UNIVERSITAT DE BARCELONA

Effect of Cpt1a deletion in the mediobasal hypothalamus in response to physical activity and aging

Kevin Ibeas Martínez

UNIVERSITAT DE BARCELONA

Facultat de Farmàcia
i Ciències de l'Alimentació

Programa de Doctorat en Biotecnologia

Effect of Cpt1a deletion in the mediobasal hypothalamus in response to physical activity and aging

Kevin Ibeas Martínez

Barcelona, 2022

UNIVERSITAT DE BARCELONA
Facultat de Farmàcia
i Ciències de l'Alimentació

Programa de Doctorat en Biotecnologia

Effect of Cpt1a deletion in the mediobasal hypothalamus in response to physical activity and aging

Memòria presentada per Kevin Ibeas Martínez per optar al títol de doctor amb mención internacional per la Universitat de Barcelona

Dolors Serra Cucurull

Laura Herrero Rodríguez

Kevin Ibeas Martínez

Barcelona, 2022

"La ciencia es más que un simple conjunto de conocimientos: es una manera de pensar".

Carl Sagan

La aventura de la ciencia

"*Última vuelta Kevin, si los neumáticos aguantan podemos alzarnos con la victoria. A por todas*"-me informaba Dolors, la directora técnica del equipo. Después de casi 5 años entrenando muy duro para alcanzar el triunfo en el campeonato Science Kart, me encontraba a escasos 2.022 metros de conseguir mi propósito. Entré en el equipo Betaoxi como un simple piloto de pruebas y puede ser que hoy acabe siendo el campeón. En ese mismo instante, mi mente se abstrajo y me recordó todas las horas de estudio, de pruebas, de análisis de resultados y dedicación que había realizado durante este tiempo.

Las primeras personas que llegaron a mi cabeza fueron mi familia. Desde pequeño, siempre me he considerado muy familiar y, cada victoria que iba consiguiendo durante el campeonato, se la dedicaba a uno de ellos y lo celebrábamos todos juntos el domingo en la playa con una buena paella y una botellita de vino. En este último gran premio, mi familia se había desplazado a Barcelona para darme todo su apoyo. Estaban sentados en primera fila y, cada vuelta que pasaba por meta notaba como se dejaban la voz para animarme. Ellos saben de primera mano que no ha sido un campeonato fácil…. Mis inicios en Science Kart no fueron sencillos: pinchazos, pérdida de potencia del motor, choques, salidas de pista, problemas con los frenos, … Sin embargo, a pesar de la distancia, siempre notaba su cariño en cada una de las etapas. Por ello, quiero agradecer a mis padres, Tinin y Marta, no sólo el apoyo incondicional, sino los valores que me habéis enseñado desde pequeño. Os quiero agradecer todas las horas en las que os explicaba las estrategias de carrera o las mejores del kart y, aunque sabía que no entendíais nada, siempre estabais allí para escucharme.

Hablando de soportar, se me vino a la cabeza la persona que nunca me ha fallado, y que estoy seguro de que nunca lo hará, mi hermana Eva. Sé que no te lo suelo decir muchas veces, pero estoy superorgulloso de ti. Desde pequeña, ya tenías claro a donde querías llegar y, a día de hoy, ya lo has conseguido. Los dos compartimos el cariño por el motor y, en estos momentos, quería agradecerte todos los consejos que me has dado gracias a los cuales estoy a punto de ganar el campeonato. Además de mi círculo cercano, también he notado el calor del resto de mi familia a los que agradezco su difusión en redes sociales, su apoyo en los programas de televisión y los ánimos recibidos previos a cualquier gran premio. Todavía me acuerdo de las primeras carreras en triciclo que hacía con mis primos en el parque de la Iglesia Real y Antigua de Gamonal en mi ciudad natal, Burgos,

y de cuando mis abuelos de Benidorm me regalaron mi primer kart, siendo mis fans incondicionales desde mis primeras carreras. Cuántos años han pasado desde entonces…

Sin embargo, el camino hasta aquí no sólo ha dependido de mi perseverancia y entrega. Ningún piloto es nada sin su equipo. Y tengo que decir que mi equipo técnico ha sido el mejor. Ellos han sido quiénes me han hecho sentir como en casa a pesar de estar lejos quiénes me han apoyado en los momentos de bajón y con los que siempre he podido contar en los momentos difíciles durante las 14 carreras de esta temporada. A pesar de que mi equipo ha ido variando durante estos años, de todos ellos he ido aprendido algo.

Mis dos grandes mentores han sido Sebastián y Mari Carmen. Dos pilotos excepcionales que ya ganaron este campeonato y que, actualmente, se encuentran trabajando en categorías superiores. Desde el primer día que conocí a Sebastián me di cuenta de que era una fuente de conocimiento. De él aprendí todo lo necesario en cuanto a estrategias, conducción y manejo de la presión. También, me llevo todas las historias y momentos que compartimos durante esas noches junto al fuego en las que no parábamos de mover el esqueleto. Eres un artista (y no sólo en la pista) y nunca dejes de indagar sobre todo aquello que es desconocido. Mari Carmen, qué quieres que te diga que no sepas ya… Sin lugar a duda, has sido lo mejor de esta experiencia, mi hermana mayor, mi novieja, la persona que, con solo mirarme a los ojos ya sabía cómo me encontraba. Desde que te fuiste, dejaste un gran vacío en el equipo y en mí. Eres una piloto excepcional, trabajadora como la que más y, sobre todo, con un corazón y una honradez envidiables. No tengo dudas de que estés donde estés vas a brillar. Gracias por todos los consejos que me diste y espero que pronto nuestros caminos se vuelvan a juntar.

Otra gran piloto que dio un giro de 360° en mi trayectoria en el equipo Betaoxi fue Paula, tres veces ganadora del Campeonato de Science Kart. Vino en el peor momento de la temporada, en el que llevaba encadenando varias derrotas consecutivas y, gracias a ella, resurgí y volví a obtener buenos resultados. Nunca olvidaré los momentos de "*desayuni*", las discusiones sobre mejoras del coche y todo lo que has hecho por mí. Eres una profesional de 10 y, aunque hayas abandonado el mundo del motor, sé que podrás conseguir todo aquello que propongas. Simplemente, gracias.

También me acuerdo de algunos ingenieros y pilotos junior que dejaron una huella en mí. Entre ellos, quiero destacar a tres pilotos junior del equipo: Mar, Pau y Meni. Llegaron al equipo siendo unos pollitos y se fueron siendo unos grandes pilotos. Yo me encargué de su formación en la disciplina de la conducción y, de cada uno de ellos, aprendí algo. Con Mar aprendí la persistencia, con Pau la paciencia, y con Meni la curiosidad, tres características básicas para cualquier buen conductor. Gracias a todos por vuestra ayuda y colaboración en la mejora del kart. Además de ellos, quiero agradecer el trabajo de todos los ingenieros que han pasado por el equipo: Sergio, Irene Lleida, Irene, Vaso y Júlia. Echo de menos nuestras reuniones comentando las estrategias de carrera, las clases de twerk con Irene Lleida, las cervecitas post-entreno con Irene, las confesiones italo-griegas con Vaso y como con Júlia nos convertimos en Tik-tokers profesionales. Gracias a todos por aparecer y compartir esta aventura a mi lado.

Ya dejaba atrás la última recta y restaban solo 905 metros para cruzar la bandera de cuadros. En ese instante, la luz roja de "*Fallo de motor*" se encendió. Recibí un mensaje de mi directora técnica: "*Kevin, baja las revoluciones. El motor está dañado y hay riesgo de explosión. Tenemos que asegurarnos de terminar la carrera"*. Mi compañera de equipo, Pía, se encontraba en segunda posición a 4 segundos de mí. Sin embargo, mi principal rival en el campeonato, Roberto, venía luchando con ella en cada curva y, si no quedaba delante de él, podría perder el campeonato. "*Pía está haciendo todo lo posible para retrasar a Roberto. Último esfuerzo, campeón*" -decía Laura, la directora de diseño y aerodinámica del equipo.

En ese momento volví de nuevo a la realidad, era el último bache que tenía que superar para conseguir este ansiado trofeo. Deposité toda mi confianza en mi compañera de escudería Pía. Empezamos en el equipo Betaoxi casi a la vez y, desde el primer momento, supe que podía contar con ella para todo. Ambos tuvimos que aprender muy rápido los trazados de las pistas, el significado de todos los pilotitos del volante y las estrategias de ahorro de neumáticos y combustible. Y ahí estábamos, en las dos primeras posiciones del Gran Premio de Barcelona después de un comienzo de temporada complicado para ambos. Gracias Pía por todos los momentos que hemos compartido juntos, por enseñarme la jerga chilena y por demostrarme que nunca en la vida me voy a poner más moreno que tú. También quiero destacar el apoyo de los pilotos de reserva del equipo: Marjorie, Marc e Ivonne. De todos ellos, quiero agradecer enormemente la ayuda de Marjorie en lo referente a la electrónica y el software

del kart. Llegó más tarde al equipo, pero, desde su llegada, la consideramos una más y, desde entonces, solo ha hecho más que mejorar. Es una piloto muy trabajadora, siempre dispuesta a ayudar y que siempre sabe sacarte una sonrisa con el pico de su muñeco. Estos meses han sido intensos para ambos, pero, finalmente, ambos lograremos nuestro objetivo. Lucha por todo lo que merezca luchar y cuida a todo el equipo como has hecho conmigo. A Marc y a Ivonne les deseo todo lo mejor y que disfruten de estos años que les falta para formarse y convertirse en los próximos campeones.

En la última recta, Roberto adelantaba a Pía y se situaba cada vez más cerca de mi kart. Ambos estudiamos en la prestigiosa Academia de Valencia donde nos hicimos inseparables. Viajábamos juntos, salíamos de fiesta, compartíamos confidencias y disfrutábamos de cada carrera como si fuéramos niños. Al año siguiente ambos fichamos por el equipo Betaoxi participar en la próxima temporada. Sin embargo, la noche previa a la primera carrera del campeonato, visitamos al experto en astrología David. Su fama era reconocida internacionalmente y queríamos saber cómo nos iba a ir la temporada. Él nos comunicó que, para conseguir el triunfo, debíamos de separar nuestros caminos. Por ello, al año siguiente, Roberto se marchó al equipo de la competencia, los ChemiArt. Sus compañeras de equipo, Mar y Maja eran las mejores pilotos de toda la parrilla y, ambos, las admirábamos desde pequeños.

No podía olvidarme de los pilotos del resto de escuderías con los que he vivido muchas aventuras y con los que, si o si, iba a celebrar esta temporada independientemente del resultado. Algunos de ellos se han ido convertido en familia, como Christopher (C!!, mi ravalader favorito, que será pequeñito pero tiene un corazón que no le cabe en el pecho), Eva, Carles, Álex, Ignasi, Simonas (mi rockero favorito), Yuanbing (thanks to you, I have a Chinese-Spanish dictionary) y la bailonga Melissa (aún recuerdo nuestro viaje a Tenerife), las secres más guapas y saladas de todas las escuderías del campeonato (Mayte, Tina, Sandra y Vanessa) a las que iba a visitar un rato y me quedaba horas pasándomelo pipa con sus historias, Consuelo (la jefa del equipo) que, aunque tuvieras un día gris, ella venía y te sacaba la mejor sonrisa o te hacía reír a carcajadas con sus alocadas ocurrencias, mi *queen* favorita, Ania, con la que he podido comprobar que viniendo de mundos totalmente diferentes, es posible tener una verdadera relación de amistad, y mi whiskera favorita, Ceci, de la que me he enamorado en muy poquitos meses. Muchisimas gracias a todos por hacerme el trabajo más ameno y conseguir que las horas se me pasarán volando.

A escasos 609 metros de la bandera de cuadros, el motor comenzó a perder potencia, y Roberto se encontraba ya a menos de 2 segundos. En ese momento, recibí un mensaje de Dolors: "*Kevin, independientemente del resultado que tengamos, estoy orgullosa de todo el recorrido que hemos realizado juntos. Recuerda que, si lo piensas con todas tus fuerzas, puedes conseguir todo lo que te propongas*". Hemos pasado muchos momentos buenos, charlas variadas que podían abarcar desde lo último sobre motores hasta las terapias alternativas o la meditación, y, también, algunos momentos de presión, tristeza y frustración por no llegar a los resultados esperados, pero siempre, en todos ellos, has estado allí para apoyarme y prestarme tu ayuda. Gracias por todo y por más calçotadas juntos. Junto a este mensaje, recibía otra conexión de Laura, la directora de diseño: "*Lucha hasta el final y lo conseguirás. Yo confío en ti*". Gracias Laura por confiar en mí desde el primer día en el que llegué al laboratorio y no sabía ni hacer una qPCR, gracias por todos los consejos que me has dado para aprovechar el tiempo al máximo y gracias por estar ahí cuando te necesitaba.

Tras estas palabras, una mezcla de sensaciones se apoderó de mí. Por un lado, no quería defraudar a mis compañeros y, por otro lado, la nostalgia de los mensajes de mis directoras y los recuerdos de mi familia me hicieron soltar más de una lágrima. Intenté mantenerme firme y, finalmente, conseguí alzarme con la victoria en el Gran Premio de Barcelona con tan sólo tres décimas de ventaja sobre Roberto. No era capaz de contener mis lágrimas de alegría y, ya en la meta, lo celebré con todos mis seres queridos con varias botellas de cava rosa.

Allí, no sólo se encontraban todas las personas que he ido nombrando, sino que también estaban el resto de mis amigos y compañeros de vida. Mis locuelos compañeros de piso y Lucía a los que, poco a poco, les he ido introduciendo en los encantos del karting y que me han visto sufrir en estos últimos meses. Gracias por todo vuestro apoyo y por cuidarme como un hermano. Mi familia barcelonesa, amigos que conoces un día y que, con el transcurso del tiempo, se convierten en familia. Gracias por estar ahí cuando tenía un problema y por todas las noches en las que, con un par de copas y unos bailes, habéis conseguido que me olvidará de todos los problemas que tenía durante el campeonato. De todos ellos, quiero agradecer especialmente a Jorge, quién empezó siendo un amigo en esta aventura, y se ha ido convirtiendo ya en parte de la familia Ibeas Martínez. Gracias por las correcciones a última hora de los cálculos de rendimiento de batería sin los cuáles no habría conseguido acabar esta carrera. Lo mismo ocurre con mi italiana Erika, con la que comparto demasiadas

cosas en común y, con la que, pase el tiempo que pase, sé que estaremos juntos en muchas más bodas próximamente. Gracias por todo lo que me has aportado en estos años y porque las resacas con Pepi y contigo se llevan mejor.

Me sorprendió enormemente encontrarme con mis compañeros de academia (Adri, Laurita, Angela y Alberto), compañeros que comparten mi afición por el motor y con los que, a pesar de estar separados, siempre he podido contar en momentos importantes. Siempre seremos el #EquipoRosa y, siempre estaremos preparados para una noche como la primera (eh, Angela). Además, también habían acudido mis amigos de Toronto, ciudad a la que fui 3 meses a realizar un curso de aerodinámica. Gracias Adri, Sara, Judith, Andy, Kim, Denise y el resto de los compañeros del curso por hacerme sentir como en casa.

Con todas estas palabras, quiero agradeceros el haberos cruzado en mi camino, el haber hecho mi vida más fácil y el haberme hecho sentir como en casa desde el primer momento en el que me mudé a Barcelona. Os voy a echar mucho de menos. Sois los mejores. ¡Os quiero mucho!

Y ahora, que corra el cava…

Abstract

Food intake and energy homeostasis are tightly regulated by the brain through a complex neuronal network located in the hypothalamus. Within this region, the mediobasal hypothalamus (MBH) acts as an interface between metabolic signals and neuroendocrine pathways governing energy balance in the central nervous system. The MBH includes two hypothalamic nuclei involved in energy balance: the ventromedial nucleus (VMN) and the arcuate nucleus (ARC). In the VMN, steroidogenic factor 1 (SF1) neurons play a critical role in the feeding and energy control. In addition, agouti-related protein (AgRP) neurons in the ARC participate in the regulation of food intake and energy expenditure.

Lipid metabolism in the MBH can modulate the whole-body energy balance. However, how changes in this pathway influence specific neuronal activity remains unclear. Carnitine palmitoyltransferase 1a (Cpt1a), which regulates the rate-limiting step in the mitochondrial fatty acid oxidation, is one of key enzymes involved in this regulation. In this work, we have analysed (1) the metabolic phenotype of mice lacking specifically *Cpt1a* in SF1 neurons (SF1 *Cpt1a* KO), and (2) the effect of Cpt1a in AgRP neurons on exercise and cognition using a mutant mouse model lacking *Cpt1a* in AgRP neurons (AgRP *Cpt1a* KO) in adult and aged mice.

Our results demonstrate that both male and female SF1 *Cpt1a* KO mice show a mild reduction in food intake without affecting body weight. Moreover, only female SF1 *Cpt1a* KO mice exhibit enhanced brown adipose tissue (BAT) activity, while this is not observed in SF1 *Cpt1a* KO male mice. Under high fat diet (HFD) conditions, male SF1 Cpt1a KO mice lost completely this moderate feeding phenotype. Because of that phenotype, we did not continue with these studies.

Exercise, the main component of energy expenditure, has a powerful action on metabolism. Specifically, in the skeletal muscle, exercise induces signalling pathways that modify the metabolism and physiological properties of muscle fibres. Regular exercise is strongly associated with increased lifespan and

decreased risk of metabolic and mental disorders during aging. In the present study, we have evaluated the physical and cognitive abilities of AgRP *Cpt1a* KO mice. Adult AgRP *Cpt1a* KO mice exhibit an improvement in endurance, motor coordination, locomotion, and exploration, without changes in anxiety-related behaviour, cognition, and strength. AgRP *Cpt1a* KO mice also show a reduction in muscle mass related to a smaller cross-sectional area (CSA) and myofibre transition from glycolytic to oxidative fibres in the gastrocnemius (GAS) and tibialis anterior (TA) muscles compared to the control group. This improvement in physical performance and muscle fibres remodelling are maintained in aged AgRP *Cpt1a* KO mice, minimising the loss of physical capacity during aging. In addition, aged AgRP *Cpt1a* KO mice displayed better cognition skills and a reduction of inflammation and oxidative stress in the hypothalamus and the hippocampus. At a central level, the deletion of *Cpt1a* in AgRP neurons from adult ZsGreen mice alters mitochondrial motility.

At a cellular level, the molecular effect produced by the silencing of *Cpt1a* were tested by two different non-coding RNAs in two AgRP hypothalamic cell lines (mHypoE-41 and E-46). Our results revealed that miRNA 6540-5p has a potential role in inhibiting *Cpt1a* gene expression. Future studies will allow us to understand the mechanisms implicated in this modulation in response to exercise and aging.

In conclusion, Cpt1a in AgRP neurons results essential to modulate exercise performance, myofibre remodelling and cognition. Nonetheless, future studies are needed to clarify the specific role of Cpt1a as a potential anti-aging candidate for the treatment of a wide-diversity disorders, where memory or physical activity are affected such as obesity, Parkinson's, and Alzheimer's diseases.

Abbreviations

α-MSH	alpha-melanocyte-stimulating hormone
Acc	Acetyl-CoA carboxylase
Adrb3	Adrenoreceptor beta 3
AgRP	Agouti-related protein
Akt	Protein kinase B
Ampk	Adenosine monophosphate-activated protein kinase
ARC	Arcuate nucleus
Atgl	Adipose triglyceride lipase
ATP	Adenosine 5'-trophosphate
AVV	Adeno-associated virus
BAT	Brown adipose tissue
BBB	Blood-brain barrier
Bdnf	Brain derived neurotrophic factor
BSA	Bovine serum albumin
CART	Cocaine and amphetamine-stimulating hormone transcript
cDNA	Complementary deoxyribonucleic acid
CNS	Central nervous system
Cpt	Carnitine palmitoyltransferase
Cpt1am	Carnitine palmitoyltransferase 1a insensitive to malonyl-CoA
$CreER^{T2}$	Mutant Cre recombinase fused to the human estrogen receptor
CSA	Cross-sectional area
Cytc	Cytochrome c oxidase
DI	Discrimination index
Dio2	Iodothyronine deiodinase 2
DMEM	Dulbecco's modified Eagle's medium
DNA	Deoxyribonucleic acid

dsRNA	Double-stranded ribonucleic acid
DREADDs	Designer receptors exclusively activated by designer drugs
EDL	Extensor-digitorum longus
EDTA	Ethylenediaminetetraacetic acid
EPM	Elevated Plus Maze
ERα	Estrogen receptor alpha
FA	Fatty acid
FAO	Fatty acid oxidation
Fas	Fatty acid synthase
Fbxo32	F-box protein 32, atrogin-1
FoxO	Forkhead box O
GABA	Gamma-aminobutyric acid
Gapdh	Glyceraldehyde-3-phosphate dehydrogenase
GAS	Gastrocnemius
Gdf8	Growth differentiation factor 8, myostatin
gDNA	Genomic deoxyribonucleic acid
GH	Growth hormone
gWAT	Gonadal white adipose tissue
H&E	Hematoxylin and eosin
HFD	High fat diet
Hprt1	Hypoxanthine phosphoribosyl-transferase 1
Hsl	Hormone-sensitive lipase
Igf-1	Insulin growth factor-1
Il	Interleukin
IR	Insulin receptor
IRES	Internal ribosome entry site
KO	Knockout

LepR	Leptin receptor
LHA	Lateral hypothalamic anterior nucleus
MBH	Mediobasal hypothalamus
Mfn	Mitofusin
MLS	Mitochondrial translocation sequence
m-HypoE	Mouse embryonic hypothalamic cell line
miRNA	Micro-ribonucleic acid
M-MLV	Moloney-murine leukaemia virus
mRNA	Messenger ribonucleic acid
mtDNA	Mitochondrial DNA
mTor	Mammalian target of rapamycin
Murf1	Muscle ring finger protein 1
Myh	Myosin heavy chain
NaCl	Sodium chloride
NCD	Normal chow diet
NORT	Novel Object Location test
NPY	Neuropeptide Y
Nrf2	Nuclear factor erythroid 2
OFT	Open Field test
OLT	Object Location test
O/N	Overnight
Opa1	Optic atrophy 1
PBS	Phosphate-buffered saline
PCR	Polymerase chain reaction
Pgc1α	Peroxisome proliferator-activated receptor γ coactivator-1α
Pi3K	Phosphatidylinositol 3-kinase
POMC	Pro-opiomelanocortin

Ppar	Peroxisome proliferator-activated receptor
PVN	Paraventricular nucleus
qRT-PCR	Quantitative real-time polymerase chain reaction
RISC	RNA-induced silencing complex
RNA	Ribonucleic acid
RNAi	Interference ribonucleic acid
ROS	Reactive oxygen species
Rpl	Ribosomal protein
Runx	Runx family transcription factor
SDS	Sodium dodecyl sulphate
SEM	Standard error of mean
SF1	Steroidogenic factor 1
siRNA	Small interfering ribonucleic acid
Slc2a	Glucose transporter solute carrier family 2 member
SNS	Sympathetic nervous system
Socs3	Suppressor of cytokine signalling 3
SOL	Soleus
sWAT	Subcutaneous white adipose tissue
TA	Tibialis anterior
TMX	Tamoxifen
Tnfα	Tumour necrosis factor alpha
Tris-HCl	Tris(hydroxymethyl)aminomethane-hydrochloric acid
Ucp	Uncoupler protein
VMN	Ventromedial nucleus
WAT	White adipose tissue

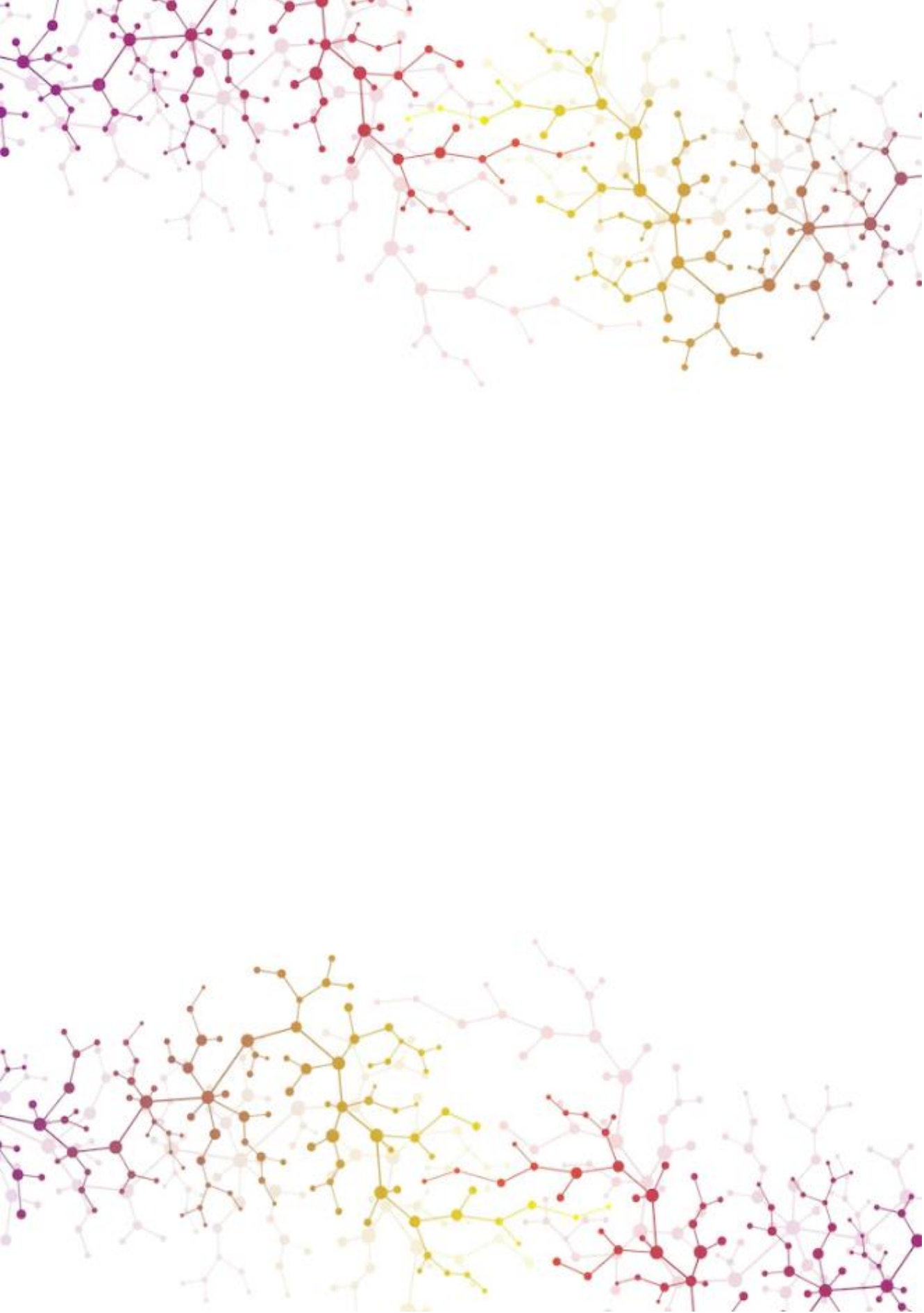

Table of contents

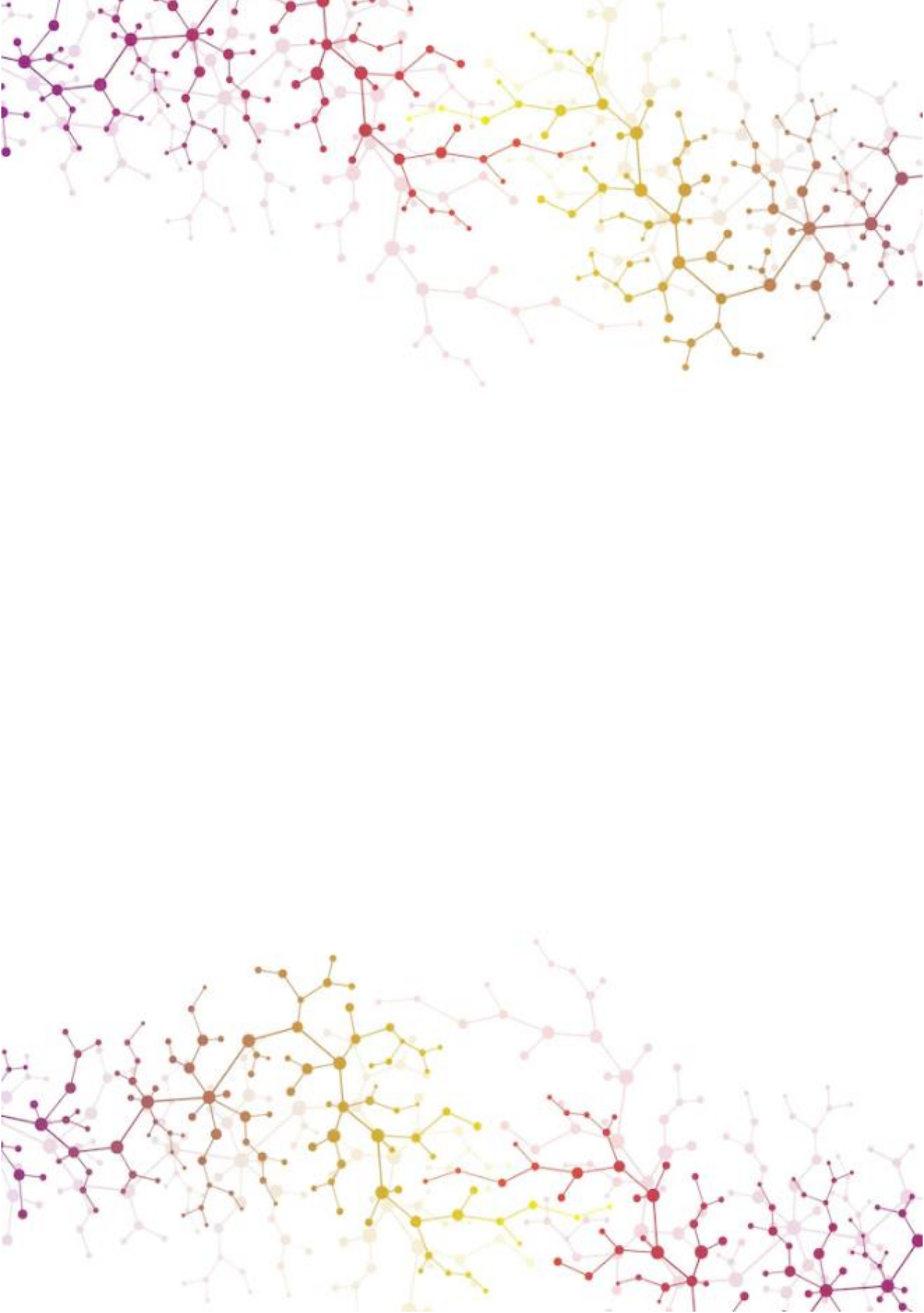

1.Introduction

1.1. Brain regulation of energy balance

The concept of energy balance is based on the fundamental thermodynamic principle that energy cannot be destroyed, and it can only be gained, lost, or stored by an organism (1). Energy balance is defined as the state achieved when the energy intake equals energy expenditure. There are two key concepts in the regulation of energy homeostasis: the energy intake (calories or energy provided into the body by food and drinks) and energy expenditure (calories or energy used in the body during physical activity or essential body functions such as digestion, circulation, respiration, or regulation of the temperature). Any alteration of this homeostatic regulation produces changes in body weight and, if this disturbance is maintained during the time, the risk of disorders such as obesity or cardiovascular diseases, increases exponentially.

Current lifestyles are responsible for the alarming growth in of the prevalence of obesity and overweight. Both terms are defined as abnormal or excessive fat accumulation in different tissues that presents a risk to health (2). An imbalance between energy intake and energy expenditure causes overweight, contributing to obesity and associated metabolic problems like type 2 diabetes, cardiovascular pathologies, osteoporosis, Alzheimer disease, depression and some types of cancer (breast, ovary, prostate, liver, kidney and colon) (3,4). Therefore, understanding the molecular and physiological mechanisms underlying the regulation of energy balance is crucial for the prevention and treatment of metabolic syndromes including obesity and overweight.

The control of energy balance is coordinated mainly by the central nervous system (CNS). This control is a multi-determined process involving a redundant and distributed network of communication that exists between several brain

regions and the body (5,6). The brain continuously receives, processes, and sends autonomic and behavioural outputs to maintain energy homeostasis. These signals are communicated to the brain either through a humoral pathway via the circulatory system, or through neuronal communication via the vagus and spinal nerves (7).

Energy intake is mainly controlled by neuronal orexigenic and anorexigenic signals in response to hormones released from different tissues and nutrients to control energy homeostasis (*Figure 1*). Ghrelin, a hunger hormone, is predominantly produced by the stomach to stimulate food intake when energy balance is negative (8).

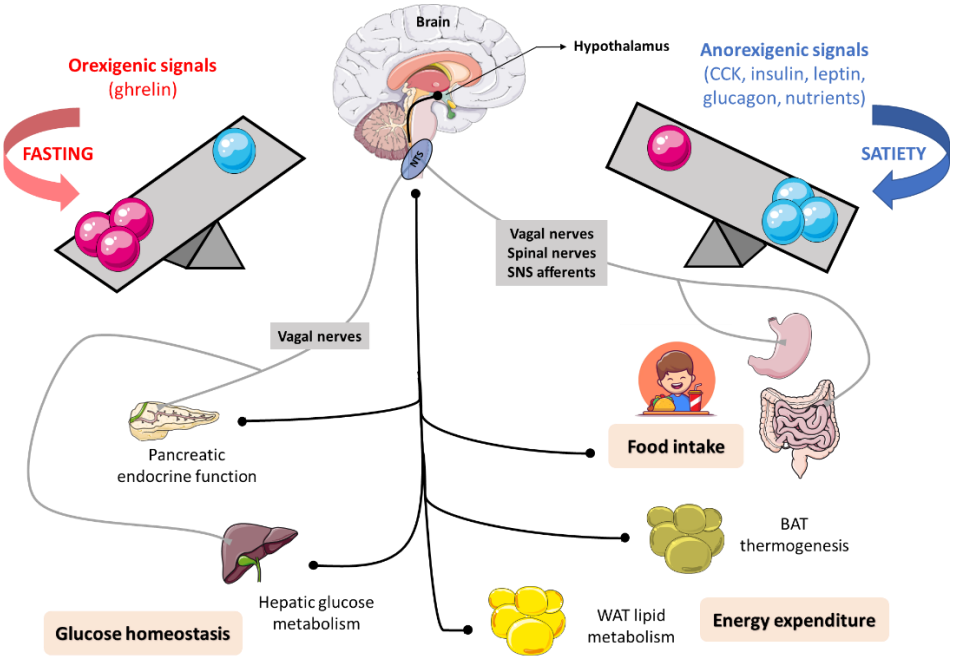

Figure 1. Regulation of energy balance by the brain. Orexigenic and anorexigenic signals act to preserve the energy homeostasis in the body. Brain also plays a crucial role in glucose homeostasis regulation. In addition, tissues can regulate brain activity through the afferent nerves and the sympathetic nervous system. NTS: nucleus of the solitary tract.

When energy balance turns positive, signals to promote satiety are released. Insulin and leptin are two hormones synthetised by the pancreas and the adipose tissue respectively, that can cross the blood-brain barrier (BBB) acting directly in numerous brain regions to inhibit food intake (9). In addition, a rise in circulating concentrations of nutrients (glucose, fatty acid, and amino acids from diet) and the cholecystokinin (CCK) hormone from the gastrointestinal system stops feeding to preserve the energy balance (10).

1.2. Hypothalamus and control of energy homeostasis

There are several brain regions involved in the modulation of energy balance. However, it has been widely known that hypothalamus is one of the most relevant area because it is at the interface between signals of metabolic state and the neuroendocrine pathways governing energy balance (11–13).

The hypothalamus is one of the oldest and smallest parts of the brain. It is composed of many neuronal nuclei that integrate multiple metabolic inputs from peripheral organs with afferent stimuli coming from other brains areas and coordinate efferent responses to control food intake, hormone secretion, body temperature, locomotion, circadian rhythm, fatigue and behaviour in order to maintain energy and glucose homeostasis (14). Anatomically, the hypothalamus is a region of the diencephalon located below the thalamus organised in various regions with different physiological functions. The anterior region is composed of lateral and medial preoptic, supraoptic, anterior hypothalamic, suprachiasmatic, and paraventricular (PVN) nuclei. The tuberal region is divided into the dorsomedial, ventromedial (VMN), arcuate (ARC) and lateral hypothalamic (LHA) nuclei. Finally, the posterior region is constituted by mammillary, tuberomammillary and posterior hypothalamic nuclei (*Figure 2*).

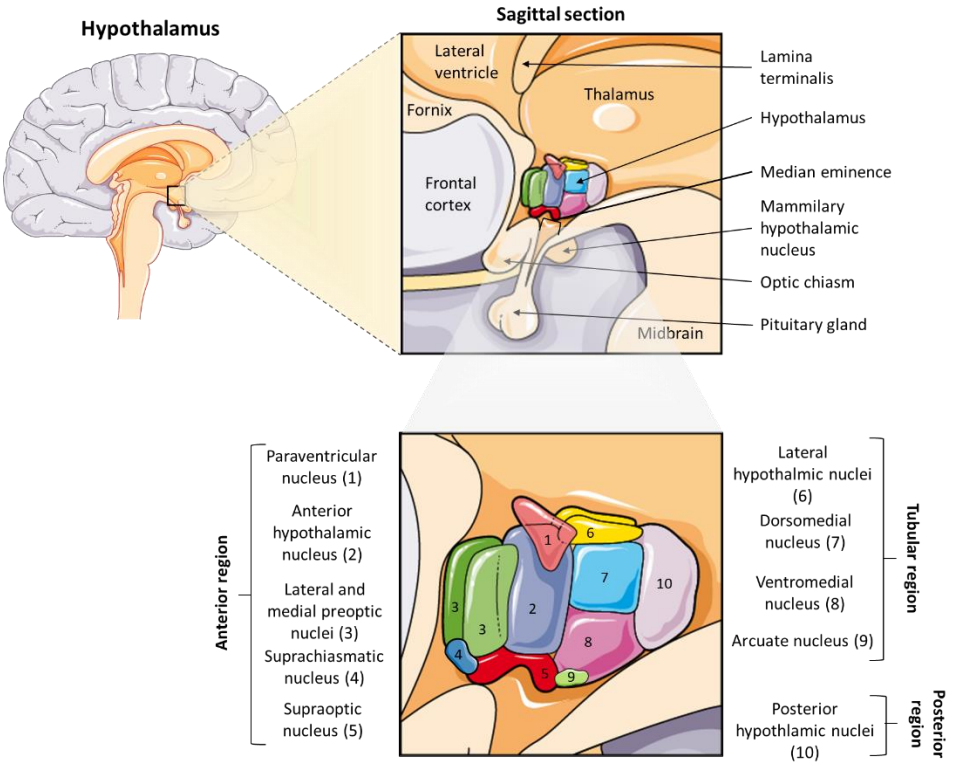

Figure 2. Hypothalamus anatomy and organization of hypothalamic nuclei. Sagittal section of hypothalamus and localization of the different hypothalamic nuclei. Parts of the figure were drawn by using pictures from Servier Medical Art. Servier Medical Art is licensed under a Creative Commons Attribution 3.0 License (https://creativecommons.org/licenses/by/3.0/).

Among these hypothalamic nuclei, the VMN was identified as the first site for body weight and energy homeostasis regulation by Bailey and Bremer in 1921 (15). In this study of diabetes insipidus, they reported that lesions in the mediobasal hypothalamus (MBH), a region that includes VMN and ARC, of dogs resulted not only in polyuria and polydipsia, but hyperphagia and obesity as well. However, the first evidence in rodents was reported by Smith (16) and Hetherington (17,18) studies, who designated the VMN as the brain "satiety centre". Since then, the VMN has remained a site of interest for regulation of food intake and glucose control (19–22). Nevertheless, the discovery of the melanocortin system in the ARC established a relevant and crucial role in the regulation of energy homeostasis. The

biological actions of α-melanocyte-stimulating hormone (α-MSH) and melanocortin receptors expressed in the CNS, melanocortin-3, and melanocortin-4 receptors (MC4R) are mainly involved in energy regulation. Indeed, mutations in MC4R are associated with obesity and high fat preference (23,24).

1.2.1. Ventromedial nucleus and SF1 neurons

The ventromedial nucleus of the hypothalamus is a bilateral region with an elliptical shape located above the median eminence. The VMN is composed of heterogeneous cell types with different gene expression patterns. Many of the genes highly expressed in the VMN have been identified and their functions have been widely analysed (13,25). As a result, the VMN plays a wide range of functions, not only associated with energy balance. Between these tasks, it is involved in the regulation of glucose and lipid metabolism, modulation of the temperature, anxiety-like behaviour, neuroendocrine control (leptin, insulin, glucagon, ghrelin and catecholamines) and reproduction (22,26).

Within these identified genes in the VMN, the steroidogenic factor 1 (SF1, officially designated NR5A1) is currently the only transcription factor whose expression is restricted in the brain to neurons in the VMN of rodents. This spatial restriction provides an excellent opportunity for studying the VMN function, as it offers a genetic target that it is exclusive to VMN adult cells. SF1 is expressed during embryonic development at E9.5 and remains confined entirely within the VMN from E10.5 to the rest of development (27). Outside the brain, SF1 can also be found in the gonads, adrenal cortex, pituitary gland and spleen (26,28).

For many years, SF1 was classified as an orphan nuclear receptor, but some evidence revealed that phospholipids can be ligands of SF1, such as phosphatidic acid (activator) or sphingosine (inhibitor) (29). In addition, SF1 can modulate the expression of some downstream genes, including brain derived neurotrophic factor (*Bdnf*), corticotropin-releasing hormone receptor 2 (*Chrh2*), estrogen receptor alpha

(*ERα*) and cannabinoid receptor 1 (*Cb1*). Considering these findings, numerous studies on mice based in targeting SF1 neurons were performed to analyse the relevance of the VMN in energy homeostasis (30).

1.2.1.1. Role of SF1 neurons in energy balance

The identification of the transcription factor SF1 as a relevant modulator of endocrine and metabolic function was reported by Parker's group (31). Knockout (KO) mice deficient in *Sf1* exhibit neonatal lethality by the lack of adrenal glands and gonads that triggers to adrenal insufficiency unless they are transplanted with adrenal glands. Transplanted *Sf1* KO mice show structural abnormalities of the VMN cytoarchitecture and, most interestingly, they exhibit massive obesity (31). A similar phenotype is described in individuals with mutations in the *Sf1* gene, who often develop mild to severe obesity (32).

To minimise the metabolic effects associated with adrenal gland transplantations in *Sf1* KO mice, Elmquist's group generated a mutant mouse model in which *Sf1* was specifically ablated after the completion of VMN development using a calmodulin-dependent protein kinase II-Cre (33). Postnatal VMN-specific *Sf1* KO mice reveal increased body weight and impaired thermogenesis under high-fat diet conditions (HFD) due to a decrease in brown the adipose tissue (BAT). In addition, the deletion of *Sf1* in the VMN of aged mice leads to a late onset of obesity due to increased food intake, blunted energy expenditure and reduced physical activity. Aged *Sf1* KO mice also exhibit a dysregulation of insulin and leptin homeostasis and a reduction in the BAT thermogenic activity (34).

Optogenetic and chemogenetic manipulation of SF1 neurons was also analysed by hM3Dq (activator) and hM4Di (inhibitor) designer receptors exclusively activated by designer drugs (DREADDs). The expression of DREADDs in SF1 neurons allows to excite or inhibit them in response to clozapine N-oxide (CNO). The administration of CNO in fasted *Sf1*-hM3Dq mice showed a reduction in food

intake and fat mass while the inhibition of SF1 neurons in fasted *Sf1*-hM4Di mice increased feeding and body weight (35).

The design of *Sf1*-Cre transgenic mice lines in which the expression of Cre recombinase is limited to SF1 neurons, has allowed a significant advance in the understanding of the VMN metabolic regulation (19,20,36–38). These mice lines have allowed the specific deletion of different targets associated with energy homeostasis by crossing them with floxed strains.

Due to the relevance of anorexigenic hormones like leptin and insulin, in the control of energy balance, the physiological effects of leptin and insulin receptors (*LepR* and *IR*, respectively) in SF1 neurons have been widely explored (*Figure 3*).

The first evidence for LepR signalling in the VMN was revealed by the generation of SF1 neurons specific *LepR* KO mice. The deletion of the *LepR* in SF1 neurons results in increased body weight without alterations in food intake. Under HFD conditions, SF1 *LepR* KO mice show a reduction in energy expenditure and an increase in body weight and food intake (19). The ablation of the suppressor of cytokine signalling 3 (*Socs3*), a negative modulator of leptin action, in SF1 neurons results in minimal effects on body weight, but shows increased insulin sensitivity in mice (39). Furthermore, a reduction in food intake and energy expenditure is observed in SF1 *Socs3* KO mice under standard or HFD conditions (39). The deletion of the α protein subunit α (*Gsα*), another negative regulator of leptin action, in SF1 neurons shows increased leptin and insulin sensitivity (40). A recent study tries to rescue the native LepR in SF1 *LepR*-null mice. However, LepR signalling in SF1 neurons is not sufficient to prevent obesity in SF1 *LepR*-null mice (41). These findings suggest that SF1 neurons interact with other cell types expressing *LepR*, and SF1 neurons by themselves cannot compensate leptin receptor deficiency.

Insulin is a hormone known for its anorexigenic and slimming effects of body weight in both rodents and humans (42,43). Deletion of *IR* in SF1 neurons in mice do not show any differences in body weight, but under HFD conditions,

mutant mice are protected against obesity and display an improvement in leptin and glucose sensitivity. Interestingly, the cellular activity of pro-opiomelanocortin (POMC) neurons in the ARC is increased under these conditions. The differential regulation of insulin action in the MBH suggests cooperation between different nuclei into the development obesity (20).

The phosphatidylinositol 3-kinase (Pi3k) is composed by two different subunits: the p85 and the catalytic subunit, p110, which p110α and p110β are responsible for hyperpolarization and depolarization processes. Mice lacking *p100α* in SF1 neurons exhibit reduced energy expenditure and leptin sensitivity in response to hypercaloric feeding without alteration in glucose and insulin homeostasis (44). SF1 *p110β* KO mice also display a decrease in energy expenditure (reduced BAT thermogenic activity) leading to an obesogenic phenotype. However, in contrast to the subunit p110α, p110β is involved in the regulation of insulin sensitivity (45). In agreement with this evidence, the deletion of forkhead box O1 (*FoxO1*), a downstream effector of Pi3k, in SF1 neurons results in a lean phenotype due to increased energy expenditure and enhanced insulin sensitivity and glucose tolerance (38). Although leptin and insulin can inhibit SF1 neurons using the same molecular pathway, their receptors are specifically distributed in the VMN, which would explain the different results observed when their receptors are deleted (*Figure 3*).

Other molecular targets involved in the homeostatic regulation are estrogens, adenosine monophosphate-activated protein kinase (Ampk). Female mice lacking the *ERα* in SF1 neurons develop obesity and adipocyte hypertrophy due to the reduction in energy expenditure (37). However, these differences are not observed in male *ERα* SF1 KO mice (46). Ampk is widely considered a master regulator of metabolism by its role as an energy sensor. The specific deletion of $Ampk\alpha_1$ in SF1 neurons leads to feeding-independent weight loss associated with an increase in energy expenditure. These mice also show an activation of BAT

function confirmed by increased BAT temperature, uncoupler protein 1 (Ucp1) protein expression and sympathetic activity (47).

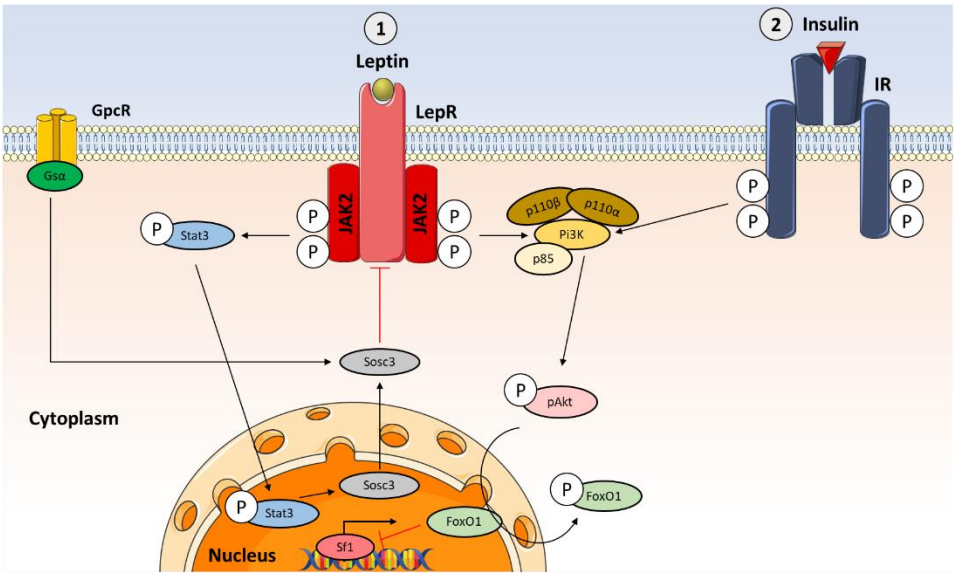

Figure 3. Leptin and insulin intracellular signalling pathways in SF1 neurons. (1) Leptin binds to LepRs and induces auto-phosphorylation of LepRs and phosphorylation of Janus kinase 2 (JAK2). Subsequently, these phosphorylated sites induce the phosphorylation of signal transducer and activator of transcription 3 (Stat3), which is translocated into the nucleus and alters the expression of several genes, including *Socs3*. Socs3 inhibits the activity of LepR. Leptin also stimulates the Pi3K-dependent pathway, particularly involving subunits p110α, which contributes to energy expenditure, and p110β, which participates in both BAT thermogenesis and glucose metabolism regulation in SF1 neurons. The Gsα subunit of G protein-coupled receptors (GpcR) negatively regulates leptin action via Socs3. The activation of leptin signalling pathway triggers protection against obesity and diabetes under HFD conditions. (2) Insulin binds to IRs and activates Pi3K that promotes the phosphorylation of FoxO1 in the nucleus via phosphorylated-protein kinase B (pAkt). pFoxO1 is translocated to the cytosol avoiding the inhibitor effect on *Sf1* gene in the nucleus. The activation of insulin signalling promotes obesity and glucose metabolism impairment under HFD conditions.

Altogether, these findings indicate that SF1 neurons play a key role in the regulation of energy homeostasis and mediates the physiological adaptation to HFD, avoiding or delaying the onset of obesity (*Table 1*). In addition, the differences observed in the phenotype of *ERα* SF1 KO mice could suggest that SF1 neurons may act on energy balance in a sex-dependent manner.

1.2.1.2. Glucose-sensing SF1 neurons impact on peripheral metabolism

In addition to the relevant role of SF1 neurons in energy balance, genetic studies have highlighted that SF1 neurons are also crucial components in the regulation of glucose homeostasis. Several studies have postulated the nature and mechanisms of VMN glucoresponsive neurons (48–50). The VMN contains a heterogeneous population of neurons. Among them, a subset of VMN neurons has been shown to sense changes in glucose levels, the glucose-excited (GE) and the glucose-inhibited (GI) neurons that exhibit antagonist effects. GE neurons are activated by leptin and glucose and lead to increased insulin sensitivity and glucose uptake in peripheral tissues through the sympathetic nervous system (SNS). Low glucose levels activate GI neurons, stimulating the glucose production and the secretion of glucagon and catecholamines by pancreas and adrenal medulla, respectively with the aim to maintain normal glucose levels (50).

The first study suggesting that SF1 neurons play a key role in the control of glucose was established by Tong *et al*., in 2007 (51). They generated a specific mouse model lacking vesicular glutamate transporter (*vGlut2*, officially designed as *Slc17a6*) in SF1 neurons, leading to a disruption in the synaptic communication by glutamate in SF1 neurons. *vGlut2* SF1 KO mice also exhibit a mild obesogenic phenotype, only under HFD conditions (*Table 1*). A partial contribution of gamma-aminobutyric acid (GABA) release, from a small population of SF1 neurons, activate POMC neurons and could explain the increase in body weight observed in *vGlut2* SF1 KO mice. Interestingly, these mice display impaired glucose homeostasis with blunted counterregulatory responses to insulin under fasted conditions. Furthermore, when they induce hypoglycemia using a hypoglycemic clamp, *vGlut2* SF1 KO mice show impaired responses of counterregulatory hormones including glucagon and adrenaline (51).

Similar results were reported by the photoinhibition of SF1 neurons. In this work, the photoinhibition of SF1 neurons had no effect on fasting blood glucose levels, but the capacity of mice to recover from insulin-induced hypoglycemia was altered, displaying a decrease in glucagon and corticosterone levels (52). Conversely, the activation of SF1 neurons raised blood glucose levels with a powerful diabetogenic effect (52).

Accumulating evidence have pointed to leptin, insulin, and their downstream effectors as regulators of glucose homeostasis. Leptin has been tightly related to glucose control improving insulin sensitivity, since intra-VMN injections of leptin increases glucose uptake in peripheral tissues through the SNS. This improvement in insulin sensitivity is blunted by the application of a Pi3k inhibitor, suggesting the potential role of leptin-Pi3k-FoxoO1 pathway in the modulation of glucose homeostasis in SF1 neurons (53). In agreement with these findings, *Socs3* SF1 KO mice exhibit improved glucose homeostasis, showing protection against hyperglycemia and hyperinsulinemia caused by HFD feeding. In addition, authors suggest that leptin-phosphorylated signal transducer and activator of transcription 3 (pStat3) pathway is also associated with the glycemic control (39). Moreover, microinjections of the neuropeptide orexin in the MBH lead to an enhancement in the liver and the skeletal muscle glucose uptake (54). Therefore, Sf1, leptin, pStat3 and FoxO1 are responsible for the glucose modulation of SF1 neurons in the VMN of the hypothalamus.

Table 1. Genetic models developed to study the role of target genes involved in energy and glucose homeostasis in SF1 neurons of the VMN.

Target	Diet	BW	FI	EE	Adiposity	Glycemia	Glucose tolerance	Insulin sensitivity	Leptin sensitivity	Source
Sf1	SD	△	-	?	△	△	▼	▼	▼	31,32,33,34
	HFD	△	-	-	-	?	?	?	?	
LepR	SD	△	-	-	△	-	?	?	?	19
	HFD	△	△	▼	△	-	?	?	?	
Socs3	SD	-	▼	▼	?	▼	△	△	△	38
	HFD	-	▼	▼	?	▼	△	△	△	
Gα	SD	-	-	-	?	-	-	-	-	39
	HFD	-	-	-	?	▼	△	△	△	
IR	SD	-	-	-	-	?	?	?	?	20
	HFD	▼	▼	-	▼	-	△	△	△	
p110α	SD	-	-	-	?	-	?	-	▼	43
	HFD	△	'	▼	△	?	?	?	?	
p110β	SD	-	-	▼	-	-	▼	▼	?	44
	HFD	△	-	▼	△	△	?	?	?	
FoxO1	SD	▼	-	△	▼	?	?	?	?	37
	HFD	▼	-	△	▼	▼	△	△	△	
ERα	SD	△ (F)	-	▼ (F)	△ (F)	?	▼ (F)	?	?	36,45
	HFD	△ (F)	-	▼ (F)	△ (F)	-	?	?	?	
AMPKα$_1$	SD	▼	-	△	▼	?	?	?	?	46
	HFD	▼	-	△	▼	▼	△	-	?	
Slc17a6	SD	-	?	?	?	▼ (M/F)	?	?	?	50
(vGlut2)	HFD	△ (M/F)	△ (M/F)	-	△ (M/F)	?	?	?	?	

-: unchanged. △: increased. ▼: decreased. ?: not measured. SD: standard diet. HFD: high-fat diet. F: female. M: male.

1.2.2. Arcuate nucleus and AgRP/NPY neurons

The arcuate nucleus of the hypothalamus is a bilateral region located in the MBH, adjacent to the third ventricle and the median eminence. The ARC nucleus is composed by two neuronal populations with antagonist effects, the co-expressing agouti-related protein (AgRP)/neuropeptide Y (NPY) neurons and the co-expressing pro-opiomelanocortin (POMC)/cocaine and amphetamine-stimulating hormone transcript (CART) neurons (55).

Both neuronal groups play a crucial role in the melanocortin system, a critical neural system underlying the control of body weight and other functions. Deficits in the melanocortin system may exacerbate comorbidities of overweight and obesity (55). While POMC/CART neurons release the precursor Pomc for the synthesis of melanocortin peptides (α, β, and γ-Msh), the AgRP/NPY neurons produce the endogenous melanocortin antagonist Agrp to control the system. Furthermore, POMC/CART neurons can express anorexigenic peptides and have appetite suppressing functions, while AgRP/NPY neurons can express orexigenic peptides and have an appetite-stimulating role (56) (*Figure 4*). AgRP/NPY neurons can also release GABA, an inhibitory neurotransmitter that may exert its orexigenic action through the GABAergic-mediated inhibition of POMC/CART neurons (57).

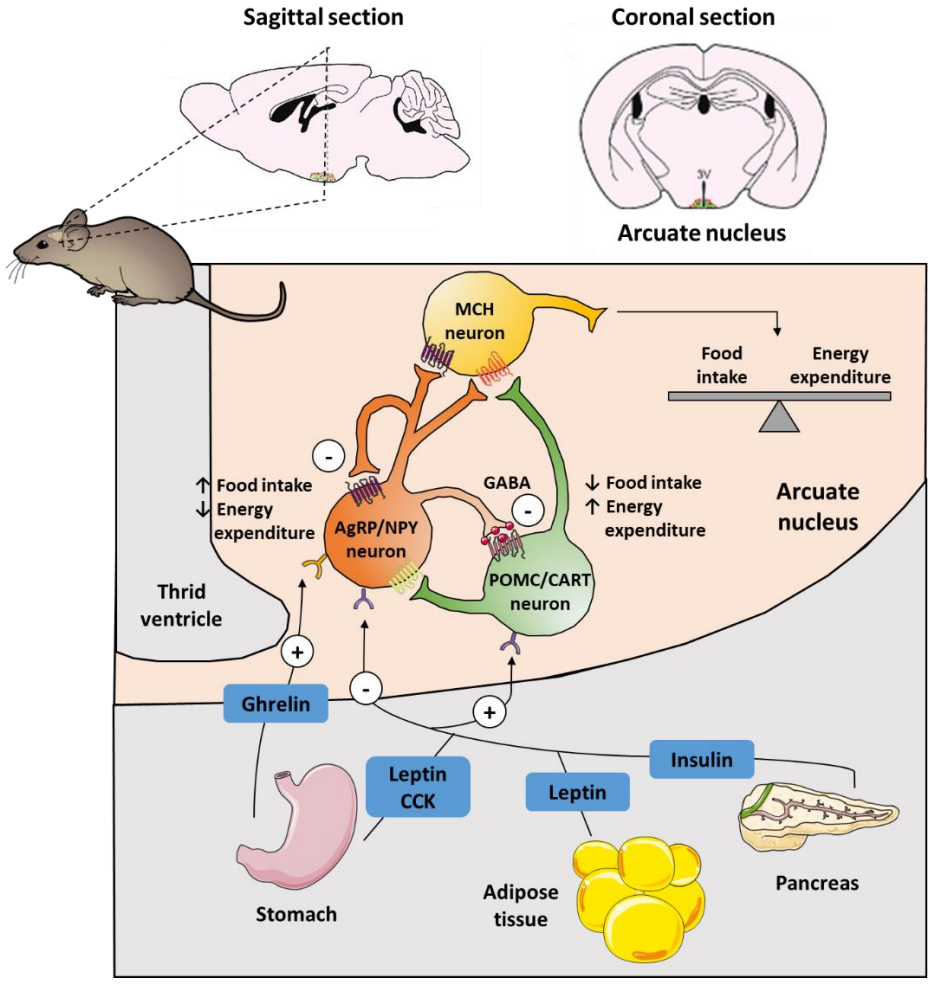

Figure 4. Regulation of appetite and energy balance in the ARC nucleus. The melanocortin system is composed by the orexigenic AgRP/NPY neurons and the anorexigenic POMC/CART neurons, which both send projections to a second order neurons to stimulate appetite or satiety. This system is also influenced by hormones secreted by peripheral organs that modulate feeding behaviour. In a fasting state, ghrelin is secreted by the stomach and released into systemic circulation, In the CNS, ghrelin stimulates AgRP/NPY neurons in the ARC. These neurons in turn have impacts on second and third order neurons that have downstream targets responsible for endocrine, behavioural, and autonomic responses in the body that drive appetite and caloric preservation. Conversely, leptin, insulin, and cholecystokinin have chronic effects of appetite regulation. Leptin is mainly secreted by adipocytes; insulin is released by pancreas; and CCK is secreted by stomach in feeding situations. These hormones cause the inhibition of AgRP/NPY neurons and the stimulation of POMC neurons. The effects of this response include the downregulation of appetite and the upregulation of metabolic rate. MCH neuron: melanocortin neuron. Parts of the figure were drawn by using pictures from Servier Medical Art. Servier Medical Art is licensed under a Creative Commons Attribution 3.0 License (https://creativecommons.org/licenses/by/3.0/).

1.2.2.1. Role of AgRP neurons in energy balance

The contribution of AgRP neurons to energy homeostasis was initially challenged by the evidence that neonatal deletion of *Npy*, *Agrp*, or both neuropeptides did not show differences in body weight and food intake (58). The differences between SF1 neurons suggest that the neurocircuit function and connectivity underlying energy balance can compensate across development and often mask the relevance of a specific gene. To test the role of AgRP neurons in food control without the possibility of developmental compensation, a specific mouse model, which human receptor for diphtheria toxin is expressed specifically in AgRP neurons was developed, allowing a temporal control depending on the diphtheria dose (59). The loss of AgRP neurons in neonatal mice revealed little effect on food intake and body weight. However, ablation of AgRP neurons in adult mice showed a dramatic decrease in food intake and produced eventual death because animals were not eaten and cannot be motivated to do so (59).

These results were confirmed using optogenetic and chemogenetic techniques. Activation of AgRP neurons results in increased food intake and body adiposity and a reduction in energy expenditure in fasted and fed mice, while chemogenetic the inhibition of AgRP neurons reduces food intake and increased energy expenditure in mice (60). Activation of AgRP neurons not only increases the respiratory exchange ratio (RER), indicating high carbohydrate utilisation (61,62), but it also suppresses the lipolytic and thermogenic programme of the white adipose tissue (WAT) (63). In addition, injections of Agrp and Npy in the MBH reveals increased food intake and reduced energy expenditure (64). These data support the idea that activation of AgRP neurons promotes the conservation of energy by the suppression of sympathetic outflow to thermogenic tissues.

The activity of AgRP neurons is activated under fasted conditions and a large amount of evidence indicate that ghrelin is involved in this stimulation (*Figure 4*). Ghrelin is a hormone predominantly produced by the stomach with orexigenic

effects. Ghrelin increases food intake by the activation of its receptor, growth hormone secretagogue receptor (Ghs-R) in AgRP neurons (65). Ghrelin also increases the messenger ribonucleic acid (mRNA) levels of *Npy* and *Agrp* in ARC neurons through the activation of transcriptional factors, such as brain specific homeobox proteins (66). These proteins interact with transcriptional factors like FoxO1, to activate the *Agrp* expression in the nucleus, and the phosphorylation of cAMP response-element-binding protein (pCreb) to stimulate *Npy* gene expression (67).

It has been suggested that the Ampk-carnitine palmitoyltransferase 1 a (Cpt1a)-uncoupler protein 2 (Ucp2) axis is a remarkable pathway in the ARC, which is involved in ghrelin's control of food intake (68). Ampk is a downstream target of the Ghs-R, and upon its activation, Ampk inhibits the acetyl-CoA carboxylase (Acc). The inhibition of Acc produces a decrease in the intracellular levels of malonyl-CoA, the physiological inhibitor of Cpt1a, which is the rate-limiting step in the mitochondrial fatty acid oxidation (FAO) pathway. Therefore, increased FAO generates a high amount of reactive oxygen species (ROS) and, the subsequent increase in Ucp2 activity. Indeed, a study using a global *Ucp2* KO mice revealed the key role of Ucp2 as an anti-oxidant player in the modulation of ghrelin's actions on AgRP neurons (69). However, it is necessary more cell-type specific studies to clarify the role of Ucp2 in food intake control in AgRP neurons.

1.2.2.2. Glucose-sensing AgRP neurons impact in peripheral metabolism

The role of AgRP neurons in glucose homeostasis is consistent with their regulation by nutrients and hormones, including insulin and leptin. Early pharmacological studies found that brain administration of Npy causes peripheral insulin resistance independent of changes in food intake. This effect was partly attributed to the decrease of glucose hepatic production (70). While the loss of

insulin receptors from AgRP neurons impairs insulin sensitivity (71), chemo- and optogenetic activation of the AgRP neurons induces insulin resistance by impairing the glucose uptake in the BAT (72). Interestingly, insulin resistance induced by the activation of AgRP neurons does not occur in *Npy* KO mice. Consistent with that, activation of POMC neurons does not appear to alter insulin sensitivity or BAT glucose uptake (72).

Overall, the relevance of SF1 and AgRP neurons on energy and glucose homeostasis has been widely by its potential therapeutic role against several disorders, such as obesity and type II diabetes, where energy balance is altered.

1.3. Mediobasal hypothalamus and lipid metabolism

The consensus established exposes that the energy requirement for the maintenance of brain function is almost entirely satisfied by glucose metabolism. However, it has been recently shown that approximately 20% of the total energy requirement for brain activity is obtained through the FAO (73).

Fatty acids (FAs) can cross the BBB and be oxidised in the brain. It has been reported that intracerebroventricular (*icv*) administration of long-chain FAs inhibits the expression of *Npy* and *Agrp* in the MBH (74). In addition, the G-protein-coupled receptor 40, a polyunsaturated fatty acid receptor, is expressed in AgRP, POMC and SF1 neurons (75). This receptor binds free FAs acting as an energy sensor in the hypothalamus. These findings suggest that the mobilisation of FAs in the MBH could have a role in the modulation of energy balance.

Several regulatory enzymes involved in the FA metabolism are expressed in the MBH region, including Ampk, Acc, Cpt1, fatty acid synthase (Fas) and malonyl-CoA decarboxylase (47,76–78). As it was described in previous sections, pharmacological and genetic manipulation of these genes in the MBH has a remarkable impact on energy balance. For example, *icv* administration of cerulenin,

a Fas inhibitor, reduces food intake and body weight in mice by a reduction in gene *Npy* and *Agrp* expression (77) .

The hypothalamus can also regulate peripheral lipid metabolism and adiposity. Disruption of the melanocortin system in mice MBH promotes lipid uptake and fat accumulation in WAT (79). The activation of AgRP neurons promotes lipogenesis via the SNS in WAT and a reduction in BAT thermogenic activity (63,64). In addition, mice lacking *p110β* in SF1 neurons show increased adiposity in WAT and BAT through the SNS (45). In contrast, mice lacking $Ampk\alpha_1$ in SF1 neurons exhibit an activation of BAT thermogenic activity and a reduction in adiposity and lipid droplets number in comparison to control mice (47).

1.3.1. Role of *Cpt1a* in the fatty acid oxidation

FA utilisation for energy uptake is performed through FAO, which takes place in the mitochondrial matrix. To be oxidised, fatty acids are converted to fatty acyl-CoA by the action of acyl-CoA synthases. The subtype of acyl-CoA synthase varies in function of the fatty acid composition (80). Then, fatty acyl-CoA is transported to the mitochondrial matrix, a process catalysed by a set of enzymes known as carnitine palmitoyltransferases (81). Cpt subtype 1 (Cpt1) is located on the outer mitochondrial membrane and allow the transport of long fatty acyl-CoA from the cytoplasm to the mitochondrial matrix, a process that represents the rate-limiting step in β-oxidation. This step is particularly important, because at this stage, fatty acyl-CoA can either be directed to oxidation for fuel or to the formation of structural glycerophospholipids depending on the energy status. Then, the acyl-carnitine translocase (Cact) transports fatty acyl-carnitine across the mitochondrial matrix. Here, Cpt2 catalyses the conversion of fatty acyl-carnitine to fatty acyl-CoA and free carnitine, that it is transported back to the cytoplasm to be reutilised. At this stage, fatty acyl-CoA is ready to enter into the β-oxidation pathway (*Figure 5*) (82).

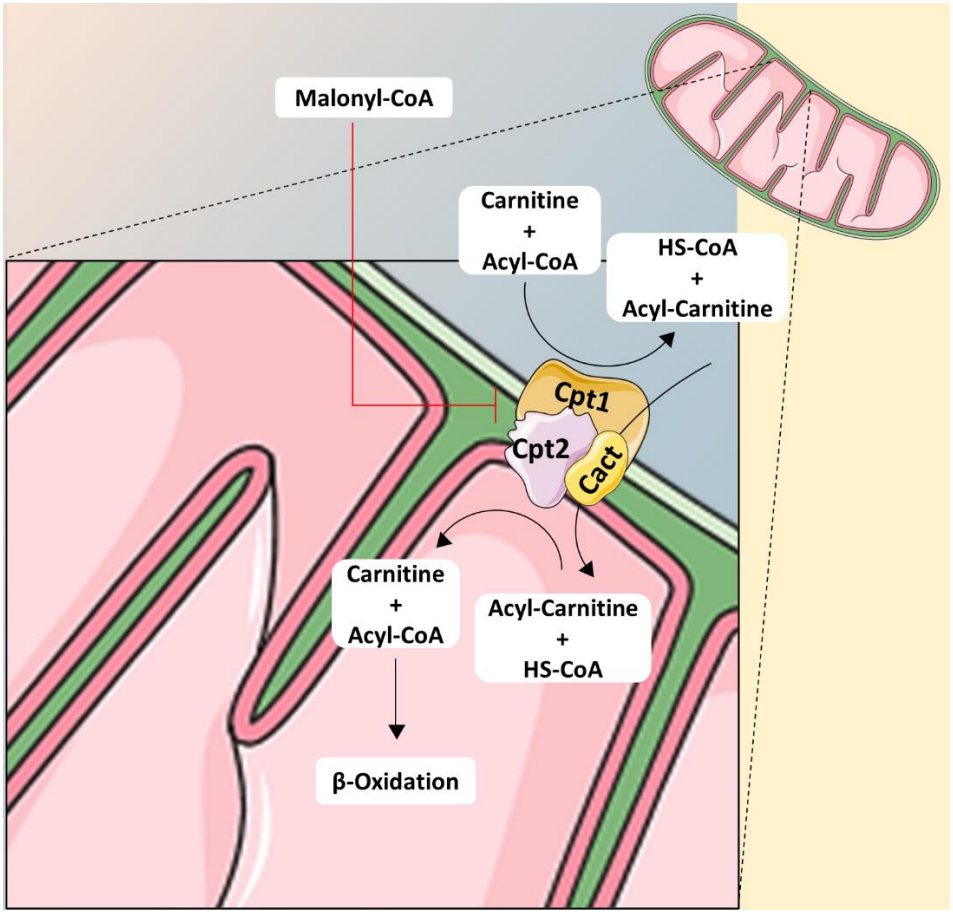

Figure 5. The carnitine palmitoyltransferase system. Schematic representation of the rate-limiting step in β-oxidation. Cpt1 is tightly regulated by malonyl-CoA, generated by acetil-CoA carboxylase (Acc) under energetic favourable situations. Parts of the figure were drawn by using pictures from Servier Medical Art. Servier Medical Art is licensed under a Creative Commons Attribution 3.0 License (https://creativecommons.org/licenses/by/3.0/).

Mammals have three different Cpt1 isoforms (Cpt1a, Cpt1b and Cpt1c) which are encoded by different genes and exhibit distinct tissue and cell distribution, and physiological and biochemical properties (*Table 2*).

Cpt1a, the liver isoform, is the most widely distributed isoform and it is expressed in liver, intestine, heart, lung, pancreas, kidney, WAT, spleen, gonads, and brain (82,83). In last decades, Cpt1a has been described as a potential therapeutic target of metabolic diseases such as obesity and type 2 diabetes, but also for

several types of cancer, including breast, ovarian and colon cancer (84–86). Cpt1b, the muscle isoform, is mainly found in skeletal muscle, heart, WAT (depending on the species), BAT and testis. Although both isoforms have a high similarity in their sequences, Cpt1b shows greater affinity for malonyl-CoA, the physiological inhibitor of Cpt1 (87). Cpt1c, the brain isoform, is expressed predominantly in brain and testis. Unlike other Cpt1 isoforms, Cpt1c is in the endoplasmic reticulum and its function is not yet fully understood. However, it has been demonstrated that Cpt1c binds to malonyl-CoA (88), and it may serve as an energy sensor in the hypothalamic regulation of energy homeostasis. Indeed, Ramirez *et al.*, reported that Cpt1c mediates ghrelin central action by altering ceramide levels (89).

Table 2. Comparative of the three isoforms of Cpt1 family.

	Cpt1a	Cpt1b	Cpt1c
Main tissue distribution	Liver, intestine, heart, pancreas, and brain	Skeletal muscle, adipose tissue, and heart	Brain and testis
Intracellular location	Outer mitochondrial membrane	Outer mitochondrial membrane	Endoplasmic reticulum
Function	Fatty acid oxidation	Fatty acid oxidation	Potential energy sensor
Substrate	Long fatty acyl-CoA	Long fatty acyl-CoA	Unknown
Inhibition by malonyl-CoA	High	Very high	-
Mouse chromosome location	Chromosome 19	Chromosome 15	Chromosome 7

1.3.2. Regulation of *Cpt1a* and relevance in the VMH

The activity of Cpt1 is tightly modulated by its physiological inhibitor, the malonyl-CoA. This molecule is produced by the condensation of two molecules of acetyl-CoA, reaction catalysed by Acc under high energy status.

In the hypothalamus, malonyl-CoA acts as an anorexigenic mediator of food intake (90,91). Central treatment with leptin (92) and Fas inhibitors such as cerulenin (77) or C75 (93) reduces food intake by an increase in hypothalamic malonyl-CoA levels. Indeed, C75 can bind directly in an irreversible way to Cpt1a, silencing its effects on feeding behaviour (94). Conversely, malonyl-CoA levels decrease in fasting conditions when ghrelin levels are high. The action of ghrelin involves the activation of Ampk, which inactivates Acc, preventing the synthesis of malonyl-CoA and, consequently, increasing the expression of Cpt1 (95). These findings suggest a potential role of Cpt1 in the control of feeding, but the mechanistic and mediators involved are still unidentified.

Two isoforms are expressed in the hypothalamus, Cpt1a and Cpt1c. However, Cpt1a is the predominant Cpt1 isoform with acyltransferase activity. Previous studies have shown that *icv* administration of selective inhibitors of Cpt1a in the hypothalamus decreases food intake (96,97). Studies carried out by our group have demonstrated that overexpression of *Cpt1a* using a permanently active mutant insensitive to malonyl-CoA (Cpt1am) in the MBH produces hyperghrelinemia and hyperphagia that lead to overweight, hyperglycemia and insulin resistance in rats (83). These changes are associated with alterations in the lipid profile and mRNA levels of glutamate and GABA transporters in the VMN (83). In addition, Gao *et al.*, revealed that the activity of Cpt1a in the VMN was altered in fasted and refeed situations, showing an increase in appetite caused by the continuous expression of *Cpt1am* (98). Nonetheless, overexpression of *Cpt1am* in the ARC does not show alterations in food intake in response to leptin (99), and injections of etomoxir, a Cpt1 inhibitor, in the ARC does not alter feeding behaviour (98).

Conversely, an unpublished work done by our team shows the relevant role of Cpt1a in AgRP neurons in food intake control. Interestingly, deletion of *Cpt1a* in AgRP neurons induces different feeding behaviour depending on the gender. Female *Cpt1a* KO mice show increased energy expenditure without changes in

food intake, while male AgRP *Cpt1a* KO mice exhibit a significant reduction in food intake without changes in energy expenditure. The lack of *Cpt1a* in AgRP enhances BAT thermogenic activity, mainly in females, and induces a decrease in fat deposits in the WAT. In addition, AgRP *Cpt1a* KO mice show polyuria and a reduction in serum angiotensin II levels, indicating a direct relation of AgRP neurons with fluid balance. These changes could be explained by the decreased in mitochondrial number and dendritic spines in AgRP neurons of AgRP *Cpt1a* KO mice. All these results indicate that each hypothalamic nucleus plays a differentiated role and, alterations in the specific neurons of these nuclei, generate changes in energy balance. Nonetheless, more studies are necessary to explore exact mechanisms of *Cpt1a* action in the hypothalamus, specially under stress conditions such as HFD or exercise.

1.4. Physical activity

It has been known that physical activity is intimately linked to human health. Susruta, a physician in India in 600 BCE., sentenced that "*diseases fly from the presence of a person, habituated to regular physical exercise…*" (100), underlying the role of physical activity in health and lifespan.

Physical activity could mitigate the progression of several disorders, including obesity, type 2 diabetes, cardiovascular diseases, osteoporosis and some types of cancer (101–103). In fact, regular exercise in the middle age reduces psychological and mental problems, such as anxiety or depression, and delays the development of dementia and Alzheimer's disease (104,105). In addition, exercise has been shown to contribute positively to cognition and memory in older adults (106). Under the dogma of "*exercise is medicine*", numerous public health agencies have recommended physical activity for the treatment of widespread disorders (2).

Exercise is an enormous challenge to whole-body homeostasis. It causes several metabolic disruptions in response to the increased energy demand of the

skeletal muscle (107). The CNS, specifically the hypothalamus, plays a crucial role in the coordination of this response (108). The hypothalamus integrates peripheral signals and delivers efferent outputs through the endocrine and nervous system to perform the necessary adaptations to maintain energy balance (109,110).

1.4.1. Skeletal muscle

Skeletal muscle comprises around 40% of total human body mass in a healthy individual and accounts for approximately 30% of total energy expenditure at rest and almost 100% during exercise (111,112). Skeletal muscle enables the maintenance of posture, stability, and the performance of a wide range of movements.

Thanks to the development of surgical techniques in the 60s, Bergström and Hultman isolated samples of human skeletal muscle for histological and biochemical analysis (113). Histologically, skeletal muscle seems uniform, but it is composed of heterogeneous fibres that differ in their physiological and metabolic properties (*Table 3*). The diversity of muscle fibres is the basis of its flexibility, which allows the same muscle to be used for a wide variety of tasks from low intensity (posture) to high intensity activity (jumping or running).

Mammalian muscle fibres are mainly classified as slow-twitch or fast-twitch based on the maximal speed of shortening (114). The variability in physiological properties of muscle fibres strongly depends on the isoform of myosin heavy chain (Myh) expressed. Indeed, myosin ATPase activity determines the sliding speed between actin and myosin, thereby shortening the speed of the fibre (115). Myosin ATPase type I histochemical staining identifies slow-twitch fibre while type II, which has the highest ATPase activity, correlates to fast-twitch myofibres. Based on the expression of predominant isoforms of Myh protein expressed, muscle fibres are classified as type I, type IIa, type IIb and type IIx/d myofibres (116) (*Table 3*).

Type I (slow-twitch) myofibres are encoded by the Myh7 isoform and exhibit a predominantly oxidative metabolism. They are characterised by high mitochondrial content, high capillary density and the mainly expression of glucose and FAO enzymes. Type I fibres are rich in myoglobin and red in appearance. In addition, they develop a slow contractile force and are specialised in endurance exercise by their high resistance to fatigue (117).

Type IIx/d (fast-twitch) myofibres express the Myh1 isoform and have a predominantly glycolytic metabolism. They are characterised by low mitochondrial content and capillary density. Type IIx/d are also poor in myoglobin and are white in appearance. They show low expression of glucose transporter 4 (Slc2a4, also known as Glut4) and have low sensitivity to insulin compared to type I myofibres playing a role in high-intensity activity such as weigh-lifting. In humans, these muscle fibres are referred to type IIx, while type IId is applied to rodents.

Table 3. Properties of skeletal muscle fibre types.

	Type I	Type IIa	Type IIx/d	Type IIb
Contraction time	Slow	Fast	Very fast	Very fast
Metabolism	Oxidative	Oxidative/ Glycolytic	Glycolytic	Glycolytic
SDH* activity	High	Intermediate	Low	Low
LDH# activity	Low	Intermediate	High	High
Resistance to fatigue	High	Moderate	Low	Low
Colour	Red	Light red	White	White
Myoglobin levels	High	Intermediate	Low	Low
Diameter	Small	Intermediate	Large	Large
Force production	Weak	Intermediate	Strong	Strong

*SDH: succinate dehydrogenase. #LDH: lactate dehydrogenase.

Type IIa (fast-twitch) myofibres have intermediate features of type I and type IIx/d muscle fibres. They show a mixed (oxidative/glycolytic) metabolism and are encoded by the Myh2 isoform. They mainly express oxidative enzymes and are light red in appearance. Although muscle endurance and resistance to fatigue rely on several cellular factors, there is a strict correlation between these properties and the high oxidative capacity and content of mitochondria of each fibre. Therefore, type IIa fibres are fast, but they have more oxidative capacity and more resistant to fatigue than type IIx/d fibres.

Rodents also possess type IIb myofibres that are encoded by Myh4 isoform. They share the same biochemical properties of type IIx/d fibres, but they exhibit a higher fast-twitch and glycolytic metabolism than type IIx/d fibres.

1.4.2. Exercise-induced skeletal muscle remodelling

Skeletal muscle is extremely adaptable to environmental changes and exhibit a high metabolic flexibility due to it is able to modify quickly the rate of adenosine 5'-phosphate (ATP) synthesis, the blood flow, and the substrate utilisation, depending on the needs (118). In response to physical activity, skeletal muscle strongly remodels their biochemical, morphological, and physiological myofibres. These changes improve skeletal muscle performance and function. The specific features of skeletal muscle adaptation to exercise depends on the modality of exercise developed (119,120). For example, resistance exercise (e.g., bodybuilding and throwing events) is generally characterised by low frequency, high resistance and intensity, and short duration. This type of activities acts mainly by increasing muscle mass and strength, displaying a transition from oxidative to glycolytic myofibres (type IIb→ type IIx/d→ type IIa→ type I). On the other hand, endurance exercise (e.g., running, cycling, and swimming events) is described by high frequency, long duration, and low power outputs. This type of exercises stimulates the mitochondrial biogenesis and the expression of mitochondrial respiration and FAO enzymes, providing a phenotypic adaptation toward a more

oxidative phenotype, where a remodelling from glycolytic to oxidative muscle fibres occurs (121). On cessation of exercise training, the myofibres transitions and metabolic changes are reverted (*Figure 6*). Although both exercise modalities are beneficial for health, endurance exercise is more effective for preventing cardiovascular diseases, while resistance exercise is indicated for the maintenance of muscle mass contrasting atrophy and age-related muscle wasting (122).

Skeletal muscle remodelling involves the activation of intracellular signalling cascades [peroxisome proliferator-activated receptor gamma coactivator-1 alpha (Pgc1α), peroxisome proliferator-activated receptor alpha and delta (Pparα and Pparδ), nuclear factor activated T cells, myocyte enhancer 2, myogenic differentiation factor (MyoD), and myogenin] to generate changes in muscle mass and mitochondrial function. The stimulation of these transcription factors induce/repress the expression of genes encoding for different Myh isoforms and metabolic enzymes that control fibre type remodelling. In addition, the transcriptional status of specific genes involved in muscle remodelling (*e.g.* Pgc1α and Ppar) may be modulated by exercise-induced epigenetic modifications [deoxyribonucleic acid (DNA) methylation, phosphorylation, acetylation and histone modifications] triggering chromatin remodelling (123,124).

Endurance exercise promotes an increased oxidative capacity of skeletal muscle and a myofibre remodelling to oxidative fibres (type I). The main regulatory elements implicated in this phenotypic adaptation are Pgc1α and Pparα (125). Accordingly, Pgc1α expression in skeletal muscle is greatly induced by a single bout of exercise and after prolonged physical activity (125,126). Pgc1α is the master regulator of mitochondrial biogenesis, and its overexpression increases mitochondrial content and function (126). Pgc1α promotes mitochondrial oxidative metabolism [pyruvate dehydrogenase 4 (Pdk4) and cytochrome c oxidase (Cytc)], glucose (Glut4) and lipid metabolism [(Cpt1b and cluster of differentiation 36 (Cd36)], and angiogenesis (127). In addition, Pgc1α is involved in slow myofibre transition and it is mainly expressed in slow muscles such as soleus (SOL) (128).

Transgenic mice overexpressing *Pgc1α* in skeletal muscle develop slower muscle mass and a phenotype characterised by high levels of mitochondrial enzymes [succinate dehydrogenase (Sdh), ATPase, Ucp1 and Cytc], high respiratory capacity, increased resistance to fatigue and protection against oxidative damage, improving exercise performance (128–130). On the other hand, mice lacking *Pgc1α* in skeletal muscle have reduced oxidative capacity, endurance performance and exhibit a slow to fast shift in muscle fibre type. Furthermore, *Pgc1α* KO mice show an increase in inflammation in peripheral tissues, such as WAT, BAT and pancreas (131).

Regular exercise triggers a rapid increase in the expression of Glut4 in human skeletal muscle (132). Pgc1α enhances insulin sensitivity, Glut4 and Akt expression in muscle. However, data from transgenic mouse models are highly controversial. Some studies reported similar data to humans, while others described the opposite effects in Glut4 and insulin sensitivity (133–135).

Pgc1α activity is modulated by transcriptional factors and post-translational modifications, including phosphorylation, deacetylation, methylation, and ubiquitination (136). A single bout of exercise induces Pgc1α deacetylation in skeletal muscle. Both deacetylation and phosphorylation of Pgc1α have been suggested to be necessary to induce the up-regulation of mitochondrial genes and *Pgc1α* gene itself (136). In addition, a wide variety of proteins and transcriptional factors are involved in the regulation of Pgc1α, including Ampk, sirtuin 1, protein kinase C, changes in intracellular calcium concentration, p38 mitogen-activated protein kinase (p38 Mapk), nitric oxide, ROS, redox balance, and hypoxia-inducible factor 1 alpha (Hif1α) (120).

While endurance exercise acts by up-regulating mitochondrial metabolism and oxidative fibre-type transformation, benefits of resistance exercise mainly depend on its ability to increase muscle mass (*Figure 6*). Skeletal muscle mass is a delicate balance between protein synthesis and protein degradation. Resistance

exercise influences both processes by activating the Pi3k/mammalian target of rapamycin (mTor) signalling (137). The kinase mTor exists in two independent complexes: mTor complex 1 and mTor complex 2. mTor complex 1 controls protein translation while mTor complex 2 prevents protein degradation by the phosphorylation and inhibition of transcriptional FoxO factors. FoxO factors induce the expression of F-box protein 32 (Fbxo32, also known as atrogin-1), muscle ring finger protein 1 (Murf1) and two E3 ubiquitin ligases, which promote the ubiquitination and the proteasome-mediated degradation of muscle proteins (138). The ubiquitin-proteasome system mediates muscle atrophy and the oxidative stress plays a key role in the regulation of the proteasome proteolytic activity (139).

The second major signalling pathway that controls skeletal muscle growth involves myostatin, a member of the transforming growth factor β superfamily also named growth differentiation factor 8 (Gdf8). Myostatin is the most well-known member of this superfamily because of the strong muscle mass developed by myostatin knockout mice (140). Myostatin acts binding to activin type IIa and IIb receptors and transforming growth factor β receptors. Through the recruitment and activation of activin receptor-like kinase-4, and -5, induces the phosphorylation of Smad2/3 to promote the formation of a heterotrimeric complex with Smad4 (*Figure 6*). Importantly, only the inhibition of Smad2/3 is sufficient to promote muscle growth, suggesting that genes involved in protein turnover are the target of these transcription factors (141). The inhibition of myostatin reduces the levels of phosphorylated Smad2/3 that allows the release of Smad4 to interact with phosphorylated Smad1/5/8 promoting protein synthesis and muscle hypertrophy (142).

Insulin growth factor-1 (Igf-1) has long been considered a key upstream regulator of mTor. Igf-1 regulates positively skeletal muscle mass via the induction of protein synthesis (138). Igf-1 acts through Pi3k/Akt pathway (*Figure 6*), resulting in an activation of mTor pathway and inhibition of FoxO factors (143).

It has been suggested that Pgc1α might also control muscle wasting pathways. Pgc1α reduces FoxO3 expression and mice overexpressing *Pgc1α* are protected from sarcopenia and exhibit increased lifespan (144). Moreover, the activation of mitochondrial oxidative metabolism and biogenesis protects against muscle atrophy, and this is achieved by endurance exercise-induced Pgc1α expression (116,145).

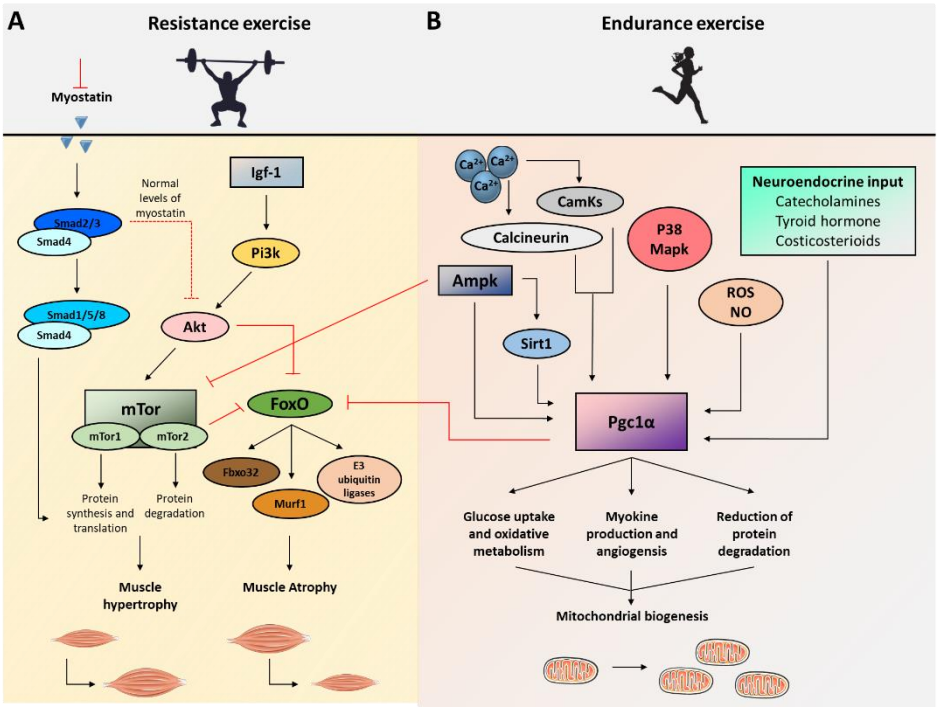

Figure 6. Skeletal muscle remodelling in response to resistance and endurance exercise. (A) In resistance exercise, mTor and myostatin are the main regulators of muscle hypertrophy. mTor is regulated by Igf-1 and Pi3k/Akt signalling pathways. The Smad4 protein derived from myostatin acts directly on the nucleus promoting protein synthesis and translation. Different FoxO factors induce muscle atrophy via activation of Fbxo32, Murf1 and two E3 ubiquitin ligases. **(B)** The crucial regulator endurance exercise is Pgc1α. Multiple signalling pathways are activated during and after endurance training and converge on Pgc1α by modulating the expression of this factor. Consequently, Pgc1α coordinates a succession of biological changes in the whole-body to promote mitochondrial biogenesis.

1.4.3. Endocrine functions of skeletal muscle

During the past decade, skeletal muscle has been identified as a secretory organ (146). In the 1960s, Goldstein suggested that humoral activity associated with skeletal muscle plays an endocrine role in the maintenance of glucose metabolism during physical exercise (147). Skeletal muscle secretes peptides and molecules called myokines that exert autocrine, paracrine, or endocrine functions. The role of these molecules varies widely and, in some cases, is antagonistic. Recent approaches have offered new perspectives of the role of skeletal muscle in homeostatic mechanisms and its inter-communication with other organs through myokines (liver, adipose tissue, bone, pancreas, heart intestine, brain, and immune cells) (146,148,149).

Some researchers have termed "exerkines" to all factors released by the skeletal muscle in response to physical activity (150). The first exerkine found to be released into the bloodstream in response to muscle activity was interleukin 6 (Il-6) (151). Although this cytokine is known for its anti-inflammatory effects, circulating Il-6 levels increases during exercise without any sign of muscle damage (152). The expression of Il-6 during physical activity is strictly independent of tumour necrosis factor alpha (Tnfα) (153). This finding suggests that muscular Il-6 has a role in metabolism rather than in inflammation. To support this idea, numerous studies have reported that intramuscular Il-6 expression is markedly enhanced when intramuscular glycogen levels are low (154,155).

Il-6 shows autocrine and paracrine functions. The autocrine regulation is through the activation of glucose uptake and fatty acid oxidation via Ampk pathway (156). Il-6 paracrine function promotes gluconeogenesis in liver, secretion of insulin in L-cells from intestine and β-cells from pancreas via glucagon-like peptide 1 and the production of osteocalcin in bone (157,158). Furthermore, Il-6 probably mediates some of the anti-inflammatory and immunoregulatory effects during exercise. Il-6 inhibits lipopolysaccharide-induced Tnfα production in cultured

human monocytes (159), and, in mice treated with an anti-Il6 antibody and in Il-6 KO mice, Tnfα levels remain high (160). Anti-inflammatory effects of Il-6 are also demonstrated the production of the classic anti-inflammatory cytokines Il-1α and Il-10, when Il-6 is stimulated (161).

Myostatin was the first muscle-secreted factor identified to fulfil all the criteria to be a myokine (162). It is a highly conserved member of the transforming growth factor β superfamily that suppresses skeletal muscle growth in an autocrine manner. Both aerobic exercise and strength training in animals and humans significantly reduced the expression of gdf8 in skeletal muscle, thus, myostatin is more like an inverse myokine compared to the rest of members that are generally upregulated by exercise (163). Mice lacking myostatin develop massive muscle hypertrophy, which is characterised by increased myofibre number and size. Myostatin decreases adiposity and enhances insulin sensitivity in adipose tissue, which leads to protection from diet-induced obesity (140,162). In addition, circulant levels of leptin, an anorexigenic hormone, are reduced in *Gdf8*-null mice, suggesting that, although a decrease in leptin secretion occurs, Gdf8-null mice are protected from the counterregulatory response of leptin signalling on energy expenditure (140). Myostatin also acts in a paracrine manner to modulate bone remodelling by the stimulation of osteoclast differentiation (164).

Brain-derived neurotrophic factor is a member of the neurotrophin family that is strongly expressed in the brain and to a lesser extent in skeletal muscle (165). In the CNS, Bdnf regulates neuronal development and modulates synaptic plasticity, playing a crucial role in the regulation of cognition and neuronal survival (166,167). Moreover, Bdnf has been identified as a key factor in the control of body mass and energy homeostasis (148). The Bdnf expression is increased in the skeletal muscle in response to exercise and contribute to stimulate FAO via Ampk (165). However, muscle derived Bdnf does not seem to be released into the circulation in significant amounts indicating that Bdnf primarily acts in an autocrine and/or paracrine manner. Besides the effects of metabolic properties, the main

consequences of modulation of muscle Bdnf extend to myogenesis, muscle satellite cell activation and muscle regeneration (168,169).

Skeletal muscle as a secretory organ opens a broad field for future research in translational medicine and inter-organ communication in response to exercise. Furthermore, benefits on health from physical activity have been widely reported (127,138,144,156), suggesting exercise as a powerful therapy to prevent several neurological and metabolic disorders.

1.4.4. Crosstalk skeletal muscle-hypothalamus

It is well established that physical activity can modulate the hypothalamic action (22,170–172). Physical activity ameliorates insulin and leptin signalling through the regulation of diverse proteins that modify levels of neuropeptides and neurotransmitters such as *Sf1*, *Agrp*/*Npy*, *Pomc*/*Cart* in the VMN and the ARC (173).

Choi *et al.,* shows that exercise training increases SF1 neuron activity in the VMN (22). Laing *et al.*, reports that 12-weeks HFD treatment dramatically reduces the expression of pStat3 in the VMN of rats, but this impairment is significantly improved by voluntary exercise training (172). In correlation with these results, humans and rodents' studies have reported that regular exercise modulates *Pomc/Cart* and *Agrp*/*Npy* expression in the ARC in different feeding conditions (174–176). However, these studies are generating conflicting results in the field. For example, Bunner *et al.*, reported that acute moderate intensity treadmill exercise increase the AgRP/NPY neuronal activity, and subsequent food intake in fed mice (177), while He *et al.*, demonstrated opposite effects after high intensity interval training (HIIT) (170). Similar results were observed in POMC neurons, where some studies revealed no changes in response to an acute moderate intensity treadmill exercise in fasted mice (177), while others observed an increase in POMC neuronal activity after fasting (178) and fed HIIT (170). All these studies analysed the neuronal activity at a single timepoint immediately after exercise, and the

exercise-mediated changes in neuronal activity in the hypothalamus can be quick and transient (179). The reported effects may reflect neuroendocrine responses during exercise, rather than changes after exercise, and may also miss critical changes in neuronal activity in the hours after exercise. In addition, these studies use electric shock to motivate mice to run, which is not controlled in the sedentary animals, and it could affect the activation of these neuronal populations. In fact, the activity of POMC neurons is stimulated by electric shock stress (180).

Another possible explanation for the variability observed in these studies is the different methodology applied in each experiment regarding intensity and duration. Variations in the energy status could modify hypothalamic neuronal activity. Therefore, the choice of type, intensity and duration of exercise training is crucial to the modulation and release of neuropeptides in the ARC.

In addition to the VMN and the ARC, other nuclei of the hypothalamus are influenced by physical activity. For example, the activation of the LHA promotes hyperlocomotion in fed mice (181). Moreover, the injection of orexin A into the PVN increases locomotor activity in mice (182). Bdnf has also been identified to be involved in physical regulation in the PVN. *Bdnf* KO mice in the single-minded 1 (Sim-1) neurons causes a decrease in ambulatory activity in the dark phase (183).

The hypothalamus modulates physical performance through the SNS and catecholamines secretion. On the one hand, an activation in the adrenergic pathway promotes activation of lipolysis, gluconeogenesis and glycogenolysis pathways in peripheral tissues to provide energy fuel for muscle activity. Furthermore, it boosts muscle hypertrophy (184). On the other hand, catecholamines act via membrane receptors divided in α and β-receptors in the whole-body. The activation of α-receptors is associated with constriction of blood vessels in bronchia and the relaxation of smooth muscle, while stimulation of β-receptors participates in the heart rate control (185). Oral administration of β_2-adrenergic receptor agonists, such as clenbuterol, in rats promotes muscle

hypertrophy by the an activation of muscle protein synthesis and/or the attenuation of protein degradation (186). Specifically, mice lacking *Sf1* in the VMN exhibit a reduction in locomotor activity and increased levels of myogenin and Fbxo32, genes implicated in protein turnover processes (11).

All these data suggest a close inter-communication between hypothalamus and skeletal muscle, playing a key role in the preservation of several physiological functions such as locomotion, appetite, cognition, and health.

1.5. Aging

Most individuals wishing to be "*forever young*", dream of a magic elixir to delay age-related changes. While many of them have searched, the proverbial "*fountain of youth*" has not been found yet, and the deterioration of cellular structure and biological function associated with aging is unavoidable.

According to the World Health Organization (WHO), aging is defined as the accumulation of a wide variety of molecular and cellular damage over the time (187). This accumulation leads to a gradual decrease in physical and mental capacity, a growing risk of disease and, finally, death. Every country in the world is experiencing a growth in the proportion of elderly people (age 65 and older). In fact, this population will double from 1 billion in 2020 to 2.1 billion in 2050, being two-thirds parts of the world's population (187).

Some evidence suggests that changes in the lifestyle, the increase in the quality of life, healthy diets and regular physical activity have been responsible for the increase in elderly population (188). Therefore, understanding the cognitive and physical changes that occurs during aging is relevant given the continuous growth in elderly population and the prevalence of age-associated problems.

1.5.1. Cognition and aging process

It has been widely found that the brain's volume peaks at the early 20s and its weight declines gradually with age at a rate of around 5% per decade after the 40s (189). The way this occurs is less clear. In the 40s, the cortex started to shrink, and aggravated neuronal atrophy and cell death (190). In addition, a decrease in dendritic synapses and the loss of synaptic plasticity has also been reported (191). The set of changes taking place in the brain with aging decreases the efficiency of cell communication, which declines learning and memory capacity (192).

Aging is associated with many neurological disorders due to the reduction in the capacity of the brain to transmit signals and communicate to other cells (*Figure 7*) (190). Loss of brain function is the main characteristic of progressive neurodegenerative disorders associated with aging, including Alzheimer's and Parkinson's diseases (193). Alzheimer's disease is characterised by a gradual cognitive deterioration with changes in behaviour-like depression and a decline in daily activities. It also causes neuronal cell death and tissue loss throughout the brain, affecting mainly areas involved in memory and thinking (194). Parkinson's disease causes unintended or uncontrollable movements, such as shaking, stiffness, and difficulty with balance and coordination. The most prominent sign of Parkinson's disease appears when neurons in the basal ganglia, a brain area involved in movement control, become impaired and/or die. The neurons of the basal ganglia are important producers of dopamine. When these neurons die or become impaired, they produce less dopamine, which causes the movement problems associated with this disease (195).

Cognition abilities also decline with age and impairments are frequently in adults over the age of 65. The decline in cognition is characterised by decreased processing speed, size of working memory and sensory receptors (196). In agreement with aging process, a variety of factors can cause cumulative damage to the brain and produce cognitive impairments, including damage to the brain due

to cerebral ischemia, head trauma, toxins, stress hormones and the development of dementia (197). The main brain region involved in memory and cognitive functions is the hippocampus. The hippocampal size is positively associated with an improvement in cognition abilities, and hippocampal atrophy is related to dementia (198). Importantly, the hippocampus possesses a high capacity for neuroplasticity and numerous studies have analysed the capacity to slow or reverse the rate of hippocampal atrophy (198).

A variety of cellular mechanisms of neurodegeneration and neuroplasticity have been proposed (199). They are being actively investigated to know how they mediate neuronal health and cognitive function. Vascular ischemia, inflammation, oxidative stress, molecular toxicity, and apoptosis are common inductors of neurodegeneration. They are involved in important signalling pathways to promote hippocampal atrophy (200). Therefore, there is emerging evidence that a healthy lifestyle improves neuroplasticity pathways to prevent cell death and neurodegeneration (200). In addition, a growing number of studies are highlighting the role of hypothalamic inflammation in cognitive dysfunction in rodent models. Despite its effects in diet-induced obesity, hypothalamic inflammation is associated with grey and white matter changes (201,202).

Diet and physical activity are two crucial factors to minimise the development of cognitive decline (203). A diet rich in calories and low in antioxidants is a risk factor for neurodegenerative disorders. However, energy restriction and the consumption of antioxidants may extend lifespan, reduce the oxidative damage, and ameliorate cognitive decline (204–206). Several studies have pointed out that exercise exhibits positive effects on cognitive decline. It has revealed that exercise training reduces the white and grey matter content, and increases the expression of Bdnf, diminishing the deleterious effects associated with age (207).

1.5.2. Skeletal muscle regulation during aging

Skeletal muscle is a tissue highly affected by aging decline, resulting in a loss of metabolic and physical function (208). The aging-related loss of muscle function involves quantitative and qualitative changes in skeletal muscle structure and function (*Figure 7*). This process is typically slow and the muscle functional loss varies significantly among individuals (209).

The decline in skeletal muscle mass and strength represents the most wide-spread, dramatic, and deleterious process during aging, also referred to as sarcopenia (210). Since then, classifications of sarcopenia have been proposed, but to establish a criterion has been difficult due to the long duration of aging process, the large variability among individuals and multiple factors that affect muscle and are not related to aging (211). Nonetheless, the reduction in muscle mass leads to a higher incidence of falls and fractures, reducing the quality of life of elderly population.

Aging-related defects in mitochondrial content and energetics have been proposed to be involved in aging muscle atrophy (212). These changes are attributed to both inactivity and age-related impairment in mitochondrial respiration, a decrease in the activity of mitochondrial enzymes, and reduced mitochondrial biogenesis, indicating a complex physiopathology involving structural changes to muscle fibres, as well as the enzymatic machinery that controls glucose and lipid metabolism (212). In fact, the loss of muscle mass is exacerbated by metabolic disorders, such as obesity due to the increased fat mass and insulin resistance (213).

The reduction in muscle mass and strength also decreases the size and the total amount of myofibres by the impairment in protein synthesis. These atrophy changes are more prominent in glycolytic fibres compared to oxidative fibres because oxidative muscles have greater number of mitochondrial content and are able to preserve their oxidative capacity during aging (214). Therefore, aging leads

to an increase in the proportion of type I in comparison to type II myofibres (215). A fast-to-slow myosin isoforms transition has been reported in both humans and animal models (216,217). This switch during aging may contribute to slowing of movement as well as decline in strength because fast muscle fibres are considered to have a higher force generation capacity than slow muscle fibres (216,217). The rate of muscle atrophy appears to be similar in women and men. However, the amount of type II myofibres atrophy and the loss may differ by gender, as type II fibres atrophy among elderly women is higher than men, particularly among type IIx myofibres (218).

In addition to muscle atrophy, a hallmark feature of aging is the decline in neuromuscular junctions. These connections allow the interaction between motor neurons to muscles being able to regulate their function. Neuromuscular junctions are key interference between terminal nerves and targeted muscle, which undergo degeneration during aging. In this context, the neuromuscular system undergoes a continual reorganization of motor neurons due to their loss and reinnervation of denervated muscle fibres (219). The increase in type I fibre composition may be due to the influence of motor neurons on muscle fibres. About, one quarter of motor neurons are inactive and non-functional during aging (220). While the number of active motor neurons decreases, each active motor neurons increases their size through the development of new branches to non-functioning myofibres (221). Therefore, with age, there is less of a contribution to tension from the higher tension type II fibres because the lower tension is now more predominant (122). Overall, the muscle mass of elderly population is smaller and weaker because of loss of type II fibres.

Favourable neuromuscular adaptations have been observed in aged population undergoing resistance training, including muscle and myofibre hypertrophy and remarkable gains in strength and power. Progressive resistance training is the most widely accepted strategy to promote muscle regrowth in atrophied muscles. For example, men over 66 years-old, who trained by

weightlifting for 12 weeks experienced strength gains of approximately 5% per day, similar to what is reported in young men (222). In addition, physical activity greatly improves cardiovascular health and diminishes the risk of muscle fragility and mortality. Training helps muscle to meet energy demands by increased mitochondrial protein production and capillary density for higher muscle metabolic demand as well as increased contractile protein production to allow greater contraction tension (222).

Figure 7. Effect of aging in skeletal muscle and brain. The progression of aging carries out several changes in the whole-body, including skeletal muscle and brain. Cognitive abilities, mitochondrial function and sarcopenia are characteristic traits of aging progression. However, exercise and other changes in the lifestyle such as diet, can avoid or delay the development of problems associated with aging.

Beyond physical activity, nutrition and hormones play a crucial role in the aging progression. Diet rich in proteins, vitamins C and D, and long-chain polyunsaturated fatty acids have been reported to improve muscle mass and

function during aging (223,224). Furthermore, the role of androgens in the muscle physiology adaptation during aging is relevant due to its decline with age. Androgens are steroid-derived hormones that contribute to many aspects of growth in youth, which continues with the maintenance of muscle and bone mass in adults. Beginning around the age of 35 years, testosterone levels in men decrease by 1 to 3% per year, while women experience the greatest drop in hormonal levels with the menopause (225). For men, the decrease in testosterone levels leads to a decrease in muscle mass and muscle strength, which increases the risk of depression and/or other disorders such as obesity and type II diabetes (226). Similarly, lower levels of estrogen lead to decreased muscle mass and increased bone fragility. Supplementation with androgen hormones can reverse or slow this trend. However, the benefits of exogenous steroid therapy are unfortunately associated with a high rate of cancer, erythrocytosis and thromboembolism (225,226).

1.5.3. Biomarkers of aging

Aging is the time-dependent physiological functional decline that affects most living organisms, which is characterised by alterations in molecular pathways, and it is a risk factor for several diseases. The identification of quantitative biomarkers of aging is necessary to measure the physiological age and, potentially, predict the lifespan. Given the complex nature of aging process, biomarkers of aging are multifaceted.

A biomarker of aging must predict the rate of aging and it must monitor a basic process that underlies the aging process. In the literature, several biomarkers of aging were reported (227,228). Most studies are related with DNA and RNA [length of telomeres, DNA repair enzymes, DNA methylation, transcriptome profile, micro-ribonucleic acid (miRNAs) and long non-coding RNAs] (229). Diet is crucial to extend lifespan in mammals and this highlights the potential role of metabolism markers for aging. These biomarkers include factors related to nutrient sensing

such as Igf-1, mTor, sirtuins, and markers associated with protein and lipid metabolism, like protein carbamylation and triglycerides (230). The products of oxidative damage α-tyrosine, 3-cholortyrosine, 3-nitrotyrosine, 8-hydroxy-2-deoxyguanosine and 8-hydroxiguanosine are also considered as aging biomarkers. In mitotic tissues, gradual accumulation of senescent cells is thought to be a causal factor of aging (231). Thus, the senescence-associated β-galactosidase is considered a biomarker of aging (232).

In addition to these molecular biomarkers, some physical and facial features have been considered aging biomarkers. Between them, the walking speed, the standing balance, the muscle mass, the body mass index, the mouth and noise width and the eye corner slope are commonly used as a markers of aging (233).

The identification of these markers has improved the knowledge of aging progression, allowing an enhancement in human health and prevention of age-associated diseases.

1.5.3.1. Insulin growth factor 1

Insulin growth factor 1 is a single chain peptide involved in many physiological, anabolic, and metabolic processes throughout the body and it is considered the major homeostatic regulator in growth, development, lifespan control and aging. Although Igf-1 can be produced in several tissues in a paracrine/autocrine manner, the liver produces approximately 75% of circulating Igf-1 in humans and rodents (234). Cellular actions of Igf-1 are mediated through the activation of Pi3k/Akt signalling pathways that regulate mTor and FoxO intracellular pathways. Igf-1 is also secreted in response to growth hormone (GH) to inhibit its action (235). Thus, GH/Igf-1 deficiencies in rodents and humans resulted in cognitive impairment and reduced growth and muscle mass (236,237).

Aging is associated with a reduction of circulating levels of Igf-1. A reduction in the signalling of GH/Igf-1 axis is related with increased longevity and, conversely,

increasing circulating Igf-1 levels promotes aging via oxidative stress and the promotion of cancer cell growth (238,239). For example, heterozygous mice for a mutated allele of the Igf-1 receptor (Igf-1 receptor null mice die at birth), show very low serum Igf-1 levels and their lifespan increase by 33% in females and 16% in males (240). The proposed mechanisms for this increase in longevity include the enhanced in insulin sensitivity and the reduction in insulin levels, inflammation, and fat content (241). Although evidence suggest that declining function of the GH/Igf-1 axis is beneficial in rodents (242–244), humans' data are contradictory. While some studies report an increased plasma Igf-1 plasma levels in healthy older humans improves insulin sensitivity and neurogenesis, other studies indicate that low levels of Igf-1 increase lifespan (245). The conflicting results observed in humans reflect the complexity of the Igf-1 system and the genetic and ethnic differences in the populations analysed.

1.6. Non-coding RNAs: siRNAs and miRNAs

The term "*non-coding RNA*" is commonly employed for RNA that does not encode a protein (246). Although the current understanding of these RNA molecules represents perhaps only the tip of the iceberg, with the rapid development of molecular biotechnology, non-coding RNAs are increasingly found to have far more relevant functions than previously recognised, and many new classes of non-coding RNA have been identified in last decades. Among them, small interfering RNAs (siRNAs) and miRNAs have attracted considerable attention because their roles in gene regulation make them likely targets for drug discovery and development. Indeed, the therapeutic potential of siRNAs and miRNAs has been demonstrated in the treatment of many different diseases including cancers (247) and infections (248,249). Compared with conventional small therapeutic molecules, siRNAs and miRNAs offer the advantage of being highly potent and able to act on "*non-druggable*" targets (for example, proteins which lack an enzymatic function or have a conformation that is inaccessible to traditional drug molecules),

since they can be designed to modulate the expression of practically any gene of interest.

Therapeutic approaches based on small RNAs involve the introduction of a synthetic siRNA/miRNA into the target cells to produce a RNA interference (RNAi), thereby inhibiting the expression of a specific mRNA to produce a gene silencing effect (250). Both RNA molecules have similar biochemical properties, but the mechanisms of action are different (*Table 4*). The requirements for sequence design and therapeutic applications of siRNAs and miRNAs are also different. The main advantage of siRNAs in comparison to miRNAs is its elevated target efficiency, which results in a high silencing efficacy. However, its effect is transient and dependent on the rate of cell division since it is not possible to amplify the RNAi. Conversely, miRNAs are less efficient, but the silencing signal is maintained over the time.

Table 4. Comparison of siRNA and miRNA properties.

	siRNA	miRNA
Structure	21-26 nucleotide RNA duplex with 2 nucleotides 3'-overhang	19-25 nucleotide RNA duplex with 2 nucleotides 3'-overhang
Complementary	Fully complementary to mRNA	Partially complementary to mRNA
mRNA target	One	Multiple
Prior to Dicer processing	Double-stranded RNA	Precursor of miRNA
Mechanism of gene regulation	Endonucleolytic cleavage of mRNA	Translational repression Degradation of mRNA Endonucleolytic cleavage of mRNA (only, when there is a high level of complementarity between miRNA and mRNA)
Applications	Therapeutic agent	Drug target Therapeutic agent Diagnostic and biomarker tool

1.6.1. Gene silencing mechanism of siRNA and miRNA

RNAi is a natural cellular process that silences the gene expression of a specific target by promoting the degradation of the mRNA. This process plays an important role in gene regulation and innate defence against viruses (251). RNAi was first described by Fire *et al.*, while studying mechanisms for effective gene inhibition by exogenous RNA in *C. elegans* (252). According to their observations, long double-stranded RNA (dsRNA) mediates potent and specific silencing of homologous genes. A similar process was described in mammals in 2007 (253). Generally, the dsRNA (either transcribed from cellular genes or artificially introduced into the cells) is processed by a specialised ribonuclease III (Dicer) in the cytoplasm into a smaller dsRNA molecule. This short dsRNA molecule is known as the siRNA and has 21-26 nucleotides with 3'-two-nucleotide overhangs. The siRNA interacts with the RNA-induced silencing complex (RISC). One component of the RISC complex, the endonuclease argonaute 2 (Ago2), cleaves the passenger strand (sense strand) of the siRNA while the guide strand (anti-sense strand) remains associated with the RISC complex. Subsequently, the anti-sense strand guides the active RISC complex to its target mRNA for cleavage by Ago2. As the anti-sense strand only binds to the mRNA that is fully complementary to it, the siRNA causes specific gene silencing (*Figure 8*) (251).

Similar to siRNAs, miRNAs also inhibit gene expression in a post-transcriptional manner. Although the gene silencing effects of siRNAs and miRNAs are distinct, miRNAs share some components with the siRNA pathway (*e.g.*, Dicer and RISC complex) (*Figure 8*).

The first miRNA was described by Lee *et al.*, while studying the developmental regulatory genes in *C. elegans* (254). miRNAs have 19-25 nucleotides with 3'-two-nucleotide overhangs and negatively regulate the gene expression of multiple genes. mRNA gene transcription is carried out by RNA polymerase II in the nucleus to give the primary miRNA (pri-miRNA), which is 5'-

capped and 3'-polyadenylated RNA with double-stranded stem-loop structure. The pri-miRNA is then cleaved by a microprocessor complex [comprising Drosha and the microprocessor complex subunit DiGeorge critical region 8 (Dgcr8)] to form the precursor of miRNA (pre-miRNA), which is a duplex that contains 70-100 nucleotides with interspersed mismatches that adopt a loop structure. Subsequently, the pre-miRNA is transported by exportin 5 to the cytoplasm, where it is further processed by Dicer into a miRNA duplex of 19-25 nucleotides. The miRNA duplex associates with the RISC complex forming a complex called miRISC. The miRNA duplex is unwound, discarding the passenger strand (sense strand)- unlike in the processing of siRNA, in which Ago2 of the RISC complex causes the cleavage of the passenger strand of siRNA. The mature single-stranded miRNA guides the miRISC to the target mRNAs and binds to them through partial complementary base pairing with the consequence that the target gene silencing occurs via translational repression, degradation and/or cleavage (255).

While the siRNA must be fully complementary to its mRNA target, the miRNA only needs to be partially complementary to it. This provides the capacity to miRNA strand to recognise an array of mRNAs. Due to the partially complementary base pairing between mRNA and miRNA, the endonuclease Ago2 of the RISC complex is not activated. Therefore, the silencing of mRNA target generally occurs through translation repression or degradation by deadenylation, decapping or exonuclease action (246).

Taken altogether, both siRNAs and miRNAs have a huge potential as therapeutic agents. In last decades, numerous works have described that miRNAs are crucial regulators in many disorders, including obesity, type II diabetes and cardiovascular diseases (249).

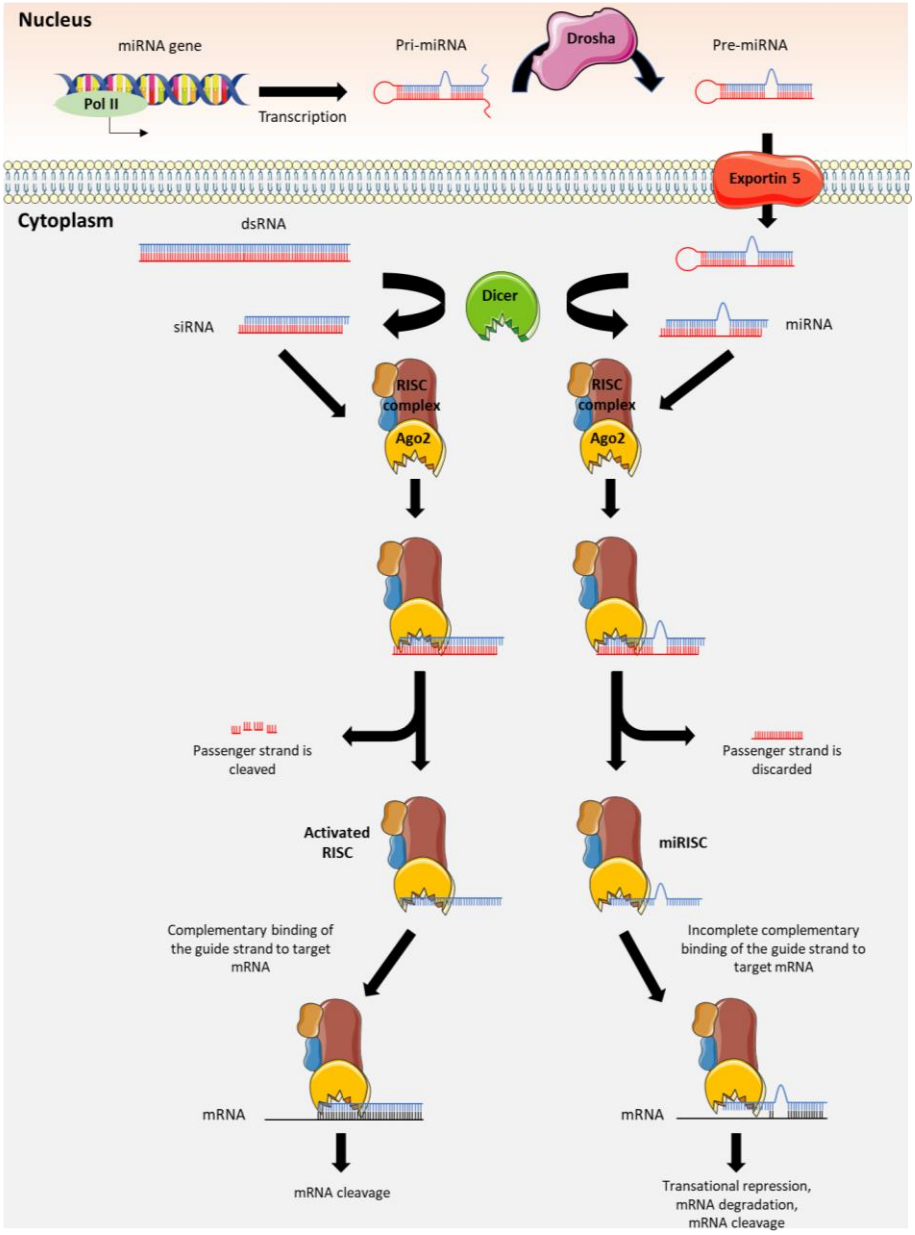

Figure 8. Gene silencing mechanisms of siRNA and miRNA. (1) dsRNA (either transcribed or artificially introduced) is processed by the Dicer into siRNA. Then, it is recognised by the RICS complex to cleave the target mRNA. (2) miRNAs are processed in the nucleus to form the pre-miRNA that is transported by exportin 5 to the cytoplasm, where it is processed by the Dicer into miRNA. The miRNA is loaded into the RISC complex, where the passenger strands is discarded and the mature miRNA guide the mRISC to inhibit the target mRNA via translational, repression, degradation, or cleavage.

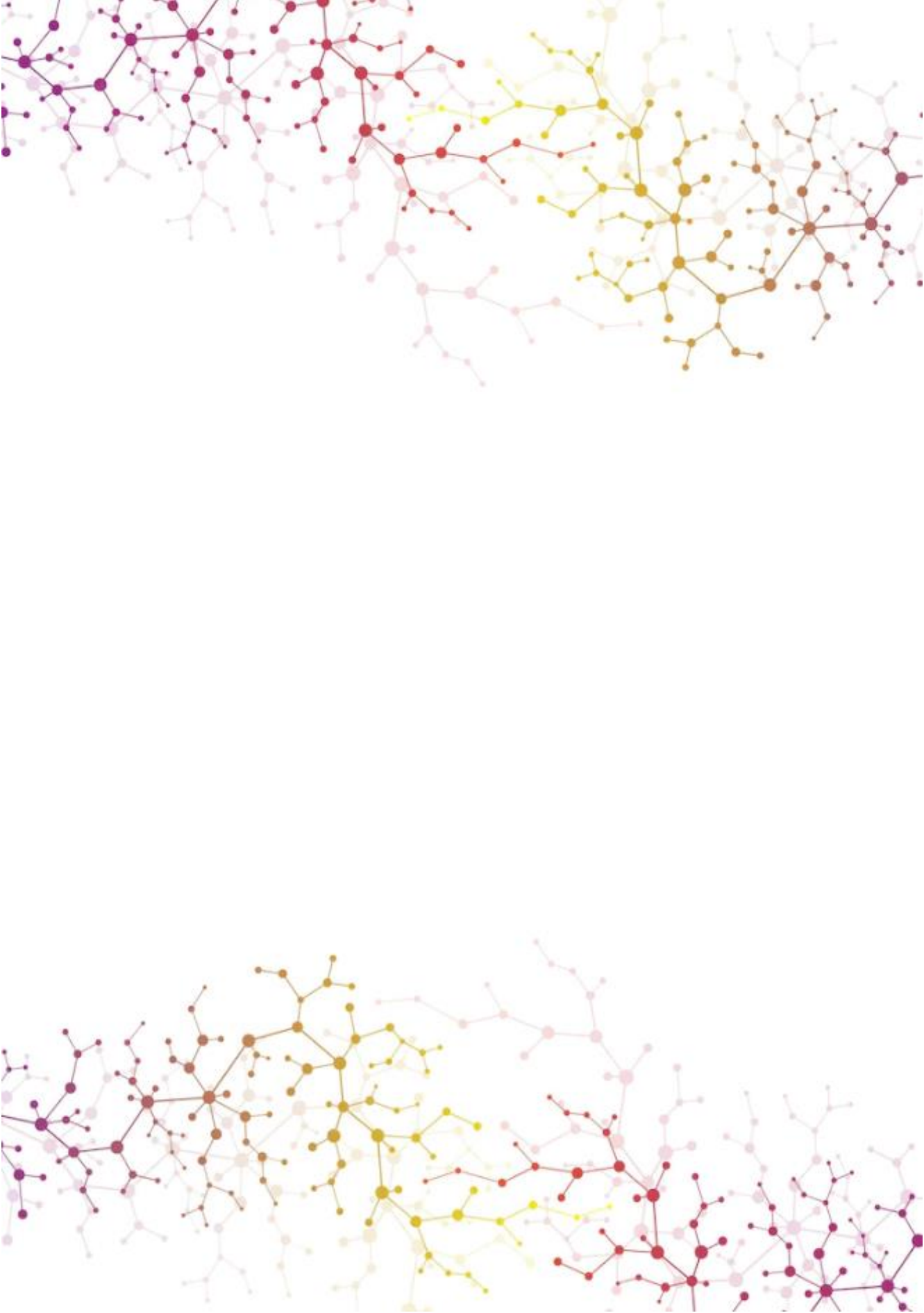

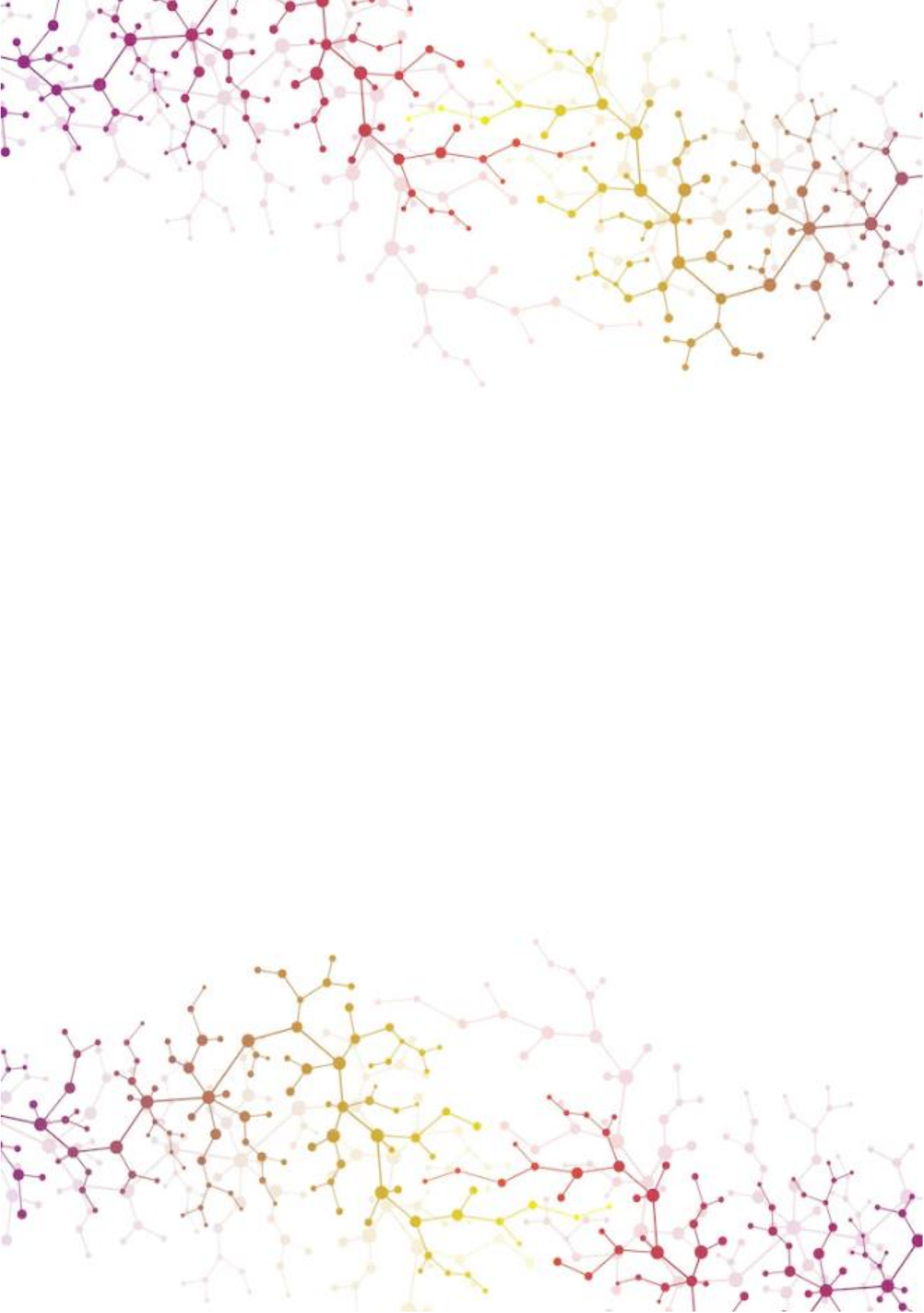

2.Objectives

The main aim of this doctoral thesis is to analyse the role of *Cpt1a* in SF1 and AgRP neurons of the mediobasal hypothalamus region in the regulation of energy balance, physical activity, and aging. To achieve this purpose, four specific objectives have been developed:

I. To study the effect of *Cpt1a* deletion in SF1 neurons on mice feeding behaviour and energy balance.

II. To analyse the exercise performance in mice lacking *Cpt1a* in AgRP neurons.

III. To establish the role of *Cpt1a* ablation in AgRP neurons in the physical and cognitive decline associated with aging.

IV. To find a potential small RNA that inhibits Cpt1a gene expression in hypothalamic cell lines to discern molecular mechanisms involved at central level.

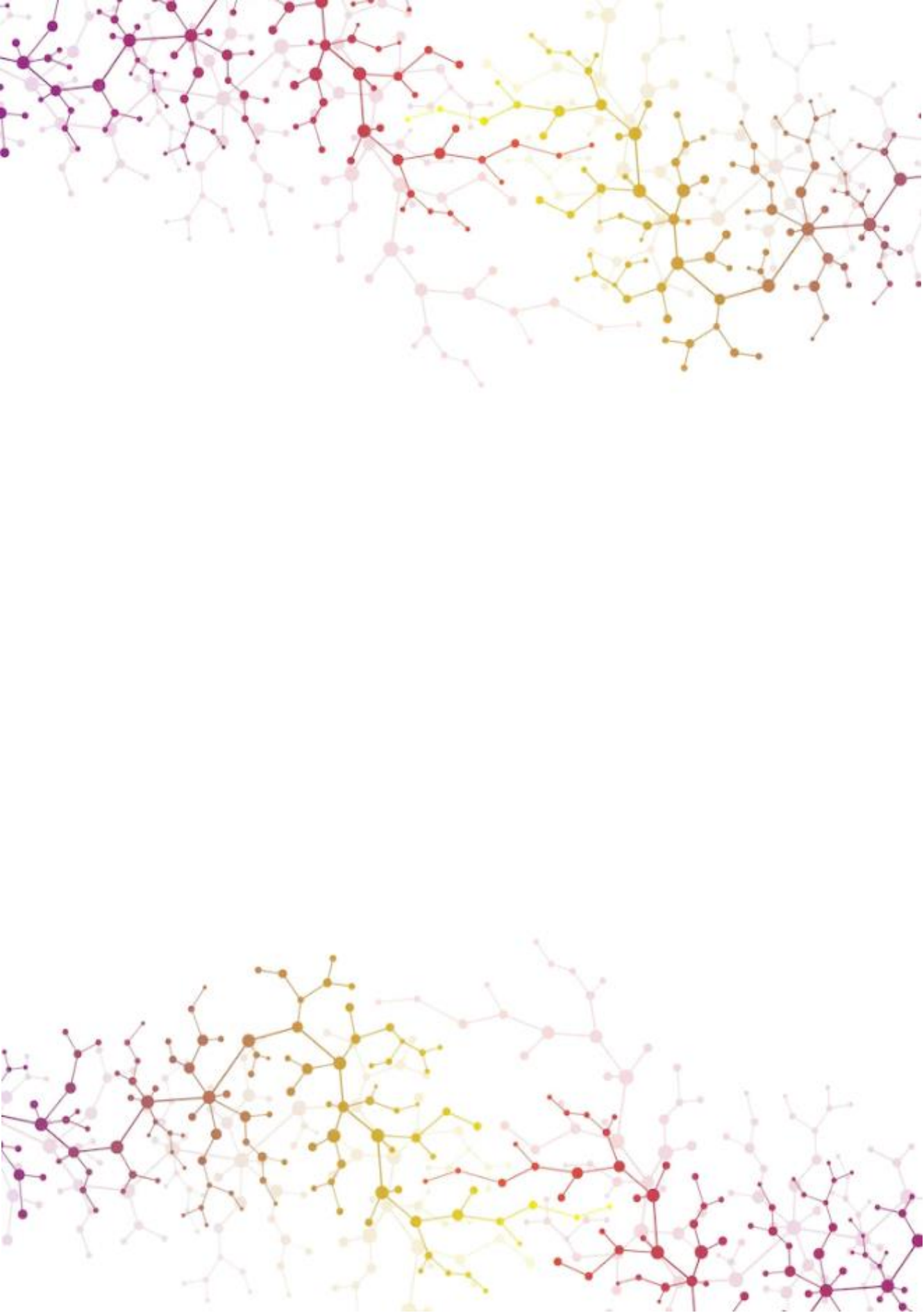

3.Materials and methods

3.1. Animal models

In the present study, several genetically modified mice were used:

-*Cpt1a* Flox mouse: A mouse strain designed to obtain the *Cpt1a* conditional KO. The homozygous *Cpt1a* Flox mouse contains two LoxP sequences surrounding the exon 4 of *Cpt1a* gene. Cpt1a enzyme is constitutively expressed in many cell types, but the presence of Cre recombinase results the excision of LoxP sites of exon 4, generating a stop codon in the exon 5 that blocks the translation of Cpt1a protein (*Figure 9*). This mouse was obtained in our laboratory in 2017 (76).

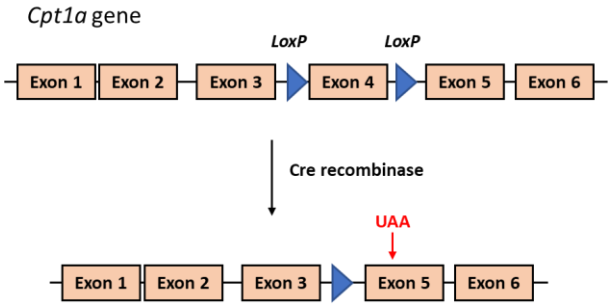

Figure 9. Scheme of *Cpt1a* Flox construct. The exon 4 of *Cpt1a* gene is flanked by two LoxP sequences in *Cpt1a* Flox mouse. The action of a Cre recombinase generates the recombination of both LoxP sites and the presence of a stop codon in the exon 5 (UAA), blocking the translation of a functional Cpt1a protein (76).

-*AgRP-CreER^{T2}* mouse: A homozygous transgenic mouse that contains DNA sequences encoding a specific-mutant Cre recombinase fused to the human estrogen receptor (*CreER^{T2}*); which does not bind to its natural ligand (estrogen) at physiological concentrations, but it binds to the synthetic ligand tamoxifen (TMX). The *CreER^{T2}* sequence is under the control of AgRP promoter, which allows the spatiotemporal gene manipulation specifically in AgRP neurons after TMX induction. This mouse was kindly provided by Prof. Joel K. Elmquist from the University of Southwestern (Dallas, United States) (256).

-*ZsGreen* mouse: The homozygous *ZsGreen* mouse contains an enhanced green fluorescent protein fused at the N-terminal with a mitochondrial translocation sequence (MLS) downstream of a floxed phosphoglycerate kinase-neomycin resistance (Pgk-Neo) cassette under the control of ubiquitous cytomegalovirus-chicken β-actin (CBA) promoter located in the Rosa26 locus. In presence of a Cre recombinase, the specific excision of LoxP sites in the Neo cassette occurs, and it starts the expression of the MLS-*ZsGreen* gene driven by CBA promoter (*Figure 10*).

The MLS used in this construct was cloned from the accessory subunit of the mitochondrial membrane respiratory chain nicotinamide adenine dinucleotide (NADH) dehydrogenase (*Ndufs4*) gene and directs ZsGreen protein to the mitochondrial matrix. This mouse was provided by Prof. Richard Palmiter from the University of Washington (Washington, United States) and Dr. Albert Quintana and Dra. Elisenda Sanz from the Universitat Autònoma de Barcelona (Bellatera, Spain).

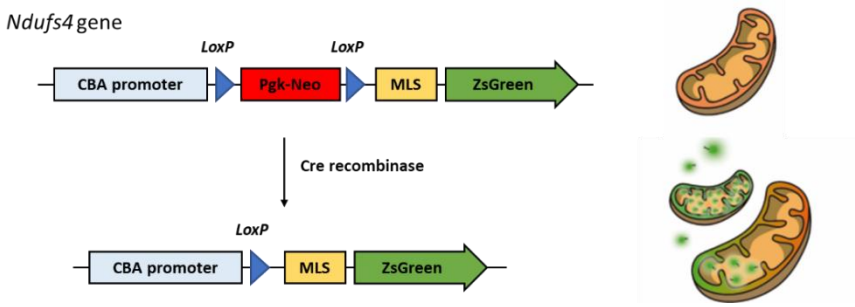

Figure 10. Scheme of the transgene construct of *ZsGreen* mice. The construct is composed by a CBA promoter followed by a floxed Pgk-Neo cassette and *ZsGreen* gene fused with the MLS. The presence of Cre recombinase triggers the recombination of the two *LoxP* sites flanked the Pgk-Neo cassette, enabling the expression of the ZsGreen protein in the mitochondrial matrix.

All animals were maintained in the Animal Experimentation Unit of the University of Barcelona, School of Pharmacy and Food Sciences at 22±2ºC and 50-60% of humidity with a 12h light/dark cycle and *ad-libitum* access to food and water. All the experiments done in this study were approved by the Ethical Committee for Animal Experimentation of the University of Barcelona, with procedure number CEEA 10994.

3.1.1. Diet

Mice were fed with a standard diet (Harlan Teklad; Harlan Ibérica, #2014) in all experimental procedures, except during the induction of obesity done in SF1 neurons experiments. In this case, 3-months-old mice were exposed to normal chow diet (NCD) [International Products Supplies Limited (IPS), TestDiet, #58Y2] or HFD (IPS, TestDiet, #58Y1). The composition of NCD is 10% of energy come from fat, 18% from protein and 72% from carbohydrates, while the composition of HFD is 60% of energy come from fat, 18% from protein and 22% from carbohydrates. Animals were fed with NCD or HFD for 10 weeks until the sacrifice.

3.2. Adeno-associated viral production

Adeno-associated viruses (AVVs) are small (20 nm) replication-defective, non-enveloped viruses with linear, single-stranded genome of 4.7 Kb that belong to the family *Parvoviridae*. AVVs are not currently known to cause human health problems. In fact, they exhibit a low capacity to induce immune response. AVVs has the advantage to infect both dividing and quiescent cells and persist in an extrachromosomal state without integrating into the genome of the host cell. These features have made AVVs as attractive candidates for gene therapy. Until now, 11th AVV serotypes are described according to their capsid proteins. Each serotype can infect cells from multiple tissue types. The AVV serotype used in this work was the serotype 9 because it shows the highest infection rate and expression in neuronal cells (257).

Plasmid design and viral production were done by the Viral Vector Production Unit (UPV) from the Universitat Autónoma de Barcelona (Bellaterra, Barcelona). Briefly, four vectors were used to obtain AVV constructions: (1) AVV9-CMV-mCherry (*Figure 11A*), (2) AVV9-CMV-internal ribosome entry site (IRES)-mCherry (*Figure 11B*) and the final plasmids (3) AVV9-SF1-mCherry (*Figure 11C*) for the control group and (4) AVV9-SF1-IRES-mCherry (*Figure 11D*) for the experimental group.

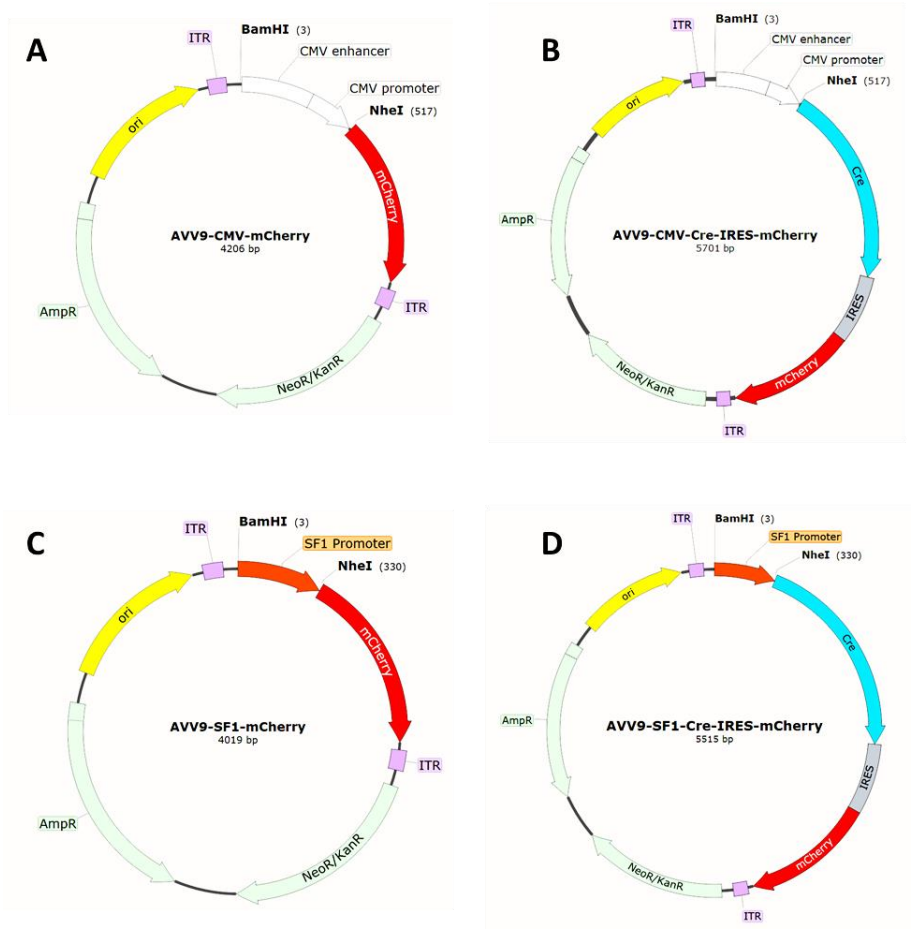

Figure 11. Plasmids utilised for the recombinant AVVs construction. **(A)** AVV9-CMV-mCherry plasmid map (4.206 bp). **(B)** AVV9-CMV-Cre-IRES-mCherry plasmid map (5.701 bp). **(C)** AVV9-SF1-mCherry plasmid map (4.019 bp). **(D)** AVV9-SF1-Cre-IRES-mCherry plasmid map (5.515 bp). Using the skeleton of plasmids,A and B, the UPV designed specific-vectors under the control of SF1 promoter. Each construction contains two inverted terminal repeat (ITR) sequences, a multicloning site flanked the promoter region, two resistance genes for bacterial selection and the fluorescent mCherry protein. The features shown in the figure are: CMV enhancer and promoter; IRES; mCherry; ITR; NeoR/KanR; neomycin and kanamycin resistance gene; AmpR, ampicillin resistance gene; ori, origin of replication; *Cre*; SF1 promoter; and two restriction sites for *BamHI* and *NheI* flanked the promoter region. Plasmid construction and design was performed using SnapGene software (Version 6.0.5).

The difference between C and D plasmids is the presence of *Cre* recombinase gene that it is necessary for the specific deletion of *Cpt1a* in SF1 neurons. The strategy used to generate C and D constructions was the replacement of the CMV promoter and the insertion of SF1 promoter through the enzymatic digestion with two restriction enzymes: *BamHI* (New England BioLabs,

#R0136S) and *NheI* (New England BioLabs, #R3131S). SF1 promoter is a DNA fragment of 706 bp that contains potential sites of regulatory elements that directly modulate the expression of *Sf1* gene [CCAAT box, GA rich region, E box and several specificity proteins (Sp) 1 and Sp3 sites], but it does not contain a recognisable TATA box (*Figure 12*). Due to the limited AVVs genome size, only the functional part of SF1 promoter (basal promoter) was used to the development of AVVs.

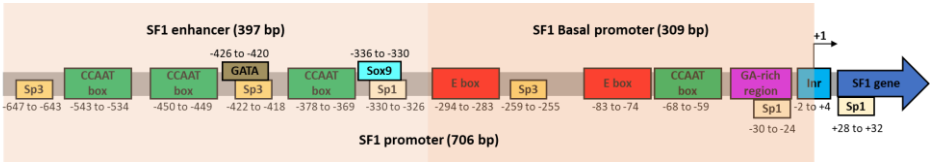

Figure 12. Cis-regulatory elements of SF1 promoter. SF1 promoter size is 706 bp and it is divided in (1) a basal promoter region (309 bp) and (2) an enhancer region (397 bp). SF1 promoter region contains the three necessary regulatory elements for a correct transcription: the E-box (-83 to -74), the CCAAT box (-68 to -59) and the Sp1 site (-30 to -24). SF1 enhancer region includes more regulatory sequences (CCAAT boxes and GATA, Sox9, Sp1 and Sp3 sites), where transcriptional factors can interact to it, modulating the transcription efficiency of the *Sf1* gene.

Recombinant AVVs were produced by triple transfection of $2{\cdot}10^8$ HEK293 cells with 250 µg of AVV plasmid designed, 250 µg of RepCap plasmid, that contains gene sequences for AAV replication paired with capsid proteins, and 500 µg of a helper adenovirus mixed with polyethyleneimine (Sigma-Aldrich, #408727). 48h after transfection, cells were harvested by centrifugation (1.000 rpm, 10 min), resuspended in 30 ml of lysis buffer (20 mM sodium chloride (NaCl), 2 mM magnesium chloride ($MgCl_2$) and 50 mM tris(hydroxymethyl)aminomethane-hydrochloric acid (Tris-HCl), pH 8.5) and lysed by three freeze-thaw cycles. Cell lysate was clarified by centrifugation (10.000 rpm, 10 min) and AVV particles were purified from the supernatant by iodixanol gradient. AVVs were quantified by Quant-iT PicoGreen dsDNA reagent (Invitrogen, #P7589) (258). AVV titers were $1.64{\cdot}10^{13}$ gc/ml for AVV9-SF1-mCherry and $1.10{\cdot}10^{13}$ gc/ml for AVV9-SF1-IRES-mCherry.

3.3. Experimental procedures on mice

3.3.1. Mice genotyping

The identification and the genotype of each animal was done following an ear code using a scissor punch (Fisherbrand, #13-820-063) to generate the different combinations (R, right; L, left; RL, right and left; 2R; 2L; 2RL; …). Ears' punches were carefully collected in 600 µl tubes (Fisherbrand, #11916955) and genomic DNA (gDNA) was extracted, as described in the following section 3.5.1.1. To confirm the genotype of each mouse, a polymerase chain reaction (PCR) was performed using the gDNA as a template (section 3.5.1.2).

3.3.2. Induction of Cre-*LoxP* system

To achieve the specific deletion of *Cpt1a* in AgRP neurons, the technology of the Cre-*LoxP* system was executed. To induce the expression of *Cre* recombinase gene, tamoxifen (Sigma, #C8267) was administered by intraperitoneal injection (*ip*). A 20 mg/ml stock solution was prepared by dissolving 100 mg of TMX in 5 ml of corn oil (Sigma, #C8267) pre-heated at 42ºC for 30 minutes. The solution was placed on a shaker (Incubator Shaker, #ExcellaE25) at 37ºC O/N protected from the light and then, TMX solution was stored at 4ºC.

8-weeks-old mice received five *ip* injections of 150 mg/kg mice weight distributed during a week. The first two doses were coupled with a 24h-food deprivation to enhance AgRP promoter activity. The last three injections were daily administered with *ad libitum* access to food and water.

3.3.3. Stereotaxis

Mouse stereotaxic instrument is an ideal tool for understanding the molecular and neural basis of behaviour and metabolism. This technology allows the administration of viruses or compounds in a site-specific brain region with a

high precision. In our studies, mouse stereotaxis was used to the administration of the recombinant AVVs (*Figure 13*).

8-weeks-old mice were anesthetised with a solution of 100 mg/kg ketamine (Richter Pharma Ag., #580393.7) and 10 mg/kg xylazine (Bayer, #580393.7). Then, they were placed in the stereotaxis instrument (Kopf instrument, #Model 900) on a heating blanket (Medisana, #CT8625) to protect them from hypothermia during the surgery and recovery. Once the mouse head was held in the device, a sagittal incision was made through the skin along the midline of the head. A hole was drilled on the skull and 500 nl of solution containing either AVV9-SF1-Cre-IRES-mCherry or AVV9-SF1-mCherry was injected using a 5 µl Hamilton Neuros syringe Model 75 RN (Hamilton, #12831293) and a Legato 130 syringe pump (KDScientific, #788130) during 8 minutes at a flux of 62.5 nl/min. After the injection, Hamilton syringe was maintained inside the skull to minimise the viral return by surface tension. The stereotaxic coordinates for the VMN are -1.7 mm posterior, -5.5 mm ventral and ±0.4 mm lateral from bregma. The injection was done in both sides of the VMN.

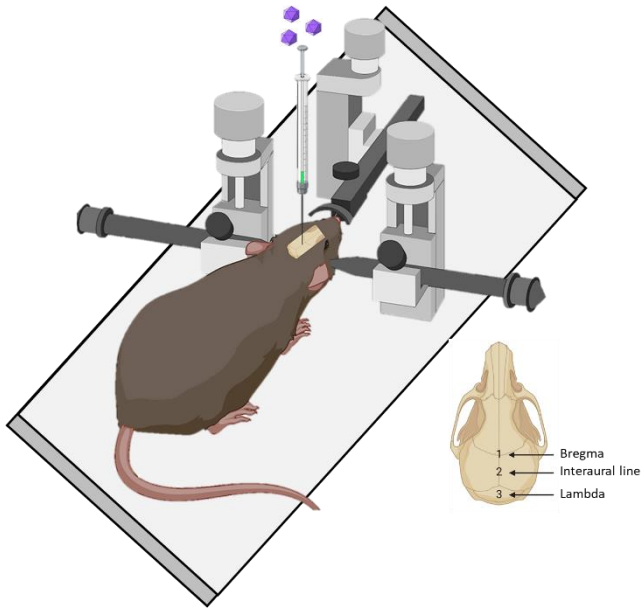

Figure 13. Scheme of stereotaxis in mouse. 8-weeks-old mice were fixed on the stereotaxic instrument to perform AVVs injections in the ventromedial hypothalamus. Bregma, interaural line and lambda were the different brain guide points used to perform the stereotaxis.

Once the procedure was finished, a super glue tissue (3M Vetbond, #1469SB) was used to close the incision. Animals were treated with 0.1 mg/kg buprenorphine (Indivior, #679588) by subcutaneous (*sc*) injections three times per day for one week as analgesic agent. In addition, daily monitoring was performed to analyse the health state of animals for three weeks.

3.3.4. Body weight and food intake control

Mice body weight of SF1 neurons experiments was monitored weekly until the sacrifice using a high precision electronic balance (Mettler Toledo, #ME54) in SF1 neurons experiments. Food intake was also monitored weekly. The initial amount of pellet was weighed at the beginning of every week using the same precision balance. Next week, remaining pellets were measured again, and new food was added up to the same amount given the previous week.

3.3.5. Fast and refeeding satiety test

Mice were housed in individual cages 2 days prior to the beginning of the experiment. In SF1 experiments, 5-months-old mice were fasted O/N and refeed with a pre-weighed meal. In AgRP physical experiments, 5-months-old mice were 6h-fasted and, some of them, were carried a treadmill training 2h before the feeding measurements (the protocol is described in section 3.3.10), while others stay fasted in the home cage. In both experiments, food intake was measured at 30 minutes, 1h, 2h, 3h and 4h after refeeding. All measurements were done using the same electronic balance.

3.3.6. Glucose analysis

Glucose levels were measured from blood samples obtained from the tail vein after O/N fasted of 3 and 4-months-old mice for SF1 experiments. In AgRP studies, 5-months-old mice were 6h-fasted with or without a single bout of exercise on a treadmill, as described in the following section 3.3.10. Fasting blood glucose

levels were measured using a hand glucometer (Bayer Contour XT, #83415194) and its test strips (Bayer Contour XT, #84191389).

3.3.7. Analysis of the BAT thermogenic activity

Mice heat production was visualised through the high-resolution infrared camera FLIR T420 (FLIR Systems AB, #62111777). The previous day, animals were anesthetised by 4% (v/v) isoflurane inhalation (Piramal Healthcare, #60307-120-25) to be shaved in the interscapular area to minimise interferences in the measurements. Mice were O/N fasted and, next day, three images of the interscapular region were taken for each mouse. Thermal data were analysed using the FLIR Tools software (Version 6.0) and adjusted by the temperature of the animal facility room and the reflected temperature (measured using an aluminium foil). The average of the corrected BAT interscapular temperature was represented in figures. These experiments were done in 14 and 18-weeks-old mice.

3.3.8. Physical and behaviour tests

Physical and behaviour tests performed in this project were done in 4-months-old mice for exercise studies and in 20-months-old mice for aging experiments.

3.3.8.1. Treadmill exhaustion test

The treadmill exhaustion test analyses endurance capacity in rodents. A difference of wheel-running activity, treadmill test does not rely upon voluntary activity. In addition, an electrified metal grid located at the bottom of treadmill forces animals to run to avoid electrical shocks. Therefore, mice are motivated to run until they are incapable of or unwilling to continue running. The test ends when mice meet the criterion for exhaustion, defined as spending five consecutive seconds on the shock grid and falling to continue running (259).

Prior the test, animals were trained three days before the exhaustion test in the treadmill Exer 3/6 (Columbus, #1050). During training, mice were acquainted with the apparatus and the electric grid. The angle of inclination of treadmill was 10º, and the intensity and frequency of the electric grid was 1.22 mA, 2Hz (*Figure 14A*). Training protocol consists in two steps: (1) Exploration time (3 minutes), where animals were free to explore the treadmill lane and the shock grid; and (2) experimental time (12 minutes), where treadmill started to work increasing the speed every 2 min. The first day of training, mice were started to run at 8m/min up to 12m/min. On the second day of training, speed was increased from 10m/min to 14m/min. On the third day of training, speed was raised from 12m/min to 16m/min. After the training phase, mice were rested one full day with no exposure to treadmill activity and, next day, they performed the treadmill exhaustion test.

In this test, mice were placed individually in the different lanes of the treadmill, and, after 5 minutes of rest, treadmill started to work following this protocol: 30 min at 10m/min, 10 min at 11m/min, 10 min at 12m/min, 10 min at 13m/min, 5 min at 14m/min and, until this point, speed was increased 1m/min every 5 minutes until exhaustion. When animals became to fatigue, they were returned to their home cages and treadmill was cleaned with 70% (v/v) ethanol (Merck Millipore, #1070172511). The total distance running, and the time spent on the treadmill are the parameters measured to analyse endurance capacity.

3.3.8.2. Open Field test

The Open Field test (OFT) is a common test used to measure locomotor activity, exploration capacity and anxiety in rodents (260). Prior the test, mice got used to the smell and handling of the manipulator to avoid changes in their behaviour. To achieve that, at least one week before the OFT, the manipulator must stay handling mice for 10 minutes every day.

Mice were placed at the centre of a white polywood box (50x50x25 cm) in which the floor was divided into two areas defined as centre and peripheral zones

(15 cm between centre area and the wall) and allowed to explore the box 10 minutes (*Figure 14B*). Mouse exploration was recorded by a camera located above the structure. Locomotion and behaviour were analysed using the SMART software (Version 3.0). After the trial, mice were returned to their home cages and the apparatus was cleaned with 70% ethanol. The parameters scored included the total distance travelled, the time spent in the centre area, and the number of entries in the centre zone, the number of grooms, rearings, defecation and urination that mice did during the test.

3.3.8.3. Elevated Plus Maze test

The Elevated Plus Maze (EPM) test is a widely used behavioural assay for rodents that it has been validated to define brain regions and mechanisms underlying anxiety-related behaviour (261). According to the OFT, mice got used to the smell and handling of the manipulator to avoid changes in their behaviour. The same acclimatation protocol described in 3.3.8.2 was followed.

In the EPM test, mice were placed at the junction of the four arms of the white structure that it is composed by two open arms without walls and two arms enclosed by 15 cm high walls. The dimensions of the arms were 15x30x5 cm and the structure is located 40 cm from the floor to prevent mice from escaping (*Figure 14C*). Mouse behaviour was recorded by a camera situated above the structure for 5 minutes, and data was analysed using the SMART software (Version 3.0). After the trial, animals were returned to their home cages and the apparatus was cleaned with 70% ethanol. The parameters scored included the total distance travelled, the time spent in the open arms and the number of grooms, rearings, urine and faecal boil that mice did during the test.

3.3.8.4. Rotarod test

Motor coordination was assessed in mice by the rotarod test following the protocol described by Deacon (262). Briefly, animals were placed on a horizontal

rod that rotated about its long axis. Mice must walk forward the rod to remain upright and not fall off. In this test, mice must acclimate to the room and the operation of the machine 30 minutes before the experimental trial.

Holding mice by the tail, animals were placed on the rotating rod (Columbus Instruments, #08915M), facing away from the direction of rotation. The rod is 3 cm diameter, supported 25 cm above the base of the apparatus (*Figure 14D*). The surface of the rod is knurled in a series of parallel ridges along the longitudinal axis, enabling mice to grip it effectively. At ten seconds after placing mice on the rod, the engine started to work from 4 rpm and speed was increased 1 rpm every 8 seconds until 40 rpm. The time spent on the rod is measured because it is correlated with motor coordination. Three continuous trials were performed by each animal with 5 minutes of rest between trials, and the best time was used for data analysis.

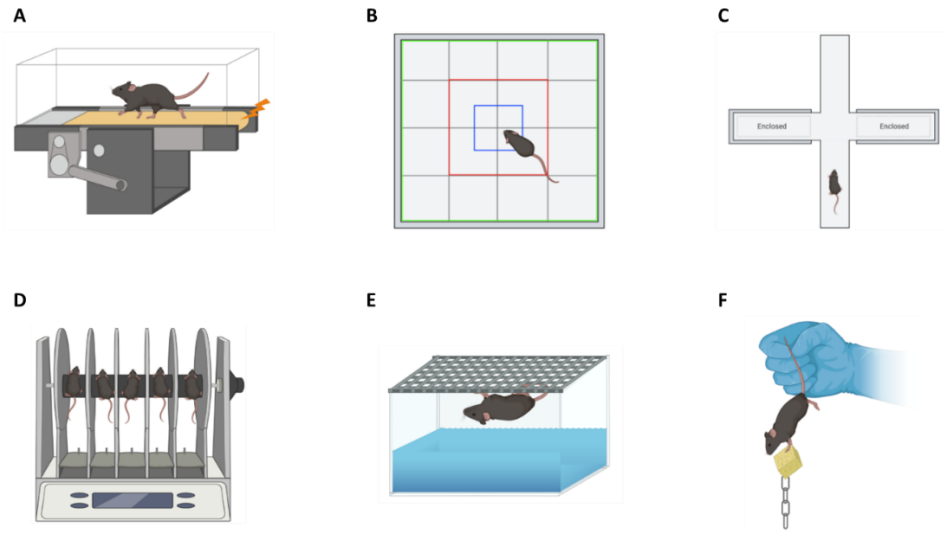

Figure 14. Scheme of different physical and behavioural tests. **(A)** Treadmill is used to perform the endurance exhaustion test. **(B)** Field and sections of the OFT. **(C)** Elevated Plus Maze structure with enclose and open arms. **(D)** Rotarod apparatus. **(E)** Inverted screen structure. **(F)** Mouse lifting weight in the weights test.

3.3.8.5. Strength tests

To assess muscle strength, two test were performed in mice: Kondziela's inverted screen (*Figure 14E*) and weights test (*Figure14F*). The material for each strength test was designed by our lab team (*Figure 15*).

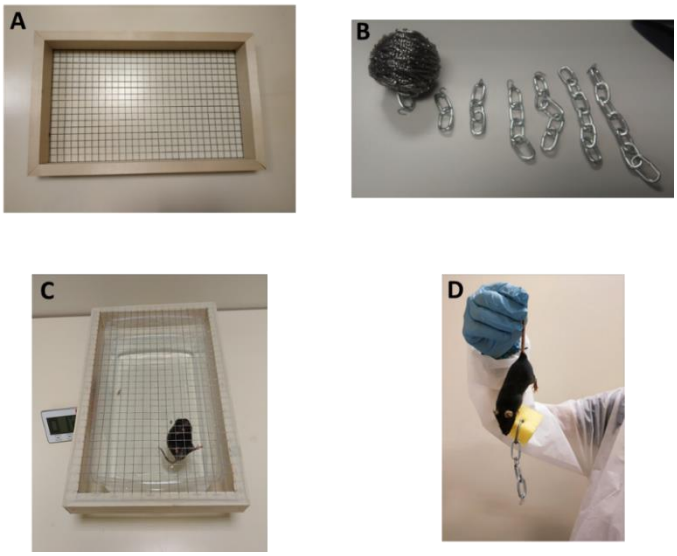

Figure 15. Images of the material used for strength tests. (A) The rectangular inverted screen of wire mesh for the Kondziela's inverted screen test. **(B)** The seven weights used in the weights test. **(C-D)** Mice performance in Kondziela's inverted screen test **(C)** and weights test **(D)**.

The inverted screen is a 15x10 cm rectangle of wire mesh surrounded by a 3 cm deep wooden which prevents occasional mouse attempts to climbing on the other side. This structure was designed to fit correctly with the experimental cage which is 25% filled with pre-heated water. The weights test consists of seven weights with different weight (8.2 g, 14.6 g, 24 g, 36.5 g, 51.2 g, 70.6 g, and 92.4 g). Each of them contained a sponge ball linked to a collector where a series of steel chain links were attached. In both tests, mice had to acclimate to the experimental room 20 minutes before testing to ensure that they were properly awake.

In the Kondziela's inverted screen test, mice were placed in the centre of the wire mesh screen and screen was rotated to an inverted position with mice heads

declining first. The screen was hold over the water cage and the time achieved until falling into the water is measured. Two continuous trials were performed by each animal with 20 minutes of rest between trials. The results obtained were analysed following the score described in the *Table 5* (263) or through the holding impulse taking into account the gravity force and mouse body weight.

Table 5. Score list of the Kondziela's inverted screen test.

	Score
1-60 sec	1
61-90 sec	2
91-120 sec	3
121-150 sec	4
151-180 sec	5
181-210 sec	6
211-240 sec	7
241-270 sec	8
271-300 sec	9
Falling more than 300 sec	10

In the weights test, mice were held by the middle base of the tail and allow them to grasp the sponge with a weight which was lying on the laboratory bench. The time was started when the last link was clear of the bench. A hold of three seconds was the criterion followed.

- If the mouse was dropped the weight in less than 3s, the mouse was rested for 1 minute and tried it on the weight once again. If the mouse failed three times, the trial was ends. The maximum time/weight achieved is assigned to each mouse.
- If the mouse held the weight for 3 s, the mouse rested for 1 minute and then, it was tried on the next heaviest weight until it failed.

The final score was calculated as the product of the number of links in the heaviest chain held for the full 3s, multiplied by the time (in seconds) that it was held. If the heaviest weight was dropped before 3s, the time held was added to its score.

3.3.9. Cognition tests

Cognition tests were performed in 4-months-old mice for exercise studies and in 20-months-old mice for aging experiments. In these tests, hippocampal activity related with memory was assessed.

3.3.9.1. Object Location test

The object location test (OLT) is a well-established test based on the spontaneous tendency of rodents to spend more time exploring a novel object location than a familiar object location, as well as to recognise when an object has been relocated (264,265). The main brain region involved in this task is the hippocampus.

The test was carried out for 3 days in a wooden box (50x50x25), the same as the OFT, but in this case one of the three walls was black (*Figure 16*). The first day of training, mice were habituated to the empty open field arena for 10 minutes. The second day, two objects (A) were placed in front of the black wall, equidistant from each other and the wall. The objects used were identical and 10-cm high. Animals were placed into the open field arena and allowed to explore both objects for 10 minutes. On the third day, one object was moved in front of the white wall to test the spatial memory (A'). Trials were recorded using a camera located above the open field arena and the total exploration time was determined by scoring the amount of time (in seconds) spent sniffing the object in the new location (A') and the object in the old location (A).

The cognitive performance was expressed using the discrimination index (DI), which is defined as (time that mice spent in A'-time spent in A)/ (time that mice spent in A'+ time spent in A). A value of DI of zero indicates that mice spend the same investigation time to both objects without any preference. After each training

day and testing, animals were returned to their home cages, and the open field arena, and the objects were cleaned with 70% ethanol.

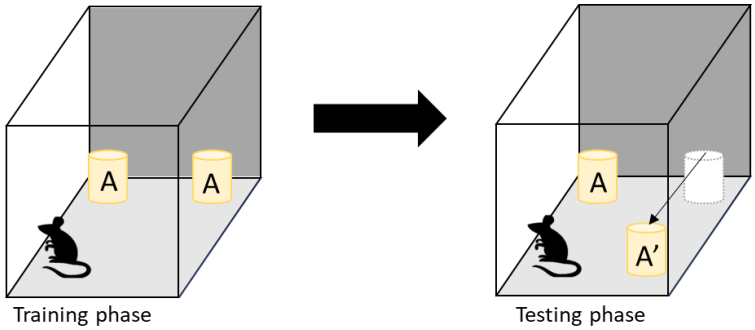

Figure 16. Scheme of the object location test. After two days of habituation to the open field arena and the two objects (A), one of them was moved to a novel location (A'). Spatial memory is analysed in this test.

3.3.9.2. Novel Object Recognition test

The novel object recognition test (NORT) allows evaluating short- and long-term recognition memory involving several brain regions, not only the hippocampus. It is based on the natural tendency of rodents to investigate new objects more than familiar objects (266).

The experimental apparatus used for the test was a 90º angle-two-arms of black polyvinyl chloride. The dimensions of this structure were 25x20x5 to facilitate the cleaning with 70% ethanol to prevent olfactory cues (*Figure 17*). The objects used were around 10-cm high and not frightened for mice. Before the test, mice were individually habituated to the apparatus for 10 minutes for 3 days. The fourth day, animals were allowed to explore freely for 10 minutes (Trial 1), where two identical objects (A) were placed at the end of each arm. Mice were removed from the two-arms structure and returned to their home cage. Two hours later, a 10-minute retention test (Trial 2) was performed. During this second trial, one of the previous objects (A) was replaced by a novel object with different colour and shape (B). Twenty-four hours later, mice were tested again with one of the previous objects (A) and a new object with different colour and shape (C) (Trial 3).

Trials were recorded using a camera located above the apparatus and the time that mice explored the novel object (B or C) and the time that mice explored the familiar object (A) were measured. The criterion of object exploration was defined as pointing the nose towards the object at a distance ≤2 cm and/or touching the object with the nose. Turning or sitting around the object was not considered exploration. To avoid object preferences biases objects A, B AND c were counterbalanced, so one third of animals were exposed to object A, one third of mice were exposed to object B, and the other third part was exposed to object C. The evaluation of the recognition memory was measured by the DI, which is defined as (time that mice spent in B/C–time spent in A)/(time that mice spent in B/C+ time spent in A).

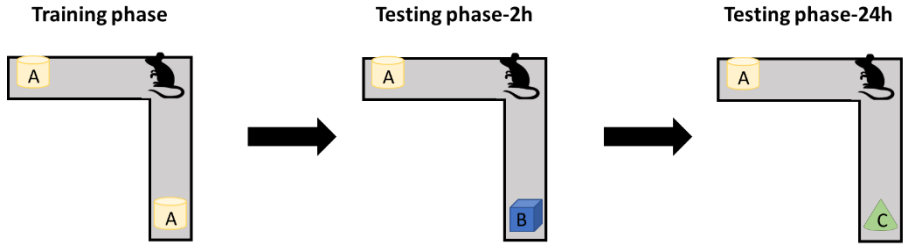

Figure 17. Scheme of the novel object recognition test. After three days of acclimation to the apparatus and the objects (A), one of them was replaced by a new object with different shape and colour (B) at 2h, and by another new object (C) at 24h. Recognition memory at 2 and 24h was analysed in this test.

3.3.10. Sacrifice procedures for mice

For the gene expression, protein content, blood metabolites and histological morphology of different tissues, animals were 2h-fasted, anaesthetised with 4% isoflurane and maintained by continuous inhalation of 2% isoflurane using a calibrated anaesthetic delivery machine (Combi-Vet Rothacher Medical, #45GMB). Quickly, blood samples were collected in heparinised tubes (Fibrilin, #0318) from the facial vein. Blood was centrifuged at 5,000 rpm at 4ºC for 15 minutes (Eppendorf Centrifuge, #5415R). The plasma supernatant was transferred to a 600 µl tube and frozen at -20ºC until measurement. Gastrocnemius (GAS), tibialis anterior (TA), quadriceps (QUA), extensor-digitorum longus (EDL), soleus (SOL),

hippocampus, hypothalamus, brown adipose tissue (BAT), subcutaneous white adipose tissue (sWAT), gonadal white adipose tissue (gWAT), liver and heart were collected and immediately stored at -80ºC until processing.

For AgRP and SF1 studies related to physical activity, a specific-sacrifice protocol in a treadmill was performed (267). Mice were subjected to a single bout of exercise in a 10º angle-treadmill before the sacrifice. Animals were habituated to the running lane and the electric grid for two days, where they performed the following running protocol: the initial speed was 10m/min and it increased 1m/min every 2 minutes until 14m/min. The experimental day, mice were run at 14m/min for 2 hours while the sedentary group remained fasted in their home cages. Blood and tissues were extracted following the general sacrifice protocol.

To obtain VMN samples, the whole-brain was collected and placed in a mouse brain matrix (Biogen, #RWD-68707) to obtain 3mm coronal sections. Once the cut was done, the section was extracted and dissected with a crosswise cut from the third ventricle to the base of the hypothalamus. Tissue samples were stored at -80ºC until their processing.

For brain immunofluorescent analysis, a 4% paraformaldehyde (PFA) pH 7.4 (Sigma-Aldrich, #158127) perfusion of the whole-animal is necessary. In this case, mice were deeply anesthetised with a solution of ketamine-xylazine. Mice were dissected and a 25-gauge blunt needle (Microlance, #613-0902) connected to a perfusion pump (Gilson, #Miniplus3pump) was inserted in the left ventricle. The perfusion process started with the injection of 75 ml of cold 1X phosphate-buffered saline (PBS) to remove blood and, after the injection the right atrium was cut to open the circulation cycle. The cold PBS was replaced by approximately 50 ml of 4% (w/v) PFA until complete animal fixation. Brains were extracted and post-fixated in 4% PFA at 4ºC for 4h. Then, brains were cryoprotected by immersion in 30% (w/v) sucrose (Panreach Applichem, #131621) solution until they sank. Brains samples were frozen by placing them into a pre-cooled 2-methylbutane (Acros Organics, #10511754) at -60ºC for 5 minutes and stored at -80ºC until processing.

For muscle immunofluorescence, mice were anesthetised with a solution of ketamine-xylazine and sacrificed by cervical dislocation. TA and GAS muscles were gently recollected and, immediately embedded in embedding molds (SPI Supplies, #2449M-AB) covered with a minimum amount of Tissue-Tek optimum cutting temperature reagent (Tissue-Tek O.C.T) (Tissue-Tek, #4583) (268). Embedded muscles were frozen by placing them into a pre-cooled 2-methylbutane solution for 5 minutes and then, muscle samples were transferred to a -80ºC for storage.

3.4. Cell culture

3.4.1. Mouse primary hypothalamic neuronal culture

Hypothalamic neurons primary culture was done in 12-weeks-old male *ZsGreen* mice after 1 month of the TMX induction. Animals were euthanised using a CO_2 chamber and cervical dislocation for subsequently hypothalamus extraction.

Once the dissection of the hypothalamus was complete, each of them was placed in a 1.5 ml Eppendorf tube with 1 ml of sterile 1X cold PBS in ice. The 1X PBS was removed and the tubes were washed three times with 1X PBS avoiding touching the whole hypothalamus. After that, 1 ml of Tryple Express with red phenol (Gibco, #11558856) was added to each tube and incubated in the water bath at 37ºC for 5 minutes. Tryple Express was removed and the tubes were washed three times with 1X PBS. Next, 1 ml of pre-heated supplemented Neurobasal Medium A (NBA), which composition is described in the *Table 6*, was added and the hypothalamus was homogenised by up and down pipetting until the medium become cloudy and most of the tissue chunks were dispersed. The triturated hypothalamus was left on ice for 5 minutes and 500 µl of the solution was added to a 2 ml of supplemented NBA medium 35 mm tissue culture plate with a 14 mm glass coverslip (MatTek, #P35G-0-14-C) coated with poly-L-Lysine (Sigma-Aldrich, #P4707).

Every three days, media were filtered using a 0.22 µm filter (Merck Millipore, #16497555) and replaced with fresh supplemented NBA media in 1:1 proportion. After approximately 9-10 days, supplemented NBA media were substituted by supplemented NBA media without red phenol (Gibco, #11570426) to avoid fluorescent interferences in the microscopic analysis.

Table 6. Supplemented NBA medium for the growth of adult neuronal primary culture.

	Volume (ml)	Product reference
50X B-27	0.8	Gibco, #175046044
1X Glutamax (2mM)	0.4	Life Technologies, #35050-038
10% Fetal bovine serum (FBS)	4	Gibco, #10270106
5% Normal horse serum (NHS)	2	Sigma-Aldrich, #H1270
1% Penicillin/streptomycin (P/S)	0.4	Gibco, #11548876
NBA medium	40	Gibco, #11540366

3.4.2. Cell lines

Immortalised murine hypothalamic cell lines of female (mHypoE-41) and male (mHypoE-46) embryonic mice were kindly provided by Dra. Denise Belsham from the University of Toronto (Toronto, Canada). Both cell lines were cultured in high glucose (1000 mg/L) Dulbecco's Modified Eagle's Medium (DMEM) (Sigma-Aldrich, #D5796) supplemented with 5% (v/v) FBS (Gibco, #11573397) and 1% (v/v) P/S (Gibco, #11548876). All cells were maintained in 5% CO_2 at 37ºC. Cells were grown in 60 mm pre-coated tissue culture plates (Sarstedt, #83.1801) for experiments and 100 mm pre-coated tissue culture plates (Corning, #CLS430167) to maintain cells stock.

3.4.2.1. Cell culture maintenance

To growth hypothalamic cells from a frozen vial, cells were placed in a 37ºC incubator to thaw them quickly. The dimethyl sulfoxide (DMSO) (Sigma, #D2438) present in the freezing medium was removed by centrifuging at 1.000 rpm for 5

minutes in a 15 ml tube (Corning, # 11765075) with a 5 ml of growth medium (GrantBio, #LMC3000). After the centrifugation, the medium was aspirated, and cells were resuspended in 2 ml of growth medium. Cell media were changed every three days or upon reaching 90-100% of cell confluency.

To make a cell passage, cell media were removed, and cells were washed twice with 1X PBS (Gibco, # 10728775). 1X PBS was aspirated and 1 ml of 1X trypsin-ethylenediaminetetraacetic acid (EDTA) with red phenol (Gibco, #11590626) was added to the plate and incubate 1-2 minutes at 37ºC. Next, 9 ml of supplemented NBA medium was added, and a 1.000 rpm centrifugation for 5 minutes was done to remove trypsin-EDTA. Finally, medium was aspirated, and cells were resuspended in the culture plates at a desired dilution.

To freeze hypothalamic cells for long storage, a freezing medium is required: high glucose DMEM supplemented with 10% FBS, 1% P/S and 10% (v/v) DMSO. Cells were trypsinised and, after the incubation, resuspended in 9 ml of growth medium in a 15 ml tube. Hypothalamic cells were centrifuged at 1.000 rpm for 5 minutes. The pellet of cells was resuspended in 17 ml of freezing medium and 1 ml aliquot was added to the cryovials (Corning, #10418571). Cryotubes were stored into a Mr. Frosty (Nalgene, #479-3200) filled with isopropanol (Acros, #12556817) and, immediately, the container was placed in -80ºC O/N. Next day, cells were stored in the liquid nitrogen tank.

3.4.3. miRNA mimic and siRNA assays

3.4.3.1. miRNA mimic and siRNA transfection

Female m-HypoE-41 and male m-HypoE-46 hypothalamic cell lines were grown to 65-75% confluency for 24h-48h miRNA/siRNA transfection in 60 mm tissue culture plates. mirVana miR 6540-5p mimic (ID: 4464084) and miR-6927-5p mimic (ID: 4464066) were purchased from Thermofisher Scientific. siRNA CPT1A (ID: mm.Ri.Cpt1a.13), negative control (NC) (ID: 51-01-14-03) and TYE 563

transfection control (ID: 51-01-20-19) were purchased from Integrated DNA technologies. The sequences of these molecules were described in the *Table 7*.

Table 7. Sequences of miRNAs and siRNA used in this study.

	Sequence (5'→3')
miR-6540-5p	CUAAGGCAGGCAGACUUCAGUG
miR-6927-5p	GUGAGGGGAUCCAGCCCAGGCU
siRNA CPT1A	AUCUGUCCAUUGCAUGUAAAUACCA

Transfection were performed using the Dharmafect 3 transfection reagent (Horizon Discovery, #77T-2003-02) following the manufacturer's protocol. Briefly, 0,25 nM miRNA mimic, siRNA and NC control and 10 nM of transfection control was prepared in 1.5 ml eppendorf tubes (Sudelab, #1002208) up to 250 µl of DMEM-serum and antibiotics free. In parallel, 2.5 µl of DharmaFect 3 transfection reagent was added to a 1.5 ml tube and filled with DMEM-serum and antibiotics free up to 250 µl. Tubes were incubated for 5 minutes at room temperature and then, the volume of both tubes was mixed and incubated for 20 minutes at room temperature. After the incubation, media were removed, washed once with 1X PBS, and replaced with 2 ml of 5% FBS DMEM without antibiotics. The transfection cocktail was added drop by drop into the plate and cells were incubated 24-48h at 37ºC until their recollection.

3.4.3.2. Mitochondrial dynamics studies

To study mitochondrial dynamics, a hypothalamic primary culture from 3-months-old ZsGreen *Cpt1a* KO and ZsGreen control were performed. TMX was administered to 8-weeks-old mice, and the hypothalamus was extracted to generate the neuronal primary cell culture. In this culture, only mitochondria from AgRP neurons were labelled with the ZsGreen fluorescent green protein. Mitochondria fluorescence of hypothalamic neurons from 9-10 days of growth was visualised in the Zeiss LSM 880 confocal microscope (Carl Zeiss, #LSM880) using a 1003 Plan Apo TIRF DIC-oil immersion objective to a total magnification of 63x.

A time-lapse of 5 minutes was recorded using the Zeiss ZEN software (Version 2.3). Mitochondrial speed and displacement were measured using the Plugin Track Mate (269) of Fiji ImageJ software (Version 1.53).

3.5. Molecular biology techniques

The analysis of tissue samples obtained from all mice and cell culture were carried out using molecular biology tools. These techniques allow to understand the biological processes that are taking place in living organisms. In this section, different techniques used in this study are described.

3.5.1. DNA manipulation

3.5.1.1. DNA extraction

Genomic DNA (gDNA) was extracted by the addition of 40 µl of QuickExtract DNA Extraction Solution (Epicenter, #QE09050) to the ears' punches collected in 600 µl tubes during mice genotyping. This reagent allows a quick and efficient gDNA extraction using a simple, one-tube protocol. Briefly, tubes were spined to ensure that ears were covered by the solution, and they were incubated at 65ºC for 6 minutes using the PCR thermocycler FlexCycler (Analytik Jena, #112B). A vigorous vortex (Comecta, #5411000) was applied to the tubes, and they were incubated in the thermocycler at 92ºC for 2 minutes. Samples were kept at 4ºC until processing.

For tissue samples, gDNA purification was performed using the proteinase K method, a broad-spectrum serine protease employed to digest contaminating proteins presented in tissue samples. Samples were incubated in 350 µl of digestion solution [0.25 mg/ml proteinase K (Promega, #17916), 1% (v/v) sodium dodecyl sulphate (SDS, Sigma-Aldrich, #L3771), 150 Mm NaCl (Sigma-Aldrich, #S7653) and EDTA (Acros Organics, #12685017)] at 55ºC for 4 h. Once digested,

10 µl of 10 mg/l RNAse (Sigma-Aldrich, #10109142001) were added into each tube and incubated at 37ºC for1h.

Genomic DNA was extracted by the addition of 350 µl of 100 mM Tris, pH 8.0 (Sigma-Aldrich, #T1378)-phenol (Acros Organics, #AM9720) solution. Tubes were mixed by inversion for 10 minutes and then, they were centrifugated at 14.000 rpm for 15 minutes. The top layer was transferred to a new tube containing 350 µl of phenol:chloroform:isoamyl alcohol (25:24:1) (Merck, #P3803). Tubes were strongly shaken for 10 minutes and centrifuged at 14.000 rpm for 10 minutes. The upper phase was placed to a new tube containing 350 µl of chloroform:isoamyl alcohol (24:1) (Sigma-Aldrich, #C0549) and samples were centrifugated at 14.000 rpm for 10 minutes. At this point, gDNA was isolated, and 350 µl of isopropanol and 15 µl of 5M NaCl were added to the tubes to enable the gDNA precipitation. Samples were vigorously shaken and centrifugated at 14.000 rpm for 15 minutes. The supernatant was removed and 100 µl of 70% EtOH were added to each tube for washing the gDNA pellet. Samples were centrifuged at 14.000 rpm for 10 minutes. The washing step was repeated and then, the gDNA pellet was resuspended in 10 µl of distilled water (dH_2O). gDNA concentrations were quantified by the NanoDrop 1000 Spectrophotometer (Thermo Scientific, #ND-1000). DNA molecules absorbed at wavelengths of 260 nm and the ratios A260/280 and A260/230 ratio were analysed to detect contamination by proteins (absorbance at 280 nm) and EDTA, carbohydrates and phenols (absorbance at 230 nm). Ratios between 1.8 to 2 are generally accepted as good DNA quality. Lower values indicate contamination of different molecules.

For the analysis of mitochondrial DNA (mtDNA) content, 25 mg of frozen gastrocnemius muscle was homogenised in a pre-cooled mortar until getting a powder that it was transferred to a new 1.5 ml tube containing 280 µl of digestion buffer, a solution from the PureLink Genomic DNA Mini Kit (Invitrogen, #1820-01). The manufacturer's guidelines were followed to extract mtDNA. mtDNA samples were quantified using the NanoDrop 1000 Spectrophotometer. A quantitative real-time PCR (qRT-PCR), described in section 3.5.2.4, was performed using a

mitochondrial gene (*Cytc*) normalised by a nuclear gene (succinate dehydrogenase complex flavoprotein subunit A, *Sdha*) for the measurement of mtDNA content in the GAS.

3.5.1.2. Polymerase chain reaction

PCR is a very useful technique to amplify DNA sequences. PCR was performed in a thermocycler FlexCycler in a final volume of 20 µl. 1 µl of extracted gDNA (~200 ng/µl) was mixed with 10 µl of 2X RED-Extract-N-Amp PCR ReadyMix (Sigma-Aldrich, #R4775), a solution that includes all the reagents needed for the PCR amplification [Taq polymerase enzyme, enzyme buffer, magnesium, deoxynucleotide triphosphates (dNTPs) and a loading dye to directly visualised the DNA molecules in a electrophoresis gel], 1 µl of 10 µM forward and reverse primers (*Table 8*) and nuclease-free water (Ambion, #AM9937) up to complete the final volume. PCR conditions were applied depending on the target gene.

For the genotyping of the *Cpt1a* Flox colony, the primers *Cpt1a* Flox forward and reverse were used. PCR conditions for the amplification of *Cpt1a* floxed gene were an initial denaturation (94ºC for 5 minutes) followed by 30 cycles of denaturation (94ºC for 30 sec), annealing (56ºC for 30 sec), extension (72ºC for 1.2 minutes) and a final extension (72ºC for 5 minutes). PCR products for the wild type allele *Cpt1a* was 990 bp, 1.030 bp for the floxed *Cpt1a*, and 219 bp for the recombined floxed *Cpt1a*.

Table 8. List of primers used for mice genotyping.

Oligonucleotides	Sequence (5'→3')
Cpt1a Flox forward	CAGGATCCCTTTGAGCAGCAG
Cpt1a Flox reverse	CAAAGTGGCCCCTAAGGCTAC
AgRP Cre-ER^{T2} forward	CAGATACCATCATCTCTCCC
AgRP Cre-ER^{T2} reverse	CCTTAAACTCGCCCATATATGTGG
AgRP Cre-ER^{T2} control reverse	GCTCTACTTCATCGCATTCCTTG
ZsGreen forward	AAAGTCGCTCTGAGTTGTTATCAG
ZsGreen reverse	GGAGCGGGAGAAATGGATATG
ZsGreen control reverse	TCACTGCATTCTAGTTGTGGTTTG

For the *AgRP-CreER^{T2}* gene, the primers *AgRP Cre-ER^{T2}* forward, reverse and *AgRP Cre-ER^{T2}* control reverse were applied. PCR conditions for the amplification were an initial denaturation (94ºC for 5 minutes), 30 cycles of denaturation (94ºC for 30 sec), annealing (56ºC for 30 sec), extension (72ºC for 30 sec) and a final extension (72ºC for 5 minutes). PCR products for the wild type allele was 514 bp and for the *CreER^{T2}* allele was 323 bp.

The primers ZsGreen forward, reverse and the ZsGreen control reverse were used for the *ZsGreen* amplification. PCR conditions for the amplification were: an initial denaturation (95ºC for 2 minutes), followed by 30 cycles of denaturation (95ºC for 30 sec), annealing (55ºC for 30 sec), extension (72ºC for 40 sec) and a final extension (72ºC for 5 minutes). The amplicon obtained for the wild type allele was 600 bp and for the *ZsGreen* allele was 500 bp.

3.5.1.3. DNA electrophoresis

PCR products were loaded into a 1-2% agarose (w/v) (Labotaq, #E5000) gel in 1X electrophoresis buffer (40 mM Tris-acetate, 1 mM EDTA, TAE) (Fisher Bioreagents, #BP13332-20). To visualise DNA bands, 5 µl of SYBR Safe (Thermo Fisher Scientific, #S33102) was added to the gel. As molecular DNA markers, 5 µl of the Gene Ruler DNA Ladder Mix 1 Kb (Thermo Fisher Scientific, #SM0311) was used for fragments greater than 1.000 bp, and the Gene Ruler DNA Ladder Mix 100 bp (Thermo Fisher Scientific, #SM0241) was performed for small fragments less than 1.000 bp. PCR products and markers were loaded into the gel and the electrophoresis was performed at 80V for 30-60 minutes in a horizontal electrophoresis system SUB-Cell GT Cell (BioRad, #1704401). After this time, gels were visualised in the Gel Doc EZ imaging system (BioRad, #1708271EDU) using the ultraviolet filter.

3.5.1.4. DNA sequencing

To confirm the VMN-specific recombination of the recombined *Cpt1a* allele, gDNA from recombined mice was purified and amplified following the PCR protocol described in the section 3.5.1.2. A PCR amplicon of 219 bp was obtained. The PCR product was visualised in an 2% agarose gel and the band of 219 bp was extracted from the gel to be sequenced. The sequencing was performed using the sequencing kit BigDye Terminator v3.1 Cycle (Applied Biosystems, #4337455). This method is based on the use of fluorescent-labelled-chain-terminating dideoxynucleotides triphosphates to reveal the DNA sequence of a PCR product.

The reaction solution used for each primer (*Cpt1a* Flox forward and reverse) was: 1 µl of Ready BigDye reaction mix, 3 µl of BigDye sequencing buffer, 2 µl of 10 µM primer, 10 µl of VMN gDNA (100 ng), and 4 µl of dH_2O to a final volume of 20 µl. The sequencing reaction was processed at the Genomic Unit from the Centres Científics i Tecnològics de la Universitat de Barcelona (CCiT-UB), and the chromatogram results were analysed using the MEGA7 software (Version 7.2.10).

3.5.2. RNA manipulation

3.5.2.1. Extraction of RNA from cultured cells

RNA extraction from cells was carried out from 60 mm plates. Cells were washed three times with 1X PBS, and 1 ml of Trizol reagent (Sigma-Aldrich, #T9424) was added pipetting up and down to homogenise the content. Cells were detached from the culture plate using a cell scraper (Thermo Fisher, #179707PK) and the homogenised solution was placed in a 1.5 ml tube containing 0.2 ml of chloroform (Biomedicals, #219400291). Solution was vigorously mixed and centrifuged at 12.000 rpm at 4ºC for 15 minutes. The aqueous phase was separated to a new tube containing 0.5 ml of isopropanol and 10 µg of the co-precipitant GlycoBlue (Invitrogen, #10391565). RNA was precipitated by a

centrifugation at 12.000 rpm at 4ºC for 15 minutes. The RNA pellet was washed three times with 75% ethanol and centrifuged at 7.500 rpm at 4ºC for 5 minutes. After the centrifugation, the RNA pellet was dried at room temperature for 10-20 minutes and then, it was eluted in a small volume of RNAse free water (10 to 40 µl, depending on the tissue). RNA samples were heated at 55ºC for 10 minutes in a thermoblock (JP Selecta, #7462200) and quantified by the Nanodrop. Ratios A260/280 and 260/230 were measured. Values between 1.8 to 2.2 are generally accepted as "pure" for RNA. Lower values indicate contamination by proteins, phenols, or carbohydrates.

3.5.2.2. RNA extraction from tissues

Depending on the type of tissue analysed, RNA was extracted by two different methods: (1) the conventional Trizol reagent protocol for non-lipid tissues and (2) the RNeasy Lipid Tissue Mini Kit (Qiagen, #74804) for tissues with a high lipid-content such as the BAT and the WAT.

Previous the RNA isolation, tissues were weighed before RNA isolation. A 30-70 mg of tissue was placed in a 2 ml tube (Fisher Scientific, #11393613) containing 1 ml of Trizol reagent. In high lipid-content tissues, 50-100 mg of tissue was homogenised in 1 ml of QIAzol lysis reagent (Qiagen, #79306). In both protocols, tissues were disrupted using 3.2 mm stainless steel beads (Qiagen, #69997) in the Tissuelyser LT (Qiagen, #85600) at 50-Hz frequency for 5 minutes. Next steps to RNA extraction were accomplished according to the manufacturer's instructions.

3.5.2.3. cDNA synthesis

Purified RNA was retrotranscribed to complementary DNA (cDNA) using the Moloney-murine leukaemia virus (M-MLV) reverse transcriptase (Invitrogen, #10338842) and following the manufacturer's instructions. Briefly, 500 ng of RNA were incubated in a tube with 1 µl of dNTPs mix (10 mM each) (Invitrogen, #16498753), 0.5 µl of 50 µM random hexamers (Applied Biosystems, #10609275)

and 0.5 µl of 50 µM oligo $d(T)_{16}$ (Applied Biosystems, #10187394) at 65ºC for 5 minutes. The content of the tube was collected by a brief centrifugation, and 4 µl of 5X first-strand buffer (Invitrogen, #10338841), 2 µl of 100 mM dithiothreitol (DTT) (Invitrogen, #10338843), and 1 µl of 40U/µl RNAseOUT recombinant ribonuclease inhibitor (Invitrogen, #10154652). The tube was incubated at 37ºC for 2 minutes. Then, 1 µl of 200U/µl of M-MLV reverse transcriptase was added to the tube mixing by pipetting. The solution was incubated in a thermocycler following the cDNA reaction: 25ºC for 10 minutes, 37ºC for 50 minutes and 70ºC for 15 minutes. The cDNA obtained was diluted with RNAse-nuclease free water up to a concentration of 5 ng/µl. Two negative control were included in the reverse transcription reaction: (1) a pool of RNA samples without the M-MLV enzyme and (2) a tube of water with the reverse transcriptase enzyme.

3.5.2.4. Quantitative real-time PCR

Quantitative real-time polymerase chain reaction (qRT-PCR) was performed using the LightCycler 480 Instrument II (Roche, #05015243001) according to the manufacturer's guidelines. Briefly, 2.5 µl of 5 ng/µl cDNA was mixed with 5 µl of 2X SYBR Green PCR Master Mix Reagent Kit (Roche, #4887352001), 0.5 µl of primer mix (forward and reverse primer, 10 µM each) and 2 µl of RNAse-free water. A qRT-PCR negative control without cDNA sample was included. All qRT-PCR reactions were carried out in duplicate on a 384 well plate (Roche, #04729749001). The plate was incubated at 95ºC for 5 minutes, followed by 45 cycles of 95ºC for 15 sec, 60ºC for 10 sec and 72ºC for 10 sec. mRNA levels were normalised using different reference genes depending on the tissue analysed: ribosomal protein L32 (*Rpl32*) for muscle and heart, ribosomal protein L7 (*Rpl7*) for cell culture and hypothalamus, *β-actin* for liver, glyceraldehyde-3-phosphate dehydrogenase (*Gapdh*) for hippocampus, and hypoxanthine phosphoribosyl-transferase 1 (*Hprt1*) for BAT and WAT samples. mRNA levels were expressed as a fold change in comparison to the control group. Primers used in this study are described in the *Table 9*.

Table 9. List of oligonucleotides used in qRT-PCR studies. All primers were provided by Merck.

Primer ID	Forward (5'→3')	Reverse (5'→3')
β-actin	ATGCTCCCCGGGCTGTAT	CATAGGAGTCCTTCTGACCCATTC
Gapdh	ACTCCACTCACGGCAAATTC	TCTCCATGGTGGTGAAGACA
Hprt1	TCCTCCTCAGACCGCTTTT	CCTGGTTCATCATCGCTAATC
Rpl7	TCGCAGAGTTGAAGGTGAAG	GCCTGTACTCCTTGTGATAGTG
Rpl32	GCTGCCATCTGTTTTACGG	TGACTGGTGCCTGATGAACT
Adrb3	ACAGCAGACAGGGACAGAGG	GCGTCCTGTCTTGACACTCC
AgRP	CGGAGGTGCTAGATCCACAGA	AGGACTCGTGCAGCCTTACAC
Arg1	CTCCAAGCCAAAGTCCTTAGAG	AGGAGCTGTCATTAGGGACATC
Atgl	TGACCATCTGCCTTCCAGA	TGTAGGTGGCGCAAGACA
Bcl2	CAGATGCACCTGACGCCCTT	AGGTCCTATTGCCTCCGACCC
Bdnf	AGTCTCCAGGACAGCAAAGC	TGCAACCGAAGTATGAAATAACC
Bnp	GTCAGTCGTTTGGGCTGTAAC	GGAAAGAGACCCAGGCAGA
Cat	GTGCATGCATGACAACCAG	TGAAGCGTTTCACATCTACAGC
Cd36	TGTACCTATACTGTGGCTAAATGAGA	TTGTGTTTTGAACATTTCTGCTT
Ck-heart	GCATCAAGGGTTACACTCTGC	CCCGTCAGGCTGTTGAGA
Cpt1a	GACTCCGCTCGCTCATTC	TCTGCCATCTTGAGTGGTGA
Cpt1b	TGCCTTTACATCGTCTCCAA	GGCTCCAGGGTTCAGAAAGT
Ctsl	GTGGACTGTTCTCACGCTCAAG	TCCGTCCTTCGCTTCATAGG
Cxcl1	AGACTCCAGCCACACTCCAA	TGACAGCGCTCATTG
Cytc	CTACAAGACGCCACAT	GAGAGGGGAGAGCAAT
Ddit3	CCCTGCCTTTCACCTTGG	CCGCTCGTTCTCCTGCTC
Dgat2	GCTGGTGCCCTACTCCAAG	CCAGCTTGGGGACAGTGA
Dio2	CCTTGGTCCCCCACTTCT	GCTTCCCCAGTCACCTTCTT
Drp1	CTGGATCACGGGACAAGG	GTTGCCTGTTGTTGGTTCCT
Fabp3	CTTTGTCGGTACCTGGAAGC	TGGTCATGCTAGCCACCTG
Fas	CAGATGATGACAGGAGATGGAA	CACTCACACCCACCCAGA
Fbxo32	AGTGAGGACCGGCTACTGTG	GATCAAACGCTTGCGAATCT
Gata4	GGAAGACACCCCAATCTCG	CATGGCCCCACAATTGAC
Gdf8	TGGCCATGATGATCTTGCTGTAA	CCTTGACTTCTAAAAAGGGATTCA
Gfap	CCTTCTGACACGGATTTGGT	ACATCGAGATCGCCACCTAC
Gpx1	GTGCTCGGTTTCCCGTG	CCTTCTCACCATTCACTTCGC
Grp78	ACTTGGGGACCACCTATTCCT	ATCGCCAATCAGACGCTCC
Hif1α	AACAGAATGGAACGGAGCAA	TTCACAATCGTAACTGGTCAGC
Hk2	TTTTGCCAAGCGTCTCCATAA	GCCGCTGCCATCCTCAGAGCGGA
Hmox1	CATAGGCGGCCAGGAACATT	TCCTCGTTCCAGAATGCAGC
Hsl	GCGCTGGAGGAGTGTTTTT	CGCTCTCCAGTTGAACCAAG
Igf-1	CAAAAGCAGCCGCTCTA	TCGATAGGGACGGGGACT
Il-1β	GCCCATCCTCTGTGACTCAT	AGGCCACAGGTATTTTGTCG
Il-6	GATGGATGCTACCAAACTG	CCAGGTAGCTATGGTACTCCAGAA
Il-10	GGTTGCCAAGCCTTATCGGA	ACCTGCTCCACTGCCTTGCT
Mbp	CTCAGAGGACAGTGATGTGTT	TGTGCTTGGAGTCTGTCACC
mCherry	TGGTGCGCAAGGGCGAGGA	GTGGCCGTTCACGGAGCC
Mfn2	CATTCTTGTGTCGGAGGAG	AAGGAGAGGGCGATGAGTCT
Murf1	TGACATCTACAAGCAGGAGTGC	TCGTCTTCGTGTTCCTTGC
Musk	TACAGAGGGGAGGTGTGTGA	TCCCGGTAGGAGGTGTTGAA
Myh-1	GAGGGACAGTTCATCGATAGCAA	TGCTAATGCCCTAATGCTAATG
Myh-2	AGGCGGCTGAGGAGCACGTA	GCGGCACAAGCAGCGTTGG

Myh-4	CACCTGGACGATGCTCTCAGA	GCTCTTGCTCGGCCACTCT
Myh-7	CGCATCAAGGAGCTCACC	CTGCAGCCGCAGTAGGTT
Ncam1	CCCAGCCAAGGAGAAATCAG	TGGCGTTGTAGATGGTGAGG
Nos2	CAGCTGGGCTGTACAAACCTT	GCATTGGAAGTGAAGCGTTTC
Npy	CAGAAAACGCCCCCAGAA	AAAGTCGGGAGAACAAGTTTCATT
Nrf2	CAGAAGGAACAGGAGAAGGC	TTTGGGAATGTGGGCAACCT
Opa1	TTCTGAGGCCCTTCTCTTGT	TGACTGTTGCTCGAAATGC
Pdk4	TTTCTCGTCTCTACGCCAAG	GATACACCAGTCATCAGCTTCG
Pepck	GTCAACACCGACCTCCCTTA	CCCTAGCCTGTTCTCTGTGC
Pgc1α	GAAAGGGCCAAACAGAGAGA	GTAAATCACACGGCGCTCTT
Plin2	GAGTCCCACTGTGTTGAGCA	CCAGGACAGTCTGGCATGT
Plin3	GGAGGAACCTGTTGTGCAG	ACCATCCCATACGTGGAACT
Pparα	CACGCATGTGAAGGCTGTAA	CAGCTCCGATCACACTTGTC
Runx1	CTCCGTGCTACCCACTCACT	ATGACGGTGACCAGAGTGC
Runx2	CGTGTCAGCAAAGCTTCTTTT	GGCTCACGTCGCTCATCT
Slc2a1	AGCTTGATCACCTCGTAGGC	TTACAGCGCGTCCGTTCT
Slc2a4	GATGACCGTGGCTCTGCT	GCTCTGCCACAATGAACCA
Socs3	CCTTCAGCTCCAAAAGCGAG	GCTCTCCTGCAGCTTGCG
Sdha	TACTACAGCCCCAAGTCT	TGGACCCATCTTCTATGC
Sod1	CAGGACCTCATTTTAATCCTCAC	CCCAGGTCTCCAACATGC
Tnfα	CTGTAGCCCACGTCGTAGC	TTTGAGATCCATGCCGTTG
Trem2	CCTGAAGAAGCGGAATGGG	CTTGATTCCTGGAGGTGCT
Ucp1	GGCCTCTACGACTCAGTCCA	TAAGCCGGCTGAGATCTTGT
Ucp2	CGGGGCCTCTGGAAAG	CCCAAGCGGAGAAAGGA
Vegf	AAGACAGAACAAAGCCAGAAAA	AGAGGTCTGGTTCCCGAAA

3.5.3. Protein manipulation

3.5.3.1. Protein extraction

Total protein extraction from 50 mg of tissue was performed by the addition of 500 µl of protein extraction buffer [(30 Mm 4-(2-hydroxyethyl)-1-piperazineethnesulfonic acid (HEPES) (Fisher Scientific, #BP310), 150 mM NaCl, 10% (v/v) glycerol (Sigma-Aldrich, #G7757), 1% (v/v) Triton X-100 (Sigma-Aldrich, #T8787), 0.5% (w/v) sodium deoxycholate (Sigma-Aldrich, #30970), Mini protease inhibitor tablet (Roche, #11836153001) and PhosSTOP phosphatase inhibitor tablet (Roche, #04906837001)]. Tissues were disrupted in the Tissuelyser LT at 50-Hz for 5 minutes. Lysates were kept shaking at 4ºC for 20 minutes to solubilise proteins. Next, samples were centrifuged at 13.000 rpm at 4ºC for 15 minutes. Supernatants were carefully collected, and protein samples were stored at -20ºC until their processing.

3.5.3.2. Protein quantification

Protein determination was carried out by the bicinchoninic acid (BCA) method using the Pierce BCA Protein Assay kit (Thermo Scientific, #23225). Protein samples were diluted 1:10 and 10 µl of diluted samples were mixed to 10 µl of dH_2O on a 96-well plate (Greiner bio-one, #655101). To prepare the standard curve, a 2 mg/ml bovine serum albumin (BSA) stock (Fisher Scientific, #V0332) was diluted within a range from 0 to 2 mg/ml (0, 0.2, 0.4, 0.8, 1.6 and 2 mg/ml). The BCA working reagent was prepared by mixing the reagent A and B in a 50:1 proportion, and 200 µl of the working solution was added to each well. Samples were covered with aluminium foil and incubated at 37ºC for 30 minutes. The amount of protein was measured by colorimetry using the microplate reader Varioskan Lux (Thermo Fisher Scientific, #VL001). Both standards and samples were performed in duplicate.

3.5.3.3. Western Blot

Western Blot is an immunodetection technique that allows the detection of a single protein from a mixture of proteins using an antibody that binds specifically to the target protein. This technique is divided into three steps: (1) the electrophoretic separation of proteins, (2) the transference of proteins to a solid support and (3) the immunodetection of interested proteins.

Protein samples were prepared for the electrophoresis migration. Samples were adjusted to a stock concentration of 1 µg/µl by the addition of 6X Loading buffer [375 Mm Tris-HCl pH 6.8, 9% SDS, 50% glycerol (Sigma-Aldrich, #G7757), 0.03% (w/v) bromophenol blue (Sigma-Aldrich, #B5525) and 9% (v/v) β-mercaptoethanol (Sigma-Aldrich, #M6250)] and the proportional volume of dH_2O depending on the amount of protein. Then, proteins were denatured at 95ºC for 5 minutes, and chilled on ice.

Protein electrophoresis was done in a system of SDS-polyacrylamide gels (SDS-PAGE) composed by a stacking gel to concentrate proteins and a separating gel, where negative charged proteins are separated according to their molecular weight. Gels were prepared using 40% (v/v) polyacrylamide (Sigma-Aldrich, #A7802), specific buffers and two polymerising agents [the N-tetramethylenediamine (TEMED) (Sigma-Aldrich, #T9281) and the ammonium persulfate (APS) (Sigma-Aldrich, #A3678)] as described in the *Table 10* and mounted in Criterion Empty Cassettes (BioRad, #3459901).

Table 10. Gel composition for protein electrophoresis.

	Separating gel (10% polyacrylamide)	Stacking gel (5% polyacrylamide)
Tris-HCl 1.5M, pH 8.9, 0.4% SDS	2.5 ml	-
Tris-HCl 0.5M, pH 6.8 0.4% SDS	-	1 ml
40% Polyacrylamide (29:1)	2 ml	0.5 ml
dH_2O	5.4 ml	2.47 ml
TEMED	10 µl	8 µl
10% APS	66.6 µl	27.2 µl

Polymerised gels were covered with running buffer (25 mM Tris-HCl pH 8.8, 192 Mm glycine (Sigma-Aldrich, #G8898) and 0.1% SDS) and 25 µg of denatured proteins were loaded in each well. In addition, 7 µl of Amersham ECL Rainbow Marker- Full range (GE Healthcare, #RPN800E) was loaded as a molecular weight reference into the first well of the gels. Protein electrophoresis was performed using the Criterion Gel Electrophoresis Cell system (BioRad, #1656001). Samples started to migrate at 80V until they exceeded the stacking gel and then, the voltage was raised up to 120V until proteins reached the end of the separating gel.

Proteins in the separating gel were transferred to a 0.45 µm nitrocellulose membrane (BioRad, #1620115) for the later incubation with specifics antibodies. The transference sandwich was composed by the electrophoresis gel and the nitrocellulose membrane surrounded by several same-size pieces of 3 mm Whatman paper (GE Healthcare, #3030) and a sponge (BioRad, #1703933) in both sides. A wet transfer was performed with continuous transfer buffer recirculation

[25 mM Tris-HCl pH 8.5, 190 mM glycine, 0.2% SDS and 20% Methanol (v/v) (Fisher Chemical, #10010240)] using the Criterion Blotter with wire electrodes (BioRad, #1704071) at 250 mA at 4ºC for 120 minutes.

Once the transference was achieved, the membrane was washed three times with 1X washing buffer [10 Mm Tris-HCl Ph 7.4, 150 mM NaCl, 0.1% (v/v) Tween 20 (Sigma-Aldrich, #P1379)]. Then, the membrane was blocked in a solution containing 5% (w/v) non-fat milk (ChemCruz, #SC2325) diluted in 1X washing buffer at room temperature for 1h in the orbital shaker Polymax 1040 (Heuldolph, #SP1040). Then, the membrane was washed three times with washing buffer for 5 minutes.

Blocked nitrocellulose membrane was incubated at 4ºC O/N in constant stirring with the specific primary antibody diluted in 5% (w/v) BSA in 1X washing buffer. The final dilution and primary antibodies used in this project are listed with *Table 11*. 24-h after the incubation, the membrane was washed three times in the washing buffer for 5 minutes and incubated with the secondary antibody at room temperature for 2h in an orbital shaker. Secondary antibodies were diluted in 5% BSA in 1X washing buffer. The final dilution and secondary antibodies used in this work are described in the *Table 12*. Then, the membrane was washed three times with 1X washing buffer for 5 minutes.

Table 11. List of primary antibodies used in the Western Blot.

Antibodies	Dilution	Source
Anti-mouse GAPDH	1:2000	Abcam, #ab8245
Anti-mouse pAKT	1:1000	Cell Signaling, #9272
Anti- rabbit AKT	1:1000	Cell Signaling, #4051S
Anti-rabbit pAMPK (Thr^{172})	1:1000	Cell Sigaling, #2531S
Anti-rabbit AMPK	1:1000	Cell Signaling, #2532S
Anti-rabbit CPT1B	1:1000	Proteintech, #22170-1-AP
Anti-rabbit pCREB (Ser^{133})	1:1000	Cell Signaling, #9198
Anti-rabbit CREB	1:1000	Cell Signaling, #4820
Anti-rabbit PSD95	1:1000	Abcam, #ab18258
Anti-rabbit TH	1:1000	Genetex, #gtx113016
Anti-rabbit UCP2	1:1000	Cell Signaling, #89326

The immunodetection was performed by enhanced chemiluminescence (ECL). The membrane was incubated with 5 ml of Pierce ECL Western Blotting substrate (Thermo Scientific, #32106) for 5 minutes. Protein detection was analysed using the Image Quant LAS 4000 Mini (GE Healthcare, #LAS4000). Images were quantified with the Image J software (Version 1.8.0).

Table 12. List of secondary antibodies used in the Western Blot.

Antibodies	Dilution	Source
Sheep anti-mouse, HRP-conjugated	1:1000	Abcam, #ab8245
Goat anti-rabbit IgG, HRP-conjugated	1:1000	Cell Signaling, #9272

HPR: horseradish peroxidase

3.5.4. Plasma analysis

Several metabolites were measured from mice plasma samples. Cortisone levels were measured using the mouse cortisone ELISA kit (Reagent Genie, #MOEB2565). Catecholamines plasma levels were analysed by the epinephrine-norepinephrine ELISA kit (ImmuSmol, #BAE5400). The aging biomarker Igf-1 was measured by the mouse/rat Igf-1 Quantikine ELISA kit (R&D System, #MG1000). The three kits were performed following the manufacturer's guidelines.

3.6. Histological analysis

3.6.1. Hematoxylin and eosin staining

After the sacrifice of mice, different tissues were fixed by immersion in 10% (v/v) formalin solution, neutral buffered (Sigma-Aldrich, #HT501128) for 24h. Then, tissues were transferred to 1X PBS and delivered to the Histology Service of the Unitat d'Experimentació Animal de la Universitat de Barcelona or to the Biobanc-Banc de Tumors de l'Institut d'Investigacions Biomèdiques August Pi I Sunyer. Tissue samples were paraffin-embedded, cut into 25 µm sections and stained with hematoxylin and eosin (H&E). Pictures of the stained samples were taken using the

inverted microscope Leica DM IL LED (Leica, #11521257) and the Leica MC190 HD camera (Leica, #MC190HD). The Image J software was used to process tissue samples.

3.6.2. Muscle and brain cross-sections obtention

To determine the skeletal muscle fibre composition, cryopreserved muscles were cross-sectioned in the cryostat Leica CM3050S (Leica, #CM3050S). Before to use the machine, the blade and samples were pre-cooled to -22 ± 2ºC for 20 minutes for thermal equilibration. Then, samples were attached to the metallic holders of the cryostat with Tissue-Tek O.C.T, and 15 µm-thick sections were collected in SuperFrost positive-charged slides (Thermo Scientific, #10149870). Slides were stored in a slide box (VWR, #631-0737) at -80ºC until processing.

Similarly, 20 µm-thick coronal sections of brain were obtained to validate the AVV injection in the VMN. The slides containing the brain sections were stored at -80ºC freezer until processing. To label the neuronal nucleus, the 4',6-diamidino-2-phenylindole (DAPI), a blue-fluorescent DNA stain that binds strongly to adenine-thymine rich regions, was used.

3.6.3. Immunostaining

Frozen slides from skeletal muscles were taken out from -80ºC to room temperature for 10 minutes for thermal equilibration. Each tissue section was surrounded by a hydrophobic liquid using a liquid blocker (ICT, #20448110068) to reduce the volume of the solutions. Tissue sections were blocked in the blocking buffer [0.9% (w/v) NaCl, 52 mM potassium phosphate dibasic (ACS Reagent, #15618020), 9.6 Mm potassium dihydrogen phosphate (Merck, #1048731000) (KPBS), 0.1% Triton X-100, 2% (v/v) goat serum (Sigma-Aldrich, #G9023) and 2% BSA] in a wet chamber for 1h. Blocking buffer was removed from slides and they were washed three times with the KPBS solution (without Triton, goat serum and

BSA) for 5 minutes. Then, primary antibodies diluted in blocking buffer were added (*Table 13*), and slides were incubated in a wet chamber at 4ºC O/N.

Table 13. List of primary antibodies used for the muscle immunostaining.

Antibodies	Dilution	Source
Anti-rabbit Dystrophin	1:1000	Abcam, #ab152777
Anti-mouse Myh2	1:300	DSHB, #2F7
Anti-mouse Myh4	1:300	DSHB, #10F5
Anti-mouse Myh7	1:300	DSHB, #BA-F8

DSHB: Development Studio Hybridoma Bank

Muscle sections were washed three times with KPBS for 5 minutes. Secondary antibodies diluted in blocking buffer were added to each section and slides were incubated for 2h at room temperature in a wet dark chamber. The list of secondary antibodies and dilutions done was defined in the *Table 14*. After the incubation, the slides were washed three times with KPBS for 5 minutes and mounted with a drop of immunostaining solution Fluoromount G (LabClinics, #00-4958-02) and covered with cover slides (Fisher Scientific, #11767394) avoiding the bubbles formation. Fluorescent images were captured using the fluorescent microscope Leica DMI4000B (Leica, #DMI4000B) equipped with a high-sensitive camera Leica DFC300 FX (Leica, #DFC3000FX)). The number of muscle fibres and composition of each muscle was analysed using the Fiji ImageJ software.

Table 14. List of secondary antibodies used for muscle immunostaing.

Antibodies	Dilution	Source
Goat anti-rabbit IgG, Alexa Fluor 405	1:1000	Invitrogen, #A31556
Goat anti-mouse IgM, Alexa Fluor 488	1:1000	Invitrogen, #A21042
Goat anti-mouse IgG1, Alexa Fluor 568	1:1000	Invitrogen, #A21124
Goat anti-mouse IgG2b, Alexa Fluor 647	1:500	Invitrogen, #A21242

3.7. Oxygen consumption measurement

5-months-old mice were anesthetised with a ketamine/xylazine solution, and the tibialis anterior muscle was collected in a 1.5 µl tube containing 1 ml of ice-cold BIOPS buffer, pH 7.1 [10 mM Ca-Egtazic acid (EGTA) buffer, 0.1 µM free calcium, 20 mM imidazole, 20 mM taurine, 50 mM 4-morpholineethanesulfonic acid potassium, 0.5 mM DTT, 6.5 Mm magnesium chloride ($MgCl_2$), 5.77 mM ATP, and 15 mM phosphocreatine]. Muscles were transferred into a small plastic petri dish on ice covered with BIOPS, where fibre bundles were separated using two pairs of very sharp forceps. Fibre bundles were permeabilised using 50 µg/ml saponin (Sigma, #S2149) in 1 ml of ice-cold BIOPS for 30 minutes. Then, fibre bundles were washed in ice-cold respiration medium MIR05, pH 7.1 (0.5 mM EGTA, 3mM $MgCl_2$, 60 mM lactobionic acid, 20 mM taurine, 10 mM potassium dihydrogen phosphate, 20 Mm HEPES, 110 mM D-sucrose and 1 g/L BSA) for 10 minutes.

Table 15. Substrates and inhibitors used to measure the oxygen consumption in skeletal muscle.

	Concentration	Product reference
Glutamate	10 mM	Sigma-Aldrich, #G1626
Malate	2 mM	Sigma-Aldrich, #M1000
ADP	2.5 mM	Cal-Biochem, #117105
Succinate	10 mM	Sigma-Aldrich, #S2378
CCCP	0.1 mM	Sigma-Aldrich, #C2920
Rotenone	0.5 µM	Sigma-Aldrich, #R8875
Antimycin	2 mM	Sigma-Aldrich, #A8674

Oxygen consumption experiments were conducted at 37ºC using a high-resolution Oxygraph-2k system (Oroboros Instruments GmbH, #PNet14.13) in collaboration with Zorzano's Lab (Institute for Research in Biomedice, IRB). 2-4 mg of wet muscle bundles were transferred into each chamber containing 2 ml of air-saturated MIR05 medium in duplicate following the sequential addition of different substrates and inhibitors: 10 mM glutamate/ 2 mM malate (complex I), 2.5 mM

ADP, 10 mM succinate (complex II), 0.1 mM carbonyl cyanide 4-(trifluoromethoxy) phenylhydrazone (FCCP, uncoupler), 0.5 µM rotenone (inhibitor of complex I) and 2 mM antimycin (inhibitor of complex III). The final concentration of substrates and drugs were optimised based on previous published studies (270) (*Table 15*). The software Datlab5 (Oroboros Instruments GmbH, Version 3.4.1) was used to analyse the oxygen consumption data from the chosen intervals.

3.8. Bioinformatics and statistical analysis

Statistical analyses were determined using the GraphPad Prism 9 software (Version 9.3.2). Two-tailed Student's t-test analysis was used to compare two groups under the same condition. One-way ANOVA followed by Tukey's test was performed when one variable was compared between more than two groups. Two-way ANOVA followed by Sidak's multiple comparisons test was used when two variables were compared between two or more groups. In survival studies, data were analysed by the Gehan-Breslow-Wilcoxon survival curves test. Data is expressed as mean ± standard error of mean (SEM). Statistically significant differences were considered when the level of confidence was above 95% (P value <0.05). The number of samples/animals per group is specified in each figure legend.

Plasmid construction and design was performed using the SnapGene software (Version 6.0.5). The chromatogram results of sequencing were analysed using the MEGA7 software (Version 7.2.10). The myofibre composition, the mitochondrial analysis and the neuronal immunofluorescence were quantified with the Image J software (Version 1.8.0). The Open Field and Elevated Plus Maze tests were analysed using the SMART software (Version 3.0).

3.8.1. miRNA databases

To find a direct miRNA target of *Cpt1a* gene, several miRNA databases combined to recent published papers were analysed. The miRNA databases employed in this work were TargetScan [https://www.targetscan.org/ (271)], miRDB [http://mirdb.org/ (272)] and miRWalk [http://mirwalk.umm.uni-heidelberg.de/ (Version 3)]. All of them are open access and evaluate biological targets of miRNAs searching for the presence of conserved octamers, heptamers and hexamers sites that match of each miRNA described. miRNA predictions are ranked according to the best score obtained. In this study, we selected two novel miRNA present in the Top10 score of all these databases.

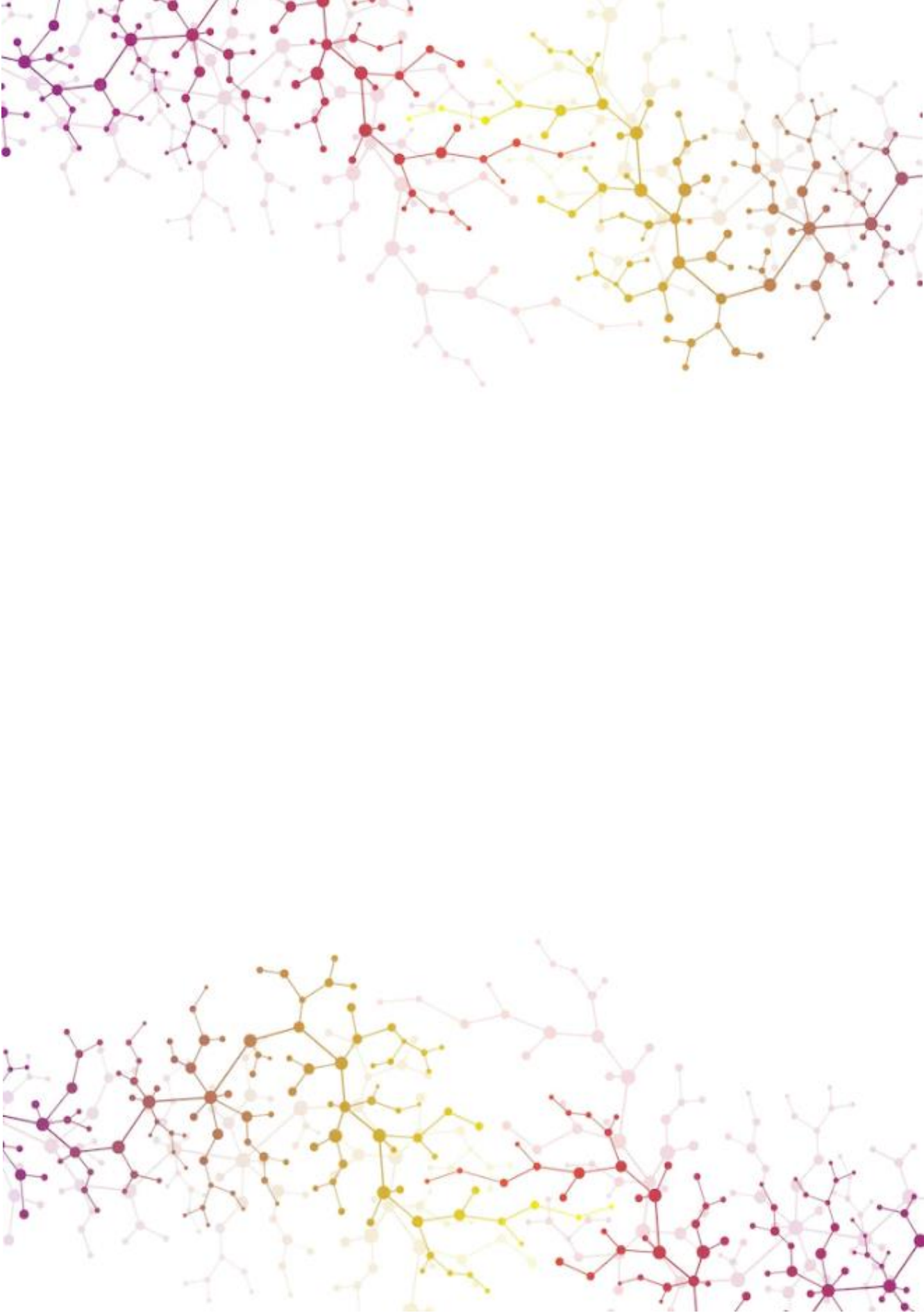

4. Results

4.1. Validation of *Cpt1a* deletion in SF1 neurons

To obtain a mutant mouse model lacking *Cpt1a* specifically in SF1 neurons (SF1 *Cpt1a* KO), two different approaches were studied (*Figure 18*). The first strategy was the generation of the SF1 *Cpt1a* KO mouse by crossing a *Cpt1a* Flox mouse with a transgenic SF1-*Cre* mouse. The Sf1 is a critical regulator of endocrine and neuronal development (31). We cannot obtain any SF1 *Cpt1a* KO mice since the Sf1 is expressed at E10.5 embryonic development in neurons, and the expression of Cpt1a in this stage results essential (273) (*Figure 18A*).

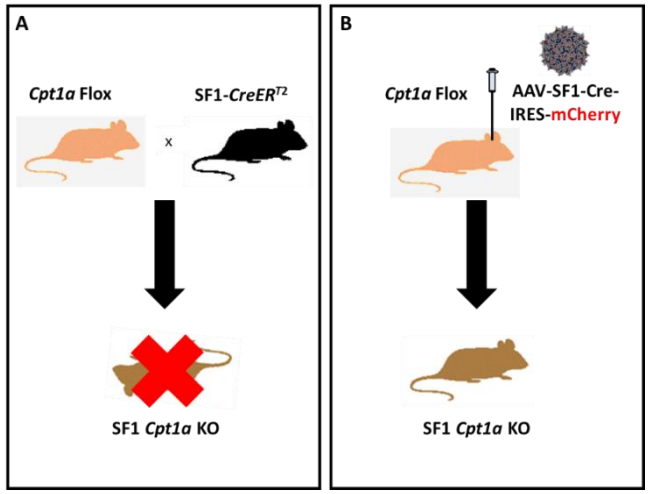

Figure 18. Strategies to obtain the SF1 *Cpt1a* KO mouse model. Different approaches were evaluated: (1) crossing the *Cpt1a* Flox mouse with a SF1-*Cre* mouse **(A)** and (2) the injection of a specific AVV-SF1-Cre-IRES-mCherry in the VMN of the *Cpt1a* Flox mouse **(B)**.

To avoid the lack of Cpt1a protein in the embryonic stage, *Cpt1a* was silenced in SF1 neurons of the VMN through the injection of an AVV9-SF1-Cre-IRES-mCherry (*Figure 18B*). This recombinant AVV contains the necessary elements to encode *Cre* recombinase and *mCherry* genes under the control of the SF1

promoter. This strategy allows, only using the *Cpt1a* Flox mouse, to induce the recombination of *Cpt1a* specifically in SF1 neurons, avoiding the neonatal lethality that occurs in the previous strategy.

Before evaluating the mouse phenotype, the Cre recombinase activity was examined. 8-weeks-old male and female *Cpt1a* Flox mice were subjected to a stereotaxis surgery, where recombinant AVVs were bilaterally injected into the VMN. The coordinates of this hypothalamic nucleus were: -1.7 mm posterior, -5.5 mm ventral and ±0.4 mm lateral from bregma. The AVV9-SF1-mCherry at $1.64 \cdot 10^{13}$ gc/ml was injected to mice from the control group (control) and the AVV9-SF1-Cre-IRES-mCherry at $1.10 \cdot 10^{13}$ gc/ml was injected to the knockout group (SF1 *Cpt1a* KO). To guarantee the maximal AVVs infection and gene expression of the *Cre* recombinase, the time of infection was set up at 3 weeks. Then, mice were sacrificed, and brains were fixed for performing the immunodetection (*Figure 19*). Both control and SF1 *Cpt1a* KO mice showed a mCherry fluorescent signal limited to the VMN, but the intensity of the fluorescent signal of SF1 *Cpt1a* KO mice was lower than control mice. In agreement with this data, the *mCherry* mRNA levels in the VMN of SF1 *Cpt1a* KO and control mice was measured by q-RT-PCR, showing a strong decrease in mRNA levels of *mCherry* in SF1 *Cpt1a* KO mice (*Figure 19B*).

Although both SF1 *Cpt1a* KO and control mice showed the *mCherry* fluorescent signal, the intensity was lower than we expected. It is widely demonstrated that physical activity increases 1.5 times the expression of *Sf1* gene and other genes related to this factor such as brain-derived neurotrophic factor (*Bdnf*), cannabinoid receptor 1 (*Cnr1*) and corticotrophin releasing hormone receptor 2 (*Crhr2*) (11). Therefore, to enhance this signal, an exercise training in a treadmill was performed the previous 3 days before the sacrifice of mice. The training protocol is described in the section 3.3.10.

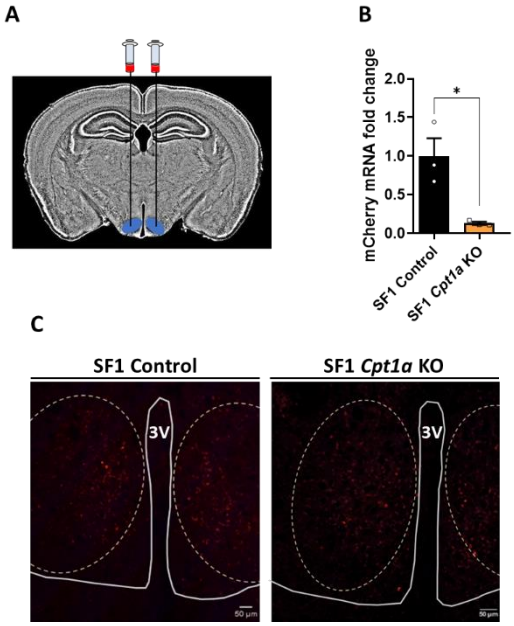

Figure 19. Validation of the Cre-mediated recombination of Cpt1a in SF1 neurons. (A) Scheme of AVV stereotaxic injections in the VMN (blue). Two bilateral injections were performed to obtain the experimental mouse model (SF1 *Cpt1a* KO mice). **(B)** *mCherry* mRNA levels from the VMN of SF1 *Cpt1a* KO and control mice normalised by the *Gapdh* gene. **(C)** Representative histological 20 µm-thick sections of the VMN of 12-weeks-old mice. Dashed lines represent the ventromedial nucleus of the hypothalamus and 3V refers to the third ventricle. Data are expressed as mean ± SEM. *P<0.05 by the two-tailed Student's t-test. n= 3 animals per experimental group. Scale bar: 50 µm.

After a single bout of exercise in the treadmill, mice were sacrificed, fixed with 4% PFA, brains were extracted and cut in sections in the cryostat. The fluorescent signal observed was similar to previous results in both SF1 *Cpt1a* KO and control groups (*Figure 20*). Even though exercise activates the expression of *Sf1* in SF1 neurons, we do not observe a remarkable increase in the fluorescent signal of brain sections analysed.

Tissue specific recombination was confirmed by PCR analysis. A 12-weeks-old SF1 *Cpt1a* KO and control littermates were sacrificed, and the VMN of each mouse was collected. The gDNA isolation was performed by the proteinase K method and analysed by PCR using the primers Cpt1a Flox.

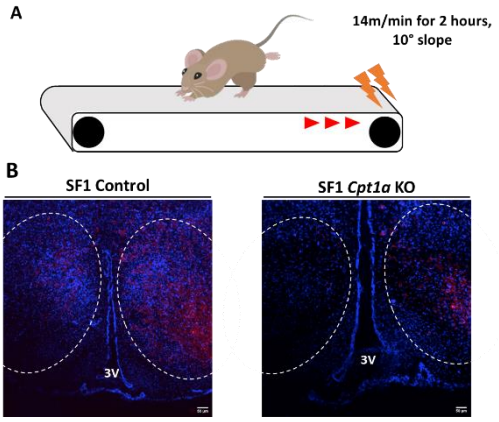

Figure 20. Histological VMN of SF1 Cpt1a KO mice after a single bout of exercise in the treadmill. (A) Scheme of the running protocol performed to enhance the *Sf1* and *mCherry* expression. **(B)** Representative histological 20 µm-thick sections of *mCherry* expression in SF1 neurons from the VMN of 12-weeks-old SF1 *Cpt1a* KO and control mice. Dashed lines represent the VMN and 3V refers to third ventricle. The neuronal nucleus is stained with DAPI. Scale bar: 50 µm.

The PCR product of the *Cpt1a* floxed region is 1.030 bp (*Figure 21A*), and the recombined amplicon is 219 bp (*Figure 21B*). No *Cpt1a* recombined amplicons were observed in samples from SF1 control mice. Surprisingly, we did not observe the recombined band in the VMN of SF1 *Cpt1a* KO mice (*Figure 21C*), probably due to the low amount of SF1 neurons in the VMN compared to other cell and neuron types. Therefore, to avoid the presence of non-recombined PCR products, the elongation time of the PCR was reduced to 1 second and the gDNA was digested using two restrictions enzymes [PstI (Fermentas, #ER0611) and AatII (Fermentas, #ER0991)], which are not in the Cpt1a recombined band (219 bp), but they are in the control band of 1.030 bp (*Figure 21A*). The gDNA from the VMN was incubated at 37ºC for 1h with these enzymes and then, a PCR was performed. Nonetheless, the intensity of recombined bands was low, and a second PCR was performed using the DNA excised from recombined bands. The results of this second PCR are shown in the *Figure 21D*, where the *Cpt1a* recombined band was only observed in the VMN of SF1 *Cpt1a* KO mice. Finally, the DNA band of 219 bp was sequenced to confirm the Cpt1a recombination (*Figure 21E*).

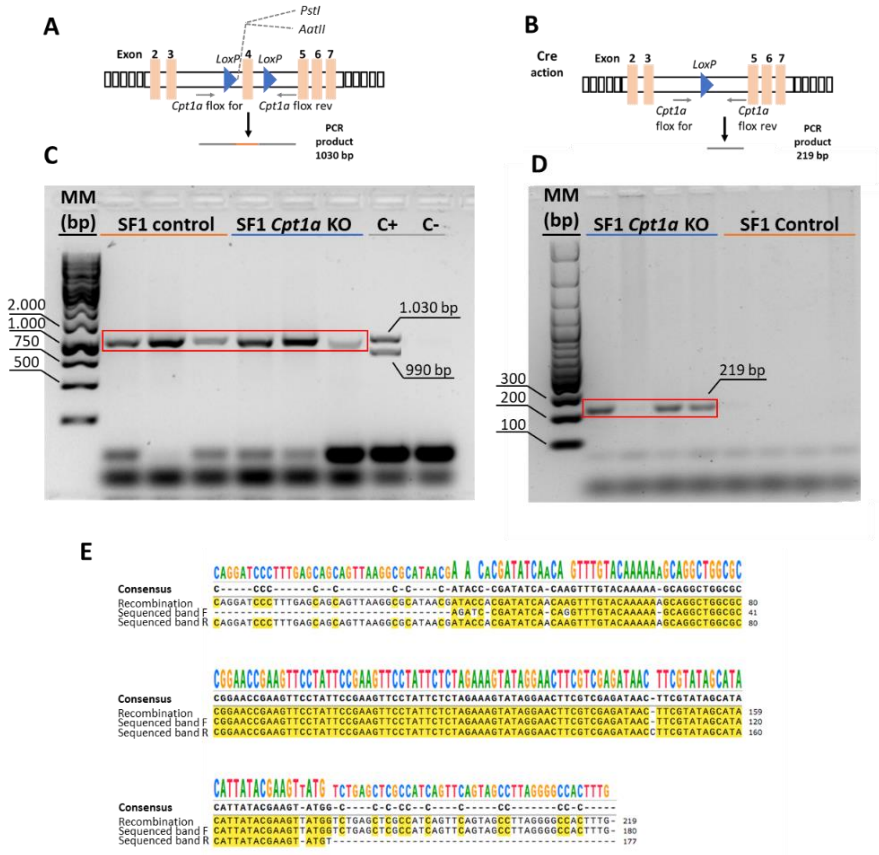

Figure 21. Validation of the *Cre-LoxP* system for the specific deletion of *Cpt1a* in SF1 neurons. (A-B) Scheme of the Cre-mediated recombination of the *Cpt1a* gene. When recombination is not activated, the floxed band (1.030 bp) containing the *LoxP* sequences surrounding the exon 4 was detected (A). The activation of the *Cre* recombinase generates a recombined PCR product of 219 bp (B). (C-D) Electrophoresis of the PCR products of SF1 *Cpt1a* KO and control mice containing the floxed band (C) and the recombined band (D) A heterozygous *Cpt1a* Flox mouse was used as a control positive (C+), to visualise the floxed and the wild-type bands (1.030 bp and 990 bp, respectively). A negative control without gDNA was performed to check DNA contaminations. The DNA molecular markers (MM) used were the 1 Kb DNA Ladder for the gel C, and the 100 bp DNA Ladder for the gel D. (E) Alignments of sequenced bands and the predicted sequence of *Cpt1a* recombination. The sequencing was performed using the *Cpt1a* Flox forward (sequenced band F) and reverse (sequenced band R). As a result, a consensus sequence was obtained mixed the average of intensity peaks of the three alignments. Yellow bars show the perfect match between the three sequences.

4.2. Cpt1a in SF1 neurons is involved in feeding behaviour

Once the deletion of *Cpt1a* in SF1 neurons was verified, mice phenotype was studied to analyse the effect of lipid metabolism in this neuronal population. 8-weeks-old male and female SF1 *Cpt1a* KO and SF1 control littermates were subjected to the AVV injection in the stereotaxic apparatus. Body weight and food intake were weekly monitored from the week 6 until the sacrifice of mice. After the AVV injection, no significant differences were observed in the body weight of males (31.93 ±4.564 g *vs*. 31.83 ±4.047 g) and females (24.11 ±1.464 g *vs.* 23.26 ±0.989 g) SF1 *Cpt1a* KO mice (*Figure 22B* and *22E*). However, both male (366.73 ±23.166 g *vs*. 388.18 ±24.275 g, **P<0.01) and female (244.48 ±6.940 g *vs*. 251.68 ±11.190 g, *P<0.05) SF1 *Cpt1a KO* mice exhibited a statistical decrease in the cumulative food intake after 6-7 weeks from the AVV injection (*Figure 22C* and *22F*).

Given the relevant role of SF1 neurons in feeding behaviour, a fast and refeed test was performed to discern if this decrease in food intake may be due to an impaired satiety. Mice were O/N fasted and the cumulative food intake was weighed during the refeeding period for 4h. No differences in the cumulative food intake after the refeeding were observed in both male and female SF1 *Cpt1a* KO mice with respect to the control mice. This demonstrates that an O/N fasting is not enough to alter the feeding behaviour (*Figure 22D* and *22G*).

Overall, these results suggest that Cpt1a in the VMN could act as a satiety signal. The specific deletion of *Cpt1a* in SF1 neurons does not produce changes in body weight but generates a mild decrease in food intake compared to the control group.

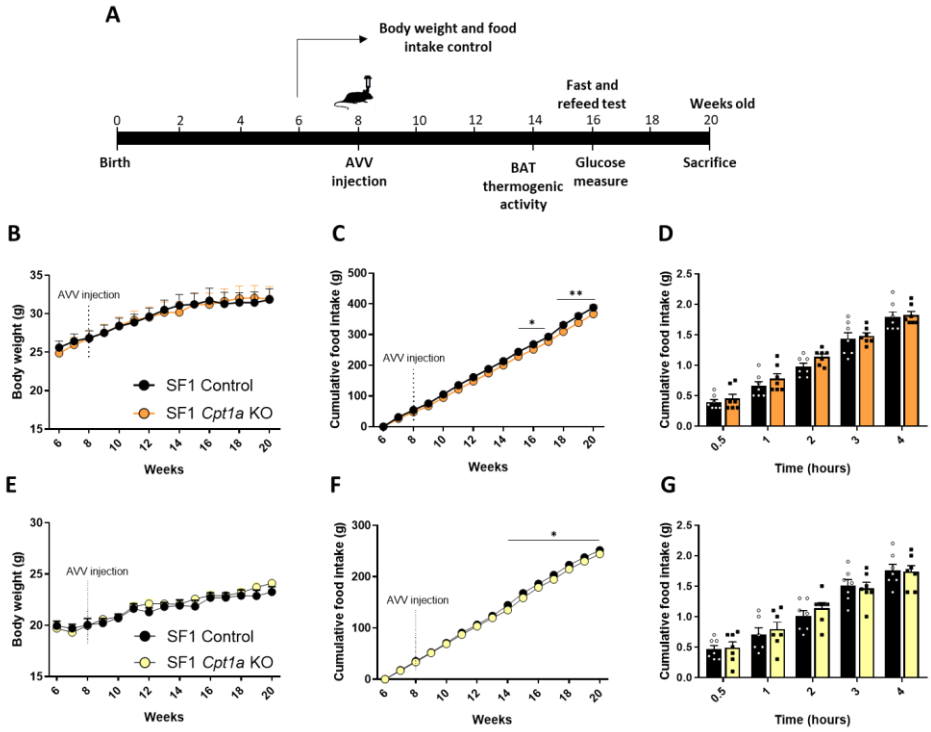

Figure 22. Body weight and food intake analysis of SF1 *Cpt1a* KO mice. **(A)** Scheme of the experimental time-course. **(B-D)** Body weight **(B)**, cumulative food intake **(C)** and fast and refeed test **(D)** of male SF1 *Cpt1a* KO and control mice. **(E-G)** Body weight **(E)**, cumulative food intake **(F)** and fast and refeed test **(G)** of female SF1 *Cpt1a* KO and control mice. Data are expressed as mean ± SEM. *P<0.05; **P<0.01 by 2way ANOVA Sidak's multiple comparisons test. n= 7-9.

4.3. Effect of *Cpt1a* deletion in SF1 neurons on peripheral tissues

It is widely established that SF1 neurons coordinate energy homeostasis and feeding control through their abilities to regulate peripheral organs activity. To analyse the role of lipid metabolism in SF1 neurons and its impact at peripheral level, different tissues directly related to the metabolism were analysed (BAT, gWAT, sWAT and liver).

4.3.1. Cpt1a in SF1 neurons affects BAT activity in a sex-dependent manner

Energy homeostasis is tightly regulated by the CNS, and the hypothalamus is the primary centre for the regulation of energy balance. In the last decades, several studies have advanced the understanding of the molecular regulation of BAT thermogenesis by the VMN thanks to the development of targeted manipulation techniques in the mouse genome and neuronal function (21,274,275). In fact, studies using a VMN-specific SF1 KO mice revealed that Sf1 is required for normal energy homeostasis by the modulation of energy expenditure specially in HFD conditions (33). Based on these data, the BAT activity was analysed to know the effect of the lack of Cpt1a in SF1 neurons.

The BAT thermogenic activity was measured after 8-weeks from the AVV injection (*Figure 23*). No differences in the BAT temperature were observed in male SF1 *Cpt1a* KO mice (37.42 ±0.244 ºC *vs*. 37.16 ±0.336 ºC) (*Figure 23B*), while an increase in the BAT temperature was detected in female SF1 *Cpt1a* KO mice compared to the control group (37.78 ±0.541 ºC *vs*. 37.1 3±0.664 ºC, *P<0.05) (*Figure 23C*).

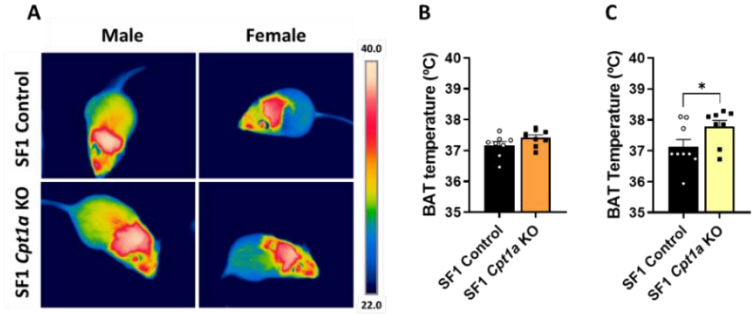

Figure 23. The BAT thermogenic activity of SF1 *Cpt1a* KO mice. (A) Representative infrared thermal images of the BAT interscapular region of male and female SF1 *Cpt1a* KO and control mice. **(B-C)** Quantification of the BAT temperature in male **(B)** and female SF1 Cpt1a KO and control mice **(C)**. Data are expressed as mean ± SEM. *P<0.05 by the two-tailed Student's t-test. n= 7-9.

The BAT histology of 5-months-old mice was analysed (*Figure 24A*). Although no differences in the BAT weight of both male and female mice (*Figure 24B and 24C*) were observed, male *Cpt1a* KO mice exhibited a higher amount of lipid content (*Figure 24A*) compared to the SF1 control group. Conversely, despite of the differences in thermogenic activity, the mRNA levels of perilipin 3 (*Plin3)*, a marker of lipid droplet content in BAT, were diminished in female *Cpt1a* KO mice (*Figure 24E*).

Due to the differences observed in the BAT thermogenesis, the mRNA levels of thermogenic markers [iodothyronine deiodinase 2 (*Dio2*), adrenoreceptor beta 3 (*Adrb3*) and *Ucp1*] and genes associated with lipid metabolism [hormone-sensitive lipase (*Hsl)*, adipose triglyceride lipase (*Atgl)* and *Cpt1b*] were analysed (*Figure 24D and 24E*).

Although we observed an increase in the thermogenic activity of female SF1 *Cpt1a* KO mice, no differences were observed in the mRNA levels of thermogenic markers (*Adrb3, Dio2* and *Ucp1)*. In male, despite of no differences in the interscapular BAT temperature, they exhibited around a 3-fold increase in the *Adrb3* mRNA levels. However, no changes in the mRNA levels of *Dio2* and *Ucp1* were observed. Dio2 is an essential component of the thyroid-sympathetic pathway required for the control of thermogenesis in mammals, while Ucp1 uncouples mitochondrial respiration from ATP synthesis inducing energy dissipation in form of heat, being the main responsible for non-shivering thermogenesis. In addition, male SF1 *Cpt1a* KO mice did not show changes in the mRNA levels of lipolytic genes (*Atgl* and *Hsl*) and the fatty acid oxidation gene *Cpt1b* (*Figure 24D*).

These results suggest that the BAT from female mice is more sensitive to alterations in lipid metabolism in the SF1 neurons compared to the male group, showing a sexual dimorphism. However, no positive correlation between the mRNA levels of thermogenic genes and activity was observed at the female group.

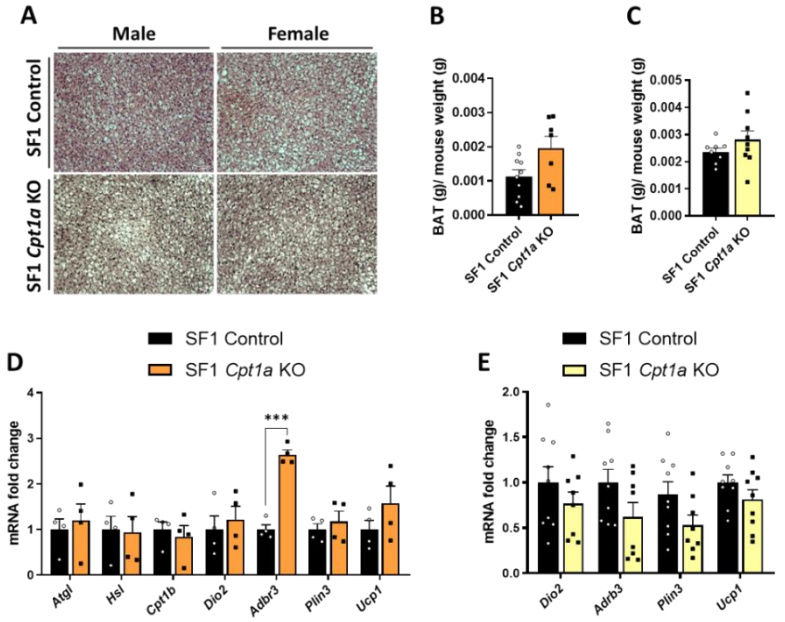

Figure 24. Histological analysis and mRNA levels of BAT from SF1 *Cpt1a* KO mice. (A) Representative images of BAT sections stained with H&E in male and female SF1 *Cpt1a* KO and control mice. Scale bar: 100 µm (magnification 20x). **(B-C)** BAT weight of 5-months-old male **(B)** and female mice **(C)**. **(D-E)** Analysis of mRNA levels of thermogenics and lipid metabolism genes by qRT-PCR in male **(D)** and female **(E)** mice normalised by the *Hprt1* gene. Data are expressed as mean ± SEM. *P<0.05; **P<0.01; ***P<0.001 by the two-tailed Student's t-test. n= 4-10.

4.3.2. Deletion of *Cpt1a* in SF1 neurons does not exhibit alterations in WAT

It has also been described that SF1 neurons play a relevant role in the modulation of white adipose tissue (13). In addition, the anorexigenic hormone leptin secreted by the WAT acts directly on the hypothalamus to control the *Sf1* expression and food intake (19).

To evaluate the potential role of fatty acid oxidation in SF1 neurons on the white adipose tissue, gWAT and sWAT were collected during the sacrifice. The weight of tissues, the H&E staining, and the mRNA levels of gWAT and sWAT from SF1 *Cpt1a* KO mice were analysed.

gWAT is considered the main fat storage of the body. Both male and female SF1 *Cpt1a* KO showed no histological differences compared to control littermates (*Figure 25A*). Moreover, the weight of gWAT remained unaltered in male and female mice (*Figure 25B* and *25C*). In agreement with these results, the mRNA levels of pro-inflammatory genes [*Il-6* and interleukin-1-beta (*Il-1β*)] and the specific isoform of the lipid droplet formation gene (*Plin2*) did not show differences between groups (*Figure 25D*).

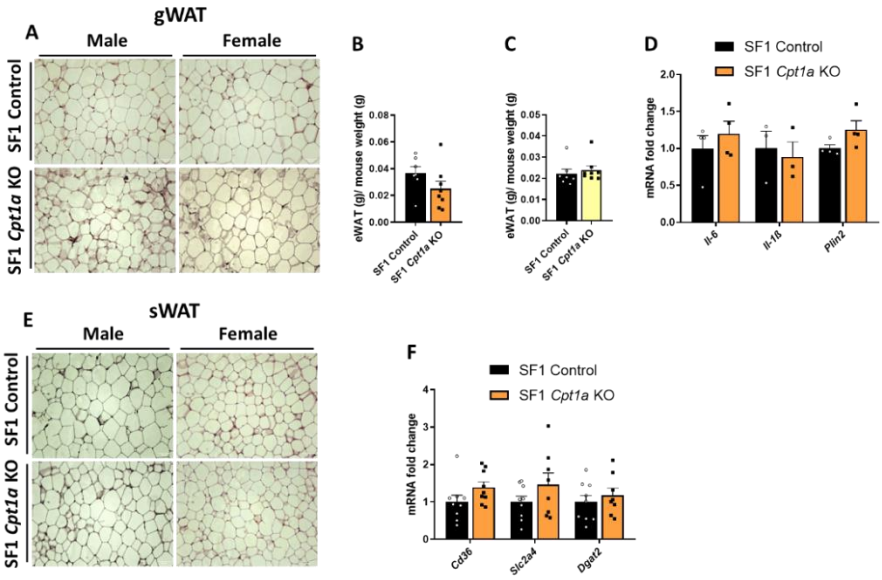

Figure 25. Histological analysis of gWAT and sWAT from SF1 *Cpt1a* KO mice. (A) Representative images of gWAT sections stained with H&E in male and female SF1 *Cpt1a* KO and control mice. Scale bar: 100 µm (magnification 20x). **(B-C)** qWAT weight of 5-months-old male **(B)** and female mice **(C)**. **(D)** mRNA levels of pro-inflammatory and lipid droplet formation genes by qRT-PCR in male SF1 *Cpt1a* KO mice. **(E)** Representative images of sWAT sections stained with H&E in male and female SF1 *Cpt1a* KO mice. Scale bar: 100 µm (magnification 20x). **(F)** mRNA levels of glucose and fatty acid transporters genes by qRT-PCR in male SF1 *Cpt1a* KO and control mice. All genes of both tissues were normalised by the *Hprt1* gene. Data are expressed as mean ± SEM. *P<0.05; **P<0.01; ***P<0.001 by the two-tailed Student's t-test. n= 4-8.

sWAT is not associated with classical pathologies such as obesity, diabetes, or cardiovascular disease. In fact, some data suggest that it could have a protective function because it is the part responsible for the release of leptin and other adipokines. Both male and female SF1 *Cpt1a* KO mice did not show changes at

histological and mRNA levels of genes related to lipid and glucose metabolism, including the fatty acid transporter cluster of differentiation 36 (*Cd36)*, the glucose transporter *Slc2a4* and the diacylglycerol O-acyltransferase 2 (*Dgat2*) in comparison to control littermates (*Figure 25E* and *25F*). Altogether, these results show that *Cpt1a* deletion in SF1 neurons did not exert any alteration in the gWAT and the sWAT of male and female mice.

4.3.3. Effect of *Cpt1a* deletion in SF1 neurons on glucose homeostasis

In addition to the role of SF1 neurons in the regulation of energy homeostasis, genetic studies have highlighted that SF1 neurons are also critical components of mechanisms controlling glucose metabolism. In fact, Borg *et al.*, (48) reported that lesions in the VMH of rats exhibited impaired glucagon, epinephrine and norepinephrine responses under hypoglycemic conditions. However, the influence of lipid metabolism in SF1 neurons on the modulation of glucose metabolism in the liver, the main tissue implicated in the glucose regulation, remains unclear.

Liver images from male and female SF1 *Cpt1a* KO mice revealed no histological alterations between groups (*Figure 26A*) and no differences in tissue weight compared to control (*Figure 26B and 26C*). Furthermore, glucose levels in plasma after O/N fasting were maintained unaltered between SF1 *Cpt1a* KO and control mice (*Figure 26D*).

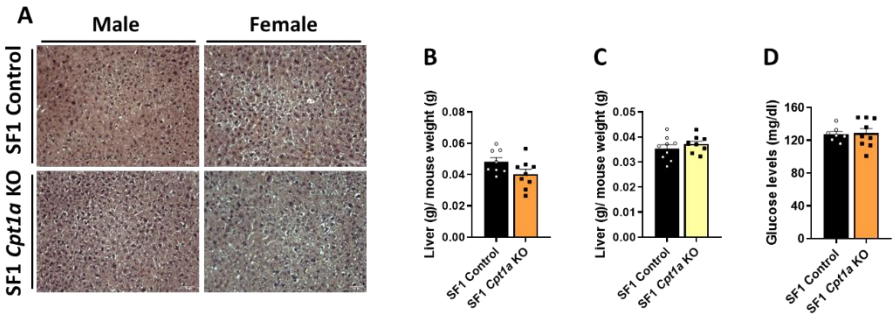

Figure 26. Histological analysis and mRNA levels of the liver from SF1 *Cpt1a* KO mice. (A) Representative images of liver sections stained with H&E in male and female SF1 *Cpt1a* KO and control mice. Scale bar: 100 µm (magnification 20x). **(B-C)** Liver weight of 5-months-old male **(B)** and female mice **(C)**. **(D)** Blood glucose levels of 4-months-old male SF1 *Cpt1a* KO and control mice. Data are expressed as mean ± SEM. *P<0.05; **P<0.01; ***P<0.001 by the two-tailed Student's t-test. n= 4-9.

4.4. Effect of HFD on the SF1 *Cpt1a* KO mouse phenotype

Since we observed some differences in food intake of SF1 *Cpt1a* KO mice, a new experiment was carried out feeding mice with HFD to determine whether the deletion of *Cpt1a* in SF1 neurons can prevent obesity. The time-course followed is described in the *Figure 27A*. Briefly, 4 weeks after the AVV injection, male mice were fed with HFD (60% fat) or NCD (10% fat) for 8 weeks until the sacrifice. In these experiments, four groups were analysed: SF1 control NCD, SF1 *Cpt1a* KO NCD, SF1 control HFD and SF1 *Cpt1a* KO HFD.

Body weight and food intake were weekly monitored until the sacrifice. No significant differences in body weight were observed under the same condition between SF1 *Cpt1a* KO and control mice. Only changes between HFD and NCD groups were observed since the 17th week of age (*Figure 27B*). In agreement with these results, food intake, expressed in kilocalories (Kcal), was lower in mice fed with NCD (SF1 *Cpt1a* KO, 868.28 ±54.422 g *vs*. 753.63 ±1.321 g, **P<0.01; SF1 control, 806.07 ±68.380 g *vs*. 762.69 ±36.336 g, **P<0.01), but no statistical

differences between SF1 *Cpt1a* KO and control mice under the same condition were detected (*Figure 27C*).

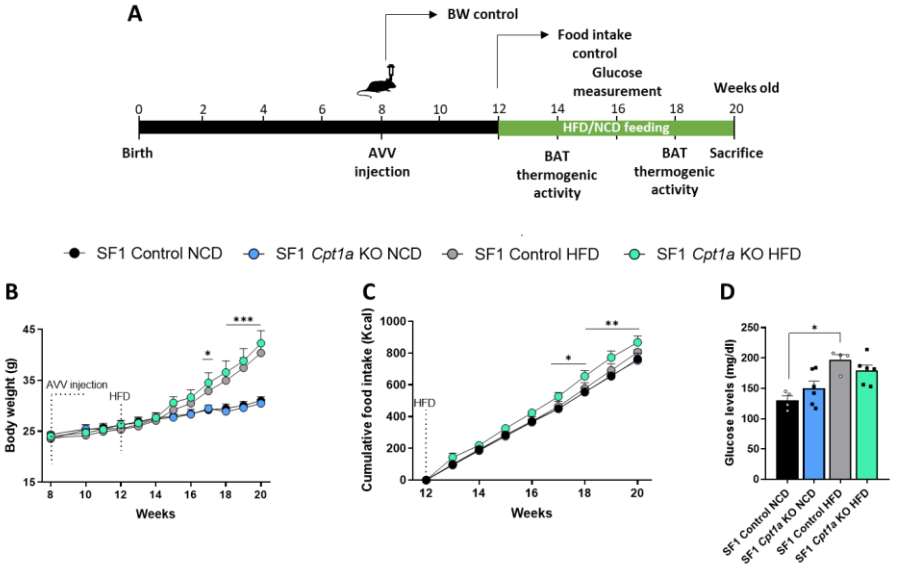

Figure 27. Body weight, cumulative food intake and glucose levels of SF1 *Cpt1a* KO mice under HFD conditions. **(A)** Scheme of the experimental time-course. **(B-C)** Body weight **(B)** and cumulative food intake **(C)** of male SF1 *Cpt1a* KO and control mice. **(D)** Blood glucose levels after O/N fasting in 16-weeks-old mice fed with HFD for 4 weeks. Data are expressed as mean ± SEM. *P<0.05; **P<0.01; ***P<0.001 by 2way ANOVA Sidak's multiple comparisons test. n= 4-14.

The VMN is also involved in the regulation of glucose. Therefore, a glucose measurement was performed to analyse the additional effect of HFD and Cpt1a deletion in SF1 neurons after 12h of fasting. Blood glucose levels of SF1 *Cpt1a* KO HFD mice did not show significant differences compared to SF1 *Cpt1a* KO NCD mice (*Figure 27D*). Conversely, the SF1 control group showed changes in glucose levels by the effect of the HFD.

It is widely described that SF1 neurons play an essential role under energy homeostasis, especially in high-fat diet conditions. We analysed the BAT thermogenesis at different time points (2 and 6 weeks after the administration of the diet), because recent studies have demonstrated a substantial activation of interscapular BAT temperature after 7-14 days of HFD (276). In contrast, longer

administration periods of HFD (from 28 days onwards) were not able to induce a considerable activation of BAT thermogenesis. At 14 days, both SF1 *Cpt1a* KO HFD and SF1 control HFD mice showed an increased in BAT temperature compared to groups fed with NCD (SF1 *Cpt1a* KO, 38.20 ±0.335 ºC *vs*. 36.50 ±0.520 ºC, *P<0.05; control, 38.21 ±0.395 ºC *vs*. 36.76 ±0.485 ºC, *P<0.05) (*Figure 28A* and *28B*). However, these differences produced by the diet were lost after 6 weeks of HFD (SF1 *Cpt1a* KO, 38.02 ±0.335 ºC *vs*. 37.48 ±1.056 ºC; SF1 control, 38.37 ±0.516 ºC *vs*. 37.56 ±0.231 ºC) (*Figure 28C*).

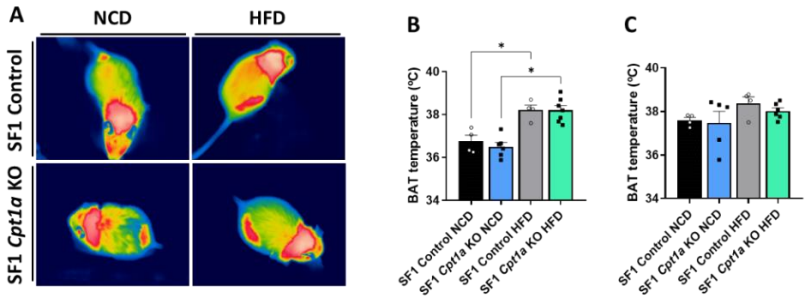

Figure 28. Analysis of the effect of HFD in the BAT thermogenic activity of SF1 *Cpt1a* KO mice. (A) Representative infrared thermal images of the interscapular BAT region of SF1 *Cpt1a* KO and control mice after 14 days of HFD/NCD administration. **(B-C)** BAT temperature quantification at 14-weeks-old **(B)** and at 18-week-old **(C)** of SF1 *Cpt1a* KO and control mice fed with HFD/NCD. Data are expressed as mean ± SEM. *P<0.05 by 2way ANOVA followed by Sidak's multiple comparisons. n= 4-7.

The histology of the BAT was also analysed. Tissue sections were stained with H&E staining and a strong increase in lipid droplet content was observed in control mice under HFD conditions (*Figure 29A*). This increase is not observed in the SF1 Cpt1a KO group. In agreement with these data, a significant increase in the BAT weight was observed in SF1 control HFD mice, but not in SF1 *Cpt1a* KO HFD mice (*Figure 29B*).

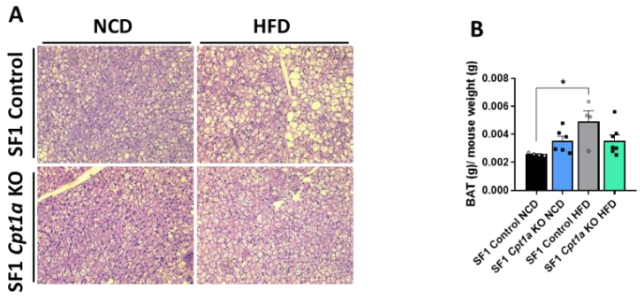

Figure 29. Histological analysis of BAT from SF1 *Cpt1a* KO mice under HFD conditions. (A) Representative images of the BAT stained with H&E from 20-weeks-old mice under different diet conditions. Scale bar: 100 µm (magnification 20x). **(B)** BAT weight from male mice was normalised by the body weight. Data are expressed as mean ± SEM. *P<0.05 by 2way ANOVA followed by Sidak's multiple comparisons. n= 4-7.

Due to their function of fat storage, the WAT increase the size of adipocytes under HFD conditions. Histological analysis of gWAT and sWAT from mice under HFD revealed an increase in adiposity, but no changes were observed between SF1 *Cpt1a* KO mice and control littermates under the same condition (*Figure 30A* and *30B*).

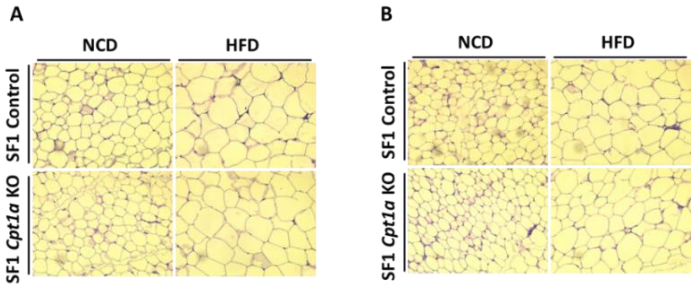

Figure 30. Histological analysis of gWAT and sWAT from SF1 *Cpt1a* KO mice under HFD conditions. Representative images of gWAT **(A)** and sWAT **(B)** stained with H&E from 20-weeks-old mice under different diet conditions (NCD and HFD). Scale bar: 100 µm (magnification 20x).

Another tissue involved in lipid metabolism is the liver. In this case, we observed an increase in lipid droplet content under HFD conditions in both SF1 *Cpt1a* KO and control groups without differences in mice under the same condition (NCD vs NCD or HFD vs HFD) (*Figure 31*).

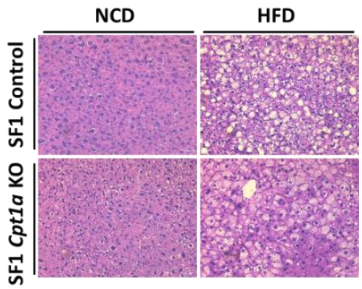

Figure 31. Histological analysis of liver from SF1 *Cpt1a* KO mice in HFD conditions. Representative images of liver stained with H&E from 20-weeks-old mice under different diet conditions (NCD and HFD). Scale bar: 100 µm (magnification 20x).

Altogether, these results do not show remarkable changes in SF1 *Cpt1a* KO mice under a metabolic stress such as HFD in comparison to control littermates. Therefore, we decided to finish this project and start a new study related to another neuronal population of the MBH, the AgRP neurons located in the ARC nucleus of the hypothalamus.

4.5. Cpt1a in AgRP neurons is necessary to regulate exercise performance in adult mice

The ARC plays a crucial role in energy homeostasis, especially in food intake regulation. Our team have demonstrated that mice lacking *Cpt1a* in AgRP neurons (AgRP *Cpt1a* KO mice) regulate energy balance in a sex-dependent manner. Although male and female mice showed a reduction in body weight, both genders afford this reduction in a different way. While male AgRP *Cpt1a* KO mice exhibited a reduction in food intake with no changes in energy expenditure, female AgRP *Cpt1a* KO mice showed increased energy expenditure without changes in food intake. However, little is known about the role of Cpt1a in AgRP neurons in response to exercise activity.

Recent studies have discovered the role of exercise to modulate the activity of AgRP neurons (27,277). Physical activity has a powerful action on metabolism,

and, during exercise, some factors such as leptin and insulin are released into the circulation modulating the expression of Agrp/Npy in the ARC.

AgRP *Cpt1a* KO mouse model was generated by crossing the inducible *AgRP-CreER*^{T2} mouse kindly provided by Prof. Joel Elmquist with the *Cpt1a* Flox mouse. Tamoxifen was administered at 2-months of age, and the recombination of *Cpt1a* gene occurs specifically in AgRP neurons. *Agrp* is also expressed in chromaffin cells of the adrenal gland, but AgRP *Cpt1a* KO mice did not exhibit histological or functional alterations in this tissue. As a control group, *Cpt1a* Flox mice were used.

The first evidence that pushed us to study the physical capacity of AgRP *Cpt1a* KO mice was the difference in the locomotor activity that AgRP *Cpt1a* KO mice showed in the house cage compared to control littermates. To confirm this evidence, different physical, cognition and behaviour tests were performed (*Figure 32A*).

4.5.1. *Cpt1a* ablation in AgRP neurons improves endurance and motor coordination

To evaluate the endurance capacity of AgRP *Cpt1a* KO male mice, a treadmill exhaustion test was performed at 4-months-old mice. Mice are forced to run until exhaustion over a conveyor belt with gradually increasing speed. AgRP *Cpt1a* KO mice showed enhanced endurance capacity compared to control littermates. They were able to stay longer on the treadmill (109.73 ±10.243 minutes *vs.* 93.60 ±12.709 minutes, **P<0.01) (*Figure 32B*), withstand higher speeds (*Figure 32D*), and run a 26% more distance (1483.35 ±249.782 m *vs.* 1176.67 ±250.316 m, **P<0.01) than control mice (*Figure 32C*).

Motor coordination is defined as the ability to coordinate muscle activation in a sequence that preserves posture. It was evaluated by the rotarod test, where mice were placed on a horizontal rod that rotates at different speeds. Mice must

walk forwards on the rod to avoid falling off. Results of this test exhibited that AgRP *Cpt1a* KO mice can spend a 69% more-time walking on the rod (100.19 ±21.642 seconds *vs.* 59.16 ±23.306 seconds, ****P<0.0001) (*Figure 32E*) and can endure higher speed compared to control mice (*Figure 32F*).

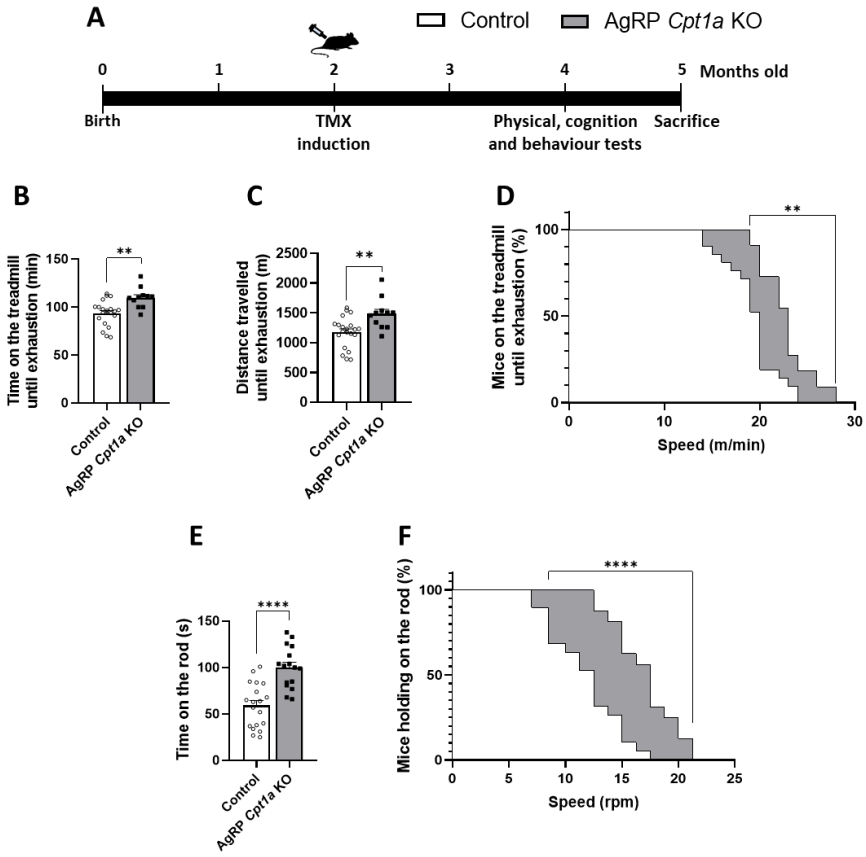

Figure 32. Evaluation of endurance and motor coordination in AgRP *Cpt1a* KO mice. (A) Scheme of the experimental time-course. (B-D) Analysis of endurance capacity by the treadmill exhaustion test. Time (B), running distance (C) and endurance capacity (D) of AgRP *Cpt1a* KO and control mice. (E-F) Analysis of the motor coordination by the rotarod test. Time (E) and endurance capacity (F) in the rod. Data are expressed as mean ± SEM. *P<0.05; **P<0.01; ***P<0.001; ****P<0.0001 by the two-tailed Student's t-test. The graphs D and F were analysed by the Gehan-Breslow-Wilcoxon survival curves test. n= 11-21.

4.5.2. Role of Cpt1a in the AgRP neurons in locomotor activity, exploration and anxiety-related behaviour

To corroborate differences observed in the endurance capacity, two tests related to locomotor activity were carried out: the Open Field test and the Elevated Plus Maze test. The OFT is a test used to analyse locomotion, exploration, and anxiety-related behaviour in rodents. EPM is a complementary test to the OFT, where anxiety-related behaviour is mainly studied. In addition, both experimental tests provide us a general overview of AgRP *Cpt1a* KO mice physical activity and exploration.

Results in the OFT demonstrated that AgRP *Cpt1a* KO mice showed an enhancement in locomotor activity as they travelled a 21% more distance than control littermates (3134.04 ±602.356 cm *vs.* 2587.49 ±535.874 cm, **P<0.01) (*Figure 33A* and *33B*). Furthermore, they exhibited a higher number of rearings (56.00 ±14.066 *vs.* 38.89 ±11.312, **P<0.01) (when mouse is moving around the environment attempting to contact relevant stimuli, *Figure 33C*) and entries in the centre area (15.17 ±6.719 *vs.* 8.78 ±3.809, **P<0.01) (*Figure 33D*), two parameters associated with the exploratory behaviour.

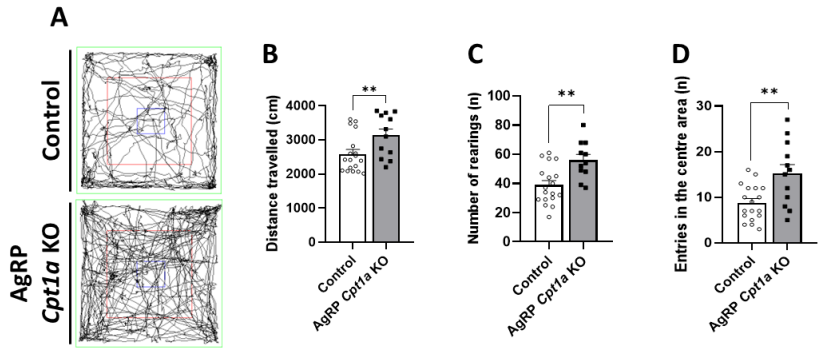

Figure 33. Analysis of the Open Field test in AgRP *Cpt1a* KO mice. (A) Representative images of control and AgRP *Cpt1a* KO mouse's travel pathway on the OFT. **(B)** Locomotor activity was analysed by the total distance travelled during the test. **(C-D)** Exploratory behaviour was measured through the number of rearings **(C)** and entries in the centre area **(D)** done by animals during the test. Data are expressed as mean ± SEM. *P<0.05; **P<0.01by the two-tailed Student's t-test. n= 15-19.

Similar results were reported in the EPM test. AgRP *Cpt1a* KO mice travelled a 18% more distance than control mice (922.72 ±186.850 cm *vs.* 780.13 ±187.905 cm, *P<0.05) (*Figure 34A* and *34B*), and they did a higher number of rearings (17.94 ±3.976 *vs.* 12.89 ±4.191, **P<0.01) (*Figure 34C*). In addition, no changes were observed in the number of entries into the open arms (9.94 ±3.230 *vs.* 8.21 ±3.563) (*Figure 34D*).

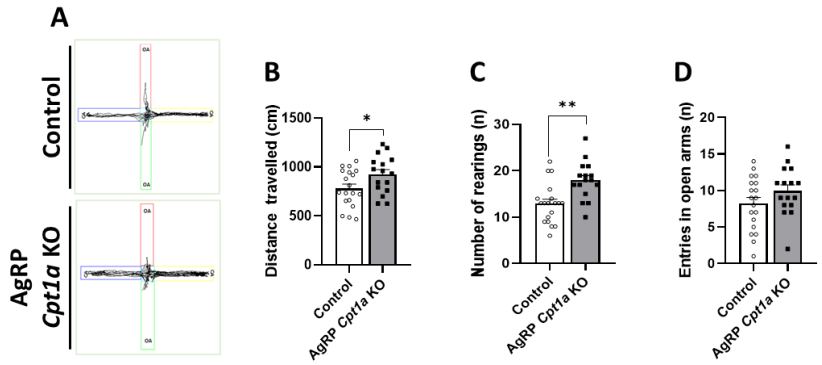

Figure 34. Analysis of the Elevated Plus Maze test in AgRP *Cpt1a* KO mice. (A) Representative images of control and AgRP *Cpt1a* KO mouse's travel pathway on the EPM. **(B)** Locomotor activity was analysed by the total distance travelled during the test. **(C-D)** Exploratory behaviour was measured through the number of rearings **(C)** and the number of entries into the open arms **(D).** Data are expressed as mean ± SEM. *P<0.05; **P<0.01by the two-tailed Student's t-test. n= 15-19.

Anxiety-related behaviour of these mice was analysed (*Figure 35*). Generally, mice display a natural aversion to open and unknown environments, and they show a preference to stay in enclosed paces or close to the walls of the field (thigmotaxis). High anxiety levels result in an increase in the proportion of time spent in the open arms and in the entries into the open arms. Low levels of anxiety lead to increased exploration and movement (261). This behaviour was observed during the performance of OFT and EPM tests.

Mice lacking *Cpt1a* in AgRP neurons did not show differences in the proportion of time spent in the centre area of the OFT (*Figure 35A*) or in the open arms of the EPM test (*Figure 35D*). In both tests, three emotional factors were analysed: grooms, urination, and defecation. Grooming is defined as a behaviour

that functions to maintain the physiological appearance and comfort of the mouse. Under stress conditions, mice exhibit an altered self-grooming. Defecation and urination are controversial parameters. It is well established that the number of faecal boles and urines increase under stress conditions. However, animals also feel relaxed or comfortable in the environment when they make these actions. Although discrepancies in the literature regarding the relation of these factors with anxiety behaviour were found, we measured these parameters in this study. AgRP *Cpt1a* KO mice showed no changes in the number of grooms, faecal bole, and urine during the performance of the OFT and EPM tests (*Figure 35B, 35C, 35E and 35F*).

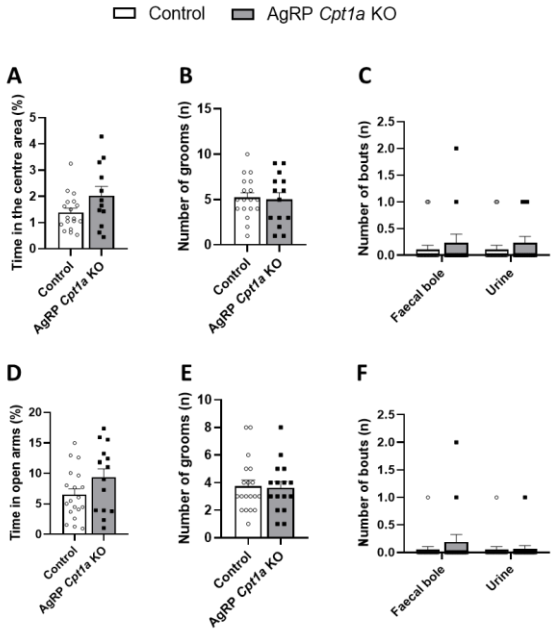

Figure 35. Anxiety-like behaviour analysis in OFT and EPM tests. (A-C) Time spent in the centre area **(A)**, number of grooms **(B)**, defecation and urination **(C)** done by mice in the OFT. **(D-F)** Time spent into the open arms **(D)**, number of grooms **(E)**, faecal bole and urine done by mice in the EPM test **(F)**. Data are expressed as mean ± SEM. *P<0.05 by the two-tailed Student's t-test. n= 15-19.

Overall, these data are in the same line as the results observed in the endurance test. AgRP *Cpt1a* KO mice exhibited an enhancement in locomotor and explorative capacity. In addition, no changes in anxiety-related behaviour were

observed, demonstrating that differences in locomotor activity were not due to anxiety behaviour. These findings suggest the relevant role of lipid metabolism in AgRP neurons in the regulation of physical activity.

4.5.3. *Cpt1a* deletion in AgRP neurons does not modulate mice strength

Considering these changes in exercise performance, we decided to measure the strength in AgRP *Cpt1a* KO mice. Muscles are activated by the brain or spinal reflexes, via neuromuscular junctions. Therefore, alterations in the lipid metabolism in AgRP neurons could affect the muscle strength.

To analyse mice strength, two different tests were performed: the Kondziela's inverted screen and the weights test. In all of them, the difference in body weight between the groups of study (27.76 ±2.115 g *vs.* 34.78 ±1.473 g, ***P<0.001) (*Figure 36A*) could affect the exercise performance because of the reduction of maximal oxygen volume (VO_2) associated with body weight. However, several studies have reported that variations in rodents weight less than 10g have a low impact on the exercise performance (278–280). In case of strength tests, it is established that heavier mice have greater lean mass and, therefore, they are generally stronger than thinner animals (263). To avoid this problem, strength capacity was expressed as holding impulse normalising the strength score by the body weight (*Figure 36C*).

The Kondziela's inverted screen test analyses the muscle strength using all four limbs while the weights test only uses their forepaws to grasp different weights. The specific deletion of *Cpt1a* in the AgRP neurons did not significantly affect muscle strength as measured either by the inverted screen test (*Figure 36B, 36C and 36D*) or weights test (*Figure 36E*).

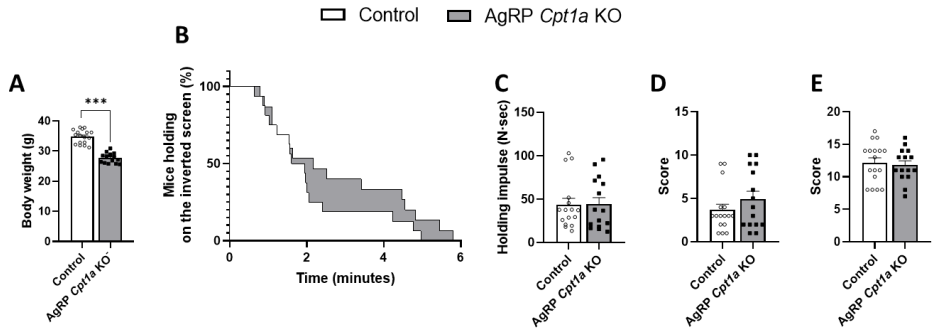

Figure 36. Evaluation of the muscle strength of AgRP *Cpt1a* KO mice. (A) Body weight of AgRP *Cpt1a* KO and control mice. **(B-D)** Percentage of mice holding on the inverted screen over time **(B)**, holding impulse **(C)** and score **(D)** of AgRP *Cpt1a* KO and control mice in the Kondzielas's inverted screen test. **(E)** Score obtained of AgRP *Cpt1a* KO and control mice in the weights test. Data are expressed as mean ± SEM. *P<0.05; **P<0.01; ***P<0.001 by the two-tailed Student's t-test. The graph B was analysed by the Gehan-Breslow-Wilcoxon survival curves test. n= 15-17.

4.5.4. Ablation of *Cpt1a* in AgRP neurons affects physical performance differently in female mice

Physical capacity was also analysed in female mice. Curiously, no differences were observed in the time (91.41 ±11.320 minutes *vs* 90.33 ±8.256 minutes) (*Figure 37A*) and distance (1208.80.41 ±234.752 m *vs* 1131.45 ±167.930 m) (*Figure 37B*) travelled until exhaustion on the treadmill. Moreover, female AgRP *Cpt1a* KO mice were unable to endure higher speeds than control littermates (*Figure 37C*) as we observed in the male group.

Muscle strength in female mice was also evaluated through the Kondziela's inverted screen test. In agreement with the male phenotype, no variations between groups were observed (206.50 ±170.875 N·sec *vs.* 271.20 ±128.629 N·sec and 9.71 ±0.451 *vs.* 10.00 ±0.000) (*Figure 37D and 37E*). Surprisingly, the score and the holding impulse normalised by the body weight (*Figure 37F*) of both female groups were approximately four times higher than both male groups. Generally, female AgRP *Cpt1a* KO and control littermates were able to maintain around 30 minutes on the inverted screen, while both male groups were held less than 10 minutes.

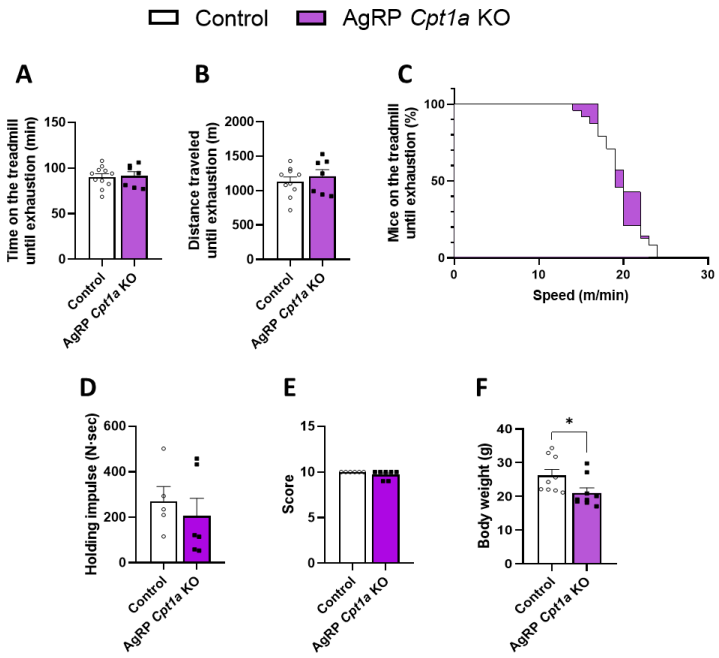

Figure 37. Analysis of physical activity and strength in female AgRP *Cpt1a* KO mice. (A-C) Performance of female AgRP *Cpt1a* KO and control mice in the treadmill exhaustion test. Time **(A)** distance **(B)** and endurance capacity **(C)** until exhaustion. **(D-E)** Holding impulse **(D)** and score **(E)** of female AgRP *Cpt1a* KO and control mice in the Kondziela's inverted screen test. **(F)** Body weight of 5-months-old female AgRP *Cpt1a* KO and control mice. Data are expressed as mean ± SEM. *P<0.05 by the two-tailed Student's t-test. The graph C was analysed by the Gehan-Breslow-Wilcoxon survival curves test. n= 6-7.

Since no remarkable changes in endurance and strength in female AgRP *Cpt1a* KO mice, only male mice were evaluated in the subsequent experiments.

4.6. Effect of exercise on feeding and glucose levels in AgRP *Cpt1a* KO mice

The role of hypothalamic AgRP neurons in the regulation of food intake is widely demonstrated (56,71) These neurons play a key role in promoting feeding. They are activated by peripheral orexigenic signals such as ghrelin (256), and inactivated by anorexigenic signals like leptin (170), insulin (71) and CCK (8).

Based on these data, a 6h fast and refeed test were performed in 5-months-old mice with and without a single acute treadmill training (14 m/min for 2h). Blood glucose levels were measured after 6h of fasting, where groups with acute exercise spent the last 2h running on the treadmill. After acute treadmill exercise, AgRP *Cpt1a* KO mice showed an increase in glycemia compared to the sedentary group, but no changes were observed in the control group due to the exercise input (*Figure 38A*). In addition, AgRP *Cpt1a* KO showed a reduction in cumulative food intake after 6h-fasted (*Figure 38B*), but this reduction was altered after a single bout of exercise (*Figure 38C*). These data support the relevance of AgRP neurons in the control of feeding behaviour and the role of exercise and lipid metabolism as modulators of AgRP neurons regulation.

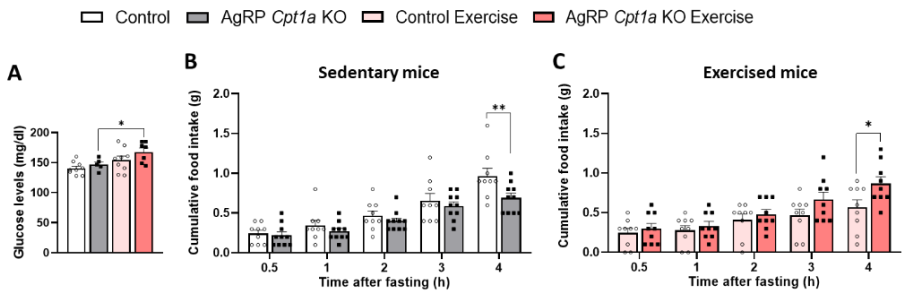

Figure 38. Evaluation of glucose and cumulative food intake under exercise conditions. (A) Blood glucose levels from 5-months-old mice AgRP *Cpt1a* KO and control mice after sedentary or an acute exercise on the treadmill. **(B-C)** Cumulative food intake after 6h-fasted in sedentary mice **(B)** or 6h-fasted, where mice run on the treadmill the two last hours **(C)**. Data expressed as mean ± SEM. *P<0.05; **P<0.01 by 2way ANOVA followed by Sidak's multiple comparisons. n= 5-10.

4.7. Effect of Cpt1a in AgRP neurons on muscle mass and CSA in the GAS muscle

To evaluate the muscle mass, mice were sacrificed at 5-months-old. After the sacrifice, different muscles (GAS, QUA, TA, EDL, and SOL) were dissected and weighed to determine the muscle mass. Instead of using the body weight to normalise the muscle mass, we decided to use the length of the tibia because it

remains constant after maturity, while fluctuations in body weight are common during aging making body weight an unreliable reference for normalising muscle and heart weight.

As a result, a dramatic reduction in the muscle mass of the QUA and GAS muscles was observed (GAS, 8.06 ±0.637 mg/mm *vs.* 8.94 ±0.557 mg/mm, **P<0.01; QUA, 10.15 ±0.981 mg/mm *vs.* 12.16 ±1.037 mg/mm, ***P<0.001) (*Figure 39A*). However, no differences were detected in the TA, EDL, and SOL muscles (*Figure 39B*). A decrease in muscle mass is generally associated with a reduction of muscle strength. However, AgRP *Cpt1a* KO mice did not show changes in the strength test performed in comparison to control mice.

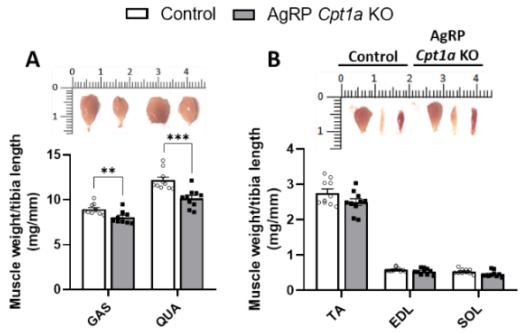

Figure 39. Analysis of the muscle mass of AgRP Cpt1a KO mice. Muscle mass of GAS and QUA muscles **(A)** and TA, EDL, and SOL muscles **(B)**. Muscle mass was normalised by the tibia length expressed in millimetres. Data are expressed as mean ± SEM. *P<0.05; **P<0.01; ***P<0.001 by the two-tailed Student's t-test. n= 9-10.

To explain these changes, we proceed to analyse the muscle histology and fibre size of the GAS and TA muscles (*Figure 40*). First, we analysed the morphology and CSA of gastrocnemius muscle sections stained with H&E. Interestingly, the GAS muscle of AgRP *Cpt1a* KO mice showed a reduction in the CSA compared to control littermates (1570.46 ±268.577 μm^2 *vs.* 1980.18 ±278.621 μm^2, ***P<0.001) (*Figure 40A and 40B*). In agreement with this result, AgRP *Cpt1a* KO mice exhibited a significant increase in the proportion of 500-1.000 μm^2 myofibres and a decrease in the number of 2.500-3.000 and 3.500-4.000 μm^2 muscle fibres (*Figure 40C*).

These alterations in the CSA and myofibre distribution could explain the differences in the physical behaviour of AgRP *Cpt1a* KO mice.

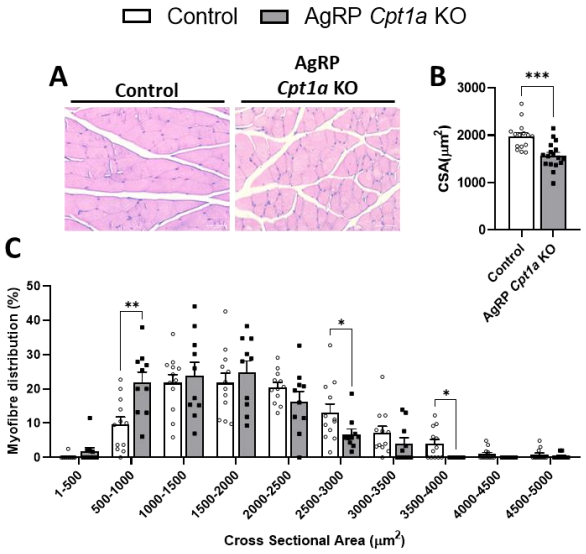

Figure 40. Morphometric analysis in the GAS muscle of AgRP *Cpt1a* KO mice. (A) Representative images of GAS muscle sections stained with H&E. Scale bar: 50 µm (magnification 40x). **(B-C)** Cross-sectional area quantification **(B)** and myofibre CSA distribution **(C)** of the GAS muscle. Data are expressed as mean ± SEM. *P<0.05; **P<0.01; ***P<0.001 by the two-tailed Student's t-test. The graph C was analysed by 2way ANOVA followed by Sidak's multiple comparisons. n= 9-10.

4.8. *Cpt1a* ablation in AgRP neurons alters myofibre composition of the GAS muscle

Type I myofibres are characterised by high oxidative capacity and red appearance due to the high mitochondria and myoglobin content. Type II myofibres are white and bigger in appearance and they exhibit a higher glycolytic capacity in comparison to type I myofibres. The fibre composition of each muscle is variable, and transition between muscle fibres can occur depending on the exercise performed. Endurance exercise promotes an increase in oxidative muscle fibres, while strength exercise increases the proportion of type II myofibres.

Myofibre composition was examined (1) by immunofluorescence using specific antibodies for the main myosin heavy chain isoforms of each muscle fibre [oxidative (type I): *Myh-7* and glycolytic (type II): *Myh-1, Myh-2,* and *Myh-4*], (2) by qRT-PCR and (3) by the mitochondrial DNA content in the GAS muscle.

Results from immunofluorescence quantification showed that AgRP *Cpt1a* KO mice exhibited a higher proportion (8.45 ±0.685 *vs.* 5.43 ±0.441, ****P<0.0001) and smaller CSA of type I myofibres (912.90 ±67.180 μm^2 *vs.* 1146.68 ±105.910 μm^2, ***P<0.001) compared to control littermates (*Figure 41*). Additionally, no changes were observed in the CSA or distribution of type II muscle fibres in the GAS of both groups of mice (*Figure 41B* and *41C*).

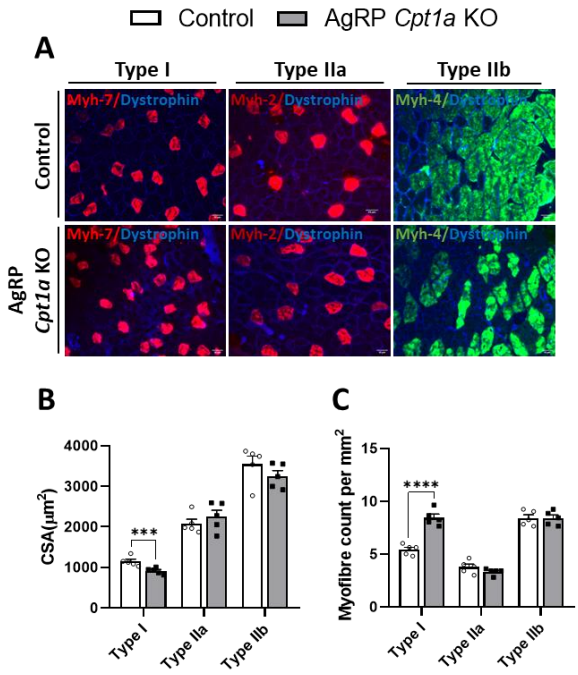

Figure 41. Analysis of the myofibre composition of the gastrocnemius muscle from *AgRP* Cpt1a KO mice. (A) Specific immunofluorescence evaluation of the different myosin heavy chain proteins. Muscle fibres are labelled with dystrophin, a protein of the muscle cell membrane (blue). Scale bar: 50 µm (magnification 40x). **(B)** Cross-sectional area of each fibre type in the GAS muscle**. (C)** Quantification of fibre types per mm^2. Data are expressed as mean ± SEM. *P<0.05; **P<0.01; ***P<0.001; ****P<0.0001 by the two-tailed Student's t-test. Six different images of the GAS were examined per mice. n= 5.

Before the analysis of the mRNA levels of the different *Myh* genes by qRT-PCR, we validated the effect of the acute exercise performed before the sacrifice by analysing the mRNA levels of three genes up-regulated after a single bout of exercise: *Il-6*, peroxisome proliferator-activated receptor alpha (*Pparα*) and *Pgc1α*. We also analysed the levels of cortisone and catecholamines (adrenaline and noradrenaline) in plasma (*Figure 42*).

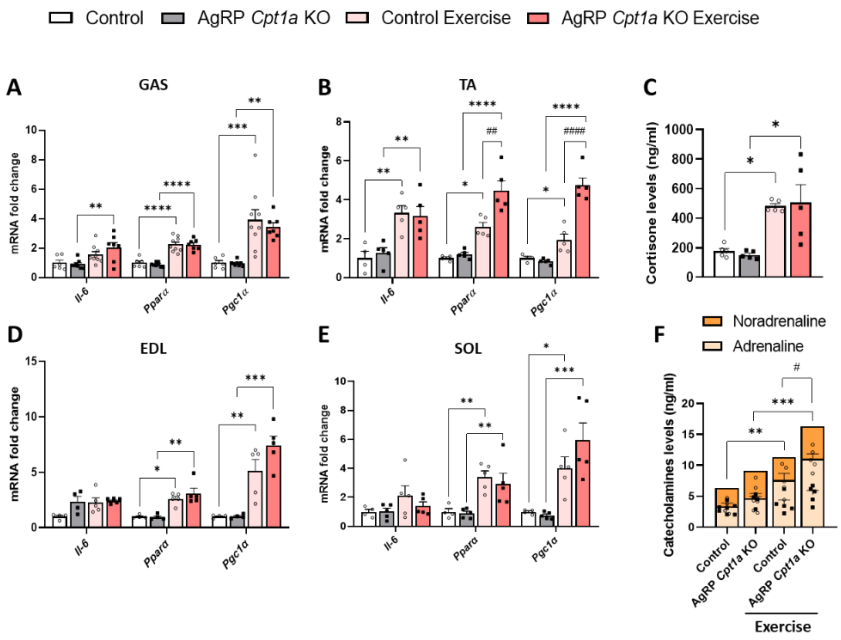

Figure 42. Validation of the exercise protocol performed before the sacrifice. Analysis of the mRNA levels of *Il-6*, *Pparα* and *Pgc1α* in the GAS **(A)** TA **(B)** EDL **(D)** and SOL **(E)** muscles of AgRP *Cpt1a* KO and control mice normalised by the *Rpl32* gene. Plasma cortisone **(C)** and catecholamines levels **(F)** of AgRP *Cpt1a* KO and control mice after sedentary or acuate exercise. Data are expressed as mean ± SEM. *P<0.05; **P<0.01; ***P<0.001; ****P<0.0001 by 2way ANOVA followed by Sidak's multiple comparisons. # is used to describe statistical differences between different genetic groups (KO and control) under the same condition (exercise or sedentary). n= 4-7.

The running protocol performed before the sacrifice of mice promoted an increase in the mRNA levels of *Pparα* and *Pgc1α* in all muscles analysed. Indeed, the TA of AgRP *Cpt1a* KO showed a significant increase compared to control mice (*Figure 42B* and *42E*). The increase in the mRNA levels of *Il-6* was controversial due to their anti- (myokine) and pro-inflammatory effects. However, in terms of

exercise, Il-6 acts as a myokine with anti-inflammatory effects. The GAS and TA muscles exhibited a stimulation in the mRNA levels of *Il-6*, while the EDL and SOL muscles show a trend to increase after the running activity.

Plasma levels of cortisone (*Figure 42C*), adrenaline and noradrenaline (*Figure 42F*) increased in both groups after exercise. In addition, exercised AgRP *Cpt1a* KO mice showed an increase in adrenaline and noradrenaline levels compared to control mice, suggesting a possible role of the SNS in response to physical activity. Altogether, these results validated the protocol of running before the sacrifice used in this study.

Once the running protocol was validated, we analysed the mRNA levels of genes associated with myofibre composition, muscle remodelling and denervation (*Figure 43*). AgRP *Cpt1a* KO mice exhibited increased mRNA levels of fibre type I (*Myh-7*) in comparison to control mice, even in sedentary conditions (*Figure 43B*). In addition, a high decrease in the mRNA levels of type IId muscle fibres (*Myh-1*) was observed under exercise conditions in AgRP *Cpt1a* KO mice compared to control littermates. Both groups displayed an increase in the mRNA levels of type IIa myofibres (*Myh-2*), the most oxidative type II fibre due to the type of exercise performed.

The mRNA levels of genes related to muscle remodelling and denervation were also studied (*Figure 43C*). AgRP *Cpt1a* KO mice did not exhibit significant changes in most of the genes analysed, but the mRNA levels of *Murf1* and the nuclear factor erythroid 2 (*Nrf2)* were increased under exercise conditions. Both genes play a relevant role in muscle remodelling. On the one hand, *Murf1* is activated under stress conditions such as exercise promoting muscle atrophy. On the other hand, *Nrf2* is involved in the maintenance of redox homeostasis and its expression starts under stress conditions. Interestingly, the mRNA levels of muscle specific receptor tyrosine kinase (*Musk),* an essential factor for neuromuscular synapse formation, is increased in acute treadmill exercise AgRP *Cpt1a* KO.

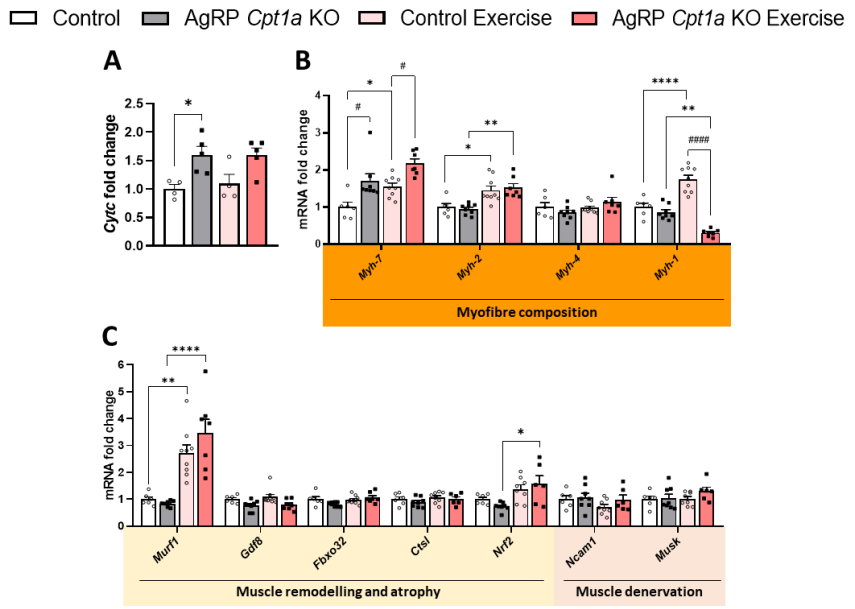

Figure 43. Analysis of myofibre composition in the gastrocnemius of *AgRP* Cpt1a KO mice. (A) Analysis of mtDNA content. **(B-C)** Analysis of mRNA levels of genes associated with myofibre composition **(B)**, muscle remodelling and denervation **(C)** of AgRP *Cpt1a* KO and control mice normalised by the *Rpl32* gene. *Ctsl*: cathepsin L1; *Fbxo32*: F-box protein 32, atrogin-1; *Gdf8*: growth differentiation factor 8, myostatin; *Musk*: muscle specific receptor tyrosine kinase and *Ncam1*: neural cell adhesion molecule 1 Data are expressed as mean ± SEM. *P<0.05; **P<0.01; ***P<0.001; ****P<0.0001 by 2way ANOVA followed by Sidak's multiple comparisons. # is used to describe statistical differences between different genetic groups (KO and control) under the same condition (exercise or sedentary). n= 4-8.

These findings suggest a myofibre transition from glycolytic type IId to oxidative type I fibres in AgRP *Cpt1a* KO mice. To confirm this, we measured the mtDNA content by the quantification of *Cytc* levels, a specific gene encoded by the mitochondrial genome, and it was normalised by the nuclear gene *Sdha*. The results of this analysis showed that AgRP *Cpt1a* KO mice exhibited a higher mtDNA content and this could explain the differences in physical activity (*Figure 43A*).

To study other pathways that could be affected by the specific deletion of *Cpt1a* in AgRP neurons, we analysed some genes associated with glucose and lipid metabolism, mitochondrial dynamics, and angiogenesis (*Figure 44*).

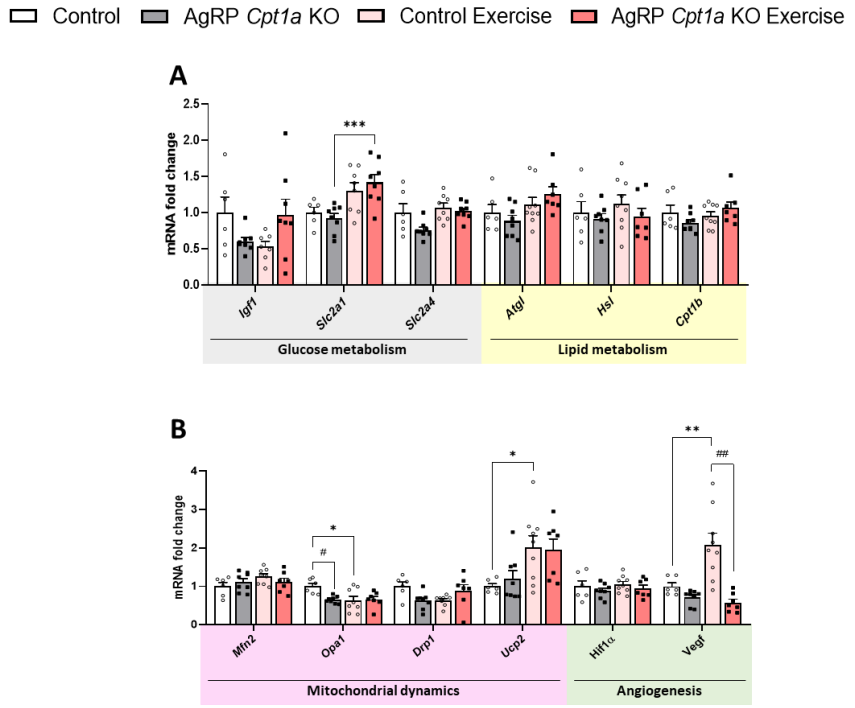

Figure 44. Analysis of different cellular pathways by qRT-PCR in the gastrocnemius of *AgRP* Cpt1a KO mice. Analysis of mRNA levels of genes associated with glucose and lipid metabolism **(A),** mitochondrial dynamics and angiogenesis **(B)** in AgRP *Cpt1a* KO and control mice normalised by the *Rpl32* gene. *Drp1*: dynamin-related protein 1; *Hif1α*: hypoxia inducible factor 1 alpha and *Mfn2*: mitofusin 2. Data are expressed as mean ± SEM. *P<0.05; **P<0.01; ***P<0.001; ****P<0.0001 by 2way ANOVA followed by Sidak's multiple comparisons. # is used to describe statistical differences between different genetic groups (KO and control) under the same condition (exercise or sedentary). n= 4-5.

No significant changes were observed in glucose and lipid metabolism of sedentary and acute exercise groups, only an increase in the glucose transporter 1 (*Slc2a1*) because of physical activity. In addition, AgRP *Cpt1a* KO mice showed a reduction in mRNA levels of optic atrophy 1 (*Opa1)* gene, a key regulator of mitochondria shape by its role in the fusion process in sedentary conditions. Moreover, acute exercise AgRP *Cpt1a* KO mice displayed a reduction in the mRNA levels of vascular endothelial growth factor (*Vegf*). The protein encoded by this gene promotes the growth of new blood vessels. A decrease in its expression during exercise is unusual, but it could occur if muscle cells are not deprived of oxygenated blood during the exercise performance.

4.9. Cpt1a in AgRP neurons is involved in myofibre composition of the TA muscle

The effect of *Cpt1a* deletion in AgRP neurons was also studied in the TA muscle. Even though we did not observe differences in the TA muscle mass, the analysis of muscle H&E cross-sections showed a 10% reduction in the CSA of AgRP *Cpt1a* KO mice in comparison to control littermates (1784.43 ±115.125 μm^2 *vs.* 1930.94 ±69.722 μm^2, *P<0.05) (*Figure 45A and 45B*). In addition, the myofibre distribution revealed the same pattern observed in the GAS muscle, where AgRP *Cpt1a* KO mice showed an increase in the CSA of TA myofibres between 500-1.000 μm^2 (*Figure 45C*).

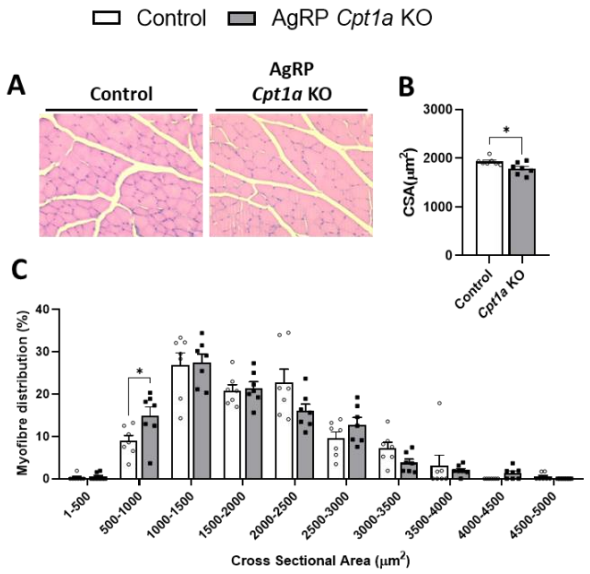

Figure 45. Morphometric analysis in the tibialis anterior muscle of AgRP *Cpt1a* KO mice. (A) TA muscle sections stained with H&E from AgRP *Cpt1a* KO and control mice. Scale bar: 50 μm (magnification 40x). **(B)** Cross-sectional area quantification of the TA muscle. **(C)** TA myofibre distribution. Data are expressed as mean ± SEM. *P<0.05; **P<0.01; ***P<0.001 by the two-tailed Student's t-test. The graph C was analysed by 2way ANOVA followed by Sidak's multiple comparisons. n= 7.

To evaluate the muscle fibres composition, 15-μm thick sections of TA muscle were incubated with specific antibodies against different myosin heavy

chain isoforms *(Figure 46A*). Interestingly, despite no showing differences in the CSA (1138.79 ±250.677 μm^2 *vs.* 1478.08 ±229.278 μm^2), the number of type I myofibres in AgRP *Cpt1a* KO mice was increased (7.57 ±1.602 *vs.* 5.51 ±0.738, *P<0.05) *(Figure 46B* and *46C*). This mouse model also showed a higher CSA in type IIa myofibres compared to control littermates, but no differences in number were detected.

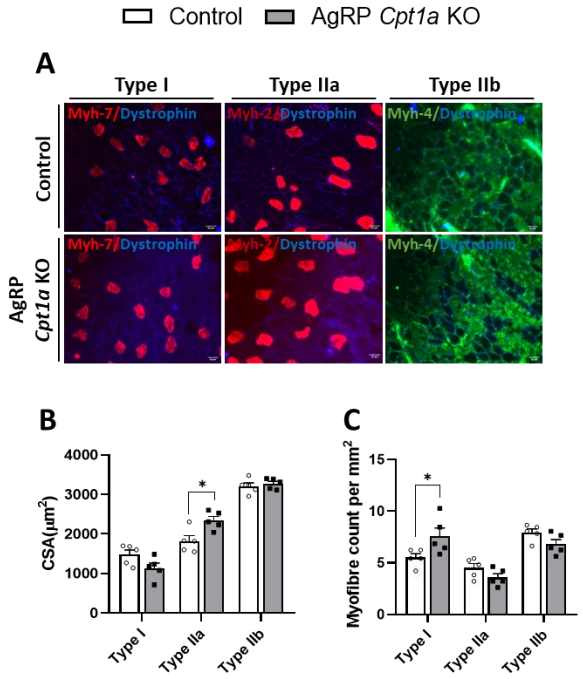

Figure 46. Analysis of myofibre composition in the tibialis anterior muscle of AgRP *Cpt1a* KO mice. (A) Specific immunofluorescence evaluation of different isoforms of the myosin heavy chain protein. Muscle fibres are co-incubated with dystrophin, a protein of the muscle cell membrane (blue). Scale bar: 50 μm (magnification 40x). **(B)** Cross-sectional area of each fibre type in the tibialis anterior muscle**. (C)** Quantification of specific fibre type per area expressed in mm^2. Data are expressed as mean ± SEM. *P<0.05 by the two-tailed Student's t-test. Five images of different TA regions per mice were examined. n= 5.

Similar results were observed in the mRNA levels of different myofibre types. Mice lacking *Cpt1a* in AgRP neurons exhibited an increase in the mRNA levels of *Myh-7* and, this increase was higher under exercise conditions compared to control

littermates. In addition, a significant increase in the mRNA levels of *Myh-2* were detected in control mice under an acute exercise on the treadmill (*Figure 47A*).

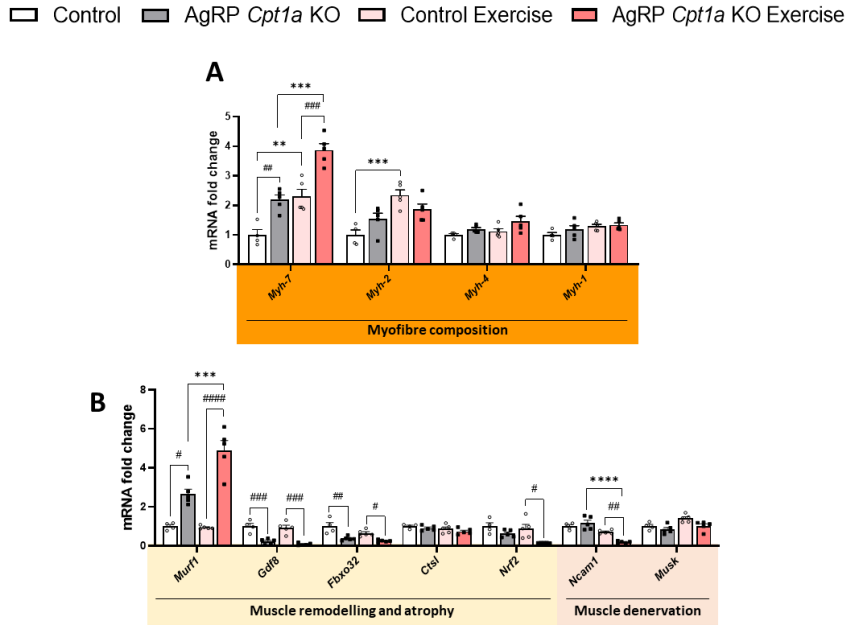

Figure 47. Analysis of myofibre composition in the tibialis anterior of AgRP *Cpt1a* KO mice. (A-B) Analysis of the mRNA levels of genes associated with myofibre composition **(A)**, muscle remodelling and denervation **(B)** of AgRP *Cpt1a* KO and control mice normalised by the *Rpl32* gene. Data are expressed as mean ± SEM. *P<0.05; **P<0.01; ***P<0.001; ****P<0.0001 by 2way ANOVA followed by Sidak's multiple comparisons. # is used to describe statistical differences between different genetic groups (KO and control) under the same condition (exercise or sedentary). n= 4-5.

Several genes related to muscle remodelling and denervation were also analysed in the TA muscle (*Figure 47B*). The atrophy gene *Murf-1* increased its mRNA levels in both sedentary and acute exercise AgRP *Cpt1a* KO mice, while a reduction in the growth differentiation factor 8 (*Gdf-8*, myostatin), *Fbxo32* (atrogin-1) and *Nrf2* was observed. Myostatin is a negative regulator of the muscle growth that acts at autocrine and paracrine levels while atrogin-1 plays a key role in muscle atrophy. A decrease in the mRNA levels of these genes suggest an inhibition of the TA atrophy and an enhancement in muscle hypertrophy. In addition, the mRNA levels of neural cell adhesion molecule 1 (*Ncam1*), a molecule that plays a key role

in the development and plasticity of the neuromuscular junction, are decreased under acute exercise in AgRP *Cpt1a* KO mice.

The mRNA levels of genes associated with glucose, lipid metabolism, mitochondrial dynamics, inflammation, and angiogenesis was analysed to determine the effect of *Cpt1a* deletion in AgRP neurons on skeletal muscle (*Figure 48*). The mRNA levels of *Igf-1* and *Slc2a1* were increased in AgRP Cpt1a KO mice in sedentary and exercise conditions, but this increase was higher in exercised animals. AgRP *Cpt1a* KO mice under acute exercise also showed an increase in the hexokinase 2 (*Hk2*), a key regulator of glycolysis pathway, suggesting an activation of glycolytic pathway in these mice. In addition, the mRNA levels of genes associated with lipolysis [fatty acid binding protein 3 (*Fabp3*), *Atgl* and *Hsl*] and fatty acid oxidation (*Cpt1b*) were increased in acute exercise and sedentary AgRP *Cpt1a* KO mice (*Figure 48A*).

Regarding mitochondrial dynamics, a significant increase in mitofusin 2 (*Mfn2*) and *Ucp2* in exercised AgRP *Cpt1a* KO mice were observed (*Figure 48B*). In addition, an increase in *Socs3*, pro- (*Il-1β*) and anti-inflammatory [interleukin 10 (*Il-10*) and CXC motif chemokine ligand 1 (*Cxcl1*)] mRNA levels were observed in acute exercise AgRP *Cpt1a* KO mice in comparison to control littermates. These changes are usual after exercise performance, but this increase in AgRP *Cpt1a* KO mice could indicate an improvement of inflammation process in response to a stress such as exercise. Moreover, acute exercise AgRP *Cpt1a* KO mice displayed a reduction in the expression of hypoxia inducible factor 1-alpha (*Hif1α*) and *Vegf* genes. As it was shown in the GAS muscle, a decrease in the mRNA levels of these genes during exercise is unusual, but it could occur if muscle cells are not deprived of oxygenated blood.

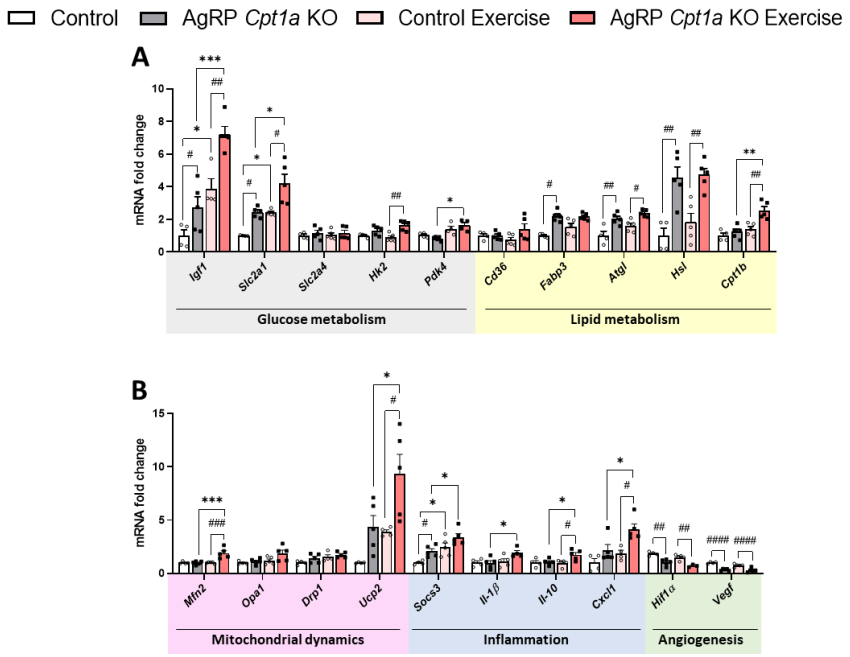

Figure 48. qRT-PCR analysis of different metabolic pathways of AgRP *Cpt1a* KO tibialis anterior muscle. **(A-B)** Analysis of the mRNA levels of genes associated with glucose and lipid metabolism **(A)**, mitochondrial dynamics, inflammation, and angiogenesis **(B)** in the TA of AgRP *Cpt1a* KO and control mice normalised by the *Rpl32* gene**.** Data are expressed as mean ± SEM. *P<0.05; **P<0.01; ***P<0.001; ****P<0.0001 by 2way ANOVA followed by Sidak's multiple comparisons. # is used to describe statistical differences between different genetic groups (KO and control) under the same condition (exercise or sedentary). n= 4-5.

To confirm these results, protein levels of different regulatory enzymes were analysed by Western Blot (*Figure 49*). Despite the changes in mRNA levels, no differences in Cpt1b and Ucp2 protein were observed. To know if the SNS was orchestrating this myofibre remodelling we also measured the protein levels of tyrosine hydroxylase (Th). However, no changes were detected in Th protein levels in the TA muscle. The pAmpk/Ampk ratio shows the cell energy status due to the role of Ampk in the regulation of energy homeostasis. AgRP *Cpt1a* KO mice showed a 2-fold increase under exercise conditions compared to the control group.

Overall, these findings suggest that the tibialis anterior muscle of AgRP *Cpt1a* KO mice show a transition from glycolytic to oxidative fibres and an

improvement in the neuromuscular denervation, glycolysis, lipolysis, and fatty acid oxidation pathways. Furthermore, they exhibit a reduction in inflammatory response and a better energy status in exercise conditions.

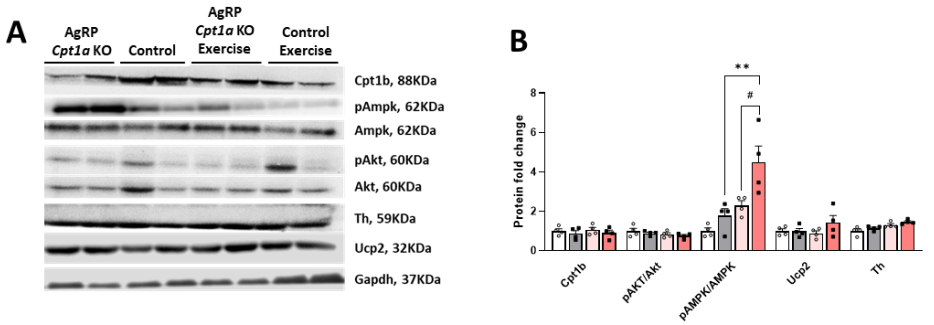

Figure 49. Analysis of protein levels in the tibialis anterior muscle of AgRP *Cpt1a* KO mice. (A) Representative Western Blot assay where 25 µg of denatured proteins were loaded in each well. **(B)** Quantification of protein levels normalised by the Gapdh protein. Data are expressed as mean ± SEM. *P<0.05; **P<0.01 by 2way ANOVA followed by Sidak's multiple comparisons. # is used to describe statistical differences between different genetic groups (KO and control) under the same condition (exercise or sedentary). n= 4-5.

4.10. *Cpt1a* deletion in AgRP neurons does not alter mitochondrial respiration in the TA muscle

Variations in the myofibre composition and mitochondrial content carried out to study the respirometry oxidative phosphorylation (OXPHOS) in the Oroboros instrument. 5-months-old mice were sacrificed u and TA muscles were collected. Using a sharp forceps, fibre bundles were separated, and 2-4 mg of fibre bundles from sedentary and acute exercise treadmill mice were transferred into the oxygraph chamber for the determination of the oxygen consumption after sequential injections of different substrates and inhibitors. (1) The addition of glutamate/malate (GM) into the chamber in saturating ADP conditions (GMD) stimulates the reduction of nicotinamide adenine dinucleotide (NAD^+ to NADH) generating electrons to the mitochondrial complex I and III. (2) The injection of succinate (Succ) activates the complex II. (3) The administration of the uncoupler

(FCCP) provides the maximal respiration rate, and inhibitors (rotenone for complex I and antimycin A for complex III) block the mitochondrial respiration.

As we can observe in the *Figure 50*, the mitochondrial respiration was not altered. We observed a higher oxygen consumption in acute exercise AgRP *Cpt1a* KO mice compared to AgRP *Cpt1a* KO sedentary group after the injection of ADP.

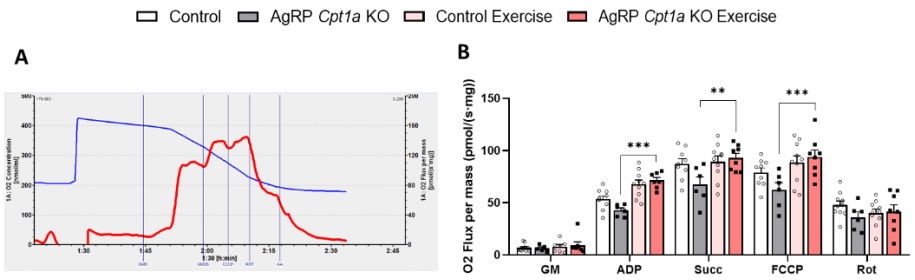

Figure 50. Mitochondrial respiration analysis of permeabilised fibres from the tibialis anterior muscle. **(A)** Representative scheme of high-resolution respirometry performed in the Oroboros Oxygraph. The blue curve shows the oxygen concentration, and the red curve shows the oxygen consumption of the fibres in the chamber. **(B)** Oxygen consumption after the addition of different substrates and inhibitors into the Oroboros chamber. Data are expressed as mean ± SEM. *P<0.05; **P<0.01 by 2way ANOVA followed by Sidak's multiple comparisons. # is used to describe statistical differences between different genetic groups (KO and control) under the same condition (exercise or sedentary). n= 5.

4.11. Effect of *Cpt1a* ablation in AgRP neurons on EDL and SOL muscles

Gastrocnemius and tibialis anterior muscles are considered as mixed muscles because they exhibit approximately a substantial proportion of both muscle fibre types (30% of type I and 70% of type II). However, the extensor digitorum longus muscle is considered as a glycolytic muscle due to the high number of type II myofibres (almost 99%), while the SOL contains predominantly around 80% of type I myofibres, considering as a oxidative muscle (114).

The fibre composition of these two muscles were measured by qRT-PCR in mice under sedentary and acute exercise treadmill conditions (*Figure 51A* and *52A*). In the EDL muscle, a decrease in the mRNA levels of *Myh-4* was observed in the

control group after exercise. However, AgRP *Cpt1a* KO mice did not show changes in the mRNA levels of different myosin heavy chains. Furthermore, no differences were observed in the oxidative SOL muscle (*Figure 52A*). In both muscles, an increase in the atrophy gene *Murf1* was detected in AgRP *Cpt1a* KO and control mice under sedentary and acute exercise conditions.

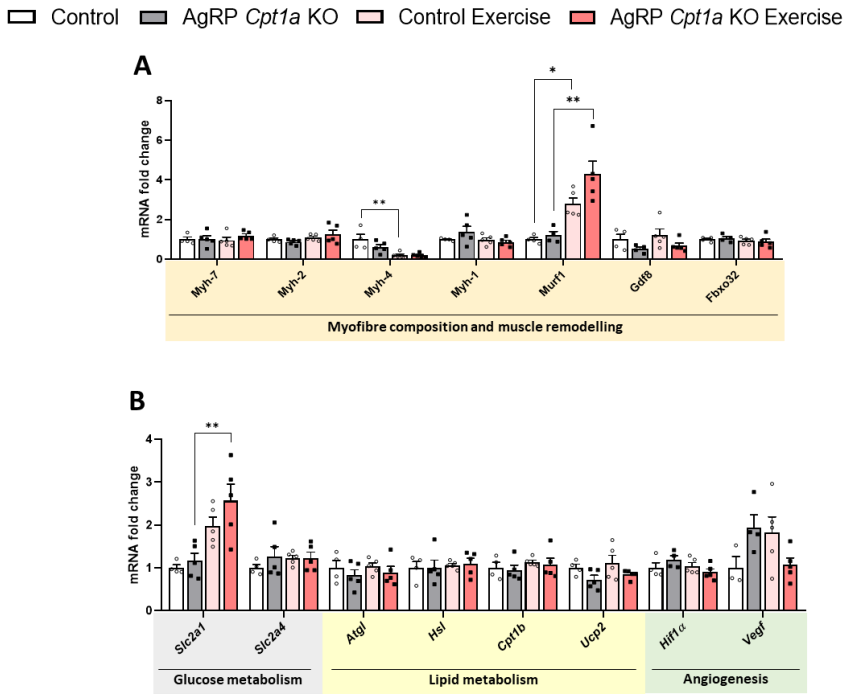

Figure 51. mRNA levels analysis of the extensor digitorium longus from AgRP *Cpt1a* KO mice. (A-B) Analysis of the mRNA levels of genes associated with myofibre composition, muscle remodelling **(A)**, glucose and lipid metabolism and angiogenesis **(B)** in AgRP *Cpt1a* KO and control mice normalised by the *Rpl32* gene. Data are expressed as mean ± SEM. *P<0.05; **P<0.01; ***P<0.001; ****P<0.0001 by 2way ANOVA followed by Sidak's multiple comparisons# is used to describe statistical differences between different genetic groups (KO and control) under the same condition (exercise or sedentary). n= 3-5.

The mRNA levels of pathways involved in exercise performance were analysed in both muscles. We observed an increase in glucose transporters genes (*Slc2a1* and *Slc2a4*) of both AgRP *Cpt1a* KO and control after exercise performance (*Figure 51B* and *52B*) in the EDL and TA muscles. Moreover, an activation of lipolysis

after an acute exercise was observed in the SOL of both control and AgRP *Cpt1a* KO mice. However, no changes in the angiogenesis process were detected in both muscles.

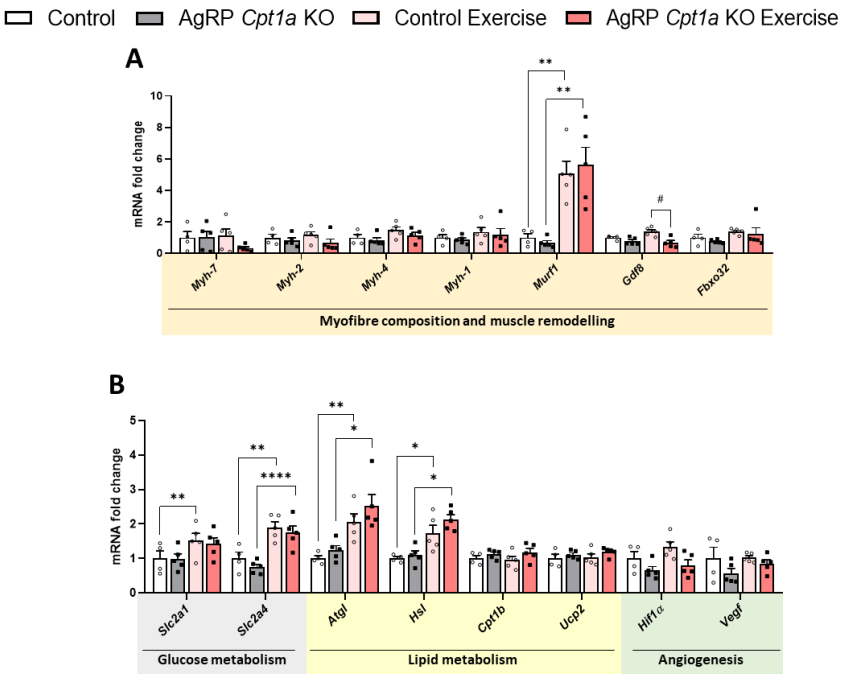

Figure 52. mRNA levels analysis of the soleus from AgRP *Cpt1a* KO mice. (A-B) Analysis of mRNA levels of genes associated with myofibre composition, muscle remodelling **(A)**, glucose and lipid metabolism and angiogenesis **(B)** in AgRP *Cpt1a* KO and control mice normalised by the *Rpl32* gene. Data are expressed as mean ± SEM. *P<0.05; **P<0.01; ***P<0.001; ****P<0.0001 by 2way ANOVA followed by Sidak's multiple comparisons. # is used to describe statistical differences between different genetic groups (KO and control) under the same condition (exercise or sedentary). n= 4-5.

Altogether, these results suggest that oxidative (SOL) and glycolytic (EDL) muscles are not dramatically affected by the lack of *Cpt1a* in AgRP neurons as opposed to mixed muscles (TA and GAS).

4.12. Analysis of the effect of *Cpt1a* deletion in AgRP neurons on other tissues

In addition to the effects in skeletal muscle, it is well-known that AgRP neurons regulate feeding behaviour through the modulation of peripheral tissues. Therefore, heart, liver and gWAT were analysed to study the impact of lipid metabolism in AgRP neurons under exercise conditions.

4.12.1. *Cpt1a* ablation in AgRP neurons exhibits an improvement in heart function

The effect of exercise in the heart is widely studied. Exercise has many benefits on heart health. Regular exercise can enhance the muscles' ability to pull oxygen out of the blood, reducing the need for the heart to pump more blood to muscles and decreasing inflammation, heart rate and blood pressure. In addition, several studies have demonstrated that regular exercise prevents the risk of suffering a sudden heart attack or cardiovascular problems (281). In addition, AgRP neurons can modulate the heart function through the SNS. Previous studies have demonstrated that an activation of this neuronal population leads to an increase in blood pressure due to the activation of the SNS (282).

Histological heart sections stained with H&E from 5-months-old mice were analysed. No morphological changes between AgRP *Cpt1a* KO mice and control littermates were observed (*Figure 53A*). However, the heart weight normalised by the tibia length showed a statistical reduction compared to the control group (62.61 ±6.628 mg/mm *vs.* 72.51 ±9.355 mg/mm, *P<0.05) (*Figure 53B*). This decrease could be explained by the difference in body weight between AgRP *Cpt1a* KO and control mice.

To go deeper in these changes, several genes related with heart function and inflammation were analysed by qRT-PCR. As it was expected, a reduction in the

mRNA levels of the heart isoform creatine kinase (*Ck*), myelin basic protein (*Mbp*) and Runx family transcription factor (*Runx*) 1 was observed under exercise conditions. Interestingly, an increase in GATA binding protein 4 (*Gata4*) in acute exercise AgRP *Cpt1a* KO mice, and a decrease in *Runx2* and brain natriuretic peptide (*Bnp*) in sedentary conditions were detected. Both genes are related with heart hypertrophy and maintenance of muscular function. These changes in the mRNA levels suggested an improvement in the cardiac function.

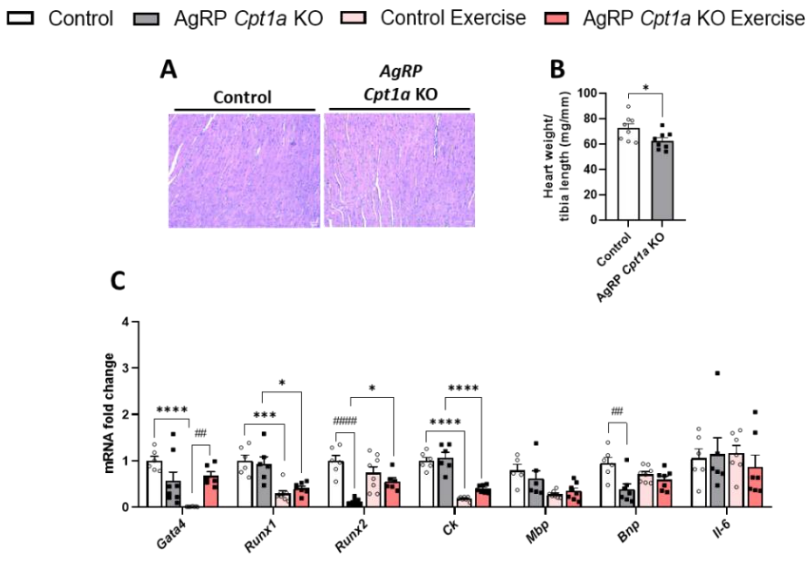

Figure 53. Morphological analysis and mRNA levels of heart from AgRP *Cpt1a* KO mice. **(A)** Representative images of heart sections stained with H&E. Scale bar: 50 µm (magnification 40x). **(B)** Heart weight was normalised by the tibia length. **(C)** Analysis of mRNA levels of genes associated with heart function and inflammation in AgRP *Cpt1a* KO and control mice normalised by the *Rpl32* gene. Data are expressed as mean ± SEM. *P<0.05; **P<0.01; ***P<0.001; ****P<0.0001 by 2way ANOVA followed by Sidak's multiple comparisons. The graph B was analysed by the two-tailed Student's t-test. # is used to describe statistical differences between different genetic groups (KO and control) under the same condition (exercise or sedentary). n= 5-8.

4.12.2. The lack of Cpt1a in AgRP neurons does not alter the liver gluconeogenesis induced by exercise

The link between AgRP neurons and liver is extensively studied. In this work, several genes associated with glucose and lipid metabolism were analysed in 5-

months-old mice after an aerobic exercise. Mice lacking *Cpt1a* in AgRP neurons showed a notably increase in phosphoenolpyruvate carboxykinase (*Pepck*) and pyruvate dehydrogenase 4 (*Pdk4)* that could indicate a higher gluconeogenesis after an exercise performance (*Figure 54*).

Regarding lipid metabolism, no changes were observed in the mRNA levels of *Cpt1a* gene. In addition, AgRP *Cpt1a* KO mice showed a reduction in the mRNA levels of Igf-1, the main mediator of growth hormone effects, in both sedentary and exercise conditions.

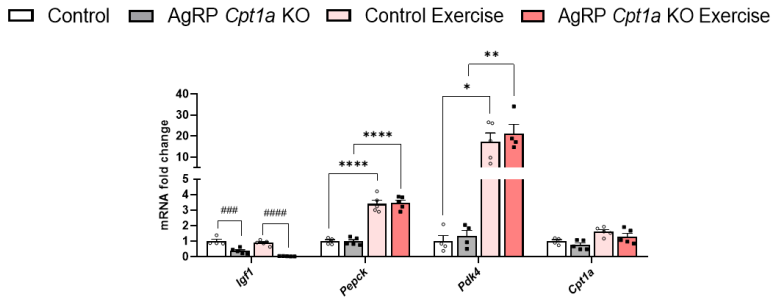

Figure 54. Evaluation of the mRNA levels in the liver of AgRP *Cpt1a* KO mice. mRNA levels were normalised by the β-actin gene. Data are expressed as mean ± SEM. *P<0.05; **P<0.01; ***P<0.001; ****P<0.0001 by 2way ANOVA followed by Sidak's multiple comparisons. # is used to describe statistical differences between different genetic groups (KO and control) under the same condition (exercise or sedentary). n= 5-8.

4.12.3. *Cpt1a* ablation in AgRP neurons decreases fatty acid synthesis in the gWAT

It is well-known that exercise increases the lipolytic pathway in the gWAT to provide glucose and free fatty acids to skeletal muscles to maintain their function. Therefore, we analysed some genes associated with lipolysis and fatty acid oxidation in the gWAT to know the effect of Cpt1a in AgRP neurons on this tissue under exercise conditions.

The results obtained by qRT-PCR suggested that AgRP *Cpt1a* KO mice show a reduction in fatty acid synthesis through the decrease in the mRNA levels of *Fas* and *Dgat2* in sedentary conditions (*Figure 55*). Furthermore, AgRP *Cpt1a* KO and

control mice showed an increase in the mRNA levels of genes related to fatty acid oxidation and transport (*Hsl* and *Cd36*) after an acute exercise. Nevertheless, no differences in *Atgl*, *Fabp3* and *Cpt1a* mRNA levels were observed between groups.

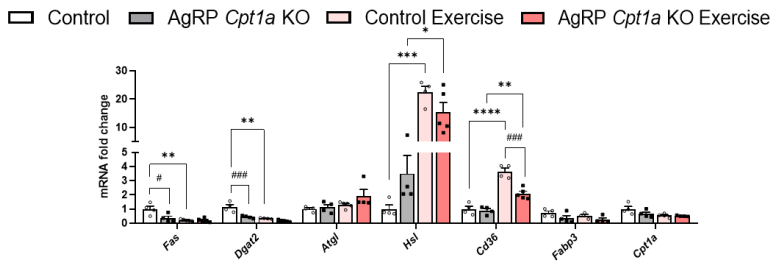

Figure 55. Evaluation of the gWAT mRNA levels from AgRP *Cpt1a* KO mice. mRNA levels were normalised by the *Hprt1* gene. Data are expressed as mean ± SEM. *P<0.05; **P<0.01; ***P<0.001; ****P<0.0001 by 2way ANOVA followed by Sidak's multiple comparisons. # is used to describe statistical differences between different genetic groups (KO and control) under the same condition (exercise or sedentary). n= 5-8.

4.13. Anti-aging effect of Cpt1a ablation in AgRP neurons

We also examined the role of *Cpt1a* deletion in AgRP neurons on exercise performance during the aging process since we observed that 10-months-old control mice have more grey hair on their backs than AgRP *Cpt1a* KO mice (*Figure 56B*). In the specific C57BL/6J mouse line, aged mice are considered from 18-24 months of age, characterised by senescent changes in aging biomarkers. In this study, several physical, cognition and behaviour tests were performed in18-months-old AgRP *Cpt1a* KO mice. Two months later, mice were sacrificed, and different tissues were collected for molecular analysis. The time-course followed is described in *Figure 56A*.

We observed a decrease of 22% in the Igf-1 levels of AgRP *Cpt1a* KO mice (368.77 ±51.855 ng/ml *vs.* 448.94 ±67.815 ng/ml, *P<0.05) (*Figure 56C*). The reduction in Igf-1 is associated with a decrease in the growth hormone signalling

and a reduction in the lifespan in rodents due to an improvement in stress defence and a lower risk for proliferative diseases (235,242,283).

Since we observed this decrease in the Igf-1 plasma levels of AgRP *Cpt1a* KO mice, we are studying the longevity of a new mice cohort which is still in progress. After 24-months-old, no differences were observed between both control and AgRP *Cpt1a* KO groups (*Figure 56D*).

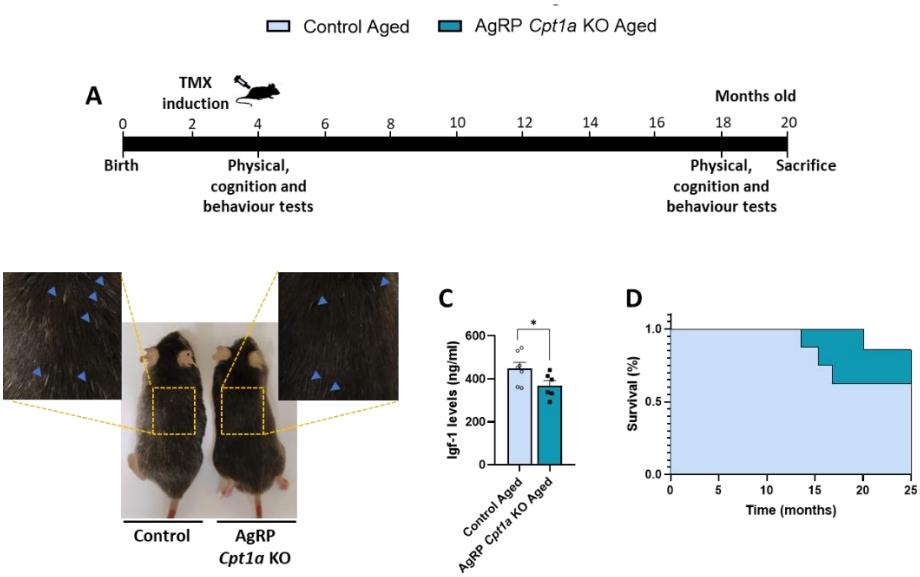

Figure 56. Analysis of the aging process in AgRP *Cpt1a* KO mice. (A) Experimental time-course. **(B)** Representative images of 20-months-old AgRP *Cpt1a* KO and control mice, focussing on the grey hair of their backs. **(C)** Plasma levels of Igf-1. **(D)** Survival rate of experimental mice after 24 months. Data are expressed as mean ± SEM. *P<0.05 by two-tailed Student's t-test. The graph D was analysed by the Gehan-Breslow-Wilcoxon survival curves test. n= 6-9.

4.14. The improvement in physical activity of young AgRP *Cpt1a* KO mice is maintained during aging

Physical capacity was assessed through the performance of different physical tests (endurance, inverted screen, and open field tests) at 18-months-old mice. Interestingly, aged AgRP *Cpt1a* KO mice exhibited a greater time on the

treadmill (97.76 ±8.945 minutes *vs.* 70.19 ±17.828 minutes, **P<0.01) and run a 58% more distance (1189.72 ±172.513 m *vs.* 750.03 ±236.907 m, **P<0.01) until exhaustion compared to control littermates (*Figure 57A* and *57B*). These data show that the decline in physical performance with the age is only shown in control mice.

Regarding muscle strength, the Kondziela's inverted screen test was performed. A reduction in the holding impulse was observed in both groups by the muscle decline during aging. However, only the aged control group exhibited a statistically decrease in strength in comparison to young groups (*Figure 57C*).

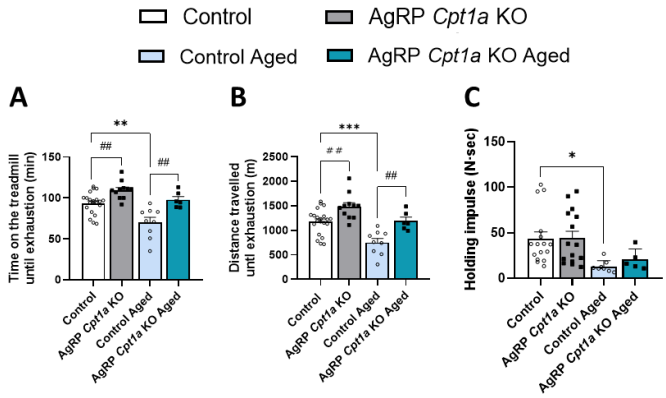

Figure 57. Evaluation of endurance and strength capacities in young and aged AgRP *Cpt1a* KO mice. (A-B) Analysis of endurance exhaustion test. Time **(A)** and distance travelled by mice until exhaustion **(B)**. **(C)** Holding impulse in the Kondziela's inverted screen test. The holding impulse was normalised by the body weight. Data are expressed as mean ± SEM. *P<0.05; **P<0.01; ***P<0.001; ****P<0.0001 by 2way ANOVA followed by Sidak's multiple comparisons. # is used to describe statistical differences between different genetic groups (KO and control) under the same age (young or old). n= 6-21.

Differences in locomotor activity, exploration and anxiety-like behaviour were analysed by the OFT. In agreement with the results of the exhaustion test, aged AgRP *Cpt1a* KO mice showed an improvement of 60% in locomotor activity (3376.47 ±799.154 m *vs.* 2050.99 ±440.764 m, **P<0.01) (*Figure 58A* and *58B*), explorative capacity (44.66 ±14.337 *vs.* 22.00 ±6.515, **P<0.01) (*Figure 58C*), and entries in the centre area (9.50 ±2.291 *vs.* 5.78 ±3.258, *P<0.05) (*Figure 58D*) in comparison to aged control mice. Aged control mice showed a reduction in locomotor and explorative capacities due to the decline in physical activity with the

age, while aged AgRP *Cpt1a* KO mice maintain their physical abilities, suggesting a possible role of Cpt1a as an anti-aging factor.

Regarding anxiety-like behaviour, aged mice did not shown changes in the time spent in the centre area (*Figure 58E*), but they exhibited increased number of grooms during the performance of the OFT (*Figure 58F*). This behaviour is a common feature in old mice. In addition, aged AgRP *Cpt1a* KO mice showed an increase in defecation during the performance of the test. These results could indicate an increase in emotional behaviour during aging.

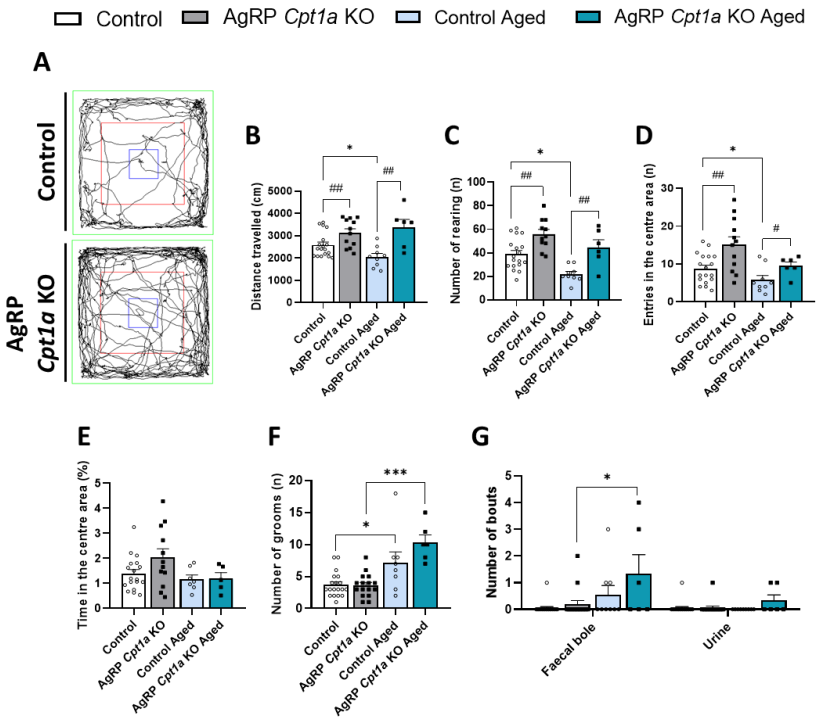

Figure 58. Analysis of the Open Field test in aged AgRP *Cpt1a* KO mice. **(A)** Illustrative images of aged control and AgRP *Cpt1a* KO mice travel pathways in the OFT. **(B)** Locomotor activity was analysed by the total distance travelled during the test. **(C-D)** Exploratory behaviour was measured through the number of rearings **(C)** and entries in the centre area **(D)** done by animals during the test. **(E-G)** Analysis of behaviour: time spent in the centre area **(E)**, number of grooms **(F)**, defecation and urination **(G)**. Data are expressed as mean ± SEM. *P<0.05; **P<0.01; ***P<0.001; ****P<0.0001by 2way ANOVA followed by Sidak's multiple comparisons. # is used to describe statistical differences between different genetic groups (KO and control) under the same age (young or old). n= 6-21.

Overall, AgRP *Cpt1a* KO mice maintain the improvement in exercise behaviour during aging, showing no signs of aging decline. Moreover, the enhancement in physical activity is not explained by changes in anxiety-like behaviour in aged mice.

4.15. *Cpt1a* ablation in AgRP neurons regulates the GAS myofibre composition in aged mice

As well as young mice, the muscle fibre composition in aged mice was studied to understand the differences in physical performance between AgRP *Cpt1a* KO and control mice. At 20-months-old, mice were sacrificed, and different muscles were collected for molecular analysis. During the sacrifice, the weight of the GAS and the QUA was measured to determine the muscle mass. Aged mice lacking *Cpt1a* in AgRP neurons displayed a reduction in muscle mass compared to control mice (GAS, 6.59 ±0.647 μm^2 *vs.* 8.43 ±0.422 μm^2, ***P<0.001; QUA, 8.31 ±0.887 μm^2 *vs.* 11.29 ±1.422 μm^2, ***P<0.001) (*Figure 59A*). The decrease in the muscle mass compared to young mice was observed in both groups due to the muscle atrophy associated with the decline of age.

Next, the morphology and the myofibre distribution of the GAS was examined in H&E muscle cross-sections (*Figure 59B, 59C and 59D*). As we have seen in the young group, aged AgRP *Cpt1a* KO mice showed a decrease in the CSA of GAS myofibres (1607.27 ±231.479 μm^2 *vs.* 1903.64 ±267.644 μm^2, *P<0.05). This reduction in the CSA could be explained by a decrease in the proportion of 2.500-3.000 μm^2 and 3.500-4.000 μm^2 GAS fibres from AgRP *Cpt1a* KO mice.

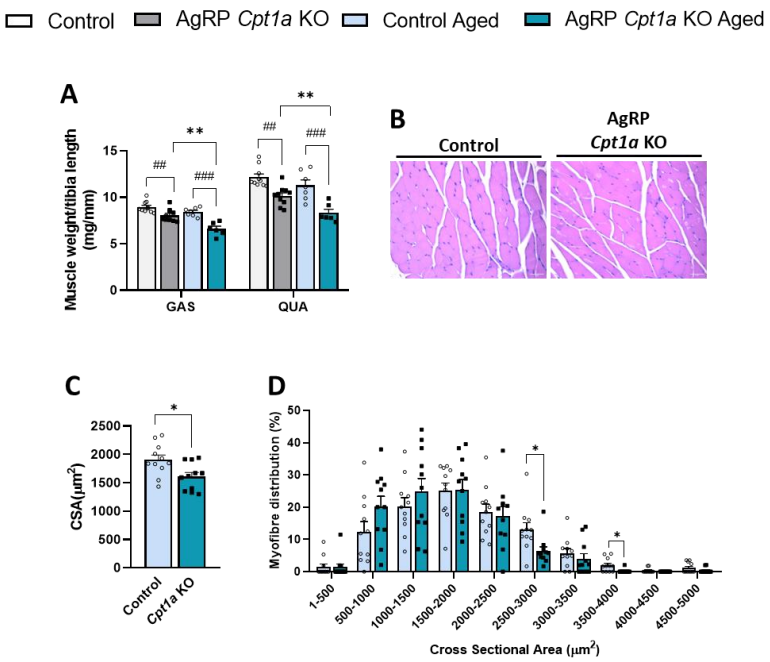

Figure 59. Morphometric analysis of the gastrocnemius muscle from aged AgRP *Cpt1a* KO mice. (A) Evaluation of muscle mass of the GAS and the QUA muscles in aged AgRP *Cpt1a* KO and control mice. **(B)** Representative images of GAS muscle cross-sections stained with H&E. Scale bar: 50 μm (magnification 40x). **(C)** Cross-sectional area quantification of the GAS muscle. **(D)** GAS myofibre distribution according to their CSA. Data are expressed as mean ± SEM. *P<0.05; **P<0.01; ***P<0.001 by the two-tailed Student's t-test. The graph A was analysed by 2way ANOVA followed by Sidak's multiple comparisons. # is used to describe statistical differences between different genetic groups (KO and control) under the same age (young or old). n= 6-9.

Once the CSA of the GAS muscle was analysed, immunofluorescent techniques were used to determine the fibre composition (*Figure 60A*). As a result, no differences were observed in the CSA of each fibre type (*Figure 60B*), but aged AgRP *Cpt1a* KO mice showed an increase in the number of type I myofibres in comparison to aged control mice (8.21 ±1.983 *vs.* 4.51 ±1.142, *P<0.05) (*Figure 60C*).

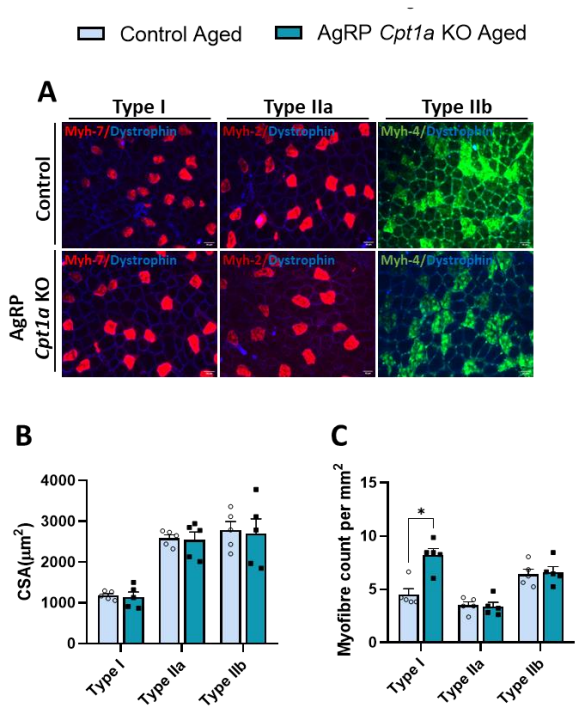

Figure 60. Myofibre composition analysis of the gastrocnemius muscle from aged AgRP *Cpt1a* KO mice. **(A)** Immunofluorescence evaluation of different myosin heavy chain proteins. The membrane of muscle fibres is labelled with dystrophin (blue). Scale bar: 50 μm (magnification 40x). **(B)** Cross-sectional area of each muscle fibre type in the GAS muscle. **(C)** Number of each fibre type per mm^2. Data are expressed as mean ± SEM. *P<0.05; **P<0.01; ***P<0.001; ****P<0.0001 by the two-tailed Student's t-test. Five images of different GAS regions per mice were examined. n= 5.

To corroborate these histological results, an analysis of the different myosin heavy chains genes was performed by qRT-PCR (*Figure 61A*). Aged AgRP *Cpt1a* KO mice showed an increase in *Myh-7* myofibres in agreement with the previous histological results. Moreover, a decrease in *Myh-2* compared to aged control mice was also observed. We studied genes associated with muscle remodelling and denervation. Mice lacking *Cpt1a* in AgRP neurons showed an increase in the mRNA levels of *Ncam1*, a protein related with neuromuscular junctions, and a decrease in muscle atrophy [Cathepsin L1 (*Ctsl*) and *Nrf2*] *(Figure 61B*). Both data could explain the differences in physical activity observed in aged mice.

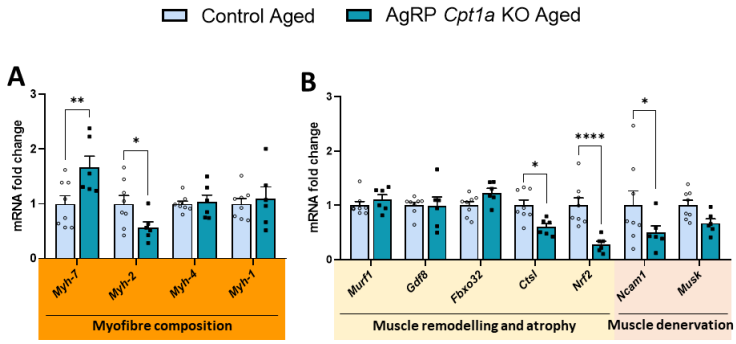

Figure 61. Evaluation of myofibres composition of the gastrocnemius from aged AgRP *Cpt1a* KO mice. Analysis of mRNA levels of genes associated with myofibre composition **(A)**, muscle remodelling and denervation **(B)** of aged AgRP *Cpt1a* KO and control mice normalised by the *Rpl32* gene. Data are expressed as mean ± SEM. *P<0.05; **P<0.01; ***P<0.001; ****P<0.0001 by the two-tailed Student's t-test. n= 6-9.

We also analysed other metabolic pathways that could be altered during aging by lipid metabolism in AgRP neurons (*Figure 62*). Unlikely to the exercise results in young mice (4 months-old), no differences were observed in the three genes selected to analyse the effect of exercise (*Il-6*, *Ppara* and *Pgc1a*). This fact could be explained because animals were not sacrificed after a single bout of aerobic exercise as we did in young groups.

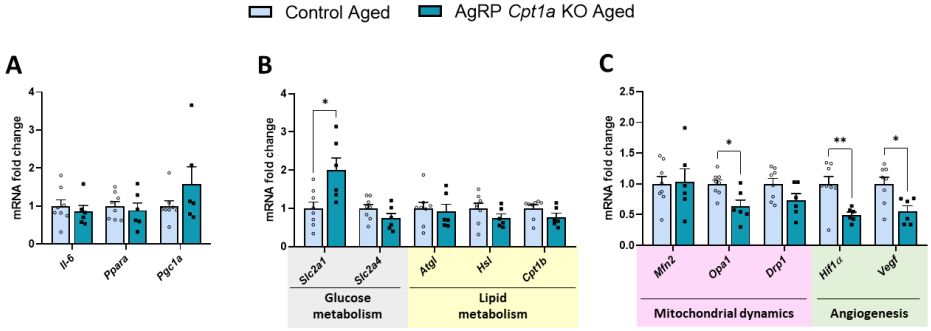

Figure 62. qRT-PCR Evaluation of different metabolic and signalling pathways in the gastrocnemius of *AgRP* Cpt1a KO mice. Analysis of mRNA levels of *Il-6*, *Ppara* and *Pgc1α* **(A),** glucose and lipid metabolism **(B),** mitochondrial dynamics and angiogenesis **(C)** of aged AgRP *Cpt1a* KO and control mice normalised by the *Rpl32* gene. Data are expressed as mean ± SEM. *P<0.05; **P<0.01by the two-tailed Student's t-test. n= 6-9.

Only the expression of the glucose transporter *Slc2a1* was increased in aged AgRP *Cpt1a* KO mice while no changes were observed in genes related to lipid metabolism (*Figure 62B*). In addition, aged mice lacking Cpt1a in AgRP neurons showed a decrease in *Opa1*, a protein involved in mitochondrial fusion process, and in the mRNA levels of *Hif1α* and *Vegf* (*Figure 62C*).

4.16. Cpt1a in AgRP neurons is involved in the TA myofibre remodelling of aged mice

The TA of aged mice was studied in the same way as the GAS muscle. However, no TA muscle was collected during the sacrifice for morphological studies. Therefore, only mRNA levels from old mice were analysed.

In agreement with GAS muscle results, a significant increase in the mRNA levels of *Myh-7* was observed in AgRP *Cpt1a* KO mice without changes in the levels of the rest of myosin heavy chain genes (*Figure 63A*). Aged AgRP *Cpt1a* KO mice also exhibited an improvement in muscle denervation and hypertrophy (*Figure 63B*). They showed a reduction in the mRNA levels of myostatin (*Gdf8*) and *Nrf2*. In addition, a high decrease in *Ncam1* mRNA levels is associated with an enhancement in neuromuscular unions and synaptic activity.

Regarding lipid and glucose metabolism (*Figure 63C*), only a decrease in the mRNA levels of *Cpt1b* was observed. Surprisingly, decreased mRNA levels in genes related to mitochondrial fusion (*Mfn2* and *Opa1*) and fission (dynamin-related protein 1, *Drp1*) were observed (*Figure 63D*). Furthermore, AgRP *Cpt1a* KO mice showed a reduction in the mRNA levels of *Hif1α* and *Vegf*.

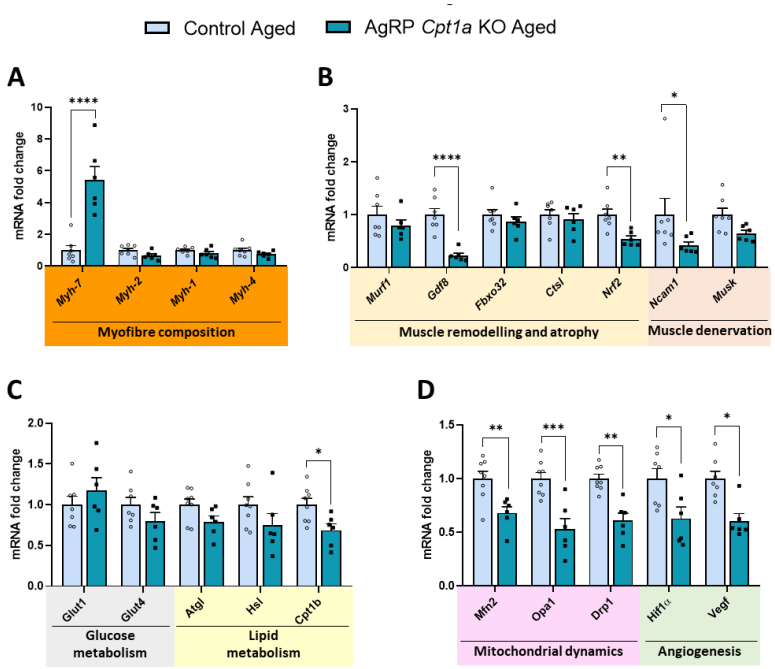

Figure 63. mRNA levels analysis of the tibialis anterior muscle from aged AgRP *Cpt1a* KO mice. Analysis of mRNA levels of genes associated with myofibre composition **(A)**, muscle atrophy and denervation **(B)**, glucose and lipid metabolism **(C)**, mitochondrial dynamics and angiogenesis **(D)** of aged AgRP *Cpt1a* KO and control mice normalised by the *Rpl32* gene. Data are expressed as mean ± SEM. *P<0.05; **P<0.01; ***P<0.001; ****P<0.0001 by the two-tailed Student's t-test. n= 6-9.

4.17. Deletion of *Cpt1a* in AgRP neurons regulates cognition in aged mice

Recent works have revealed that AgRP neurons are not only critical regulators of food intake, but they also have involved in cognitive processes (196). However, the effect of lipid metabolism in AgRP neurons in cognition and memory remains unknown. Therefore, two cognition tests were assessed to characterise the role of *Cpt1a* and aging in this field.

The object location test (OLT) is a typical cognition test, where spatial memory is analysed. This type of memory is mainly regulated by the hippocampus. While young AgRP *Cpt1a* KO mice did not showed differences in the DI compared

to control mice, aged AgRP *Cpt1a* KO mice exhibited a higher DI, and remained more time investigating the moved object than control littermates (0.47 ±0.144 *vs.* -0.17 ±0.229, ***P<0.001) (*Figure 64A*). The novel object recognition test (NORT) analyses recognition memory in which hippocampus and other brain areas such as hypothalamus are involved. In agreement with the OLT, no differences were observed in young mice. However, despite no changes were detected after 2h of replacement by a new object (0.19 ±0.102 *vs.* -0.02 ±0.174) (*Figure 64B*), aged AgRP *Cpt1a* KO mice showed a better recognition memory after 24h (0.33 ±0.134 *vs.* -0.06 ±0.063, ***P<0.001) (*Figure 64C*).

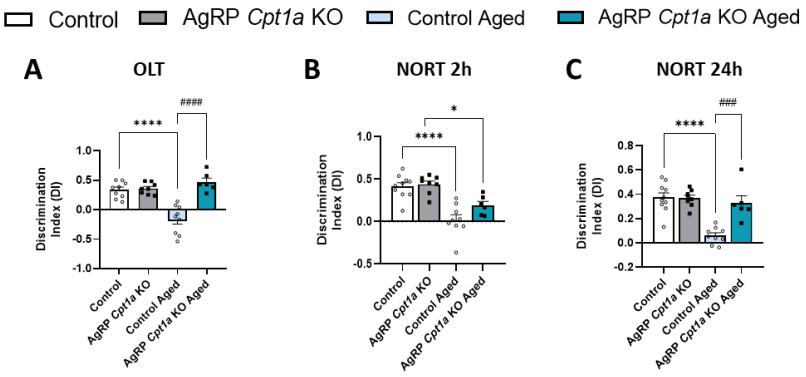

Figure 64. Evaluation of cognition and memory in AgRP *Cpt1a* KO mice. (A) Analysis of spatial memory in the OLT. The investigation time of moved object was measured through the DI. **(B-C)** Analysis of recognition memory in the NORT. The DI at 2h **(B)** and 24h **(C)**. Data are expressed as mean ± SEM. *P<0.05; **P<0.01; ***P<0.001; ****P<0.0001 by 2way ANOVA followed by Sidak's multiple comparisons. # is used to describe statistical differences between different genetic groups (KO and control) under the same age (young or old). n= 6-9.

These results suggest that Cpt1a in AgRP neurons can modulate cognition during aging. In addition, aged AgRP *Cpt1a* KO mice maintain the spatial and the recognition memory in comparison to young mice, while aged control mice exhibited the typical decline in memory associated with the age.

4.18. *Cpt1a* ablation in AgRP neurons reduces neuroinflammation and increases plasticity in the hippocampus of aged mice

Hippocampus is the main brain region involved in memory, learning and the processing of external stimuli. To go deeper into these cognition differences in aged mice, the hippocampus was collected during the sacrifice at 20-months-old.

The hippocampal mRNA levels analysis showed an improvement in neuroinflammation, microglia activation and neuronal plasticity in AgRP *Cpt1a* KO mice (*Figure 65A*). The glial fibrillary acidic protein (Gfap), an essential protein in cell communication and function of the BBB, increases its mRNA levels in aged AgRP *Cpt1a* KO mice. In addition, an increase in the Il-6 mRNA levels and a decrease in the Tnfα mRNA levels was observed. Il-6 diminished the neural inflammation, while Tnfα is expressed under stress conditions increasing neuroinflammation. Therefore, these data suggest that aged AgRP *Cpt1a* KO mice showed a reduction in hippocampal inflammation. Microglia activation was observed by the increase in the mRNA levels of arginase 1 (*Arg1*) and a decrease in oxidative stress was analysed by the nitric oxide synthase 2 (*Nos2*).

Neuroplasticity was assessed through the mRNA levels of *Bdnf* and the protein levels of phosphorylated cAMP response element binding (Creb) and the postsynaptic density protein 95 (Psd95). Aged AgRP *Cpt1a* KO mice exhibited an increase in *Bdnf* mRNA levels compared to control littermates. This factor plays an essential function in the synaptic regulation and neuroplasticity changes related to learning or memory. Moreover, aged mice lacking *Cpt1a* in AgRP neurons showed an increase in the protein levels of the ratio pCreb/Creb and Pd95 (*Figure 65B and 65C*). These two factors are involved in the maturation of excitatory and post-synaptic signalling complexes. Altogether, these results suggest an improvement

in neuronal plasticity in aged AgRP *Cpt1a* KO mice compared to control littermates that could explain the differences in memory observed in the OLT and NORT.

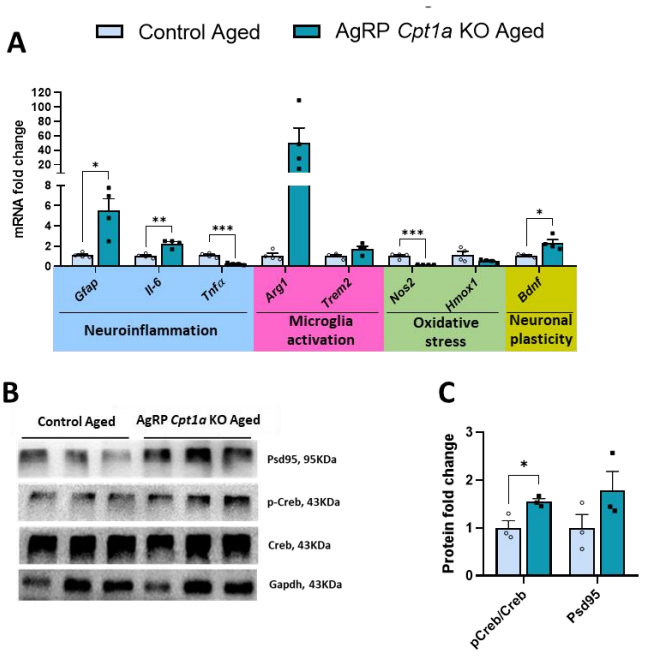

Figure 65. Analysis of the mRNA levels of the hippocampus from aged AgRP *Cpt1a* KO mice. (A) Evaluation by qRT-PCR of the mRNA levels of genes associated with neuroinflammation, microglia activation, oxidative stress, and neuroplasticity of aged AgRP *Cpt1a* KO and control mice normalised by the *Gapdh* gene. **(B-C)** Analysis by Western Blot of proteins involved in neuronal plasticity. Representative Western Blot **(B)** and quantification normalised by the Gapdh protein **(C)**. *Trem2*: Triggering receptor expressed on myeloid cells 2; *Hmox1*: Heme Oxygenase 1. Data are expressed as mean ± SEM. *P<0.05; **P<0.01; ***P<0.001; ****P<0.0001 by the two-tailed Student's t-test. n= 3-4.

4.19. Effect of Cpt1a in AgRP neurons on the hypothalamus of aged mice

Hypothalamus is mostly involved in the maintenance of whole-body homeostasis acting as a link between endocrine and nervous systems. However, hypothalamic inflammation levels are associated with a loss of cognitive skills and behaviour (280). Therefore, several genes related with inflammation and oxidative stress were analysed by qRT-PCR (*Figure 66*).

Aged AgRP *Cpt1a* KO mice showed a reduction in the mRNA levels of pro-inflammatory Il-1β, suggesting a protective neuroinflammatory effect since this molecule is only released during stress conditions or infections in the hypothalamus. In addition, aged AgRP *Cpt1a* KO mice exhibited a decrease in the mRNA levels of different genes involved in oxidative stress [superoxide dismutase type 1 (*Sod1*), *Nrf2*, DNA damage-inducible transcript 3 (*Ddit3*, or also known as *Chop*) and *Nos2*] (*Figure 66B*). These results suggest that aged AgRP *Cpt1a* KO mice exhibited a reduction in neuroinflammation and oxidative stress, displaying a better neuronal communication and function.

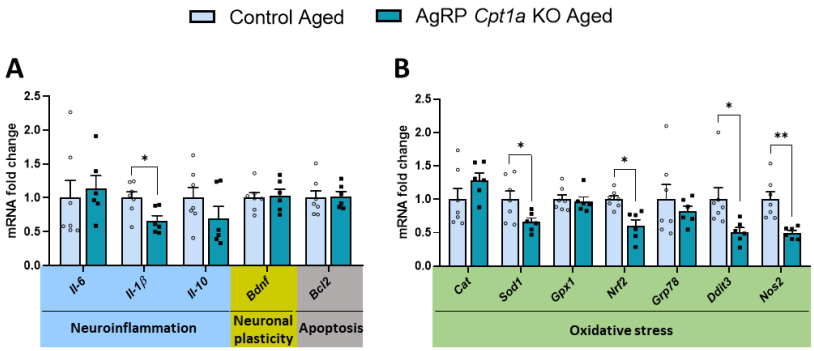

Figure 66. Analysis of the mRNA levels of the hypothalamus from aged AgRP *Cpt1a* KO mice. Evaluation by qRT-PCR of the mRNA levels of genes associated with neuroinflammation, neuroplasticity, apoptosis **(A)** and oxidative stress **(B)** of aged AgRP *Cpt1a* KO and control mice normalised by the *Rpl7* gene. *Bcl2*: B-cell lymphoma 2; *Gpx1*: Glutathione peroxidase 1; *Grp78*: glucose-regulated protein, Bip. Data are expressed as mean ± SEM. *P<0.05; **P<0.01; ***P<0.001; ****P<0.0001 by the two-tailed Student's t-test. n= 6-9.

4.20. *Cpt1a* ablation in AgRP neurons alters neuronal mitochondrial dynamics

Cpt1a is a mitochondrial enzyme located in the mitochondrial outer membrane that catalyses the rate-limiting step of the FAO. Once the phenotype was studied, we decided to analyse the effect of *Cpt1a* deletion on mitochondrial

dynamics using adult primary hypothalamic neuronal culture from the ZsGreen *Cpt1a* KO mouse.

To obtain this mouse model, the *Cpt1a* floxed *AgRP-CreER*^{T2} mouse was crossed with the ZsGreeen mouse kindly provided by Prof. Richard Palmiter from the University of Washington (Washington, United States) and Dr. Albert Quintana and Dra. Elisenda Sainz from the Universitat Autònoma de Barcelona (Bellatera, Spain). As a control, a *Cpt1a* wild-type *AgRP-CreER*^{T2} was crossed to the ZsGreen mouse to generate the ZsGreen control mouse. In both cases, the presence of the Cre recombinase is necessary to generate the *Cre-LoxP* recombination, and the expression of the fluorescent protein ZsGreen.

Animals were induced with TMX at 2-moths-old. One month later, mice were sacrificed, and hypothalamus was extracted to generate the neuronal primary cell culture. Hypothalamic neurons were growing in poly-L-lysine coated plates and, at 9th day, the ZsGreen fluorescent generated only in AgRP neurons was visualised in the confocal microscope. A video of 5 minutes was recorded to measure the speed and the distance migrated by mitochondria.

As a results, ZsGreen *Cpt1a* KO mice showed a higher mitochondrial movement, whit no changes in mitochondrial speed compared to the control group (*Figure 67*). These results could suggest that, despite no differences in speed, the mitochondria anterograde and retrograde transport in AgRP neurons of AgRP Cpt1a KO mice could be altered, and the Cpt1a enzyme might play a role in its regulation.

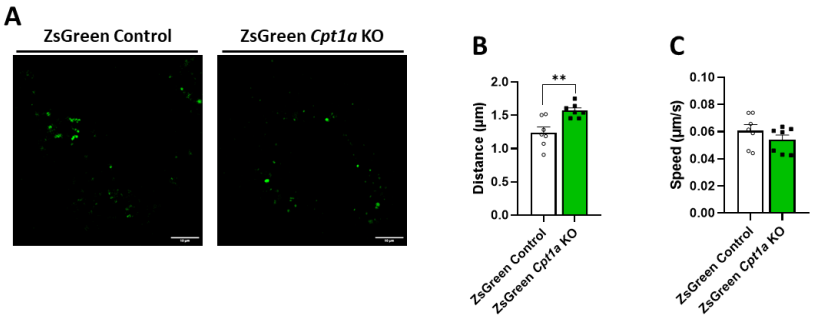

Figure 67. Analysis of mitochondrial dynamics in primary hypothalamic neuronal culture from ZsGreen *Cpt1a* KO mice. (A) Representative images of primary culture from 3 months-old mice, where mitochondria are labelled with the ZsGreen fluorescent protein. Scale bar: 10 µm (magnification 63x). **(B-C)** Mitochondrial distance displaced **(B)** and mitochondrial speed **(C)** of mitochondria from the AgRP neurons **(C).** Data are expressed as mean ± SEM. *P<0.05; **P<0.01; ***P<0.001; ****P<0.0001 by the two-tailed Student's t-test. Two-three images were taken from each animal. n= 3.

4.21. *In vitro* analysis of *Cpt1a* silencing using siRNA and miRNA mimics

To study the molecular mechanism of *Cpt1a* deletion in hypothalamic *Agrp*-expressing cell lines (mHypoE-41 and mHypoE-46), a CPT1A siRNA and two novel miRNAs were used to silence *Cpt1a* gene expression. Briefly, siRNAs and miRNAs are two RNA oligonucleotides with a high-specific sequence of the target mRNA sequence, binding to it and interfering the gene expression.

Synthetic miRNAs mimics can assume the regulatory role of natural miRNAs. The two miRNAs' mimics used to reduce the gene expression of *Cpt1a* were the miRNA 6540-5p and the miRNA 6927-5p. Although there is not enough literature about these miRNAs (284), we chose them because both molecules obtained best scores as a target of the *Cpt1a* in the different miRNA databases described in the section 3.8.1.

mHypoE-41 and mHypoE-46 were grown to 65-75% of confluency in 100 mm tissue culture plates. The transfection with the miRNAs and the siRNA was analysed at 24h and 48h. Before the siRNA and miRNAs experiments, a

transfection with 0.25 µM of TYE 563 Transfection control was carried out to check the efficiency of the DharmaFect transfection. The transfected cells expressed the red fluorescent dye TYE 563 at 24 and 48h in both hypothalamic cell lines, without changes in cell viability (*Figure 68A*). A reduction in cell survival was observed after the transfection but no differences in cell number were detected between the negative control and the siRNA/miRNAs (*Figure 68B*).

The CPT1A siRNA and the miRNA 6540-5p showed a reduction in the *Cpt1a* mRNA levels in both hypothalamic cell lines at 24h (*Figure 68C* and *68D*). Surprisingly, the miRNA 6927-5p showed an increase in *Cpt1a* mRNA levels in the mHypoE-41, while no differences were observed in the mHypoE-46. In addition, the mRNA levels of the neuropeptides *AgRP* and *Npy* in both hypothalamic cell lines after the transfection with the siRNA and miRNAs did not exhibit changes in comparison to the negative control. No differences in *Cpt1a* and neuropeptides mRNA levels were also observed after 48h of transfection (*Figure 68E*).

Altogether, these results suggest that the optimum time for doing Cpt1a silencing experiments was 24h. In addition, the CPT1A siRNA and the miRNA 6540-5p showed a potential inhibitory role in the regulation of *Cpt1a* gene expression. However, it could be necessary more studies and analyse Cpt1a protein levels to understand the molecular mechanisms of *Cpt1a* modulation in both hypothalamic *Agrp*-expressing cell lines.

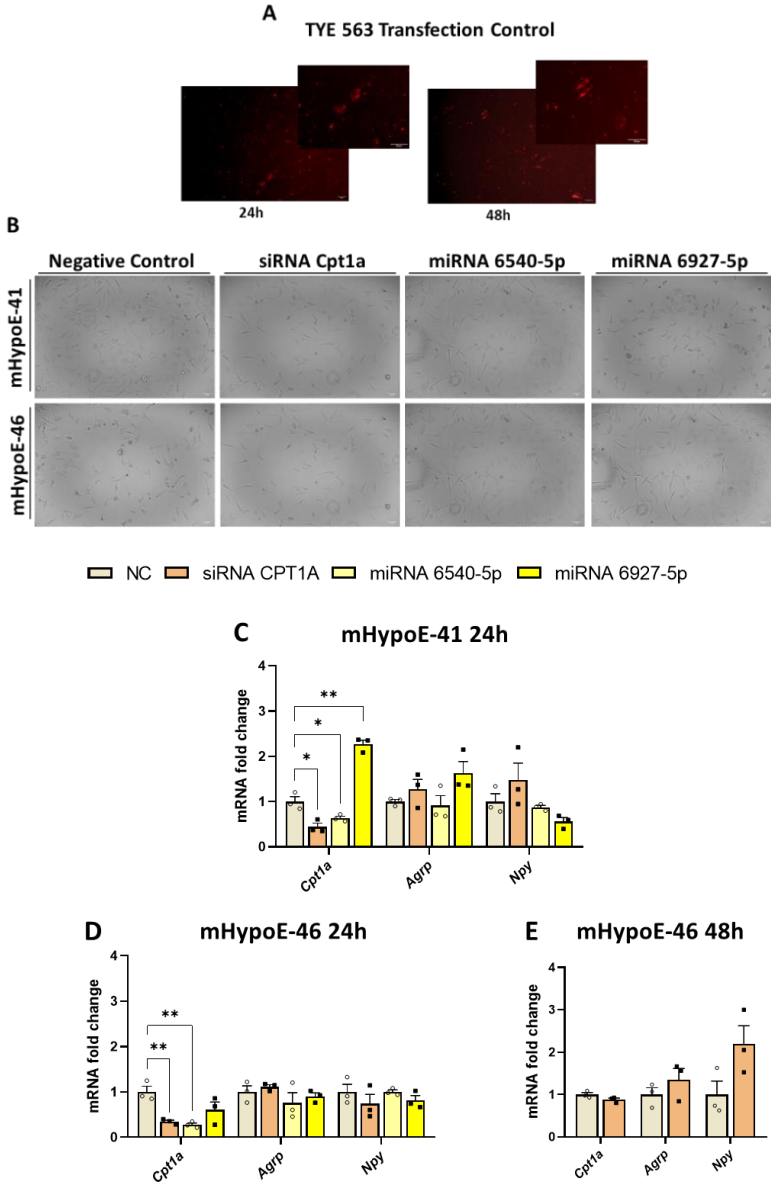

Figure 68. Analysis of the effect of CPT1A siRNA, miRNA 6540-5p and miRNA 6927-5p on *Cpt1a* silencing. (A) Representative images of 24h and 48h transfection with TYE 563 Transfection control in m-HypoE-46 Scale bar: 100 µm **(B)** Representative images of neuronal confluency after 24h of transfection in different conditions. Scale bar: 100 µm. **(C-D)** Analysis of the mRNA levels of *Cpt1a, Agrp* and *Npy* after 24h of transfection in mHypoE-41 **(C)** and mHypoE-46 **(D)** cells normalised by the *Rpl7* gene. **(E)** Analysis of the mRNA levels of *Cpt1a*, *Agrp* and *Npy* analysis after 48h of transfection in mHypoE-46 normalised by the *Rpl7* gene. Data are expressed as mean ± SEM. *P<0.05; **P<0.01by one-way ANOVA followed by Tukey's post hoc test. n=3.

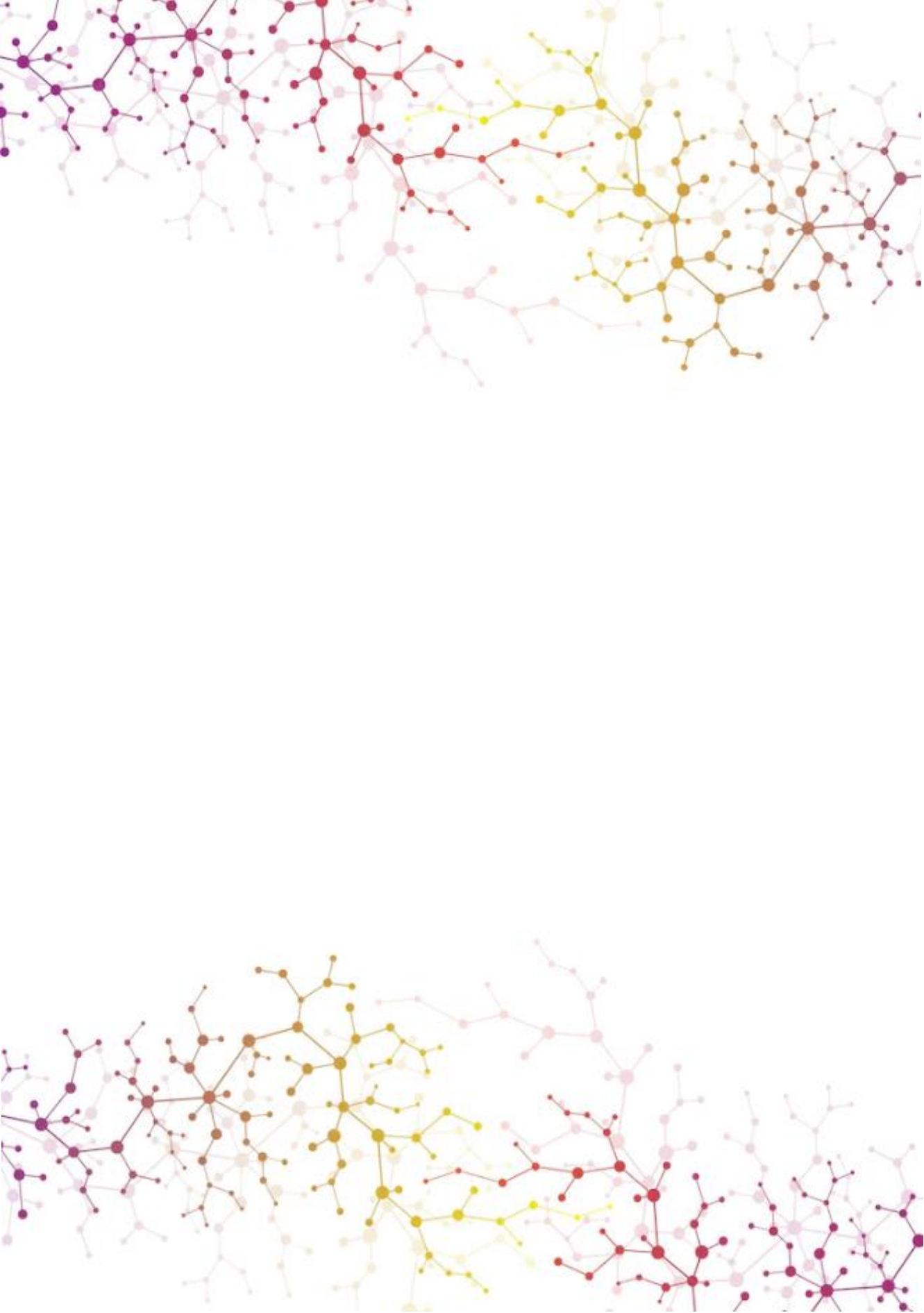

5. Discussion

The hypothalamus is a critical brain region involved in the regulation of food intake and energy homeostasis. In the last decade, lipid metabolism has been postulated to have a crucial role in neuronal physiology. In this context, increasing evidence indicates that the modulation of lipid metabolism in the hypothalamus play a key role in energy balance (75,76,285). Furthermore, although the exact mechanism remains unknown, many studies supported the role of hypothalamus in the modulation of exercise training (181,184).

In this study, we focus on understanding the specific function of Cpt1a in hypothalamic SF1 neurons and the role of this enzyme in AgRP neurons in response to physical activity and aging. The main results of this project revealed that (1) *Cpt1a* deletion in SF1 neurons exhibits a mild-impact on feeding behaviour and energy expenditure in a sex dependent-manner; (2) AgRP *Cpt1a* KO mice show an enhancement in physical performance via myofibre remodelling; and (3) mice lacking *Cpt1a* in AgRP neurons maintain this improvement in physical and cognitive abilities during aging through the increase in neuroplasticity and the reduction in oxidative stress and inflammation in the hippocampus and hypothalamus.

5.1. *Cpt1a* ablation in SF1 neurons induces a sex-based differential effect on energy balance

The VMN has been considered the "*satiety centre*", since lesions in this nucleus induce hyperphagia and obesity (16,18,30). Considering the relevant role of SF1 neurons in energy homeostasis, they have been established as a target to the treatment of some disorders such as obesity and cardiovascular disease. Lipid metabolism plays a critical role in the VMN control of energy balance. Indeed, the effect of some enzymes (Ampk, Acc, Cpt1a, Cpt1c, Fas, and malonyl-CoA decarboxylase) and intermediates of fatty acid metabolism (malonyl-CoA, acetyl-

CoA, and several long fatty acids-CoA) on different hypothalamic nuclei have been studied in last decades (47,74,76–78,276).

The first evidence of the role of Cpt1a in the hypothalamus was reported by Obici *et al.,* (97). In this work, *icv* administration of a ribozyme-containing plasmid designed to decrease the expression of Cpt1a in rats showed a reduction in food intake. Previous studies in our group revealed that the overexpression of a permanently active Cpt1a mutant insensitive to malonyl-CoA in rats increased food intake and led to an obesogenic phenotype, characterised by hyperglycemia and insulin resistance (83). Furthermore, Cpt1am expression increased the mRNA levels of vesicular GABA transporters and two key transcription factors involved in the expression of orexigenic peptides (*Creb* and *FoxO1*) in the VMN of rats (83).

Given the obesogenic phenotype in rats overexpressing *Cpt1a* in the VMN, in the present study we decided to study the role of *Cpt1a* deletion specifically in SF1 neurons of the VMN. We tried to generate a mutant mouse model lacking *Cpt1a* IN SF1 neurons by crossing a *Cpt1a* Flox mouse with a transgenic SF1-*Cre* mouse. However, due to the relevant role of Cpt1a during embryonic development, mice exhibited neonatal lethality and we were not able to generate this mouse model (273). Finally, we deleted *Cpt1a* in SF1 neurons using a recombinant AAV that expressed the Cre recombinase under the control of the SF1 promoter. Both male and female SF1 *Cpt1a* KO mice did not exhibit differences in body weight, but they showed a mild reduction in food intake.

According to this feeding behaviour, other studies based on the specific ablation of *Socs3*, a negative regulator of leptin, in the VMN of mice fed with standard chow and HFD have obtained similar results (39). However, mice lacking up-stream enzymes of Cpt1a such as Ampkα_1 (21,47) and transcriptional factors like FoxO1(38) in the SF1 neurons did not show alterations in food intake, but they exhibited a notable decrease in body weight. Therefore, the inhibition of Cpt1a in SF1 neurons may be caused by the accumulation of long fatty acids in the VMN,

which triggers a satiety signal, leading to a decrease in food intake. However, this neurocircuitry is complex and more studies in this field would be necessary to understand the precise mechanism involved.

One remarkable characteristic of hypothalamic SF1 neurons is their abilities to monitor signals that reflect the energy status and promote appropriate behavioural and metabolic responses to maintain energy and glucose homeostasis. The modulation of SF1 neurons has demonstrated its capacity to modulate peripheral nutrient utilisation, glucose production, thermoregulation and fat accumulation (45,46,50). A recent study reported that mice lacking the BBSome, a protein complex composed of 8 Bardet-Biedl syndrome (BBS) proteins, in SF1 neurons showed increased body weight and adiposity caused by a reduction in energy expenditure. This decrease was associated with the reduction in BAT thermogenic activity and increased lipid storage in the WAT by a lower sympathetic tone in both tissues. Furthermore, inhibition of the BBSome in SF1 neurons revealed normal glucose metabolism, insulin sensitivity and blood pressure (286).

There are numerous studies where the connection between SF1 neurons and BAT has been established, but how the VMN stimulation couples the SNS activation to the BAT remains unclear. The BAT is the only tissue able to convert chemical energy directly into heat by activation of the SNS, and its thermogenic capacity is due to its high mitochondria content and Ucp1 expression. Chronic lesions in the VMN of rats led to a decrease in the sympathetic activity (287). Ablation of *Sf1* in the VMN of mice resulted in an impaired thermogenesis after HFD exposure and decreased mRNA levels of *Ucp1* (33). Conversely, the activation of SF1 neurons using the DREADD technology induces BAT activation (282). Furthermore, the specific deletion of *Cpt1c* in the VMN showed a reduction in BAT activity and the mRNA levels of *Ucp1* in response to metabolic challenges, such as HFD or leptin administration (288). In agreement with these evidence, mice lacking $Ampk\alpha_1$ in the VMN showed similar results (47), highlighting the role of lipid metabolism in the regulation of BAT thermogenic activity.

Interestingly, despite no differences in BAT weight, female SF1 *Cpt1a* KO mice, but not male, exhibited an increase in BAT activity. However, female SF1 *Cpt1a* KO mice did not show changes in the mRNA levels of thermogenic markers (*Dio2*, *Adrb3* and *Ucp1*), while male SF1 *Cpt1a* KO mice showed a strong increased in the mRNA levels of *Adrb3*, the main adrenergic receptor that interconnect the BAT with the SNS. In addition, Adrb3 is also responsible of the browning of beige and white adipose tissue (289).

The WAT also plays a critical role in the regulation of SF1 neurons through the secretion of the anorexigenic hormone leptin. WAT is considered the main fat storage of the body that it is mobilised under low energy conditions. There are several studies that indicate that specific deletions of enzymes implicated in lipid metabolism such as Ampk, and signalling proteins as Pi3k, LepR, IR and FoxO1 in SF1 neurons can alter mice adiposity and weight (13,19,22). In the present study we have not seen differences in the histology and weight of gWAT and sWAT. Moreover, no changes in the mRNA levels of inflammatory, lipid and glucose transporters were observed in both types of white adipose tissue.

Numerous studies have demonstrated the critical role of SF1 neurons in the modulation of glucose homeostasis (290). Some populations of SF1 neurons can sense glucose levels and exert changes in peripheral tissues through the SNS. Insulin is one of the hormones involved in this regulation. Specific deletion of IR in SF1 neurons showed an enhancement in insulin and leptin sensitivity and glucose hepatic production (20). However, both male and female SF1 *Cpt1a* KO mice did not show differences in weight and histological analysis. Therefore, despite its role in glucose regulation, Cpt1a in SF1 neurons seems not to be involved in the regulation of glucose metabolism.

Most of the studies have been done in male mice, and little is known about the energy balance in female mice. It is logical to assume sex-based differences in food intake and energy expenditure exist due to distinct physiological, metabolic,

and hormonal patterns. For example, sex-based differences of feeding behaviour in mammals have been attributed mainly to the effect of gonadal hormones (estrogens and androgens) which regulate food intake by acting on brain and peripheral tissues (291). The VMN contains ERα neurons that control an array of sex-specific responses to coordinate the regulation of sexual behaviour and gonads development. In fact, mice lacking *Sf1* exhibit neonatal lethality by the absence of adrenal glands and gonads (31). Even if no measurements of hormonal levels have been made, it is possible that the sexual dimorphism observed in our mouse model could be consequence of different levels of sexual hormones.

Altogether, Cpt1a in SF1 neurons seems to play a weak role in energy homeostasis. While female SF1 *Cpt1a* KO mice exhibited a faint decrease in food intake and an activation of BAT activity maintaining their body weights, male SF1 *Cpt1a* KO mice also showed a mild decrease in food intake without changes in body weight and BAT activity. Although it has not been studied, another possible explanation of the maintenance of body weight could be that both male and female SF1 *Cpt1a* KO mice could exhibit a reduced physical activity compared to control mice. In fact, some studies have shown that activation of *Sf1* in the VMN increases locomotor activity in mice, highlighting the role of SF1 in physical activity (11).

5.2. Male SF1 *Cpt1a* KO mice do not show alterations in energy and glucose regulation under HFD

Most of the metabolic effects described in the literature about the regulation of energy balance in SF1 neurons have been studied under HFD conditions. For example, mice lacking *IR* in SF1 neurons did not exhibit physiological changes in animals fed with standard diet. However, mice fed with HFD exhibited a strong decrease in body weight, adiposity and food intake (20).

Studies based on specific deletion of *vGlut2* in SF1 neurons reported increased body weight and adiposity caused by an increase in food intake under

HFD conditions (51). Conversely, mice lacking *Ampkα*$_1$ in SF1 neurons and fed with HFD showed a reduction in body weight due to an increase in energy expenditure and BAT thermogenic activity (47). We expected similar results to the Ampk study, but SF1 *Cpt1a* KO mice did not exhibit any change in body weight, food intake and blood glucose levels compared to control littermates. The diet-induced obesity worked and, after 5 weeks of diet, both SF1 *Cpt1a* KO and control mice showed an increase in body weight in comparison to NCD groups, but not between the same nutritional condition.

The thermogenic activity of the BAT under HFD conditions remains unaltered in SF1 *Cpt1a* KO mice. We measured the thermogenesis twice (after 14 days and 1 month of diet) because recent studies have revealed a strong activation of the BAT thermogenesis after 7-14 days of diet. Longer administration periods of HFD are considerably losing the thermogenic efficiency caused mainly by an adaptation of brown adipocytes (276,288). In the same way, although gene expression analysis in these tissues were not done, there were no differences in the histological images of BAT, gWAT, sWAT and liver. In all these tissues, we only observed the increase in adiposity or adipocyte size by the diet.

The duration, the amount of fat in the diet, the age and the mice strain are critical factors in the HFD effect (292,293). Generally, most studies used the 60% fat diet in C57BL/6 mice strain starting at 6-12 weeks of age. In addition, several differences in mice phenotype were observed depending on the diet duration. In our case, 12-weeks-old mice were fed with 60% HFD for 8 weeks. Therefore, it is possible that we could observe differences in SF1 *Cpt1a* KO mice phenotype by changing the duration of the diet administration.

After several cohorts of animals without conclusive phenotypical results, we decided to stop the study. Several factors may be involved in the lack of relevant differences in this project. In first place, the genome contained in the AVV9-SF1-Cre-IRES-mCherry was 5.515 bp, while the maximal genome encapsidation size is

approximately 4.700 bp. The large genome encapsidated of the AVVs used in this study could generate problems in their abilities to infect neurons. Since we observed that the m-Cherry fluorescent signal in SF1 neurons was low in control and SF1 *Cpt1a* KO mice, we tried to increase the expression of the Cre recombinase and the m-Cherry through the activation of SF1 promoter with exercise as it is described in the literature (11,29). Although a little increment in the m-Cherry fluorescent signal was detected, no significant differences were observed between exercise and sedentary mice. Secondly, SF1 promoter used in the construction of the AVVs did not have enough activity to direct the Cre recombinase expression. SF1 promoter contains all the necessary elements to start the transcription (initiator element, CCAAT and E box for RNA polymerase binding and Sp1 sites, where regulatory elements bind to modulate the transcriptional process). Although SF1 basal promoter is adequate to drive specific gene expression in SF1 neurons (21), some studies in mice have revealed that large fragments are necessary to mimic the endogenous SF1 promoter expression (29). Additional regulatory elements located in SF1 enhancer region such as GATA, Sox9 and CCAAT boxes, are necessary to fully recapitulate Sf1 expression *in vivo* (*Figure 12*). Overall, new strategies would be necessary to reveal the specific function in energy balance regulation of Cpt1a in the VMN of the hypothalamus.

5.3. AgRP neurons require Cpt1a enzyme to modulate exercise performance in adult mice

Exercise can influence the activity of different neuronal populations in the MBH. In fact, several studies have reported the potential role of physical activity in the regulation of SF1, AgRP and POMC neurons through the SNS and the secretion of myokines that can cross the BBB (11,170,173). Exercise increases insulin sensitivity leading to an enhancement of glucose uptake in muscles, hepatic glucose production and lipolysis in the WAT. Specifically, within the ARC nucleus, the melanocortin system acts as an interface between signals of metabolic state

and neuronal pathways governing energy balance, glucose, and lipid metabolism. The activity of AgRP neurons has been shown to change in response to metabolic hormones, such as leptin, ghrelin and insulin (66,72,294). However, the effect of lipid metabolism in AgRP neurons on exercise performance still unknown.

In this project, we have elucidated for the first time that Cpt1a in AgRP neurons plays a crucial role in the regulation of locomotion, motor coordination and exploration by the evaluation of different physical and behavioural tests. AgRP *Cpt1a* KO mice displayed an improvement in motor coordination, exploration, locomotor activity and endurance compared to control littermates. This increase in physical capacity could be due to different factors: 1) the reduction in body weight; 2) the activation of the SNS; and 3) the myofibre remodelling in the skeletal muscle. AgRP *Cpt1a* KO mice showed a reduction of 7g in body weight compared to control group, but several studies have described that differences in body weight less than 10g have a low impact on exercise performance (278–280). Therefore, we considered that body weight is not a factor involved in these physical differences. The SNS is a powerful modulator of physical activity in several tissues, including skeletal muscle. However, the expression of the Th in the TA muscle did not show any different pattern compared to the control group. Surprisingly, a muscle fibre transition was observed in the TA and GAS of AgRP *Cpt1a* KO mice that will be widely discussed in the following section.

Recently, AgRP neurons have also been associated with non-feeding behaviour, including those associated with reward, anxiety and compulsive behaviour (179,295). For this reason, mouse behaviour was analysed in the OF and EPM tests to examine alterations in behaviour. AgRP *Cpt1a* KO mice did not show changes in the time spent in the open arms, the number of grooms, defecation, and urination, showing no differences in anxiety-like behaviour in comparation to control mice. This fact reinforces that the improvement in physical performance is not due to changes in behaviour, suggesting a potential role of Cpt1a in AgRP neurons in the regulation of physical activity.

AgRP *Cpt1a* KO mice not only show sexual dimorphism regarding feeding and energy expenditure, but they also exhibited different phenotype in response to exercise. Interestingly, female mice lacking *Cpt1a* in AgRP neurons did not exhibit differences in locomotor activity measured by the exhaustion test on the treadmill. These data strengthen the idea of different sexual behaviour in response to exercise.

Neurons expressing AgRP in the ARC nucleus of the hypothalamus have also been well characterised for their role in appetite behaviour. These neurons are stimulated in fasted conditions, orchestrating orexigenic signals to promote food intake. In addition, several studies have identified that activation of AgRP projections to paraventricular, LHA, thalamus, parabrachial, and bed nucleus of the stria terminalis is sufficient to stimulate food intake (56,296). In addition, AgRP neurons are also involved in energy expenditure and, therefore, in body weight control (60,297). According to these works, in the present study and previous results in our group, we have observed that both AgRP *Cpt1a* KO male and female mice exhibited a decrease in body weight. This decrease could affect to the mouse physical capacity by a reduction in motor skills and the maximal oxygen volume. However, mice ranging a difference less than 10g, the impact of body weight in exercise performance is minimal (279,280) and, thus, the results obtained could be considered in an independent manner of body weight.

Interestingly, we observed an impairment in feeding behaviour after an acute exercise on the treadmill in AgRP *Cpt1a* KO mice. The response of appetite after a single bout of exercise is highly variable and is poorly understood (170,177). Indeed, several studies have suggested that physical activity reduces appetite signals, a phenomenon referred to as “exercise-induced anorexia” (179). Generally, fasting conditions activate AgRP neurons promoting hunger signals. Nonetheless, our results showed a reduction in food intake after 6h-fasted in sedentary AgRP *Cpt1a* KO mice, while an increase in feeding behaviour was observed in exercise conditions. This result suggests exercise as a regulator of AgRP activity on feeding

behaviour. The increase in food intake after exercise could be explained by an inhibition of the melanocortin tone as it was observed in the work of He *et al.,* (170). The activation of the melanocortin system works under fasting conditions to maintain energy and glucose homeostasis, but it fails during exercise activity suggesting that Cpt1a in AgRP neurons is involved in feeding behaviour.

5.4. Cpt1a in AgRP neurons regulates muscle mass and myofibre composition

Skeletal muscle is an adaptable tissue able to change its physiological, morphological, and metabolic properties in response to external stimuli. The hypothalamus, specially the MBH, regulates skeletal muscle physiology through the SNS and the release of catecholamines and hormones, such as growth hormone, glucagon, testosterone, and cortisone. Although the MBH-SNS axis is likely the key regulator of skeletal muscle adaptations to exercise, whether AgRP neurons regulate the SNS activity during/post exercise is still an open question.

To further understand the enhancement in physical performance of AgRP *Cpt1a* KO mice, muscle strength was measured. Both male and female mice did not show differences in strength capacity. As well as previous tests, the body weight can influence strength, but, in this case, we normalised the strength activity by the body weight (holding impulse).

During resistance exercise, muscles can grow up because new proteins and organelles are accumulated in the cytosol, increasing the cellular volume (hypertrophy). Muscle mass is a balance between protein synthesis and degradation. Muscle hypertrophy is mainly regulated by Pi3k-pAkt-mTor and myostatin pathways, while muscle atrophy is mainly orchestrated by FoxO factors and Pgc1α (137,138). In AgRP *Cpt1a* KO mice, we have observed a reduction in the muscle mass of the GAS and QUA muscles in comparison to control mice. The decrease in muscle mass is associated with a reduction in muscle strength, but in

our mouse model we did not observe changes in the strength capacity. These muscle mass differences could be explained by the activation of certain hormonal and metabolic pathways, such as insulin and Pgc1α, that can counter the effect on muscle mass. Gdf8 and Fbxo32 mRNA levels are also reduced in AgRP Cpt1a KO mice, resulting in increased muscle hypertrophy, supporting the hypothesis that strength remains unaltered despite the differences in muscle mass. However, AgRP *Cpt1a* KO mice also showed an increase in the TA mRNA levels of *Murf1* that promote muscle atrophy. These data are controversial, and more studies would be necessary to understand the role of Cpt1a in AgRP neurons on strength capacity.

The reduction in muscle mass is related to an increase in the number of type I myofibres, characterised by a low CSA and a high oxidative capacity. Recent studies reported that deletion of *mTOR* in skeletal muscle of male mice shows a decrease in muscle mass and CSA in SOL and TA muscles (298). In addition, mice lacking *Sox6*, a fast myofibre enriched repressor of slow muscle fibres, in skeletal muscle had an increased number of slow myofibres and mitochondrial activity, displaying an enhanced muscle endurance (299). In agreement with these results, AgRP *Cpt1a* KO mice exhibited a reduction in the CSA of GAS and TA muscles, associated with a high number of type I muscle fibres. To boost the effect in myofibre transition, a single acute exercise on the treadmill was performed before the sacrifice of mice. As a results, the mRNA levels of *Myh-7* and *Myh-2* from the GAS and TA muscles of AgRP *Cpt1a* KO mice were strongly higher compared to sedentary mice, and this increase was higher under exercise conditions.

According to these data, the GAS mtDNA content of SF1 *Cpt1a* KO mice was higher than control littermates in sedentary and exercise conditions. However, no changes were observed in the oxidative metabolism. In addition, TA muscle of AgRP *Cpt1a* KO mice showed increased mRNA levels in genes associated with FAO and mitochondrial biogenesis. However, mitochondrial respiration was unaltered in both exercise and sedentary conditions, suggesting that mitochondrial function was maintained in the control group despite of the reduction in the mtDNA content

and type I myofibres. In agreement with these findings, no differences in Cpt1b, Ucp2 and pAkt/Akt protein levels were observed in the TA of AgRP *Cpt1a* KO mice.

During physical activity, especially endurance training, muscles need glucose to maintain their function. In this study, AgRP *Cpt1a* KO mice exhibited an increase in glucose transporters and glycolysis in TA and GAS muscles. Exercise induces angiogenesis by increasing capillary growth, and reduces inflammation in skeletal muscle (300). The TA muscle of AgRP *Cpt1a* KO mice displayed an enhancement in inflammation response, specially under exercise conditions through the activation of *Cxcl1* and *Socs3*, two factors associated with the release of Il-6 and its metabolic benefits in exercise training. In addition, the mRNA levels of *Il-1β* and *Il-10* increased in AgRP *Cpt1a* KO mice after an acute exercise by limiting host immune response to pathogens and preventing tissue damage. The enhancement in physical performance in AgRP *Cpt1a* KO mice could be produced by an increased oxygen transport, which could improve their ability to continue doing exercise in comparison to control littermates. However, GAS and TA muscles exhibited a reduction in angiogenesis, mimicking the natural process that happens during aging. The decrease in the mRNA levels of these genes influences the oxygen transport and metabolism in AgRP *Cpt1a* KO mice. Therefore, angiogenesis is not involved in the improvement in physical activity of AgRP *Cpt1a* KO mice.

In contrast to GAS and TA muscles, the SOL, an oxidative muscle composed by a high proportion of type I fibres, and the EDL, a glycolytic muscle characterised by high amounts of type II fibres, of AgRP *Cpt1a* KO mice did not show differences in the mRNA levels of the different Myh isoforms. Furthermore, exercise induced an increase in glucose uptake and in the mRNA levels of *Murf1* in SOL and EDL muscles. In addition, the SOL of AgRP *Cpt1a* KO mice showed an improvement in the mRNA levels of genes associated with lipolysis and a reduction in the mRNA levels of *Gdf8*.

Overall, although the muscle strength was unaltered, the specific deletion of *Cpt1a* in AgRP neurons affects the muscle mass in GAS and QUA muscles. Moreover, AgRP *Cpt1a* KO mice exhibited a myofibre transition from glycolytic to oxidative fibres in TA and GAS muscles. These changes in morphology and biochemical status of the fibres are associated with an activation of the mitochondrial biogenesis and oxidative metabolism, and an enhancement in the inflammation response. These results suggest that Cpt1a inAgRP neurons could play a crucial role in the myofibre remodelling and, this process is enhanced in response to physical activity. However, further studies would be necessary to elucidate the molecular mechanisms involved in the phenotype observed in AgRP *Cpt1a* KO mice.

5.5. Cpt1a is necessary in AgRP neurons to modulate peripheral tissue metabolism in response to exercise

It is well-known that AgRP neurons regulate feeding behaviour through signals that modulate the activity of peripheral tissues depending on the energy status. AgRP neurons also release central signals in response to exercise that promote energy and nutrients for the muscle activity. The mechanisms behind the improvement in physical activity of AgRP *Cpt1a* KO mice remains unknown. Therefore, we decided to study different pathways in peripheral tissues to understand the phenotype of these mice.

One possible mechanism involved could be the enhancement in the heart function. The increased in heart force may lead to an improvement in cardiac activity, oxygen transport and endurance capacity (281). The heart weight of AgRP *Cpt1a* KO mice was smaller than control mice and it did not exhibit histological disruptions. Exercise activity is a potent stress for the heart and reduces the expression of genes associated with muscle function such as *Ck*, *Mbp*, *Runx1*,

Runx2, and *Gata4*, a transcriptional factor that regulates the expression of genes involved in cardioprotection and muscle hypertrophy signalling. In agreement with this observation, control and AgRP *Cpt1a* KO mice exhibited a decrease in the mRNA levels of *Runx1* and *Ck* after an acute exercise on the treadmill. Interestingly, a significant increase in the mRNA levels of *Gata4* was observed in exercised AgRP *Cpt1a* KO mice, suggesting an enhancement in the heart function of AgRP *Cpt1a* KO mice. These findings reveal that Cpt1a in AgRP neurons could modulate the cardiac function, and the enhancement of heart activity could explain the differences in endurance capacity observed in AgRP *Cpt1a* KO mice.

The liver is also tightly related to physical activity. During exercise, the liver increases gluconeogenesis to provide energy for skeletal muscle function. AgRP neurons can modulate the metabolic activity of the liver through the SNS (301). On the one hand, mice lacking *IR* in AgRP neurons showed a strong suppression in hepatic glucose production (71). On the other hand, the deletion of carnitine acetyltransferase (*Crat*) in AgRP neurons reduced the hepatic glycogen content and increased the triglycerides levels during the fasted state (302). In agreement with these data, exercise induced an increase in the mRNA levels of *Pepck* and *Pdk4* in the liver of AgRP *Cpt1a* KO mice, suggesting an activation of the gluconeogenesis pathway. However, no significant changes were observed between mice under the same condition (sedentary and exercise).

The Igf-1 is mostly secreted by the liver, and it is the main mediator of growth hormone effects. It is involved in many metabolic and physiological processes including aging and energy homeostasis. In fact, specific deletion of *Igf-1* in the liver resulted in a moderate increase in lifespan and a reduction in body weight and fat mass (303). Mice lacking *Igf-1* receptor in gonadotropin releasing hormone neurons showed normal growth, but at 14 weeks of age, male and female mice displayed a reduction in body weight due to an increase in energy expenditure (304). In agreement with these studies, AgRP *Cpt1a* KO mice showed a decrease

in body weight and in the liver mRNA levels of *Igf-1* that could suggest an increase in lifespan.

The WAT is the main lipid storage of the body, and it provides glucose and fatty acids to skeletal muscle to maintain its activity through the SNS. Several studies also highlighted the role of AgRP neurons in the modulation of lipid metabolism in the WAT (62). For example, deletion of ghrelin receptor in AgRP neurons increases adiposity in WAT by an increase in food intake. Importantly, the deletion of the ghrelin receptor attenuated the effect of diet-induced obesity due to an increase in energy expenditure and browning in the WAT via activation of the SNS (305). Our mice model showed a reduction in fatty acid synthesis compared to control mice in sedentary conditions probably because they did not store fatty acids or did not use them as an energy fuel. In addition, AgRP *Cpt1a* KO and control mice under acute exercise exhibited a stimulation in the lipolysis, but not in FAO. However, no changes were observed between groups at the same condition.

Altogether, the specific deletion of *Cpt1a* in AgRP neurons has a strong impact on heart function. Nonetheless, no great differences were observed in liver and WAT mRNA levels, only those because the effect of exercise. These results provide evidence that AgRP neurons have the potential capacity to adapt to changing metabolic substrates, which is important in some metabolic disorders such as obesity or cardiovascular diseases.

5.6. Cpt1a in AgRP neurons as an anti-aging enzyme and its role in exercise activity

In the last decades, lifespan has been increasing, and it is expected to continue to increase in the following years. Therefore, the study of the molecular mechanisms of the aging progress results essential. Aging is a process characterised by the progressive accumulation of damage that leads to tissue dysfunction. Skeletal muscle is one of the tissues most affected by aging. Several

studies have reported that, during aging, accumulation of ROS and changes in metabolism and physiology are associated with the gradual loss of muscle mass and function (sarcopenia) (210,211). Hypothalamus is also affected by the progression of aging. Recent studies have revealed that hypothalamic dysfunction in sensing or processing signals may have strong effects on metabolic and physiological functions (306), even in challenging situations such as exercise or HFD.

Generally, aging process causes a reduction in exercise performance mainly due to a reduction in muscle function and oxygen transport. One study compared the exercise capacity in adult (6 months of age), old (24 months of age) and elderly (28 months of age) mice through the performance of rotarod, forelimb strength, inverted screen (four limb strength) and treadmill endurance tests. In all tests, old and elderly mice showed a reduction in the exercise capacity associated with the aging decline. However, only in the endurance test, adult and old mice did not have significant differences but, eldery mice showed a reduction of 34% and 27% in endurance capacity compared to adult and old mice, respectively (307). In agreement with these data, 18-months-old control mice exhibited a reduction in endurance, strength and exploration compared to control young mice (5-months-old). However, aged AgRP *Cpt1a* KO mice were able to maintain the same levels of endurance, strength, and explorative capacity compared to young mice, showing an improvement in exercise performance compared to aged control mice. These differences could be explained by a myofibre remodelling from glycolytic to oxidative fibres as we observed in the adult stage. In addition, although no differences in anxiety-like behaviour were observed between groups, aged control and AgRP *Cpt1a* KO mice showed an increase in grooming and defecation during the performance of the OFT. This augment could be associated with a higher emotional behaviour and the disability to adapt to the novel environmental situation, a general characteristic of aged mice.

Unexpectedly, over the months, we realised that control mice exhibited more grey hair on their backs than AgRP *Cpt1a* KO mice. This phenotypic trait led us to measure the plasma levels of Igf-1, a common marker of cellular growth and aging (283). Interestingly, aged AgRP *Cpt1a* KO mice showed a decrease in the Igf-1 levels that it is associated with an increased lifespan. Therefore, it seems that AgRP *Cpt1a* KO mice exhibit a delay in the aging progression that could explain the improvement in exercise performance compared to aged control mice. Moreover, to determine if Cpt1a play a role as an anti-aging enzyme, a study of longevity is ongoing. After 24 months, no changes have been observed between groups, but a trend toward increased lifespan in AgRP *Cpt1a* KO is expected.

During aging, muscles are subjected to metabolic changes. For instance, mitochondrial activity impairment and changes in energy metabolism are crucial to the development of sarcopenia and myofibre transformation. Glycolytic muscles are more prone to become impaired due to the low number in mitochondria. Therefore, muscle loss in sarcopenia results from a fibre type-specific loss of muscle mass and a reduced number of specific fibre types. According to this data, we observed a reduction in the GAS and QUA muscle mass that was heightened in aged AgRP *Cpt1a* KO mice. Furthermore, like young mice, aged AgRP *Cpt1a* KO mice showed a decrease in the CSA of the GAS muscle due to an increase in the number of type I myofibres and the mRNA levels of *Myh-7*. In fact, the GAS muscle of AgRP *Cpt1a* KO mice showed a reduction in the mRNA levels of type IIa, suggesting a possible transition from type IIa to type I fibres in these mice.

Although no histological alterations were observed in the TA muscle of aged mice, both TA and GAS muscles of aged AgRP *Cpt1a* KO mice exhibited an increase in the mRNA levels of *Myh-7* and glucose metabolism, and a decrease in angiogenesis and atrophy genes. Indeed, the TA of aged AgRP *Cpt1a* KO mice showed decreased mRNA levels of *Gdf8*, suggesting a reduction in muscle atrophy induced by aging.

These results are in concordance with the overexpression of *Pgc1α* and *Ampk* in the skeletal muscle. Overexpression of *Pgc1α* in mice skeletal muscle activates mitochondrial oxidative metabolism and the transition to oxidative myofibres, leading to a strong increase in endurance and protection against age-associated sarcopenia (308). In the same way, overexpression and deletion of *Ampkα*$_1$ and *Ampkα*$_2$ in the skeletal muscle highlights the role of Ampk in the myofibre remodelling (309).

Mitochondrial dynamics is a critical process not only for mitochondrial morphology, but also for the regulation of mitochondrial function and quality control. This process is controlled mainly by fusion (Mfn1,Mfn2 and Opa1) and fission proteins (Drp1 and fission 1 protein), and its balance is essential for the mitochondria function (270,310). In the TA muscle of aged AgRP *Cpt1a* KO mice, it was observed a dramatic decrease in the mRNA levels of mitochondrial fusion and fission proteins. These data suggest an impairment in the mitochondrial dynamics that could lead to a reduction in mitochondrial quality. However, despite the impaired mitochondrial dynamics, other compensatory mechanisms such as a high peripheral oxidation in other tissues or autophagy could be compensate this reduction in mitochondria function.

Another consequence associated with the age is the decline in neuromuscular junctions. Muscle denervation is a crucial factor in age-related muscle weakness. Adult (5-months-old) AgRP *Cpt1a* KO mice exhibited an improvement in muscle denervation in the TA muscle. As adults, aged AgRP *Cpt1a* KO mice showed an enhancement in muscle denervation in the TA and GAS muscles compared to control mice. These observations suggest that these mice exhibit less signs of muscle weakness and wasting, especially during aging,where the effect of muscle atrophy is more pronounced.

All these findings in aged mice emphasise the role of Cpt1a in AgRP neurons in aging. It seems that aged AgRP *Cpt1a* KO mice showed a reduction in the

deleterious effects associated with aging decline, but more evidence are necessary to know if Cpt1a is involved in lifespan. In addition, these animals exhibited a better performance in locomotion and exploration without changes in strength and anxiety-like behaviour. The improvement in physical capacity was associated with an increased number and mRNA levels of oxidative myofibres and an enhancement in muscle denervation.

5.7. *Cpt1a* ablation in AgRP neurons improves cognition in aged mice

Several studies have demonstrated that hypothalamic neurons are essential for diverse types of learning and memory. Among them, hypothalamic melanocortin neurons in the LHA were shown to be required for the learning to select nutrient-containing foods, as well as non-food-related object recognition memory formation (311), while hypothalamic orexin neurons were found to be involved in associative learning and memory, including spatial memory (312).

Our results showed that, although young mice did not show differences in memory, aged AgRP *Cpt1a* KO mice exhibited a better performance in spatial and recognition memory compared to control littermates. In addition, cognitive abilities of AgRP *Cpt1a* KO mice were maintained during the aging process, without any alteration associated with age.

To explain this improvement in memory and cognition, it was evaluated the neuronal proliferation, plasticity and inflammation in the hippocampus and the hypothalamus. During aging, neurons undergo increased amounts of oxidative stress, perturbed energy homeostasis, mitochondrial impairment, accumulation of damaged proteins, DNA lesions, and apoptosis (199). All these changes make neurons vulnerable to degeneration and loss of function.

The hippocampal mRNA levels and expression showed an enhancement in neuronal plasticity, neuroinflammation and microglia activation accompanied by a

reduction in oxidative stress in aged AgRP *Cpt1a* KO mice. In addition, the hypothalamus of aged AgRP *Cpt1a* KO mice exhibited a reduction in neuroinflammation, and oxidative stress compared to aged control mice. These data are correlated with better cognitive abilities and could explain the benefits in memory observed in aged AgRP *Cpt1a* KO.

All these findings suggest the potential role of Cpt1a in AgRP neurons in the regulation of memory and cognitive skills by the improvement in hippocampal and hypothalamic neuroplasticity and neuroinflammation. However, more studies will be necessary to understand the molecular mechanisms underlying these changes in the mouse phenotype.

5.8. Cpt1a is involved in the mitochondrial movement in AgRP neurons

Cpt1a is a mitochondrial enzyme, and its deletion in neurons affects mitochondrial activity and fatty acid metabolism. Previous studies have been shown that neuronal activation of AgRP/NPY neurons during fasting or after ghrelin administration is associated with an increase in mitochondria number and decrease in mitochondria size (69). Diet-induced obesity mice reduces the NPY/AgRP neuronal activity and increases the size and elongation of mitochondria (313), indicating that changes in mitochondrial dynamics may play a role in the activation of AgRP/NPY neurons to regulate energy balance. Particularly, in AgRP neurons, previous results in our group have revealed that, although neuronal viability was not affected, male mice lacking *Cpt1a* in AgRP neurons showed a reduction in mitochondria number and size. In addition, AgRP neurons lacking Cpt1a showed a reduction in the number of dendritic spines, and neuronal projections to other nuclei such as paraventricular or LHA.

In this project, using mouse primary hypothalamic neuronal culture (3-month-old), whose mitochondria were labelled with the ZsGreen fluorescent

protein, we analysed the speed and the distance migrated by mitochondria. As a results, we observed that the specific deletion of *Cpt1a* in AgRP neurons affected mitochondrial movement, while mitochondrial speed was unaltered.

Neurons are particularly susceptible to disturbance in mitochondria motility and the regulation of mitochondrial movement play a crucial role in the neuronal health and death. Mitochondrial fission and fusion are two processes dependent on mitochondrial motility. A decrease in motility causes neuronal dysfunction due to the accumulation of ROS, and abnormalities in mitochondrial movement are implicated in a wide range of neurodegenerative and psychiatric problems, such as amyotrophic lateral sclerosis, Alzheimer's and Parkinson's disease (314). Therefore, the increase in mitochondria displacement could be implicated in an improvement in the mitochondrial function of AgRP neurons in compensation of the reduction in mitochondria number and dendritic spines observed in AgRP *Cpt1a* KO mice.

This experiment had some limitations according to the experimental procedure. We found a low quantity of neurons-expressing the ZsGreen fluorescent protein in each cell culture plate. The reduced number of positive cells may be due to the small proportion of AgRP neurons in the whole hypothalamus and, although the medium promotes the growth of neurons instead of other neuronal cell types, only 5-10 fluorescent neurons were observed in the 60 mm^2 culture plate. In addition, the value of mitochondrial speed obtained in these studies is relatively low compared to other studies [0.05 µm/s in this study *vs.* 0.1-0.2 µm/s (315)]. Although the specific deletion of *Cpt1a* in AgRP neurons increased mitochondrial motility, it would be interesting to study the role of proteins involved in anterograde (kinesins) and retrograde (dyneins) transport to complete the study of mitochondrial dynamics and to know the specific role of Cpt1a.

5.9. Potential role of miRNA mimic 6540-5p for *Cpt1a* silencing *in vitro* studies

In the last decade, the discovery of microRNAs as important regulatory agents of gene expression has opened therapeutic opportunities for these oligonucleotides. Since then, a large literature focusing on their biological basis, dysregulation in diseases, and their potential therapeutic role have been published. The main advantages of these molecules are their strong activities and their capacities to act on proteins which lack enzymatic function or have an inaccessible conformation to the traditional drug molecules.

Recent studies have reported the role of miRNAs in *Cpt1a* regulation in multiple health problems, including breast cancer and type 2 diabetes (247,316–318). In breast cancer, the Cpt1a/FAO axis is responsible of metastasis. Zeng *et al.*, reported that miRNA 328-3p can downregulate *Cpt1a* expression and it could be a potential therapeutic target for the treatment of breast cancer (316). In type II diabetes patients, the miRNA 324-5p regulates negatively *Cpt1a* expression, producing an inhibitory effect on inflammation in blood vessels (317). Specifically in dendritic cells, Sun *et al.*, revealed that miRNA 142-5p is involved in the downregulation of *Cpt1a* (318).

Considering these findings, we decided to silence the expression of *Cpt1a* in AgRP hypothalamic cell culture lines to understand the molecular mechanisms in neurons responsible of the improvement in physical and cognitive performance of AgRP *Cpt1a* KO mice. The effect of the two miRNAs recently described in the literature (miRNA 6540-5p and 6927-5p) was opposite. While miRNA 6540-5p showed a decrease in the mRNA levels of *Cpt1a* compared to the negative, miRNA-6927-5p exhibited a strong increase in *Cpt1a* mRNA levels in mHypoE-41 and no changes in mHypoE-46. New experiments would be necessary to confirm the silencing role of miRNA 6540-5p and to discern possible mechanisms behind the changes in phenotype observed in AgRP *Cpt1a* KO mice.

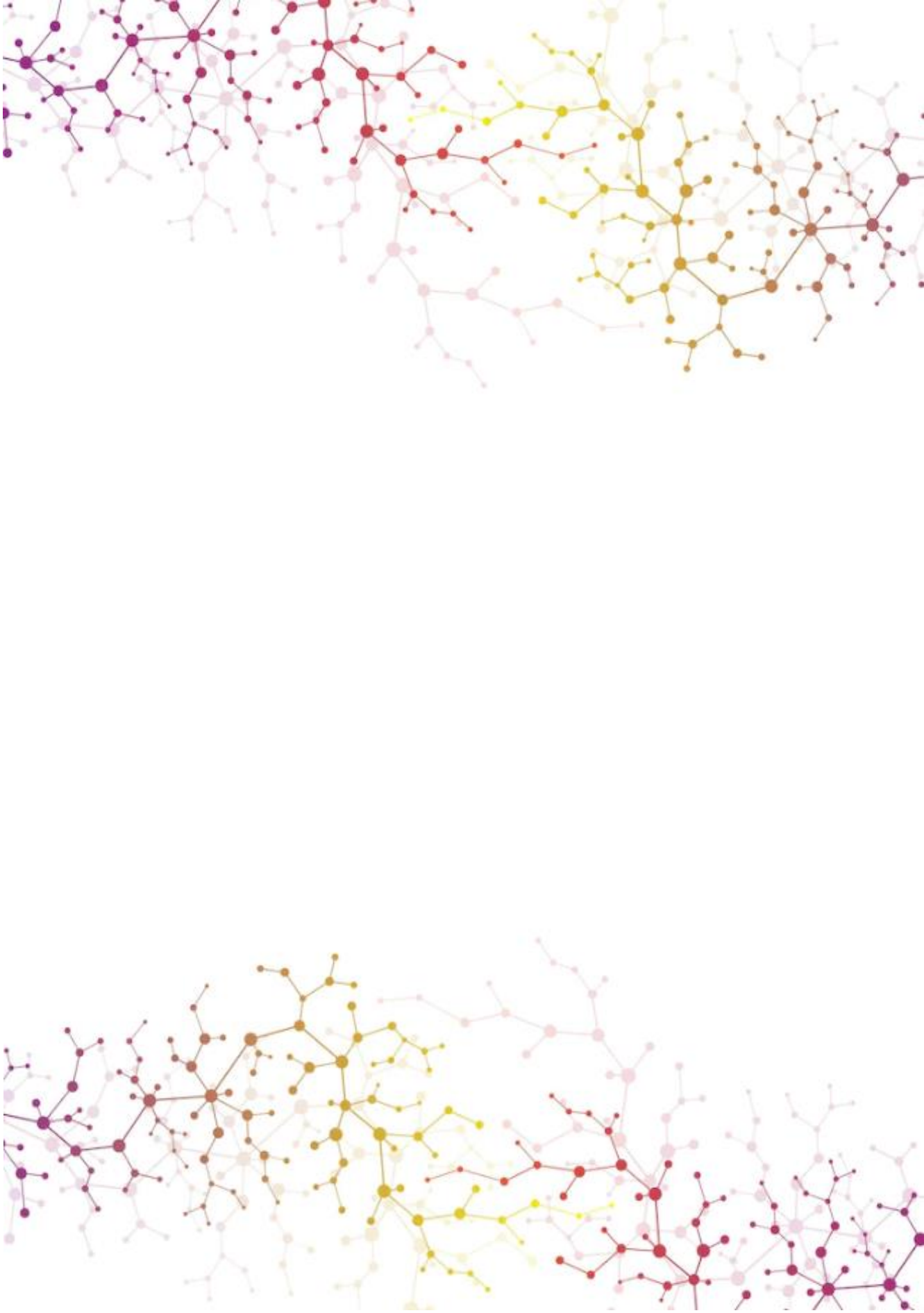

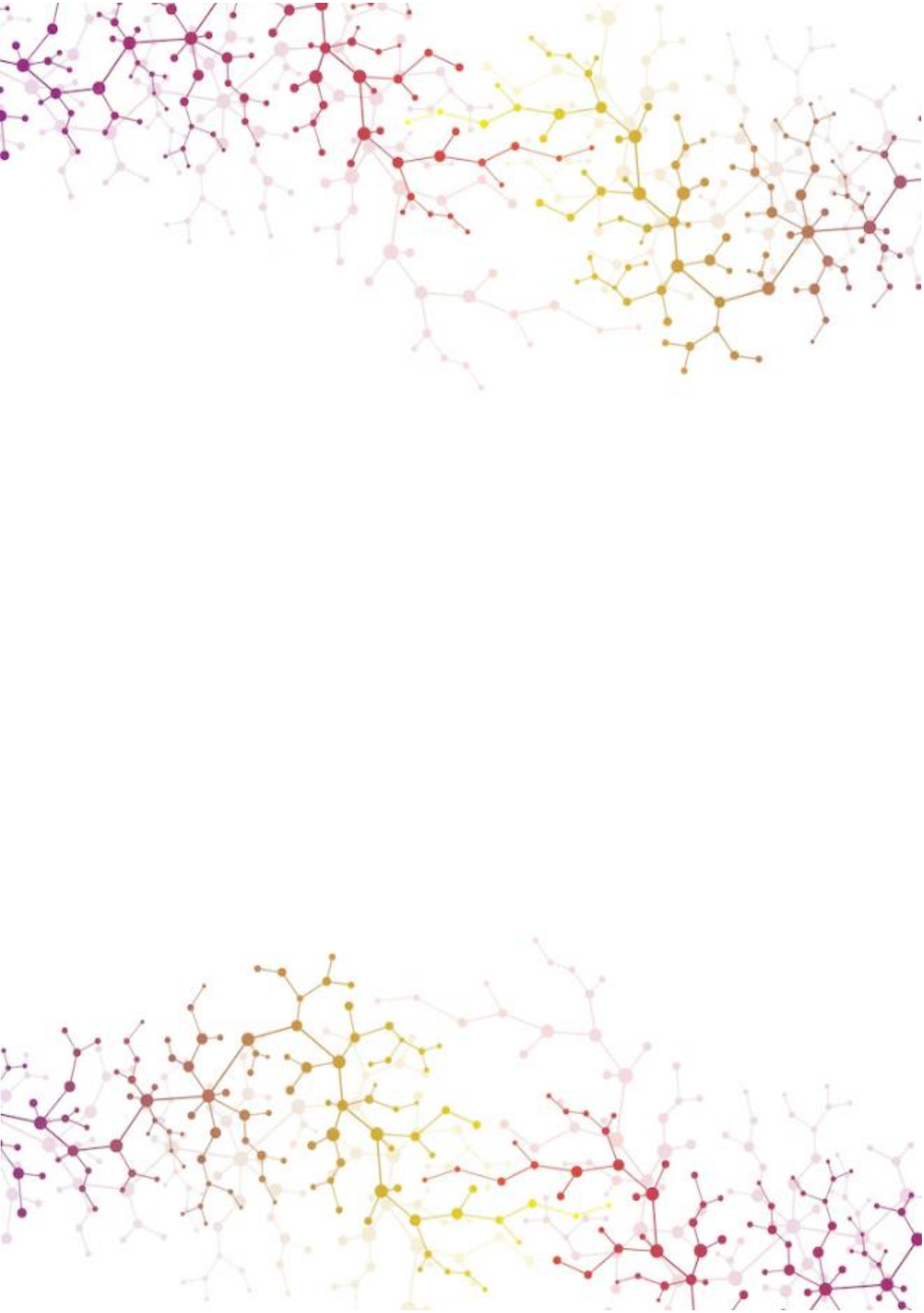

6. Conclusions

- The specific deletion of *Cpt1a* in SF1 neurons produce a mild reduction in food intake in both male and female mice. However, this phenotype is lost under HFD conditions.

- Male and female SF1 *Cpt1a* KO mice show different BAT thermogenic activity. While male mice do not exhibit changes, female mice show an increase in the BAT activity,

- A sexual dimorphism in response to physical activity was observed in AgRP *Cpt1a* KO mice. Male mice lacking *Cpt1a* in AgRP neurons exhibit an improvement in locomotor activity, motor coordination and exploratory capacity, with no changes in strength and anxiety-like behaviour. Female AgRP *Cpt1a* KO mice do not show differences in exercise performance.

- AgRP *Cpt1a* KO male mice show a decrease in muscle mass characterised by a transition from glycolytic to oxidative myofibres in the TA and GAS muscles. This fibre remodelling is accompanied by an increase in oxidative metabolism.

- Cpt1a in AgRP neurons can modulate the heart activity in response to exercise. The improvement in cardiac function in AgRP *Cpt1a* KO mice could be associated with better physical skills.

- Ablation of *Cpt1a* in AgRP neurons has anti-aging effects. AgRP *Cpt1a* KO mice display better exercise performance induced by a higher proportion of oxidative myofibres and the improvement in muscle denervation in the TA and GAS muscles.

- Aged AgRP *Cpt1a* KO mice show an enhancement in cognition and memory that could be a consequence of increased mRNA levels of genes associated with neuronal plasticity and a reduction in the genes involved in neuroinflammation and oxidative stress in the hippocampus and the hypothalamus.

- The specific deletion of *Cpt1a* in AgRP neurons shows an increase in motility in the mitochondria of AgRP neurons that could improve the mitochondrial function and dynamics.

- The miRNA 6540-5p downregulates *Cpt1a* gene expression in the m-HypoE41 and the m-HypoE46, showing a interesting tool to study the molecular mechanism involved in the activation of AgRP neurons.

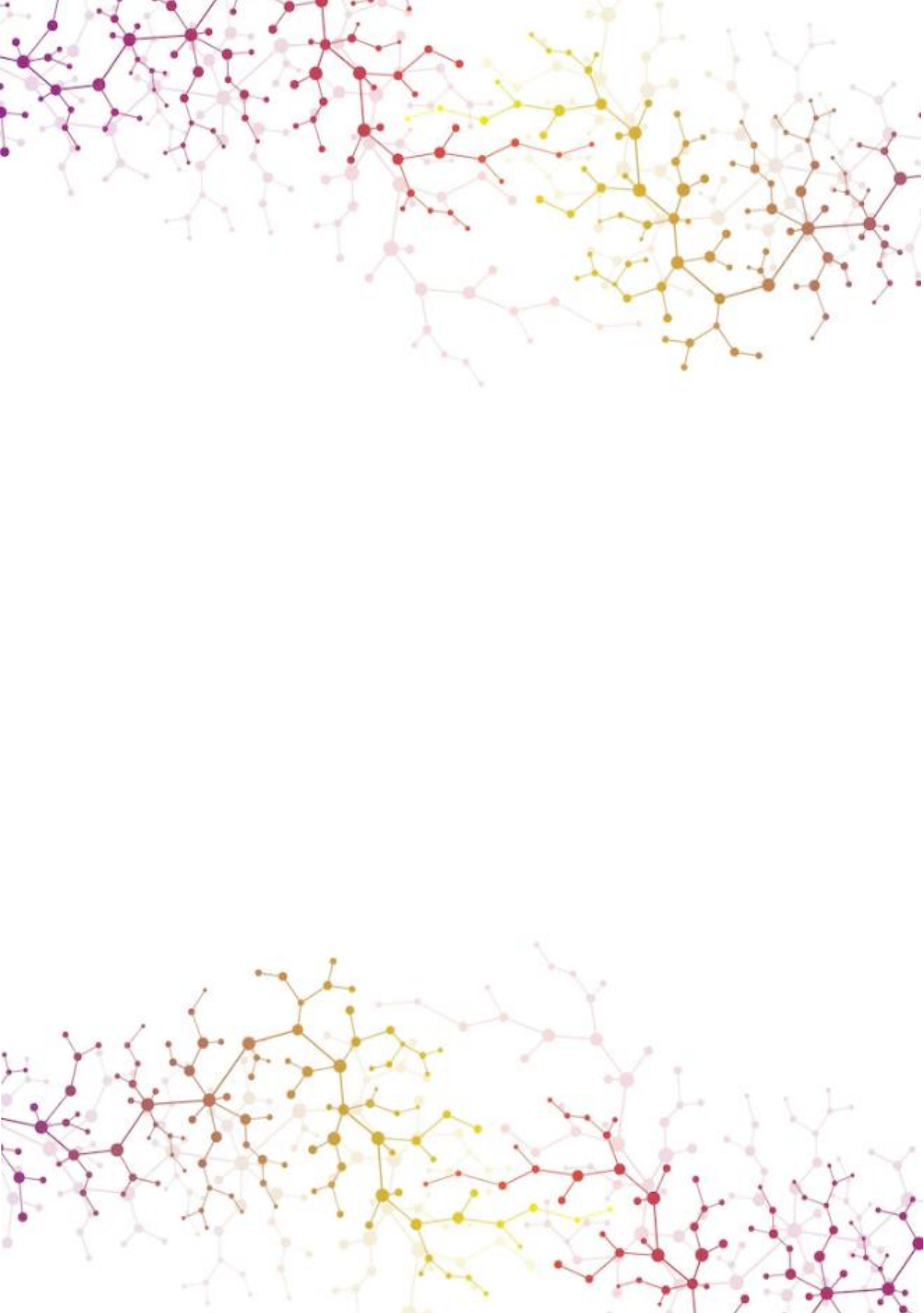

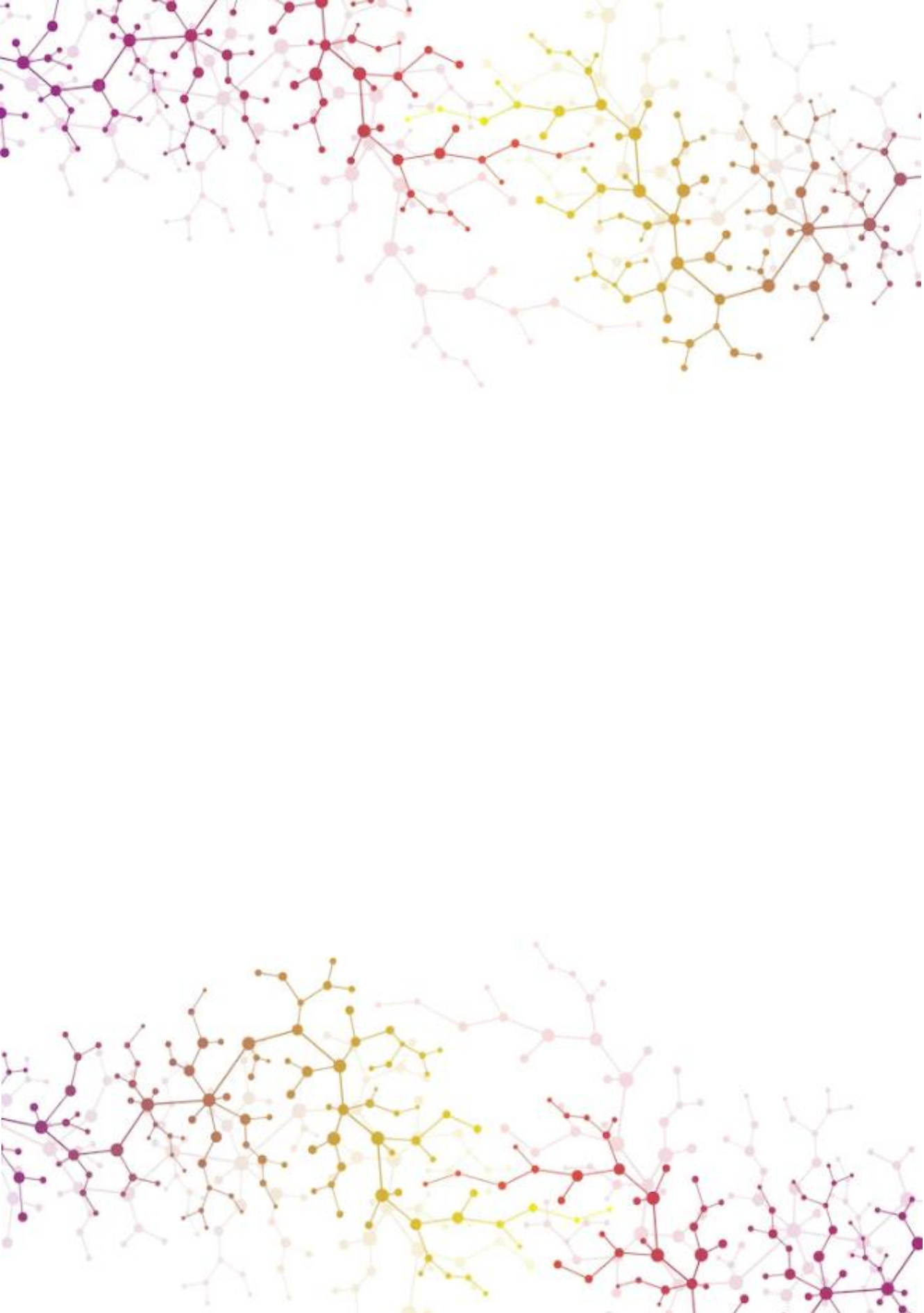

7. Bibliography

1. Hill JO, Wyatt HR, Peters JC. The importance of energy balance. *Eur Endocrinol*. 2013;9(2):111–5.

2. World Health Organization. Guidelines on physical activity, sedentary behaviour and sleep. For children under 5 years of age. *World Health Organization*. 2019. 4 p.

3. Wolin KY, Carson K, Colditz G. Obesity and cancer. *Oncologist*. 2010;15:556–65.

4. Finck BN. Targeting metabolism, insulin resistance, and diabetes to treat nonalcoholic steatohepatitis. *Diabetes*. 2018;67(12):2485–93.

5. Faulconbridge LF, Hayes MR. Regulation of energy balance and body weight by the brain: A distributed system prone to disruption. *Psychiatr Clin North Am*. 2011;34(4):733–45.

6. Myers MG, Olson DP. Central nervous system control of metabolism. *Nature*. 2012;491(7424):357–63.

7. Sandoval D, Cota D, Seeley RJ. The integrative role of CNS fuel-sensing mechanisms in energy balance and glucose regulation. *Annu Rev Physiol*. 2008;70:513–35.

8. Smitka K, Papezova H, Vondra K, Hill M, Hainer V, Nedvidkova J. The role of "mixed" orexigenic and anorexigenic signals and autoantibodies reacting with appetite-regulating neuropeptides and peptides of the adipose tissue-gut-brain axis: Relevance to food intake and nutritional status in patients with anorexia nervosa. I*nt J Endocrinol*. 2013;1(4):100-10..

9. Meek T, Morton G. Leptin, diabetes, and the brain. *Indian J Endocrinol Metab*. 2012;16(9):534.

10. Miller LJ, Harikumar KG, Wootten D, Sexton PM. Roles of Cholecystokinin in the Nutritional Continuum. Physiology and Potential Therapeutics. F*ront Endocrinol (Lausanne)*. 2021;12:1–7.

11. Fujikawa T, Castorena CM, Pearson M, Kusminski CM, Ahmed N, Battiprolu PK, *et al.* SF-1 expression in the hypothalamus is required for beneficial metabolic effects of exercise. *Elife*. 2016;5:1–17.

12. de Git KC, Adan RA. Leptin resistance in diet-induced obesity: The role of hypothalamic inflammation. *Obes Rev*. 2015;16(3):207–24.

13. Fosch A, Zagmutt S, Casals N, Rodríguez-Rodríguez R. New insights of sf1 neurons in hypothalamic regulation of obesity and diabetes. *Int J Mol Sci*. 2021;22(12):1–22.

14. Saper CB, Lowell BB. The hypothalamus. *Curr Biol*. 2014;24(23):1111–6.

15. Bailey P, Bremer F. Experimental diabetes insipidus. *Arch Intern Med*. 1921;28(6):773–803.

16. Smith PE. Hypophysectomy and a replacement therapy in the rat. *Am J Anat.* 1930;45(2):205–73.

17. Hetherington AW. Obesity in the rat following the injection of chromic acid into the hypophysis. *Endocrinology.* 1940;26(2):264–8.

18. Hetherington AW, Ranson AN. the Relation Of various hypothalamic lesions to adiposity in the rat. *J Comp Neurol.* 1942;76:475–99.

19. Dhillon H, Zigman JM, Ye C, Lee CE, McGovern RA, Tang V, *et al.* Leptin directly activates SF1

neurons in the VMH, and this action by leptin is required for normal body-weight homeostasis. *Neuron*. 2006;49(2):191–203.

20. Klöckener T, Hess S, Belgardt BF, Paeger L, Verhagen LAW, Husch A, *et al*. High-fat feeding promotes obesity via insulin receptor/PI3K-dependent inhibition of SF-1 VMH neurons. *Nat Neurosci.* 2011;14(7):911–8.

21. Martínez-Sánchez N, Seoane-Collazo P, Contreras C, Varela L, Villarroya J, Rial-Pensado E, *et al.* Hypothalamic AMPK-ER Stress-JNK1 Axis Mediates the Central Actions of Thyroid Hormones on Energy Balance. *Cell Metab*. 2017;26(1):212-229.e12.

22. Choi YH, Fujikawa T, Lee J, Reuter A, Kim KW. Revisiting the ventral medial nucleus of the hypothalamus: The roles of SF-1 neurons in energy homeostasis. *Front Neurosci*. 2013;7:1–9.

23. Anderson EJP, Çakir I, Carrington SJ, Cone RD, Ghamari-Langroudi M, Gillyard T, *et al.* Regulation of feeding and energy homeostasis by α-MSH. *J Mol Endocrinol*. 2016;56(4):157–74.

24. Van Der Klaauw AA, Keogh JM, Henning E, Stephenson C, Kelway S, Trowse VM, *et al.* Divergent effects of central melanocortin signalling on fat and sucrose preference in humans. *Nat Commun*. 2016;7:1–5.

25. McClellan KM, Parker KL, Tobet S. Development of the ventromedial nucleus of the hypothalamus. *Front Neuroendocrinol*. 2006;27(2):193–209.

26. Zhao L, Ki WK, Ikeda Y, Anderson KK, Beck L, Chase S, *et al.* Central nervous system-specific knockout of steroidogenic factor 1 results in increased anxiety-like behavior. *Mol Endocrinol.* 2008;22(6):1403–15.

27. MacKay H, Scott CA, Duryea JD, Baker MS, Laritsky E, Elson AE, *et al.* DNA methylation in AgRP neurons regulates voluntary exercise behavior in mice. *Nat Commun.* 2019;10(1).

28. Parker KL, Rice DA, Lala DS, Ikeda Y, Luo X, Wong M, *et a*l. Steroidogenic factor 1: An essential mediator of endocrine development. *Recent Prog Horm Res.* 2002;57:19–36.

29. Hoivik EA, Lewis AE, Aumo L, Bakke M. Molecular aspects of steroidogenic factor 1 (SF-1). *Mol Cell Endocrinol.* 2010;315(1–2):27–39.

30. King BM. The rise, fall, and resurrection of the ventromedial hypothalamus in the regulation of feeding behavior and body weight. *Physiol Behav.* 2006;87(2):221–44.

31. Majdic G, Young M, Gomez-Sanchez E, Anderson P, Szczepaniak LS, Dobbins RL, *et al.* Knockout mice lacking steroidogenic factor 1 are a novel genetic model of hypothalamic obesity. *Endocrinology*. 2002;143(2):607–14.

32. Achermann JC, Ito M, Ito M, Hindmarsh PC, Jameson JL. A mutation in the gene encoding steroidogenic factor-1 causes XY sex reversal and adrenal failure in humans. *Nat Genet.* 1999;22(2):125–6.

33. Kim KW, Zhao L, Donato J, Kohno D, Xu Y, Eliasa CF, *et al.* Steroidogenic factor 1 directs programs regulating diet-induced thermogenesis and leptin action in the ventral medial hypothalamic nucleus. *Proc Natl Acad Sci U S A*. 2011;108(26):10673–8.

34. Kinyua AW, Yang DJ, Chang I, Kim KW. Steroidogenic factor 1 in the ventromedial nucleus of the hypothalamus regulates age-dependent obesity. *PLoS One*. 2016;11(9):1–12.

35. Viskaitis P, Irvine EE, Smith MA, Choudhury AI, Alvarez-Curto E, Glegola JA, *et al.* Modulation of SF1 Neuron Activity Coordinately Regulates Both Feeding Behavior and Associated

Emotional States. *Cell Rep*. 2017;21(12):3559–72.

36. Bingham NC, Anderson KK, Reuter AL, Stallings NR, Parker KL. Selective loss of leptin receptors in the ventromedial hypothalamic nucleus results in increased adiposity and a metabolic syndrome. *Endocrinology*. 2008;149(5):2138–48.

37. Xu Y, Nedungadi TP, Zhu L, Sobhani N, Irani BG, Davis KE, *et al.* Distinct hypothalamic neurons mediate estrogenic effects on energy homeostasis and reproduction. *Cell Metab.* 2011;14(4):453–65.

38. Kim KW, Donato J, Berglund ED, Choi YH, Kohno D, Elias CF, *et al.* FOXO1 in the ventromedial hypothalamus regulates energy balance. *J Clin Invest.* 2012;122(7):2578–89.

39. Zhang R, Dhillon H, Yin H, Yoshimura A, Lowell BB, Maratos-Flier E, *et al*. Selective inactivation of Socs3 in SF1 neurons improves glucose homeostasis without affecting body weight. *Endocrinology*. 2008;149(11):5654–61.

40. Berger A, Kablan A, Yao C, Ho T, Podyma B, Weinstein LS, *et al.* Gsα deficiency in the ventromedial hypothalamus enhances leptin sensitivity and improves glucose homeostasis in mice on a high-fat diet. *Endocrinology*. 2016;157(2):600–10.

41. Senn SS, Le Foll C, Whiting L, Tarasco E, Duffy S, Lutz TA, *et al.* Unsilencing of native LepRs in hypothalamic SF1 neurons does not rescue obese phenotype in LepR-deficient mice. *Am J Physiol - Regul Integr Comp Physiol*. 2019;317(3):R451–60.

42. Air EL, Benoit SC, Blake Smith KA, Clegg DJ, Woods SC. Acute third ventricular administration of insulin decreases food intake in two paradigms. *Pharmacol Biochem Behav*. 2002;72(1–2):423–9.

43. Jauch-Chara K, Friedrich A, Rezmer M, Melchert UH, Scholand-Engler HG, Hallschmid M, *et al.* Intranasal insulin suppresses food intake via enhancement of brain energy levels in humans. *Diabetes*. 2012;61(9):2261–8.

44. Xu Y, Hill JW, Fukuda M, Gautron L, Sohn JW, Kim KW, *et al.* PI3K signaling in the ventromedial hypothalamic nucleus is required for normal energy homeostasis. *Cell Metab.* 2010;12(1):88–95.

45. Fujikawa T, Choi YH, Yang DJ, Shin DM, Donato J, Kohno D, *et al.* P110β in the ventromedial hypothalamus regulates glucose and energy metabolism. *Exp Mol Med.* 2019;51(4).

46. Correa SM, Newstrom DW, Warne JP, Flandin P, Cheung CC, Lin-Moore AT, *et al.* An estrogen-responsive module in the ventromedial hypothalamus selectively drives sex-specific activity in females. *Cell Rep.* 2015;10(1):62–74.

47. Seoane-Collazo P, Roa J, Rial-Pensado E, Liñares-Pose L, Beiroa D, Ruíz-Pino F, *et al.* SF1-specific AMPKa1 deletion protects against diet-induced obesity. *Diabetes*. 2018;67(11):2213–26.

48. Borg WP, During MJ, Sherwin RS, Borg MA, Brines ML, Shulman GI. Ventromedial hypothalamic lesions in rats suppress counterregulatory responses to hypoglycemia. *J Clin Invest.* 1994;93(4):1677–82.

49. Kang L, Routh VH, Kuzhikandathil E V., Gaspers LD, Levin BE. Physiological and Molecular Characteristics of Rat Hypothalamic Ventromedial Nucleus Glucosensing Neurons. *Diabetes*. 2004;53(3):549–59.

50. Song Z, Routh VU. Differential effects of glucose and lactate on glucosensing neurons in the ventromedial hypothalamic nucleus. *Diabetes*. 2005;54(1):15–22.

51. Tong Q, Ye CP, McCrimmon RJ, Dhillon H, Choi B, Kramer MD, *et al.* Synaptic Glutamate Release by Ventromedial Hypothalamic Neurons Is Part of the Neurocircuitry that Prevents Hypoglycemia. *Cell Metab*. 2007;5(5):383–93.

52. Meek TH, Nelson JT, Matsen ME, Dorfman MD, Guyenet SJ, Damian V, *et al.* Functional identification of a neurocircuit regulating blood glucose. *Proc Natl Acad Sci U S A*. 2016;113(14):E2073–82.

53. Minokoshi Y, Haque MS, Shimazu T. Microinjection of leptin into the ventromedial hypothalamus increases glucose uptake in peripheral tissues in rats. *Diabetes*. 1999;48(2):287–91.

54. Shiuchi T, Haque MS, Okamoto S, Inoue T, Kageyama H, Lee S, *et al.* Hypothalamic Orexin Stimulates Feeding-Associated Glucose Utilization in Skeletal Muscle via Sympathetic Nervous System. *Cell Metab*. 2009;10(6):466–80.

55. Zagmutt S, Mera P, Soler-Vázquez MC, Herrero L, Serra D. Targeting AgRP neurons to maintain energy balance: Lessons from animal models. *Biochem Pharmacol*. 2018;155(May):224–32.

56. Deem JD, Faber CL, Morton GJ. AgRP neurons: Regulators of feeding, energy expenditure, and behavior. *FEBS J*. 2022;289(8):2362–81.

57. Tong Q, Ye CP, Jones JE, Elmquist JK, Lowell BB. Synaptic release of GABA by AgRP neurons is required for normal regulation of energy balance. *Nat Neurosci*. 2008;11(9):998–1000.

58. Qian S, Chen H, Weingarth D, Trumbauer ME, Novi DE, Guan X, *et al.* Neither Agouti-Related Protein nor Neuropeptide Y Is Critically Required for the Regulation of Energy Homeostasis in Mice. *Mol Cell Biol*. 2002;22(14):5027–35.

59. Luquet S, Perez FA, Hnasko TS, Palmiter RD. NPY/AgRP neurons are essentials for feeding in adult mice but can be ablated in neonates. *Science* (80). 2005;310(5748):683–5.

60. Aponte Y, Atasoy D, Sternson SM. AGRP neurons are sufficient to orchestrate feeding behavior rapidly and without training. *Nat Neurosci.* 2011;14(3):351–5.

61. Joly-Amado A, Denis RGP, Castel J, Lacombe A, Cansell C, Rouch C, *et al.* Hypothalamic AgRP-neurons control peripheral substrate utilization and nutrient partitioning. *EMBO J.* 2012;31(22):4276–88.

62. Cavalcanti de Albuquerque JP, Bober J, Zimmer MR, Dietrich MO. Regulation of substrate utilization and adiposity by Agrp neurons. *Nat Commun.* 2019;10(1).

63. Ruan H Bin, Dietrich MO, Liu ZW, Zimmer MR, Li MD, Singh JP, *et al.* O-GlcNAc transferase enables AgRP neurons to suppress browning of white fat. *Cell*. 2014;159(2):306–17.

64. Hagan MM, Benoit SC, Rushing PA, Pritchard LM, Woods SC, Seeley RJ. Immediate and prolonged patterns of Agouti-related peptide-(83-132)-induced c-Fos activation in hypothalamic and extrahypothalamic sites. Endocrinology. 2001;142(3):1050–6.

65. Sun Y, Wang P, Zheng H, Smith RG. Ghrelin stimulation of growth hormone release and appetite is mediated through the growth hormone secretagogue receptor. *Proc Natl Acad Sci U S A.* 2004;101(13):4679–84.

66. Goto M, Arima H, Watanabe M, Hayashi M, Banno R, Sato I, *et al.* Ghrelin increases neuropeptide Y and agouti-related peptide gene expression in the arcuate nucleus in rat hypothalamic organotypic cultures. *Endocrinology*. 2006;147(11):5102–9.

67. Nogueiras R, López M, Lage R, Perez-Tilve D, Pfluger P, Mendieta-Zerón H, *et al.* Bsx, a novel hypothalamic factor linking feeding with locomotor activity, is regulated by energy availability. *Endocrinology*. 2008;149(6):3009–15.

68. Lage R, Diéguez C, Vidal-Puig A, López M. AMPK: a metabolic gauge regulating whole-body energy homeostasis. *Trends Mol Med*. 2008;14(12):539–49.

69. Andrews ZB, Liu ZW, Walllingford N, Erion DM, Borok E, Friedman JM, *et al.* UCP2 mediates ghrelin's action on NPY/AgRP neurons by lowering free radicals. *Nature*. 2008;454(7206):846–51.

70. Van Den Hoek AM, Heijboer AC, Corssmit EPM, Voshol PJ, Romijn JA, Havekes LM, *et al.* PYY3-36 reinforces insulin action on glucose disposal in mice fed a high-fat diet. *Diabetes*. 2004;53(8):1949–52.

71. Könner AC, Janoschek R, Plum L, Jordan SD, Rother E, Ma X, *et al.* Insulin Action in AgRP-Expressing Neurons Is Required for Suppression of Hepatic Glucose Production. *Cell Metab*. 2007;5(6):438–49.

72. Steculorum SM, Ruud J, Karakasilioti I, Backes H, Engström Ruud L, Timper K, *et al.* AgRP Neurons Control Systemic Insulin Sensitivity via Myostatin Expression in Brown Adipose Tissue. *Cell*. 2016;165(1):125–38.

73. Ebert D, Haller RG, Walton ME. Energy contribution of octanoate to intact rat brain metabolism measured by 13C nuclear magnetic resonance spectroscopy. *J Neurosci.* 2003;23(13):5928–35.

74. Obici S, Feng Z, Morgan K, Stein D, Karkanias G, Rossetti L. Central administration of oleic acid inhibits glucose production and food intake. *Diabetes*. 2002;51(2):271–5.

75. Dragano NRV, Solon C, Ramalho AF, de Moura RF, Razolli DS, Christiansen E, *et al.* Polyunsaturated fatty acid receptors, GPR40 and GPR120, are expressed in the hypothalamus and control energy homeostasis and inflammation. *J Neuroinflammation.* 2017;14(1):1–16.

76. Mir JF, Zagmutt S, Lichtenstein MP, García-Villoria J, Weber M, Gracia A, *et al.* Ghrelin Causes a Decline in GABA Release by Reducing Fatty Acid Oxidation in Cortex. *Mol Neurobiol.* 2018;55(9):7216–28.

77. Loftus TM, Jaworsky DE, Frehywot CL, Townsend CA, Ronnett G V., Daniel Lane M, *et al.* Reduced food intake and body weight in mice treated with fatty acid synthase inhibitors. *Science* (80). 2000;288(5475):2379–81.

78. Swierczynski J, Goyke E, Korczynska J, Jankowski Z. Acetyl-CoA carboxylase and fatty acid synthase activities in human hypothalamus. *Neurosci Lett.* 2008;444(3):209–11.

79. Nogueiras R, Wiedmer P, Perez-Tilve D, Veyrat-Durebex C, Keogh JM, Sutton GM, *et al*. The central melanocortin system directly controls peripheral lipid metabolism. *J Clin Invest.* 2007;117(11):3475–88.

80. Eaton S, Bartlett K, Pourfarzam M. Mammalian mitochondrial β-oxidation. *Biochem J.* 1996;320(2):345–57.

81. McGarry JD, Brown NF. The mitochondrial carnitine palmitoyltransferase system. From concept to molecular analysis. *Eur J Biochem*. 1997;244(1):1–14.

82. Serra D, Mera P, Malandrino MI, Mir JF, Herrero L. Mitochondrial fatty acid oxidation in obesity. *Antioxidants Redox Signal.* 2013;19(3):269–84.

83. Mera P, Mir JF, Fabriàs G, Casas J, Costa ASH, Malandrino MI, *et al.* Long-term increased carnitine palmitoyltransferase 1A expression in ventromedial hypotalamus causes hyperphagia and alters the hypothalamic lipidomic profile. *PLoS One.* 2014;9(5):1–13.

84. Huang D, Chowdhury S, Wang H, Savage SR, Ivey RG, Kennedy JJ, *et al.* Multiomic analysis identifies CPT1A as a potential therapeutic target in platinum-refractory, high-grade serous ovarian cancer. *Cell Reports Med.* 2021;2(12):100471.

85. Pucci S, Zonetti MJ, Fisco T, Polidoro C, Bocchinfuso G, Palleschi A, *et al.* Carnitine palmitoyl transferase-1A (CPT1A): A new tumor specific target in human breast cancer. *Oncotarget*. 2016;7(15):19982–96.

86. Xiong X, Wen YA, Fairchild R, Zaytseva YY, Weiss HL, Evers BM, *et al.* Upregulation of CPT1A is essential for the tumor-promoting effect of adipocytes in colon cancer. *Cell Death Dis*. 2020;11(9).

87. Calderon-Dominguez M, Mir JF, Fucho R, Weber M, Serra D, Herrero L. Fatty acid metabolism and the basis of brown adipose tissue function. *Adipocyte*. 2016;5(2):98–118.

88. Sierra AY, Gratacós E, Carrasco P, Clotet J, Ureña J, Serra D, *et al.* CPT1c is localized in endoplasmic reticulum of neurons and has carnitine palmitoyltransferase activity. *J Biol Chem.* 2008;283(11):6878–85.

89. Ramírez S, Martins L, Jacas J, Carrasco P, Pozo M, Clotet J, *et al*. Hypothalamic ceramide levels regulated by cpt1c mediate the orexigenic effect of ghrelin. *Diabetes*. 2013;62(7):2329–37.

90. Wolfgang MJ, Lane MD. The role of hypothalamic malonyl-CoA in energy homeostasis. *J Biol Chem.* 2006;281(49):37265–9.

91. Lopaschuk GD, Ussher JR, Jaswal JS. Targeting intermediary metabolism in the hypothalamus as a mechanism to regulate appetite. *Pharmacol Rev.* 2010;62(2):237–64.

92. Gao S, Kinzig KP, Aja S, Scott KA, Keung W, Kelly S, *et al*. Leptin activates hypothalamic acetyl-CoA carboxylase to inhibit food intake. *Proc Natl Acad Sci U S A.* 2007;104(44):17358–63.

93. López M, Lelliott CJ, Tovar S, Kimber W, Gallego R, Virtue S, *et al.* Tamoxifen-induced anorexia is associated with fatty acid synthase inhibition in the ventromedial nucleus of the hypothalamus and accumulation of malonyl-CoA. *Diabetes*. 2006;55(5):1327–36.

94. Mera P, Bentebibel A, López-Viñas E, Cordente AG, Gurunathan C, Sebastián D, *et al.* C75 is converted to C75-CoA in the hypothalamus, where it inhibits carnitine palmitoyltransferase 1 and decreases food intake and body weight. *Biochem Pharmacol*. 2009;77(6):1084–95.

95. Gao S, Casals N, Keung W, Moran TH, Lopaschuk GD. Differential effects of central ghrelin on fatty acid metabolism in hypothalamic ventral medial and arcuate nuclei. *Physiol Behav*. 2013;118:165–70.

96. Schwartz MW, Woods SC, Jr DP, Seeley RJ, Baskin DG. Central nervous system control of food intake.*Nature*. 2000;404(6778):661–71.

97. Obici S, Feng Z, Arduini A, Conti R, Rossetti L. Inhibition of hypothalamic carnitine palmitoyltransferase-1 decreases food intake and glucose production. *Nat Med.* 2003;9(6):756–61.

98. Gao S, Serra D, Keung W, Hegardt FG, Lopaschuk GD. Important role of ventromedial hypothalamic carnitine palmitoyltransferase-1a in the control of food intake. *Am J Physiol*

Endocrinol Metab. 2013;305(3):336–47.

99. Gao S, Keung W, Serra D, Wang W, Carrasco P, Casals N, *et al.* Malonyl-CoA mediates leptin hypothalamic control of feeding independent of inhibition of CPT-1a. *Am J Physiol - Regul Integr Comp Physiol*. 2011;301(1):209–17.

100. Tipton CM. Susruta of India, an unrecognized contributor to the history of exercise physiology. *J Appl Physiol.* 2008;104(6):1553–6.

101. Garrett NA, Brasure M, Schmitz KH, Schultz MM, Huber MR. Physical inactivity: Direct cost to a health plan. *Am J Prev Med.* 2004;27(4):304–9.

102. Monninkhof EM, Elias SG, Vlems FA, Van Der Tweel I, Schuit AJ, Voskuil DW, *et al.* Physical activity and breast cancer: A systematic review. *Epidemiology*. 2007;18(1):137–57.

103. Ruegsegger GN, Booth FW. Running from disease: Molecular mechanisms associating dopamine and leptin signaling in the brain with physical inactivity, obesity, and type 2 diabetes. *Front Endocrinol (Lausanne)*. 2017;8:1–8.

104. Taylor CB, Sallis JF, Needle R. The relation of physical activity and exercise to mental health. *Public Health Rep.* 1985;100(2):195–202.

105. Rovio S, Kåreholt I, Helkala EL, Viitanen M, Winblad B, Tuomilehto J, *et al.* Leisure-time physical activity at midlife and the risk of dementia and Alzheimer's disease. *Lancet Neurol.* 2005;4(11):705–11.

106. Chekroud SR, Gueorguieva R, Zheutlin AB, Paulus M, Krumholz HM, Krystal JH, *et al.* Association between physical exercise and mental health in 1·2 million individuals in the USA between 2011 and 2015: a cross-sectional study. *The Lancet Psychiatry.* 2018;5(9):739–46.

107. Hawley JA, Hargreaves M, Joyner MJ, Zierath JR. Integrative biology of exercise. *Cell*. 2014;159(4):738–49.

108. Pedersen BK. Physical activity and muscle–brain crosstalk. *Nat Rev Endocrinol*. 2019;15(7):383-392

109. St-Pierre, David H. and Richard D. The effect of Exercise on the Hypothalamic-Pituitary-Adrenal Axis. In: *Endocrinology of Physical Activity and Sport. Second Edi.* 2013. p. 37–44.

110. Ibeas K, Herrero L, Mera P, Serra D. Hypothalamus-skeletal muscle crosstalk during exercise and its role in metabolism modulation. *Biochem Pharmacol.* 2021;190:114640.

111. Gallagher S, Butterworth GE, Lew A, Cole J. Hand-mouth coordination, congenital absence of limb, and evidence for innate body schemas. *Brain Cogn.* 1998;38(1):53–65.

112. Rolfe DFS, Brown GC. Cellular energy utilization and molecular origin of standard metabolic rate in mammals. *Physiol Rev.* 1997;77(3):731–58.

113. Berström J, Hultman E. Muscle Glycogen Synthesis after exercise: an Enhancing Factor localized to the Muscle Cells in Man. *Nature*. 1966;210:309–10.

114. Schiaffino S, Reggiani C. Fiber types in Mammalian skeletal muscles. *Physiol Rev*. 2011;91(4):1447–531.

115. Scott W, Stevens J, Binder-Macleod SA. Human skeletal muscle fiber type classifications. *Phys Ther*. 2001;81(11):1810–6.

116. Ferraro E, Giammarioli AM, Chiandotto S, Spoletini I, Rosano G. Exercise-induced skeletal muscle remodeling and metabolic adaptation: Redox signaling and role of autophagy.

Antioxidants Redox Signal. 2014;21(1):154–76.

117. Bottinelli R. Functional heterogeneity of mammalian single muscle fibres: Do myosin isoforms tell the whole story?. *Arch Eur J Physiol.* 2001;443(1):6–17.

118. Pilegaard H, Saltin B, Neufer DP. Exercise induces transient transcriptional activation of the PGC-1α gene in human skeletal muscle. *J Physiol.* 2003;546(3):851–8.

119. Handschin C, Chin S, Li P, Liu F, Maratos-Flier E, LeBrasseur NK, *et al*. Skeletal muscle fiber-type switching, exercise intolerance, and myopathy in PGC-1α muscle-specific knock-out animals. *J Biol Chem.* 2007;282(41):30014–21.

120. Narkar VA, Downes M, Yu RT, Embler E, Wang YX, Banayo E, *et al.* AMPK and PPARδ Agonists Are Exercise Mimetics. *Cell*. 2008;134(3):405–15.

121. Luquet S, Lopez-Soriano J, Holst D, Fredenrich A, Melki J, Rassoulzadegan M, *et al.* Peroxisome proliferator-activated receptor δ controls muscle development and oxidative capability. *FASEB J.* 2003;17(15):2299–301.

122. Larsson L, Degens H, Li M, Salviati L, Lee Y Il, Thompson W, *et al*. Sarcopenia: Aging-related loss of muscle mass and function. *Physiol Rev.* 2019;99(1):427–511.

123. McGee SL, Fairlie E, Garnham AP, Hargreaves M. Exercise-induced histone modifications in human skeletal muscle. *J Physiol.* 2009;587(24):5951–8.

124. Williams K, Carrasquilla GD, Ingerslev LR, Hochreuter MY, Hansson S, Pillon NJ, *et al.* Epigenetic rewiring of skeletal muscle enhancers after exercise training supports a role in whole-body function and human health. *Mol Metab.* 2021;53:101290.

125. Hawley JA, Lessard SJ. Exercise training-induced improvements in insulin action. *Acta Physiol.* 2008;192(1):127–35.

126. Calvo JA, Daniels TG, Wang X, Paul A, Lin J, Spiegelman BM, *et al.* Muscle-specific expression of PPARγ coactivator-1α improves exercise performance and increases peak oxygen uptake. *J Appl Physiol.* 2008;104(5):1304–12.

127. Chinsomboon J, Ruas J, Gupta RK, Thom R, Shoag J, Rowe GC, *et al.* The transcriptional coactivator PGC-1α mediates exercise-induced angiogenesis in skeletal muscle. *Proc Natl Acad Sci U S A.* 2009;106(50):21401–6.

128. Lin J, Wu H, Tarr PT, Zhang CY, Wu Z, Boss O, *et al*. Transcriptional co-activator PGC-1α drives the formation of slow-twitch muscle fibres. *Nature*. 2002;418(6899):797–801.

129. Handschin C and SB. The role of exercise and PGC1a in inflammation and chronic diasease. *Nature*. 2008;454(7203):463–9.

130. Tadaishi M, Miura S, Kai Y, Kawasaki E, Koshinaka K, Kawanaka K, *et al.* Effect of exercise intensity and AICAR on isoform-specific expressions of murine skeletal muscle PGC-1α mRNA: A role of β2-adrenergic receptor activation. *Am J Physiol - Endocrinol Metab.* 2011;300(2):341–9.

131. Dillon L, Rebelo A, Morales C. The role of PGC1 coactivator sin Aging Skeletal Muscle and Heart. *IUBMB Life*. 2012;64(3):231–41.

132. Frøsig C, Jørgensen SB, Hardie DG, Richter EA, Wojtaszewski JFP. 5'-AMP-activated protein kinase activity and protein expression are regulated by endurance training in human skeletal muscle. *Am J Physiol - Endocrinol Metab.* 2004;286(3 49-3):411–7.

133. Nader GA, Esser KA. Intracellular signaling specificity in skeletal muscle in response to different modes of exercise. *J Appl Physiol.* 2001;90(5):1936–42.

134. Geng T, Li P, Okutsu M, Yin X, Kwek J, Zhang M, *et al*. PGC-1α plays a functional role in exercise-induced mitochondrial biogenesis and angiogenesis but not fiber-type transformation in mouse skeletal muscle. *Am J Physiol - Cell Physiol.* 2010;298(3):572–9.

135. Lira VA, Benton CR, Yan Z, Bonen A. PGC-1α regulation by exercise training and its influences on muscle function and insulin sensitivity. *Am J Physiol - Endocrinol Metab.* 2010;299(2).

136. Cantó C, Jiang LQ, Deshmukh AS, Mataki C, Coste A, Lagouge M, *et al.* Interdependence of AMPK and SIRT1 for Metabolic Adaptation to Fasting and Exercise in Skeletal Muscle. *Cell Metab.* 2010;11(3):213–9.

137. Small EM, O'Rourke JR, Moresi V, Sutherland LB, McAnally J, Gerard RD, *et al.* Regulation of PI3-kinase/Akt signaling by muscle-enriched microRNA-486. *Proc Natl Acad Sci U S A.* 2010;107(9):4218–23.

138. Bodine SC, Latres E, Baumhueter S, Lai VKM, Nunez L, Clarke BA, *et al.* Identification of ubiquitin ligases required for skeletal Muscle Atrophy. *Science*. 2001;294(5547):1704–8.

139. Powers SK, Kavazis AN, McClung JM. Oxidative stress and disuse muscle atrophy. *J Appl Physiol.* 2007;102(6):2389–97.

140. Lin J, Arnold HB, Della-Fera MA, Azain MJ, Hartzell DL, Baile CA. Myostatin knockout in mice increases myogenesis and decreases adipogenesis. *Biochem Biophys Res Commun.* 2002;291(3):701–6.

141. Winbanks CE, Weeks KL, Thomson RE, Sepulveda P V., Beyer C, Qian H, *et al.* Follistatin-mediated skeletal muscle hypertrophy is regulated by Smad3 and mTOR independently of myostatin. *J Cell Biol.* 2012;197(7):997–1008.

142. Sartori R, Romanello V, Sandri M. Mechanisms of muscle atrophy and hypertrophy: implications in health and disease. *Nat Commun.* 2021;12(1):1–12.

143. Coffey VG, Hawley JA. Molecular basis of training adaptation. *Sport Med.* 2007;37(9):737–63.

144. Sandri M, Lin J, Handschin C, Yang W, Arany ZP, Lecker SH, *et al.* PGC-1α protects skeletal muscle from atrophy by suppressing FoxO3 action and atrophy-specific gene transcription. *Proc Natl Acad Sci U S A.* 2006;103(44):16260–5.

145. Jahnke VE, Van Der Meulen JH, Johnston HK, Ghimbovschi S, Partridge T, Hoffman EP, *et al.* Metabolic remodeling agents show beneficial effects in the dystrophin-deficient mdx mouse model. *Skelet Muscle.* 2012;2(1):1.

146. Pedersen BK, Febbraio MA. Muscles, exercise and obesity: skeletal muscle as a secretory organ. *Nat Rev Endocrinol.* 2012;8(8):457–65.

147. Goldstein MS. Humoral nature of the hypoglycemic factor of muscular work. *Diabetes*. 1961;10(3):232–4.

148. Delezie J, Handschin C. Endocrine crosstalk between Skeletal muscle and the brain. *Front Neurol.* 2018;9:698–702.

149. Rai M, Demontis F. Systemic Nutrient and Stress Signaling via Myokines and Myometabolites. *Annu Rev Physiol.* 2016;78:85–107.

150. Safdar A, Saleem A, Tarnopolsky MA. The potential of endurance exercise-derived exosomes

to treat metabolic diseases. *Nat Rev Endocrinol.* 2016;12(9):504–17.

151. Steensberg A, Van Hall G, Osada T, Sacchetti M, Saltin B, Pedersen BK. Production of interleukin-6 in contracting human skeletal muscles can account for the exercise-induced increase in plasma interleukin-6. *J Physiol.* 2000;529(1):237–42.

152. Philip C, Fischer P. Interleukin-6 in acute exercise and training : what is the biological relevance. *Exerc Immu Rev*. 2016;1991:6–33.

153. Keller C, Hellsten Y, Steensberg A, Klarlund Pedersen B. Differential regulation of IL-6 and TNF-α via calcineurin in human skeletal muscle cells. *Cytokine*. 2006;36(3–4):141–7.

154. Pedersen BK. Muscular interleukin-6 and its role as an energy sensor. *Med Sci Sports Exerc.* 2012;44(3):392–6.

155. Hoene M, Weigert C. The role of interleukin-6 in insulin resistance, body fat distribution and energy balance. *Obes Rev.* 2008;9(1):20–9.

156. Carey AL, Steinberg GR, Macaulay SL, Thomas WG, Holmes AG, Ramm G, *et al.* Interleukin-6 increases insulin-stimulated glucose disposal in humans and glucose uptake and fatty acid oxidation in vitro via AMP-activated protein kinase. *Diabetes*. 2006;55(10):2688–97.

157. Ellingsgaard H, Hauselmann I, Schuler B, Habib AM, Baggio LL, Meier DT, *et al.* Interleukin-6 enhances insulin secretion by increasing glucagon-like peptide-1 secretion from L cells and alpha cells. *Nat Med.* 2011;17(11):1481–9.

158. Chowdhury S, Schulz L, Palmisano B, Singh P, Berger JM, Yadav VK, *et al.* Muscle-derived interleukin 6 increases exercise capacity by signaling in osteoblasts. *J Clin Invest*. 2020;130(6):2888–902.

159. Schindler R, Mancilla J, Endres S, Ghorbani R, Clark S, Dinarello C. Correlations and interactions in the production of interleukin-6 (IL- 6), IL-1, and tumor necrosis factor (TNF) in human blood mononuclear cells: IL-6 suppresses IL-1 and TNF. *Blood*. 1990;75(1):40–7.

160. Mizuhara BH, Neill EO, Ogawa T, Kusunoki C, Otsuka K, Satoh S, *et al*. T Cell Activation-associated Hepatic Injury: mediation by tumor necrosis factors and protection by interleukin 6. *J Exp Med*. 1994;179:884–6.

161. Steensberg A, Fischer CP, Keller C, Møller K, Pedersen BK. IL-6 enhances plasma IL-1ra, IL-10, and cortisol in humans. *Am J Physiol - Endocrinol Metab*. 2003;285(2 48-2):433–7.

162. McPherron AC, Lawler AM, Lee SJ. Regulation of skeletal muscle mass in mice by a new TGF-beta superfamily member. *Nature*. 1997;387(6628):83–90.

163. Schnyder S, Handschin C. Skeletal muscle as an endocrine organ : PGC-1 α , myokines and exercise. *Bone*. 2015;80(1):115–25.

164. Dankbar B, Fennen M, Brunert D, Hayer S, Frank S, Wehmeyer C, *et al.* Myostatin is a direct regulator of osteoclast differentiation and its inhibition reduces inflammatory joint destruction in mice. *Nat Med*. 2015;21(9):1085–90.

165. Matthews VB, Åström MB, Chan MHS, Bruce CR, Krabbe KS, Prelovsek O, *et al*. Brain-derived neurotrophic factor is produced by skeletal muscle cells in response to contraction and enhances fat oxidation via activation of AMP-activated protein kinase. *Diabetologia*. 2009;52(7):1409–18.

166. Nitta A, Ohmiya M, Sometani A, Itoh M, Nomoto H, Furukawa Y, *et al.* Brain-derived neurotrophic factor prevents neuronal cell death induced by corticosterone. J *Neurosci Res*.

1999;57(2):227–35.

167. Tyler WJ, Alonso M, Bramham CR, Pozzo-miller LD. From acquisition to consoliadation: on the role of BDNF signaling in hippocampal-dependent learning. *Learn Mem.* 2002;9(5):224–37.

168. Sleiman SF, Henry J, Al-Haddad R, El Hayek L, Haidar EA, Stringer T, *et al.* Exercise promotes the expression of brain derived neurotrophic factor (BDNF) through the action of the ketone body β- hydroxybutyrate. *Elife*. 2016;5(JUN2016):1–21.

169. Clow C, Jasmin BJ. Brain-derived neurotrophic factor regulates satellite cell differentiation and skeltal muscle regeneration. *Mol Biol Cell.* 2010;21(13):2182–90.

170. He Z, Gao Y, Alhadeff AL, Castorena CM, Huang Y, Lieu L, *et al.* Cellular and synaptic reorganization of arcuate NPY/AgRP and POMC neurons after exercise. *Mol Metab*. 2018;18:107–19.

171. Shin MS, Kim H, Chang HK, Lee TH, Jang MH, Shin MC, *et al.* Treadmill exercise suppresses diabetes-induced increment of neuropeptide Y expression in the hypothalamus of rats. *Neurosci Lett.* 2003;346(3):157–60.

172. Laing BT, Do K, Matsubara T, Wert DW, Avery MJ, Langdon EM, *et al.* Voluntary exercise improves hypothalamic and metabolic function in obese mice. *J Endocrinol.* 2016;229(2):109–22.

173. Benite-Ribeiro SA, Putt DA, Santos JM. The effect of physical exercise on orexigenic and anorexigenic peptides and its role on long-term feeding control. *Med Hypotheses.* 2016;93:30–3.

174. Onambélé-Pearson GL, Breen L, Stewart CE. Influence of exercise intensity in older persons with unchanged habitual nutritional intake: Skeletal muscle and endocrine adaptations. *Age (Omaha)*. 2010;32(2):139–53.

175. Caruso V, Bahari H, Morris MJ. The beneficial effects of early short-term exercise in the offspring of obese mothers are accompanied by alterations in the hypothalamic gene expression of appetite regulators and FTO (fat mass and obesity associated) gene. *J Neuroendocrinol.* 2013;25(8):742–52.

176. Cowley MA, Smart JL, M. R, G. CM, Diano S, Horvath TL, *et al.* Leptin activates anorexigenic POMC neurons through a neural network in the arcuate nucleus. *Nature*. 2001;411(6836):480–4.

177. Bunner W, Landry T, Laing BT, Li P, Rao Z, Yuan Y, *et al.* ARCAgRP/NPY Neuron Activity Is Required for Acute Exercise-Induced Food Intake in Un-Trained Mice. *Front Physiol*. 2020;11(May):1–12.

178. Jeong JH, Lee DK, Liu SM, Chua SC, Schwartz GJ, Jo YH. Activation of temperature-sensitive TRPV1-like receptors in ARC POMC neurons reduces food intake. *PLoS Biol.* 2018;16(4):1–24.

179. Miletta MC, Iyilikci O, Shanabrough M, Šestan-Peša M, Cammisa A, Zeiss CJ, *et al.* AgRP neurons control compulsive exercise and survival in an activity-based anorexia model. *Nat Metab.* 2020;2(11):1204–11.

180. Calvez J, Fromentin G, Nadkarni N, Darcel N, Even P, Tomé D, *et al.* Inhibition of food intake induced by acute stress in rats is due to satiation effects. *Physiol Behav.* 2011;104(5):675–83.

181. Pei H, Patterson CM, Sutton AK, Burnett KH, Myers MG, Olson DP. Lateral hypothalamic Mc3R-expressing neurons modulate locomotor activity, energy expenditure, and adiposity in

male mice. *Endocrinology*. 2019;160(2):343–58.

182. Kosse C, Schöne C, Bracey E, Burdakov D. Orexin-driven GAD65 network of the lateral hypothalamus sets physical activity in mice. *Proc Natl Acad Sci U S A*. 2017;114(17):4525–30.

183. Kim ER, Xu Y, Cassidy RM, Lu Y, Yang Y, Tian J, *et al.* Paraventricular hypothalamus mediates diurnal rhythm of metabolism. *Nat Commun*. 2020;11(1):1–17.

184. Droste SK, Gesing A, Ulbricht S, Müller MB, Linthorst AE, Reul JM. Effects of long-term voluntary exercise on the mouse hypothalamic-pituitary-adrenocortical axis. *Endocrinology*. 2003;144(7):3012–23.

185. Garcia-Sainz JA. Adrenaline and its receptors: one hundred years of research. *Arch Med Res.* 1995;26(3):205–12.

186. Choo JJ, Horan MA, Little RA, Rothwell NJ. Anabolic effects of clenbuterol on skeletal muscle are mediated by β2- adrenoceptor activation. *Am J Physiol - Endocrinol Metab.* 1992;263(6-1).

187. World Health Organization. Ageing and Health. *World Health Organization*. 2021;1.

188. Booth FW, Laye MJ, Roberts MD. Lifetime sedentary living accelerates some aspects of secondary aging. *J Appl Physiol*. 2011;111(5):1497–504.

189. Svennerholm L, Boström K, Jungbjer B. Changes in weight and compositions of major membrane components of human brain during the span of adult human life of Swedes. *Acta Neuropathol*. 1997;94(4):345–52.

190. Peters R. Ageing and the brain. *Postgrad Med J*. 2006;82(964):84–8.

191. Barnes CA. Long-term potentiation and the ageing brain. *Philos Trans R Soc B Biol Sci.* 2003;358(1432):765–72.

192. Besdine RW, Wu D. Aging of the human nervous system: what do we know? *Med Health R I.* 2008;91(5):129–31.

193. Esopenko C, Levine B. Aging, neurodegenerative disease, and traumatic brain injury: The role of neuroimaging. *J Neurotrauma.* 2015;32(4):209–20.

194. Mayeux R, Stern Y. Epidemiology of Alzheimer disease. *Cold Spring Harb Perspect Med.* 2012;2(8).

195. Benabid AL. Deep brain stimulation for Parkinson's disease. *Curr Opin Neurobiol*. 2003;13(6):696–706.

196. Salthouse TA. Selective review of cognitive aging. *J Int Neuropsychol Soc.* 2010;16(5):754–60.

197. Sonnen JA, Larson EB, Crane PK, Haneuse S, Li G, Schellenberg GD, *et al.* Pathological correlates of dementia in a longitudinal, population-based sample of aging. *Ann Neurol.* 2007;62(4):406–13.

198. Fotuhi M, Do D, Jack C. Modifiable factors that alter the size of the hippocampus with ageing. *Nat Rev Neurol.* 2012;8(4):189–202.

199. Mattson MP, Magnus T. Ageing and neuronal vulnerability. *Nat Rev Neurosci.* 2006;7(4):278–94.

200. Bano D, Agostini M, Melino G, Nicotera P. Ageing, neuronal connectivity and brain disorders: An unsolved ripple effect. *Mol Neurobiol.* 2011;43(2):124–30.

201. Marks BL, Katz LM, Styner M, Smith JK. Aerobic fi tness and obesity: Relationship to cerebral white matter integrity in the brain of active and sedentary older adults. *J Sports Med.* 2011;45(15):1208–15.

202. Puig J, Blasco G, Daunis-I-Estadella J, Molina X, Xifra G, Ricart W, *et al.* Hypothalamic damage is associated with inflammatory markers and worse cognitive performance in obese subjects. *J Clin Endocrinol Metab.* 2015;100(2):276–81.

203. Otsuka M, Yamaguchi K, Ueki A. Similarities and differences between Alzheimer's disease and vascular dementia from the viewpoint of nutrition. *Ann NY Acad Sci.* 2002;977:155–61.

204. Mattson MP. Will caloric restriction and folate protect against AD and PD? *Neurology*. 2003;60(4):690–5.

205. Zandi PP, Anthony JC, Khachaturian AS, Stone S V., Gustafson D, Tschanz JA, *et al.* Reduced Risk of Alzheimer Disease in Users of Antioxidant Vitamin Supplements: The Cache County Study. *Arch Neurol.* 2004;61(1):82–8.

206. Barja G. Free radicals and aging. *Trends Neurosci.* 2004;27(10):595–600.

207. Colcombe SJ, Erickson KI, Raz N, Webb AG, Cohen NJ, McAuley E, *et al.* Aerobic fitness reduces brain tissue loss in aging humans. J*ournals Gerontol - Ser A Biol Sci Med Sci.* 2003;58(2):176–80.

208. Janssens GE, Grevendonk L, Perez RZ, Schomakers B V., de Vogel-van den Bosch J, Geurts JMW, *et al.* Healthy aging and muscle function are positively associated with NAD+ abundance in humans. *Nat Aging*. 2022;2(3):254–63.

209. Cheng S, Degens H, Evans M, Cheng SM, Selänne H, Rittweger J, *et al.* What makes a 97-year-old man cycle 5,000 km a year? *Gerontology*. 2016;62(5):508–12.

210. Rosenberg IH. Symposium: Sarcopenia: Diagnosis and Mechanisms Sarcopenia: Origins and Clinical Relevance 1. *J Nutr.* 1997;127:990–1.

211. Beaudart C, Reginster JY, Slomian J, Buckinx F, Dardenne N, Quabron A, *et al.* Estimation of sarcopenia prevalence using various assessment tools. *Exp Gerontol.* 2015;61:31–7.

212. Gouspillou G, Bourdel-Marchasson I, Rouland R, Calmettes G, Biran M, Deschodt-Arsac V, *et al.* Mitochondrial energetics is impaired in vivo in aged skeletal muscle. *Aging Cell.* 2014;13(1):39–48.

213. Cleasby ME, Jamieson PM, Atherton PJ. Insulin resistance and sarcopenia: Mechanistic links between common co-morbidities. *J Endocrinol.* 2016;229(2):R67–81.

214. Merritt EK, Stec MJ, Thalacker-Mercer A, Windham ST, Cross JM, Shelley DP, *et al.* Heightened muscle inflammation susceptibility may impair regenerative capacity in aging humans. *J Appl Physiol.* 2013;115(6):937–48.

215. Larsson L, Karlsson J. Isometric and dynamic endurance as a function of age and skeletal muscle characteristics. *Acta Physiol Scand.* 1978;104(2):129–36.

216. Schultz A, Ashton-Miller J, Alexander N. What leads to age and gender differences in balance maintenance and recovery? *Muscle*. 1997;5:60–4.

217. Caccia MR, Harris JB, Johnson MA. Morphology and physiology of skeletal muscle in aging rodents. *Muscle Nerve*. 1979;2(3):202–12.

218. Kim JS, Kosek DJ, Petrella JK, Cross JM, Bamman MM. Resting and load-induced levels of

myogenic gene transcripts differ between older adults with demonstrable sarcopenia and young men and women. *J Appl Physiol.* 2005;99(6):2149–58.

219. Einsiedel LJ, Luff AR. Effect of partial denervation on motor units in the ageing rat medial gastronemius. *J Neurol Sci.* 1992;112(1–2):178–84.

220. Brown WF. A method for estimating the number of motor units in thenar muscles and the changes in motor unit count with ageing. *J Neurol Neurosurg Psychiatry.* 1972;35(6):845–52.

221. Kirkendall DT, Garrett WE. Current Concepts The Effects of Aging and Training on Skeletal Muscle. *J Am Sports Med* 1998;26(4):598–602.

222. Frontera WR, Meredith CN, O'reilly KP, Knuttgen HG, Evans WJ. Strengh conditioning in older men: skeletal muscle hypertrophy and improved function. *Pap Knowl Towar a Media Hist Doc*. 1988;7:1038–44.

223. Robinson S, Cooper C, Aihie Sayer A. Nutrition and sarcopenia: A review of the evidence and implications for preventive strategies. *J Aging Res*. 2012;2012.

224. Millward DJ. Nutrition and sarcopenia: Evidence for an interaction. *Proc Nutr Soc.* 2012;71(4):566–75.

225. Horstman AM, Dillon EL, Urban RJ, Sheffield-Moore M. The role of androgens and estrogens on healthy aging and longevity. *Journals Gerontol - Ser A Biol Sci Med Sci.* 2012;67(11):1140–52.

226. Siparsky PN, Kirkendall DT, Garrett WE. Muscle Changes in Aging: Understanding Sarcopenia. *Sports Health*. 2014;6(1):36–40.

227. Xia X, Chen W, McDermott J, Han JD. Molecular and phenotypic biomarkers of aging. *F1000Research*. 2017;6.

228. Engelfriet PM, Jansen EH, Picavet HS, Dollé ME. Biochemical markers of aging for longitudinal studies in humans. *Epidemiol Rev.* 2013;35(1):132–51.

229. Rehkopf DH, Needham BL, Lin J, Blackburn EH, Zota AR, Wojcicki JM, *et al.* Leukocyte Telomere Length in Relation to 17 Biomarkers of Cardiovascular Disease Risk: A Cross-Sectional Study of US Adults. *PLoS Med.* 2016;13(11).

230. Gorisse L, Pietrement C, Vuiblet V, Schmelzer CEH, Köhler M. Protein carbamylation is a hallmark of aging. *Proc Natl Acad Sci USA.* 2016;113(5):1191–6.

231. Syslová K, Böhmová A, Mikoška M, Kuzma M, Pelclová D, I PK. Multimarker Screening of Oxidative Stress in Aging. *Oxid Med Cell Longev*. 2014;2014:562860.

232. Matjusaitis M, Chin G, Anders E, Stolzing A. Biomarkers to identify and isolate senescent cells. *Ageing Res Rev.* 2016;29:1–12.

233. Chen W, Qian W, Wu G, Chen W, Xian B, Chen X, *et al.* Three-dimensional human facial morphologies as robust aging markers. *Nat Publ Gr.* 2015;25(5):574–87.

234. Frater J, Lie D, Bartlett P, Mcgrath JJ. Insulin-like Growth Factor 1 (IGF-1) as a marker of cognitive decline in normal ageing : A review. *Ageing Res Rev.* 2018;42:14–27.

235. Brown-borg HM, Borg KE. Dwarf mice and the ageing process. *Nature*. 1996;384:180.

236. Ashpole NM, Sanders JE, Hodges EL, Yan H, Sonntag WE. Growth hormone , insulin-like growth factor-1 and the aging brain IGF-1 Protein Levels. *Exp Gerontol* . 2015;68:76–81.

237. Milman S, Huffman DM, Barzilai N. Review The Somatotropic Axis in Human Aging : Framework for the Current State of Knowledge and Future Research. *Cell Metab*. 2016;23(6):980–9.

238. Gubbi S, Quipildor GF, Barzilai N, Huffman DM, Milman S. 40 years of IGF1: IGF1: The Jekyll and Hyde of the aging brain. *J Mol Endocrino*l. 2018;61(1):T171–85.

239. Piriz J, Muller A, Trejo JL. IGF-I and the aging mammalian brain. *Exp Gerontol.* 2011;46(2–3):96–9.

240. Holzenberger M, Dupont J, Ducos B, Leneuve P, Géloên A, Even PC, et al. IGF-1 receptor regulates lifespan and resistance to oxidative stress in mice. *Nature*. 2003;421.

241. Bartke A. Healthspan and longevity can be extended by suppression of growth hormone signaling. *Mamm Genome*. 2016;27(7):289–99.

242. Junnila RK, List EO, Berryman DE, Murrey JW, Kopchick JJ. The GH / IGF - 1 axis in ageing and longevity. *Nat Rev Endocrinol.* 2013;9:366–76.

243. Vitale G, Pellegrino G, Vollery M, Hofland LJ. ROLE of IGF-1 system in the modulation of longevity: Controversies and new insights from a centenarians' perspective. *Front Endocrinol (Lausanne)*. 2019;10(2):1–11.

244. Berryman DE, Sandahl J, Johannsson G, Thorner MO, Kopchick JJ. Role of the GH / IGF-1 axis in lifespan and healthspan : Lessons from animal models. *Growth Horm IGF Res.* 2008;18(6):455–71.

245. Paolisso G, Ammendola S, Del Buono A, Gambardella A, Riondino M, Tagliamonte MR*, et al.* Serum levels of insulin-like growth factor-I (IGF-I) and IGF-binding protein-3 in healthy centenarians: Relationship with plasma leptin and lipid concentrations, insulin action, and cognitive function. *J Clin Endocrinol Metab.* 1997;82(7):2204–9.

246. Lam JK, Chow MY, Zhang Y, Leung SW. siRNA Versus miRNA as Therapeutics for Gene Silencing. *Mol Ther Nucleic Acids.* 2015;4(9):252.

247. Bader AG, Brown D, Stoudemire J, Lammers P. Developing therapeutic microRNAs for cancer. *Gene Ther.* 2011;1121–6.

248. Chandra PK, Kundu AK, Hazari S, Chandra S, Bao L, Ooms T, *et al.* Inhibition of Hepatitis C Virus Replication by Intracellular Delivery of Multiple siRNAs by Nanosomes. *Mol Ther.* 2012;20(9):1724–36.

249. Maegdefessel L. The emerging role of microRNAs in cardiovascular disease. *J Intern Med.* 2014; 276(6);663–44.

250. Carthew RW, Sontheimer EJ. Origins and mechanisms of miRNAs and siRNAs. *Cell*. 2009;136(4):642–55.

251. Agrawal N, Dasaradhi PVN, Mohmmed A, Malhotra P, Bhatnagar RK, Mukherjee SK. RNA Interference : Biology , Mechanism , and Applications. *Microbiol Mol Biol Rev.* 2003;67(4):657–85.

252. Fire A, Xu S, Montgomery M, Kostas S, Driver S, Mello C. Potent and specific interference by double-stranded RNA in Caenorhabditis elegans. *Nature*. 1998;391:806–11.

253. Elbashir SM, Harborth J, Lendeckel W, Yalcin A, Weber K, Tuschl T. Duplexes of 21 ± nucleotide RNAs mediate RNA interference in cultured mammalian cells. *Nature*. 2001;411(6836):494–8.

254. Lee R, Feinbaum R, Ambros V. The C . elegans Heterochronic Gene lin-4 Encodes Small RNAs with Antisense Complementarity to lin-14. *Cell*. 1993;75(5):843–54.

255. Svoboda P. Key Mechanistic Principles and Considerations Concerning RNA Interference. *Front Plant Sci.* 2020;11:1237.

256. Wang Q, Liu C, Uchida A, Chuang JC, Walker A, Liu T, *et al.* Arcuate AgRP neurons mediate orexigenic and glucoregulatory actions of ghrelin. *Mol Metab.* 2014;3(1):64–72.

257. Zincarelli C, Soltys S, Rengo G, Rabinowitz JE. Analysis of AAV serotypes 1-9 mediated gene expression and tropism in mice after systemic injection. *Mol Ther.* 2008;16(6):1073–80.

258. Piedra J, Ontiveros M, Miravet S, Penalva C, Monfar M, Chillon M. Development of a rapid, robust, and universal PicoGreen-based method to titer adeno-associated vectors. *Hum Gene Ther Methods*. 2015;26(1):35–42.

259. Dougherty JP, Springer DA, Gershengorn MC. The treadmill fatigue test: A simple, high-throughput assay of fatigue-like behavior for the mouse. *J Vis Exp*. 2016;2016(111):1–7.

260. Wilson RC, Vacek T, Lanier DL, Dewsbury DA. Open-field behavior in muroid rodents. *Behav Biol.* 1976;17(4):495–506.

261. Walf A, Frye C. The use of the elevated plus maze as an assay of anxiety-related behavior in rodents. *Nat Protoc.* 2007;2(2).

262. Deacon RMJ. Measuring motor coordination in mice. *J Vis Exp.* 2013;(75):1–8.

263. Deacon RMJ. Measuring the strength of mice. *J Vis Exp.* 2013;(76):1–4.

264. Ennaceur A, Meliani K. A new one-trial test for neurobiological studies of memory in rats. III. Spatial vs. non-spatial working memory. *Behav Brain Res.* 1992;51(1):83–92.

265. Companys-Alemany J, Turcu AL, Bellver-Sanchis A, Loza MI, Brea JM, Canudas AM, *et al.* A novel NMDA receptor antagonist protects against cognitive decline presented by senescent mice. *Pharmaceutics.* 2020;12(3):1–17.

266. Ennaceur A, Delacour J. A new one-trial test for neurobiological studies of memory in rats. 1: Behavioral data. *Behav Brain Res.* 1988;31(1):47–59.

267. Knudsen JG, Gudiksen A, Bertholdt L, Overby P, Villesen I, Schwartz CL, *et al.* Skeletal muscle IL-6 regulates muscle substrate utilization and adipose tissue metabolism during recovery from an acute bout of exercise. *PLoS One*. 2017;12(12):1–19.

268. Wang C, Yue F, Kuang S. Muscle Histology Characterization Using H&E Staining and Muscle Fiber Type Classification Using Immunofluorescence Staining. *Bio Prtotoc*. 2017;7(10).

269. Ershov D, Phan M, Pylvänäinen JW, Rigaud SU, Blanc L Le, Conway JRW, et al. Bringing TrackMate in the era of machine-learning and deep-learning. BioRxiv. 2021;20:1–4.

270. Sebastián D, Sorianello E, Segalés J, Irazoki A, Ruiz-Bonilla V, Sala D, *et al.* Mfn2 deficiency links age-related sarcopenia and impaired autophagy to activation of an adaptive mitophagy pathway. *EMBO J.* 2016;35(15):1677–93.

271. Lewis BP, Burge CB, Bartel DP. Conserved seed pairing, often flanked by adenosines, indicates that thousands of human genes are microRNA targets. *Cell*. 2005;120(1):15–20.

272. Liu W, Wang X. Prediction of functional microRNA targets by integrative modeling of microRNA binding and target expression data. *Genome Biol.* 2019;20(1):1–10.

273. Cheung C, Kurrasch D, Liang J, Ingraham H. Genetic Labeling of Steroidogenic Factor-1 (SF-1) Neurons in Mice Reveals Ventromedial Nucleus of the Hypothalamus (VMH) Circuitry Beginning at Neurogenesis and Development of a Separate Non-SF-1 Neuronal Cluster in the Ventrolateral VMH. *J Comp Neurol.* 2013;521(6):1268–88.

274. Labbé SM, Caron A, Lanfray D, Monge-Rofarello B, Bartness TJ, Richard D. Hypothalamic control of brown adipose tissue thermogenesis. *Front Syst Neurosci.* 2015;9:1–13.

275. Tran LT, Park S, Kim SK, Lee JS, Kim KW, Kwon O. Hypothalamic control of energy expenditure and thermogenesis. *Exp Mol Med*. 2022;54(4);354-69.

276. Miralpeix C, Fosch A, Casas J, Baena M, Herrero L, Serra D, *et al.* Hypothalamic endocannabinoids inversely correlate with the development of diet-induced obesity in male and female mice. *J Lipid Res.* 2019;60(7):1260–9.

277. Landry T, Shookster D, Chaves A, Free K, Nguyen T, Huang H. Exercise increases NPY/AgRP and TH neuron activity in the hypothalamus of female mice. *J Endocrinol.* 2022;252(3):167–77.

278. Bishop PA, Crowder TA, Fielitz LR, Lindsay TR, Woods AK. Impact of body weight on performance of a weight-supported motor fitness test in men. *Mil Med.* 2008;173(11):1108–14.

279. Barrow P, Leconte I. The influence of body weight on open field and swimming maze performance during the post-weaning period in the rat. *Lab Anim.* 1996;30(1):22–7.

280. Shoji H, Takao K, Hattori S, Miyakawa T. Age-related changes in behavior in C57BL/6J mice from young adulthood to middle age. *Mol Brain.* 2016;9(1):1–18.

281. Jeong SW, Kim SH, Kang SH, Kim HJ, Yoon CH, Youn TJ, *et al.* Mortality reduction with physical activity in patients with and without cardiovascular disease. *Eur Heart J.* 2019;40(43):3547–55.

282. Jiang J, Morgan DA, Cui H, Rahmouni K. Activation of hypothalamic AgRP and POMC neurons evokes disparate sympathetic and cardiovascular responses. *Am J Physiol - Hear Circ Physiol.* 2020;319(5):1069–77.

283. Mao K, Quipildor GF, Tabrizian T, Novaj A, Guan F, Walters RO, *et al.* Late-life targeting of the IGF-1 receptor improves healthspan and lifespan in female mice. *Nat Commun.* 2018;9(1):1–12.

284. Xiao Y, Chen W, Chen R, Luo A, Chen D, Liang Q, *et al.* Exosomal MicroRNA Expression Profiling Analysis of the Effects of Lycium Barbarum Polysaccharide on Gestational Diabetes Mellitus Mice. *Evidence-based Complement Altern Med.* 2020;2020:29533502.

285. Diéguez C, Frühbeck G, López M. Hypothalamic lipids and the regulation of energy homeostasis. *Obes Facts*. 2009;2(2):126–35.

286. Rouabhi M, Guo DF, Morgan DA, Zhu Z, López M, Zingman L, *et al.* BBSome ablation in SF1 neurons causes obesity without comorbidities. *Mol Metab.* 2021;48:101211.

287. Sakaguchi T, Bray GA, Eddlestone G. Sympathetic activity following paraventricular or ventromedial hypothalamic lesions in rats. *Brain Res Bull.* 1988;20(4):461–5.

288. Rodríguez-Rodríguez R, Miralpeix C, Fosch A, Pozo M, Calderón-Domínguez M, Perpinyà X, *et al.* CPT1C in the ventromedial nucleus of the hypothalamus is necessary for brown fat thermogenesis activation in obesity. *Mol Metab.* 2019;19:75–85.

289. de Jong JM, Wouters RT, Boulet N, Cannon B, Nedergaard J, Petrovic N. The β3-adrenergic receptor is dispensable for browning of adipose tissues. *Am J Physiol - Endocrinol Metab.* 2017;312(6):508–18.

290. Yoon NA, Diano S. Hypothalamic glucose-sensing mechanisms. *Diabetologia*. 2021;64(5):985–93.

291. Mauvais-Jarvis F. Sex differences in metabolic homeostasis, diabetes, and obesity. *Biol Sex Differ.* 2015;6(1):1–9.

292. Speakman JR. Use of high-fat diets to study rodent obesity as a model of human obesity. *Int J Obes*. 2019;43(8):1491–2.

293. de Moura e Dias M, dos Reis SA, da Conceição LL, Sediyama CMN de O, Pereira SS, de Oliveira LL, *et al.* Diet-induced obesity in animal models: points to consider and influence on metabolic markers. *Diabetol Metab Syndr*. 2021;13(1);654-61

294. Tan K, Knight ZA, Friedman JM. Ablation of AgRP neurons impairs adaption to restricted feeding. *Mol Metab.* 2014;3(7):694–704.

295. Dietrich MO, Zimmer MR, Bober J, Horvath TL. Hypothalamic Agrp neurons drive stereotypic behaviors beyond feeding. *Cell*. 2015;160(6):1222–32.

296. Padilla SL, Qiu J, Soden ME, Sanz E, Nestor CC, Barker FD, *et al.* Agouti-related peptide neural circuits mediate adaptive behaviors in the starved state. *Nat Neurosci*. 2016;19(5):734–41.

297. Morselli L, Claffin K, Cui H, Grobe JL. Control of Energy Expenditure by AgRP Neurons of the Arcuate Nucleus: Neurocircuitry, Signaling Pathways, and Angiotensin. *Curr Hypertens Rep.* 2018;20(3):112–25.

298. Zhang Q, Duplany A, Moncollin V, Mouradian S, Goillot E, Mazelin L, *et al.* Lack of muscle mTOR kinase activity causes early onset myopathy and compromises whole-body homeostasis. *J Cachexia Sarcopenia Muscle.* 2019;10(1):35–53.

299. Quiat D, Voelker KA, Pei J, Grishin N V., Grange RW, Bassel-Duby R, *et al.* Concerted regulation of myofiber-specific gene expression and muscle performance by the transcriptional repressor Sox6. *Proc Natl Acad Sci U S A.* 2011;108(25):10196–201.

300. Shin KO, Bae JY, Woo J, Jang KS, Kim KS, Park JS, *et al.* The effect of exercise on expression of myokine and angiogenesis mRNA in skeletal muscle of high fat diet induced obese rat. *J Exerc Nutr Biochem.* 2015;6(1):91–8.

301. Lezi E, Lu J, Burns JM, Swerdlow RH. Effect of exercise on mouse liver and brain bioenergetic infrastructures. *Exp Physiol.* 2013;98(1):207–19.

302. Reichenbach A, Stark R, Mequinion M, Lockie SH, Lemus MB, Mynatt RL, *et al.* Carnitine acetyltransferase (Crat) in hunger-sensing AgRP neurons permits adaptation to calorie restriction. *FASEB J.* 2018;32(12):6923–33.

303. Svensson J, Sjögren K, Fäldt J, Andersson N, Isaksson O, Jansson JO, *et al.* Liver-Derived IGF-I regulates mean life span in mice. *PLoS One.* 2011;6(7):1–9.

304. Al-Samerria S, Radovick S. The role of insulin-like growth factor-1 (Igf-1) in the control of neuroendocrine regulation of growth. *Cells*. 2021;10(10):1–13.

305. Wu CS, Bongmba OYN, Yue J, Lee JH, Lin L, Saito K, *et al.* Suppression of GHS-R in AgRP neurons mitigates diet-induced obesity by activating thermogenesis. *Int J Mol Sci.* 2017;18(4).

306. Liu T, Xu Y, Yi CX, Tong Q, Cai D. The hypothalamus for whole-body physiology: from metabolism to aging. *Protein Cell.* 2022;13(6):394–421.

307. Graber TG, Maroto R, Fry CS, Brightwell CR, Rasmussen BB. Measuring Exercise Capacity and Physical Function in Adult and Older Mice. *Journals Gerontol - Ser A Biol Sci Med Sci*. 2021;76(5):819–24.

308. Yang S, Loro E, Wada S, Kim B, Tseng WJ, Li K, *et al.* Functional effects of muscle PGC-1alpha in aged animals. *Skelet Muscle*. 2020;10(1):1–8.

309. Lantier L, Fentz J, Mounier R, Leclerc J, Treebak JT, Pehmøller C, et al. AMPK controls exercise endurance, mitochondrial oxidative capacity, and skeletal muscle integrity. *FASEB J.* 2014;28(7):3211–24.

310. Liesa M, Shirihai OS. Mitochondrial dynamics in the regulation of nutrient utilization and energy expenditure. *Cell Metab.* 2013;17(4):491–506.

311. Domingos AI, Sordillo A, Dietrich MO, Liu ZW, Tellez LA, Vaynshteyn J, *et al.* Hypothalamic melanin concentrating hormone neurons communicate the nutrient value of sugar. *Elife*. 2013;2013(2):1–15.

312. Mavanji V, Butterick TA, Duffy CM, Nixon JP, Billington CJ, Kotz CM. Orexin/hypocretin treatment restores hippocampal-dependent memory in orexin-deficient mice. *Neurobiol Learn Mem.* 2017;146:21–30.

313. Dietrich MO, Liu ZW, Horvath TL. Mitochondrial dynamics controlled by mitofusins regulate agrp neuronal activity and diet-induced obesity. *Cell*. 2013;155(1):188.

314. Lovas JR, Wang X. The meaning of mitochondrial movement to a neuron's life. *Biochim Biophys Acta - Mol Cell Res*. 2013;1833(1):184–94.

315. Chen M, Li Y, Yang M, Chen X, Chen Y, Yang F, *et al*. A new method for quantifying mitochondrial axonal transport. *Protein Cell.* 2016;7(11):804–19.

316. Zeng F, Yao M, Wang Y, Zheng W, Liu S, Hou Z, *et al.* Fatty acid β-oxidation promotes breast cancer stemness and metastasis via the miRNA-328-3p-CPT1A pathway. *Cancer Gene Ther.* 2022;29(3–4):383–95.

317. Wu G, Zhang J, Fan GG, Zou ZY, Yin YL, Li GX. MiRNA-324-5p inhibits inflammatory response of diabetic vessels by targeting CPT1A. *Eur Rev Med Pharmacol Sci.* 2020;24:12836–43.

318. Sun Y, Oravecz-Wilson K, Bridges S, McEachin R, Wu J, Kim SH, *et al.* MiR-142 controls metabolic reprogramming that regulates dendritic cell activation. *J Clin Invest.* 2019;129(5):2029–42.

8. Scientific production

1. Reyes M*, González L*, Ibeas K*, Cereijo R, Taxeràs SD, Pellitero S, Martínez E, Tarascó J, Moreno P, Malagón P, Higueras C, Soria A, Puig-Domingo M, Villarroya F, Serra D, Herrero L, Sánchez-Infantes D. White adipose tissue-infiltrated CD11b+ myeloid cells are a source of S100A4, a new potential marker of hepatic damage. *Eur J Endocrinol*. 2021;184(4):533-41. doi: 10.1530/EJE-20-1130.

2. Ibeas K, Herrero L, Mera P., Serra D. Hypothalamus-skeletal muscle crosstalk during exercise and its role in metabolism modulation. *Biochem Pharmacol*. 2021;190:114640. doi: 10.1016/j.bcp.2021.114640.

3. Ibeas K. La obesidad, la pandemia silenciosa. *Rincón del profesor, sección de divulgación de la SEBBM*. 2021. doi: 10.18567/sebbmdiv_RPC.2021.11.1.

4. (*submitted*) Zagmutt S, Mera P, González-García I, Ibeas K, Obri A, Martin B, Esteve A, Soler-Vázquez MC, Bastias-Pérez M, Cañes L, Augé E, Pelegri C, Vilaplana J, Ariza X, García J, Martinez-González J, Casals N, López M, Sanz E, Quintana A, Herrero L, Serra D. Cpt1a is required in AgRP neurons to control food intake and thirst in a sex-dependent manner.

5. (*submitted*) Soler-Vázquez MC, Delgado K, Calatayud C, Mera P, Zagmutt S, Bastías-Pérez M, Ibeas K, Casals N, Consiglio A, Serra D, Herrero L. Implantation of CPT1AM-expressing adipocytes reduces obesity and glucose intolerance in mice

*Authors contributed equally to this work